TECHNIQUES FOR MONITORING THE PERFORMANCE OF PHASED-ARRAY ANTENNAS

by

JACOB RONEN

A Thesis submitted for the Degree of Doctor of Philosophy in the Faculty of Engineering, University of London and the Diploma of Membership of the Imperial College (DIC)

Department of Electrical Engineering
Imperial College of Science and Technology
Exhibition Road, London, S.W.7

January, 1981

ABSTRACT

This thesis is concerned with the problem of monitoring phased-array antennas in general and Microwave Landing System (MLS) phased arrays in particular.

Various novel methods of monitoring phased-array antennas are suggested. One is based on changes in the far-field radiation pattern arising from defects in the array. Another method uses the near-field to far-field transformation, based on the concept of the plane-wave spectrum, for the detection of defects in the antenna. A third method is based on near-field measurements and uses the properties of the Fresnel integral.

The methods were simulated on the computer and, where possible, were tested by experiment. A comparative assessment of the methods is given, and an operational monitoring system is suggested for the Microwave Landing System phased array.

ACKNOWLEDGEMENTS

The author would like to thank a number of people who aided him throughout this project and in the preparation of the resulting thesis.

Formost he would like to acknowledge his gratitude to his supervisor Dr. R.H. Clarke who guided his efforts and shared his enthusiasm, assistance and valuable suggestions in this project, and for constant encouragement and kindly criticism.

The author is deeply indebted to the discussions held in the first phases of the work with Prof. J. Brown for crystallizing the subject.

He much appreciates the enlightening discussions held with his colleagues in the Microwave Laboratory. To Mr. P.J. Taylor who helped in the initiation of the subject and for his preparedness in constant supplying of any data required. And to his former colleague Dr. I.A. Mashhour.

Also he would like to thank Dr. M. Enein of the Plessey Company for constructively criticizing the interim conclusions of the work. He is very grateful to the College Computer Center for using the Draft-Format typing, to Mrs. T. Shahak and Mr. R. Puddy for the drawings, to Mrs. R. Zilbrass and Mr. N. Hazan for some of the computer runs and to Mr. N.J. Miles for the Photograghs.

The work described in this thesis was carried out while the author was supported by RAFAEL - Israel Ministry of Defence. This is also gratefully acknowledged.

To my dear wife Ruth

TABLE OF CONTENTS

		Page
ABSTRACT		ii
ACKNOWLEDGMENTS		iii
TABLE OF CONTENTS		1
CHAPTER 1	INTRODUCTION	9
1.1	A short review of methods for monitoring the performance of phased array antennas	10
1.2	Description of the MLS	12
1.3	Expected types of defects in phased array antennas	14
1.4	Tecniques dealt with in this study	16
CHAPTER 2	THE SUBSTITUTE ELEMENT TECHNIQUE	19
2.1	Patterns of uniformly illuminated ideal arrays	19
2.2	The concept of an equivalent substitute array	21
2.3	Sensitivity of antenna patterns to defective elements in the array	22
2.4	Static and dynamic patterns and defects in phased array antennas	22
2.5	The equivalent substitute field of a defective element in an N-element array	24
2.6	Examples of defective elements in an N-element array	25
2.7	Demonstration of defective array patterns in the far side-lobe region	27

		Page
2.8	A method to extract the location of a defective element	31
2.9	Identification of the defect	33
2.10	Some computer simulations	33
2.11	Non necessity of measuring in far field	37
2.12	Applicability of the subtraction method	37
2.13	Conclusions	38
CHAPTER 3	APPLICATION OF THE SUBSTITUTE ELEMENT TECHNIQUE	39
3.1	Performance of an array of isotropic elements with random phase error	39
	3.1.1 The mean far-field radiation	40
	3.1.2 The variance of the far-field radiation	41
	3.1.3 The incoherent to coherent far-field power ratio	42
3.2	Use of the proposed subtraction method in the presence of random phase-shift errors	44
	3.2.1 The static case	44
	3.2.2 The dynamic case	45
3.3	Array center reference phase for defective and non-defective arrays	46
3.4	Computer simulation of defects in presence of random phase excitation	47

		Page
3.5	Inadvertently latched (stuck) phase-shifter feeding a single element	50
	3.5.1 The equivalent substitute element representation of a stuck phase-shifter feeding a single element	51
	3.5.2 A modification in the subtraction method for a stuck phase-shifter	54
3.6	The equivalent-substitute array of a stuck phase-shifter feeding a single subarray	55
3.7	A stuck phase-shifter feeding an M-element subarray with a switched beam-forming network (B.F.N.)	57
3.8	Simulation of stuck phase-shifters in ideal arrays	58
3.9	Discussion	61
CHAPTER 4	MUTUAL COUPLING EFFECTS	62
4.1	Mutual coupling effects between array elements	63
4.2	Mutual coupling effects in a two element array	64
4.3	The equivalent substitute array in a two element array	67
4.4	Defects in an infinitely long array	71
4.5	Effects of reflected power due to a defect in array elements	75
4.6	Simulation of defective elements in actual arrays	78

		Page
	4.6.1 Simulation parameters	78
	4.6.2 Assessment of the results	81
4.7	Discussion (expected usefulness of the subtraction method in actual arrays - deterministic case)	81
CHAPTER 5	APPLICATION OF THE ANGULAR SPECTRUM CONCEPT	84
5.1	Summary of the angular spectrum concept	84
	5.1.1 The angular spectrum of two dimensional fields	89
	5.1.2 Determination of far-field from near field measurements	91
5.2	Use of the angular spectrum method to locate defects in antenna arrays	93
	5.2.1 Demonstration of the angular spectrum method	95
5.3	Use of the angular autocorrelation (a.c.f.) of the angular spectrum to locate defects in the presence of random errors	101
	5.3.1 The a.c.f. and the aperture illumination	101
	5.3.2 Demonstration of the a.c.f. method	102
5.4	Discussion	107
CHAPTER 6	MONITORING IN THE NEAR FIELD	109
6.1	A focused near-field monitoring antenna	109

		Page
	6.1.1 Fresnel diffraction in the near field	110
	6.1.2 Several properties of the Fresnel integral and the recommended monitoring technique	112
	6.1.3 The near-field monitoring technique	117
6.2	Simulation experiments with a near-field monitoring antenna	117
	6.2.1 Uniform transmitting antenna aperture field	119
	6.2.2 Half-cosine aperture field	124
	6.2.3 Sine aperture field	129
	6.2.4 Raised cosine (cosine square over pedestal) aperture field	132
	6.2.5 Summary of the near-field simulation experiment	138
6.3	Internal/integral monitoring of Phased array antennas	140
	6.3.1 Sampling the aperture field of the array	140
	6.3.2 Internal sampling of the radiating elements	142
6.4	Discussion	145
CHAPTER 7	EXPERIMENTAL INVESTIGATION	148
7.1	The experimental set-up	148
	7.1.1 The Geometry	148
	7.1.2 antenna array and probes	149

		Page
	7.1.3 The near-field set-up	153
7.2	Data collection and processing	156
	7.2.1 Recording and preprocessing	156
	7.2.2 Near field processing	157
	7.2.3 Simulation of near-field measurements	157
7.3	The near-field experimental results	158
	7.3.1 open waveguide patterns	158
	7.3.2 The subtraction method	165
	7.3.3 The angular spectrum method	169
	7.3.4 The autocorrelation (a.c.f.) method	170
	7.3.5 Sensitivity to instability (and thresholds)	174
7.4	Details of some supporting tests	180
	7.4.1 Static and dynamic errors	180
	7.4.2 Antenna tests (and stray radiation)	182
	7.4.3 Comparison of far field measurements	185
	7.4.4 Discussion of the results of the preliminary tests	187
7.5	Summary and discussion	188
CHAPTER 8	COMPARISON OF THE METHODS	190
8.1	Analysis tools used	190
	8.1.1 The equivalent substitute element technique	190
	8.1.2 The approximation to the Fresnel integral	191

		Page
	8.1.3 Simulation models used	191
8.2	A summary and comparison of the monitoring methods suggested	194
8.3	A summary of the experimental investigation	198
8.4	Comparison of the required processing	200
	8.4.1 Preprocessing and signal measurements	200
	8.4.2 Processing	203
8.5	A tentative proposal for a practical monitoring system (MLS phased-array)	206
	8.5.1 Definition of the monitoring system	208
	8.5.2 A simplified block diagram	210
CHAPTER 9	CONCLUSIONS	217
APPENDIX A	Reproduced selected sections from ICAO (SARPS) report [6]	225
APPENDIX B	Expected error in estimating phase reference (the random case)	239
APPENDIX C	Angular a.c.f. of the angular-spectrum	242

		Page
APPENDIX D	Approximations to the near-field of a half-cosine aperture fields	244
APPENDIX E	Listing of computer programs	249
APPENDIX F	Commercially advertized electronic products	297
REFERENCES		323

CHAPTER 1

INTRODUCTION

Phased array antennas represent one of the most important types of modern antenna. They play a major role in the introduction of novel and sophisticated systems, where performance of agile beam scanning and/or multi-object detection and tracking are called upon.

An inherent feature of these antennas is their "graceful" degradation in performance as elements fail. If a small percentage of array elements fail the directivity is practically unchanged and the effective radiated power (ERP) changes only by a few percent. The advantage of graceful degradation is also a source of difficulty in monitoring element failure in such arrays.

Phased array antennas are mostly used in two-way (transmit/receive) systems, for example, in modern Radar systems. However, they are also used in important one-way systems as in the proposed Microwave Landing System (MLS), transmit only, phased-array antennas. There, monitoring is of major importance as there is no other means available to indicate that the array is performing normally, such as a Radar display or a communication-system output.

Monitoring of every single element of the array, although sometimes used, can be undesirable in a multi-element array where the reliability of monitoring these multiconnections leads to new uncertainties.

The purpose of the present work is to look for monitoring methods based on a composite signal, rather than on the accumulation of a multitude of individual signals. Specifically, the MLS phased array parameters will be used whenever possible in the application of the suggested monitoring methods.

Not much published work has been found that deals with this kind of monitoring. A short review of known phased-array monitoring methods is presented in section 1.1. A description of the MLS will be summarized in 1.2. Expected types of defects in phased-array antennas will be discussed in section 1.3. Monitoring techniques presented in the present work will be summarized in 1.4.

1.1 A short review of methods for monitoring the performance of phased array antennas.

Blake, Schwartzman and Esposito [1] described two techniques for monitoring large phased array antennas, used in the " Hard Point Demonstration Array Radar " (HAPDAR).

The first technique makes use of testing the fault signals resulting in response to the applied control current feeding the diode phase shifters of the array. Each pulse repetion period a different phase shifter is sampled. The information deduced on diode malfunctioning is recorded as a short or open circuit condition.

The second technique is a "maintenance system check". This is a low level (receive only) R.F. check based on a special phase coding (say between 0 and 45 degrees) of each specific phase shifter in turn, while the antenna beam is kept in a fixed

direction. A transmitter on a test tower directs a C.W. signal towards the array and the resulting received beam phase and amplitude modulation are analyzed in the computer to calculate the phase shifts of the tested element. The necessary time stated for performing the tests over a 2165-element array is 16 minutes.

Neither of these techniques is satisfactory. The first is an indirect check that does not measure the R.F. performance of the elements. The second method, besides being too lengthy, interrupts the normal operation of the system by the requirement to point the array beam in a fixed direction, and moreover the phase shifters are not examined with the full transmitted R.F. power.

Ransom and Mittra [2] suggested a method of locating defective elements in large arrays based on near field (Fresnel region) recording of phase and amplitude over a plane parallel to, and of the same size as, the aperture. The solution is based on the reconstruction of the aperture field by inversion of the recorded field, using the diffraction formula. Subtracting the expected correct field from the reconstructed field, gives the error field whose maxima indicate the presence of defective elements.

This method which can be used in a near field antenna measurement is impractical in field-operated systems, such as MLS, where such obstructions are not permitted.

Another method for pattern measurements of phased-array antennas is suggested by Scharfman and August [3], by focusing the transmitting antenna into the near zone. As in the previous

case this is not desirable as it changes the original patterns and it also interrupts the normal operation of the system.

An experimental investigation by a team from the Bendix Company [4] checked the degradation in the performance of MLS antenna patterns due to array elements failure, using two methods. The first as in [3], focusing the transmitting antenna array (a 60λ aperture), into the near field (to a distance twice the array aperture). The second method used a waveguide line integral monitor. Both test results showed good agreement with patterns measured previously on an antenna test range. It was found that 10% of array components can fail before the side-lobe increases to 17 db and the beam pointing error exceeds .02 degrees. However as in the previous paper, no specific proposal has been made for the inverse problem of identifying defective elements based on monitoring.

No other methods for the monitoring and detection of defects in operational phased-array antennas are known to the author. Therefore alternative methods, or modification of present methods will be sought in the present study.

1.2 Description of the MLS

The Microwave Landing System (MLS) is proposed to replace the global standard of the present Instrument Landing System (ILS) in 1985 ; although both systems will coexist for another decade. The expected improvements of the MLS over the ILS are [5] :

- A larger coverage area, up to ± 60 degrees in azimuth and up to 30 degrees in elevation, enabling proportional guidance; compared to only one straight approach path in the ILS.

- Two hundred frequency channels allocated in the C-band (5.031 to 5.090 GHz) compared to the 40 channels in the VHF and UHF presently allocated to the ILS.

- The time multiplex signal format will enable angle and data functions (Azimuth, elevation plus optional capabilities like flare elevation plus missed approach guidance) to be communicated.

Out of several contending proposals, the time-referenced Scanning Beam (TRBS) system was finally endorsed by the International Civil Aviation Organization (ICAO) as the standard for MLS on April 1978. The operation of the system is as follows.

The coverage area of the (TRBS) MLS is continuously and linearly swept by two fan beams - one in azimuth and the other in elevation. In each scan, two pulses (main beams) are received by the aircraft, the "to" and the "fro" scans. The on-board receiver, derives the azimuth and elevation from the time difference between the scans. The final specifications of the MLS are not yet available. However, Standards And Recommended Practices (SARPS), are given in the ICAO SARPS report [6], parts of which are reproduced in Appendix A.

The main recommended approximate specifications are as follows :

-Linear angle scan rate (Azimuth and Elevation)		20000 deg/sec
-Antenna beam-widths(in the plane of angle scan)		1 deg.
(Resulting antenna aperture		60 λ)
-Data rates	Azimuth	13.5 Hz
	Elevation	40.5 Hz
-Accuracy		0.01 deg.
-Linearly allowable error degradation to 20 nautical miles along centerline		0.2 deg.

Each functional element of the MLS (e.g, Azimuth, Elevation etc.) is to be associated with monitor and control equipment [6]. Monitors shall assure the appropriate guidance qualities. When malfunctions occur, the monitors shall initiate action to restore normal operations, downgrade performance categories, or remove the element from service, as appropriate to the situation.

The requirement is to cause the radiation to cease if malfunction persists for more than one second (details in reference [6] or Appendix A). This leads to a requirement on the monitoring measurements including the processing response time.

1.3 Expected types of defects in phased array antennas

Phased-arrays can be represented [7] as being composed of the following sections :

- Feed network ; power distribution (in transmit) or combining (in receive) network.

- Phase control and beam switching network.

- Radiating elements (and sub-arrays).

Defects could be in amplitude, phase or a combination of the two.

Classified according to their origin, defects can be thought of as either "static" or "dynamic". Defects in the feed network and the radiating elements are in general of a static nature. While those in the electronically controlled elements like phase-shifters and beam switches are generally time dependent, and hence dynamic.

It is possible to control phased array antennas, with only phase-shifters feeding each element of the array. However, it can be shown that more economical systems can be derived based on "thinned" phase-shifters, where each is feeding a sub-array of the antenna. If larger angle coverage than that provided by the sub-array is required, then these subarrays could be fed by beam-switching networks (e.g., Rotman lenses in one proposal [8] for the MLS phased-array).

Dynamic defects in digital phase shifters are caused when one or more of the digital phase bits are not responsive to the digital command ("stuck" phase). This may be accompanied by one or more non-responsive beam switches. In systems like the MLS, where solid-state components of very high reliability are used, it is very unlikely that a defect will be initiated in more than one component of the array at one time. On the other hand, the

graceful degradation in the array performance due to defcts in a small number of the array components, presents, as already explained, a problem of identifying these defects.

The methods developed in this work to monitor different kinds of defects, are summarized in the next section.

1.4 Techniques dealt with in this study

The basic idea in the analysis of the effects of array component failure, on the performance of an array, is to find a technique to represent defective elements in a convenient way. The technique of the "equivalent substitute element" to represent defective elements in an array, is put forward in chapter 2. Based on the equivalent substitute technique the "subtraction method" is suggested which enables the inverse process, i.e., given the far-field patterns, a defect in a single element of otherwise ideal arrays, can be traced. Application of the substitute element technique and the subtraction method in actual arrays is first demonstrated by the introduction of defects in the presence of random phase excitation errors in chapter 3. The random phase excitation is, in part, representing the quantum behaviour of digital phase shifters ; rather than the ideal analogue ones. Defects of a dynamic nature ; the stuck phase shifter feeding a single element or a subarray, are also represented in the same chapter.

A more realistic representation of defects in actual arrays is described in chapter 4. There, defects in the presence of mutual coupling are discussed. The mutual coupling effects are demonstrated using Carter`s equations [9,10,11].

Another method of monitoring defects in antenna arrays is given in chapter 5. There, the application of the angular spectrum concept [12,13] is used to represent the aperture field of the array as a transform of the far field. The angular spectrum direct method, is given first. Another method, based on the Wiener-Khinchin or Van Cittert - Zernike principle [14,18], makes use of the autocorrelation function (a.c.f.) of the angular spectrum to derive the aperture power distribution across the array. The a.c.f. method is presented and demonstrated. The determination of far-field patterns from near-field measurements, based on the angular spectrum concept, which is widely used [13,14,15,17], is also summarized in this chapter. Use is made of this technique in the experiments described in chapter 7. Near-field analysis based on the Huygens-Fresnel diffraction formula [13,18] is given in chapter 6. Use is made of an approximation to the Fresnel integral to derive another type of near-field (Fresnel region) monitoring technique. This technique enables real time monitoring of the main beam scan of the array, without the need to focus the transmitting antenna (as has been done, for example, in [3,4]). The integral/internal monitoring technique, as a form of very close-in field monitoring, is described, also based on the Huygens-Fresnel diffraction formula. The normalized far-field patterns derived from integral/internal monitoring suggested the application of the far field monitoring techniques of chapters 2, 3, 4 and 5 to this method of monitoring also. Simulation on the computer of defects in arrays and the application of the far-field and near-field techniques, has accompanied the analysis throughout. However, it was thought to be vital to obtain experimental verification where possible. The

experimental investigation is described in chapter 7. A laboratory test set-up has been used, employing waveguide slot arrays available in the Departmet Microwave laboratory. Defects were introduced into the arrays and, using the near-field to far-field transformation, the various monitoring methods were examined. A detailed comparison of the methods suggested is given in chapter 8. The conclusions in chapter 9 also contain recommendations for future work.

CHAPTER 2

THE SUBSTITUTE ELEMENT TECHNIQUE

A method for the detection of defective elements in antenna arrays, based on a simple idea which uses familiar array theory [10,20], is described in this chapter. The method emphasizes the engineering significance of using rather simple formulas for accurately determining the location and type of defective elements in the array, based on changes in the far-field pattern. The idea of an "equivalent substitute element" is proposed in order to represent defective elements in an array. Defects of both "static" and "dynamic"(i.e. with the beam being swung) nature are discussed and defects of a static nature in ideal arrays are considered in detail.Other types of defect of a dynamic and static nature will be discussed in chapters 3 and 4. The "subtraction method", based on the equivalent substitute element technique, is presented and the applicability of the method is discussed.

For simplicity two-dimensional situations will be used throughout most of the work, as it is easier to appreciate the underlying concepts and methods. In addition most results can be used almost directly for MLS phased arrays which are characterized by their two dimensional beam scanning (see section 1.2).

2.1 Patterns of uniformly illuminated ideal arrays.

In this section a summary of known formulas will be given.

The normalized far-field E_N of an N element, isotropic, equally spaced and uniformly illuminated linear array is given by [10,20]

$$E_N = \frac{1}{N} \sum_{i=1}^{N} e^{j[i-(\frac{N+1}{2})]\phi}$$

$$= \frac{1}{N} \frac{\sin(N\phi/2)}{\sin(\phi/2)} \qquad (2.1)$$

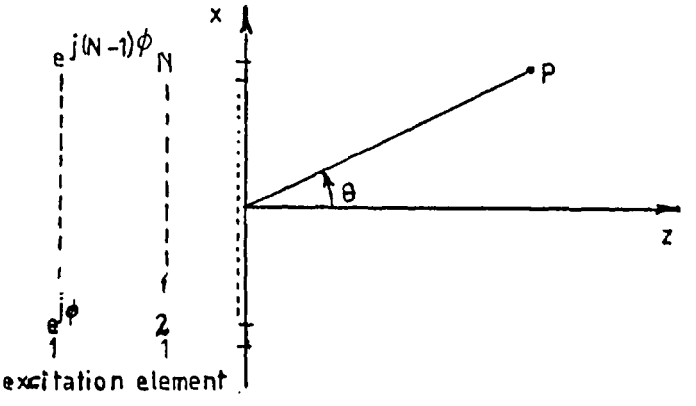


Fig. 2.1 Array geometry.

where ϕ is the total phase-difference as viewed from the far-field, between successive elements of the array, and consists of the internal phase-shift α introduced between the elements and the additional spatial phase-shift due to differential free-space propagation delay between succesive elements. Thus

$$\phi = kd \sin\theta + \alpha \qquad (2.2)$$

where d is the spacing between elements and θ is the angle of observation, measured to the broadside direction. The propagation constant is $k=2\pi/\lambda$, where λ is the wavelength of the radiation. As a variable of the geometry $s=\sin\theta$ rather than θ will be used, thus simplifying the analysis. For a broadside array $\alpha=0$ and the peak lobe amplitude decays approximately hyperbolically with s except for the main-beam region, where the maximum normalized amplitude is limited to unity, and the far side-lobe levels are tending to the value 1/N . The phase pattern will be an oscillatory square-wave symmetrical to the broadside direction (s=0). It is the changes in the far-field patterns in

the side-lobe region that leads to the detection of defective elements as described in the following section.

2.2 The concept of an equivalent substitute array.

An "equivalent substitute array" is an array of "equivalent substitute elements". It is derived by considering the actual defective array to be the sum of an ideal array, which has no defective elements, and the equivalent substitute array. This decomposition is justified by the linear relation between the elements' excitation and the radiation. An example of this is given in Fig. 2.2.

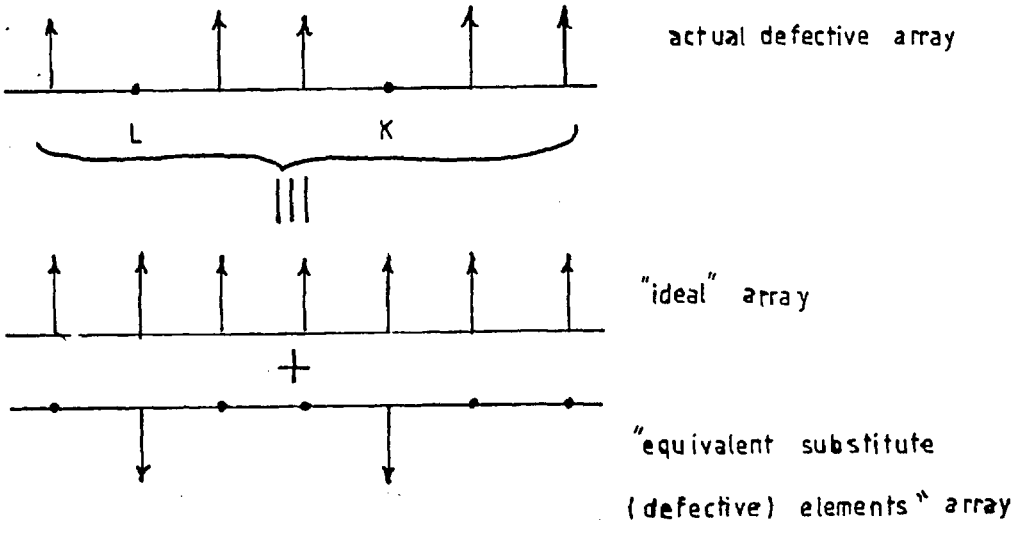


Fig. 2.2 Demonstration of equivalent substitute elements

An additional virtue of using the equivalent substitute array, is the insight it gives into the selection of the pattern region for the detection of defective elements. This is best done by looking

for the sensitivity of antenna patterns to defects in the array, which follows.

2.3 Sensitivity of antenna patterns to a defective element in the array.

The field pattern envelope of a unity amplitude excitation N element array is comparable to a single element antenna in the far side-lobe region and will be N times higher in the main-beam region. The substitute array of a missing (defective) element in the array will be equal to a single element antenna. Therefore, the effect of a defective element in the array will be N times larger in the far side-lobe region than in the main-beam region. It is therefore recommended that use be made of the far side-lobe region to monitor defects in the antenna array.

2.4 Static and dynamic patterns and defects in phased array antennas.

Phased array antenna patterns can be divided into two main categories : static patterns and dynamic patterns. The difference is essentially one of method of measurement. The static pattern of an array could be measured by the conventional antenna range instrumentation where the antenna phase control and beam switching networks are fixed throughout the measurement. The antenna is then rotated relative to the measuring probe and the pattern recorded. The dynamic pattern, in contrast, will be recorded when the antenna and the measuring probe are fixed and the array beam is scanning by dynamically controlling its phase and beam switching network. If ideal arrays of identical elements

are considered then the main difference between the static and the dynamic patterns of the array will be due to the element gain factor and the changing projected aperture area. Differences between a static pattern and a dynamic pattern measured with the probe in the broadside direction of the array, are due only to the element gain factor.

Defects in antenna arrays can similiarly be categorized into the two main classes of static and dynamic, depending on whether they affect the static or the dynamic pattern. A static defect in an array element can be described by a fixed change in magnitude and phase with respect to the ideal element excitation. The result is normally a constant error in the pattern beam pointing, the beam-width and increased side-lobe level. While a dynamic defect will exhibit a time-dependent shift of the excitation magnitude and phase. Hence, dynamic errors in the pattern beam pointing, the beam-width and dynamic changes in the side-lobe level will be noticed. In realistic phased arrays the dynamic control of the phase and beam switching networks is often performed in discrete (quantized) steps rather than continuously, hence introducing dynamic quantization of the beam scan and the resulting pattern. Over and above these built-in phase excitation errors due to quantization, a defect like an unintentionally stuck phase shifter can occur causing dynamic changes in the array beam pointing, the beam-width and the side-lobe level.

In the present chapter simple defects of a static nature will be analyzed, based on the substitute element representation. Defects of a dynamic nature will be described in chapter 3. While more complex defects of a static nature (mutual coupling effects)

will be described in chapter 4.

2.5 The equivalent substitute field of a defective element in an N-element array

Expressions will now be developed for the equivalent substitute excitation and the resulting far-field radiation for defects of a static nature in a simple, though important, case. Combined amplitude and phase defects in a single element of the array (element K) are assumed. The effect is conveniently demonstrated by the phasor representation, of Fig. 2.3. (The analysis for a single defective element also applies to the case of many elements through the principle of superposition.)

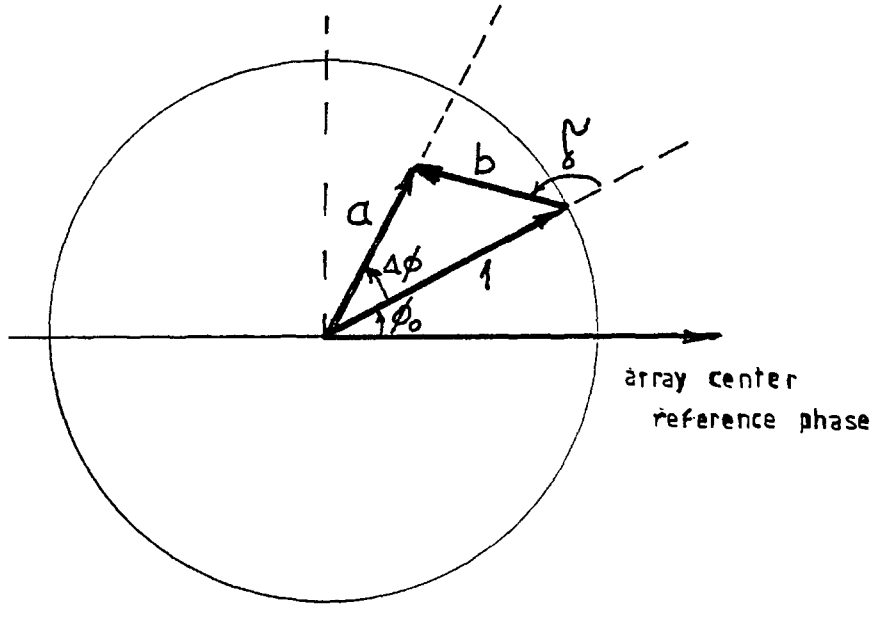


Fig. 2.3 Phasor representation of phase and amplitude defect, the equivalent substitute element.

Fig. 2.3 shows the ideal element of unit amplitude and phase ϕ_0 referred to the array centre reference phase, where, from equation (2.1),

$$\phi_o = [\, K - (\tfrac{N+1}{2})\,]\,\phi \qquad (2.3)$$

and K is the element number concerned. The defective Kth element has an amplitude ratio of a:1 to the ideal, and is shifted $\Delta\phi$ radians in phase. The following expressions are derived for the normalized magnitude b and the phase shift γ of the substitute element,

$$\left.\begin{aligned} b &= (1 + a^2 - 2a\cos\Delta\phi)^{1/2} \\ \text{and} \\ \gamma &= \pi - \arcsin(\tfrac{a}{b}\sin\Delta\phi) \end{aligned}\right\} \qquad (2.4)$$

and the radiated normalised far-field E of the defective array will, therefore, be a superposition of the good array and the substitute element far fields, giving

$$E = \frac{1}{N}\left[\frac{\sin\frac{N\phi}{2}}{\sin\frac{\phi}{2}} + b e^{j\gamma} e^{j[K-(\frac{N+1}{2})]\phi}\right] \qquad (2.5)$$

it can be seen immediately that information on the defective element location (K) and the nature of the defect (b, γ) is contained in equation (2.5). Use will be made of this information in suggesting the subtraction method of monitoring, and in the simulation on the computer of defective array patterns. It also demonstrates the higher sensitivity of the far field pattern to defects in the far side-lobe region, as explained in section 2.3.

2.6 Examples of defective elements in an N - element array.

Expressions will now be given for the following examples;

a) The Kth element missing.

Here, $\gamma = \pi$ and b=1, therefore the normalized far-field of the array will be given by

$$E = \frac{1}{N}\left[\frac{\sin\frac{N\phi}{2}}{\sin\frac{\phi}{2}} - e^{j[K-(\frac{N+1}{2})]\phi}\right] \qquad (2.6)$$

b) The Kth element with a phase defect only.

Here $b=2\sin(\Delta\phi/2)$ and $\delta=1/2(\pi+\Delta\phi)$ therefore

$$E=\frac{1}{N}\left[\frac{\sin(N\phi/2)}{\sin(\phi/2)}+2\sin\Delta\phi/2\,\exp\{j\frac{1}{2}(\pi+\Delta\phi)\}\exp\{j[K-(\frac{N+1}{2})\phi]\}\right] \qquad (2.7)$$

c) Two missing elements, K and L.

This can be represented by a two-element substitute subarray. The array far field will be given by

$$E = \left[\frac{\sin(N\phi/2)}{\sin(\phi/2)}-2\cos\frac{D\phi}{2}\,\exp\{j(K+\frac{D}{2}-(\frac{N+1}{2}))\phi\}\right] \qquad (2.8)$$

where D=(L-K) is the difference in element numbers between the missing elements, and 2 cos $D\phi/2$ is the interference pattern of two elements seperated D elements apart. It is clear that the cosine term will not introduce additional phase jumps of π radian as long as

$$\left|\frac{D\phi}{2}\right| < \frac{\pi}{2} \qquad (2.9)$$

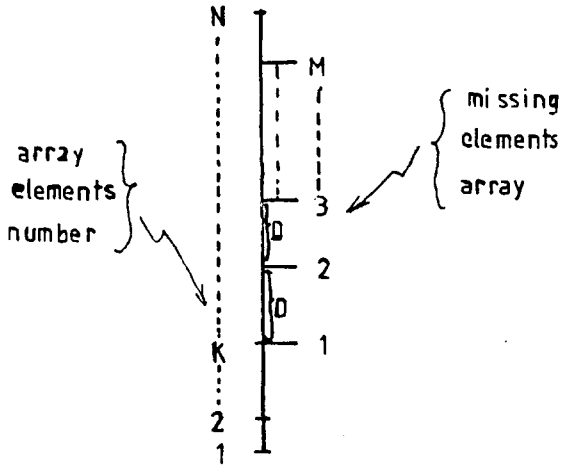


Fig. 2.4 M missing elements equidistantly seperated.

d) M missing elements equidistantly spaced.

Fig. 2.4 shows an N-element array where M of its elements are missing. The Kth is the first missing element, and each subsequent Dth element is also missing. The far-field of the defective array will be,

$$E = \frac{1}{N}\left[\frac{\sin\frac{N\phi}{2}}{\sin\frac{\phi}{2}} - \frac{\sin(M D\phi/2)}{\sin(D\phi/2)} \exp\{ j(K + (\tfrac{M-1}{2})D - (\tfrac{N+1}{2}))\phi \}\right] \qquad (2.10)$$

This expression will be compared to that used in the case of a defective subarray described in chapter 3, when defective subarrays will be dealt with in more detail. A pictorial representation of some of these effects will now be given.

2.7 Demonstration of defective array patterns in the far side-lobe region.

In order to emphasize the sensitivity of the far-sidelobe region to the presence of defective elements, the following three cases will be considered using equation (2.5) as a basis.

Case 1 Missing center element of the array (Fig. 2.5)

Case 2 Defect of $\pi/4$ phase shift error and +3db amplitude error in the center element (Fig. 2.6).

Case 3 Off-centre defect, described over the entire angular region (side-lobe and main-lobe). (Fig. 2.7)

Case 1 Missing centre element:far field far side- lobe region

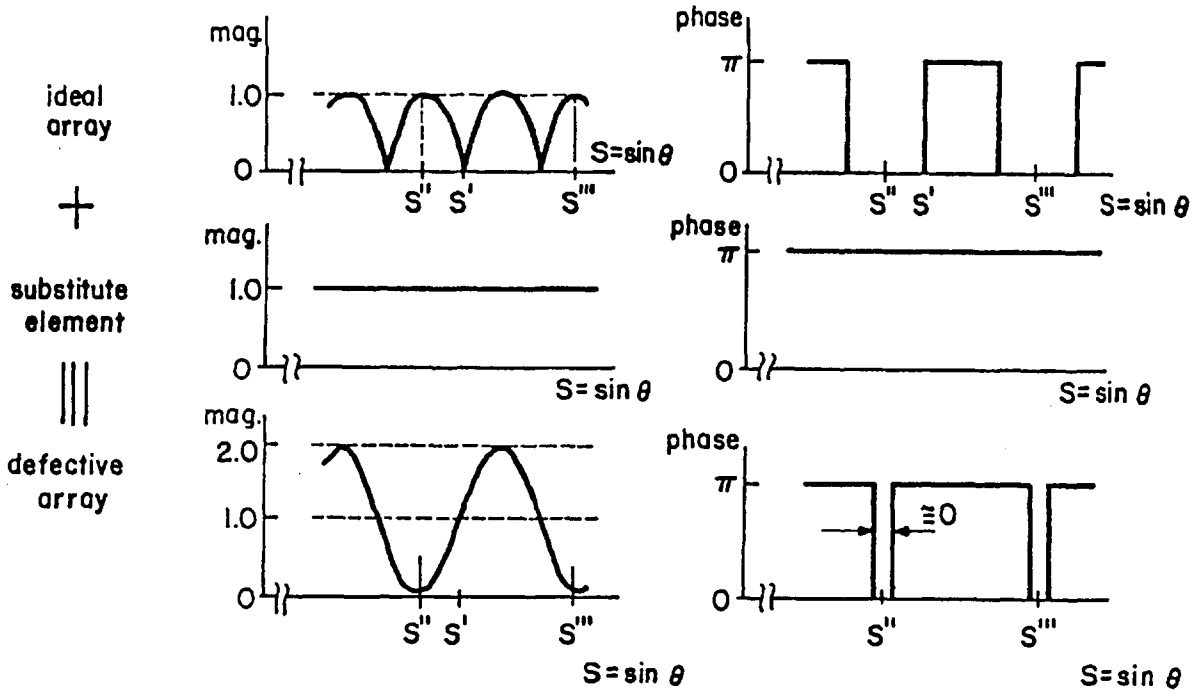


Fig. 2.5 array pattern for case 1 : missing centre element of the array.

Referring to Fig. 2.5 ; the defective array pattern is there derived from the ideal array and the substitute element. The far side-lobe level of the field magnitude is increased by almost 6db. The number of side-lobes is divided by a factor of 2. The phase pattern also changes, instead of being a square-wave phase of 0 and π, the phase remains almost constant at π, apart from narrow gaps of 0 phase (the period remains the same but the duty-cycle has changed appreciably.)

Case 2 Phase and amplitude defects in centre element ; far-field far side-lobe region.

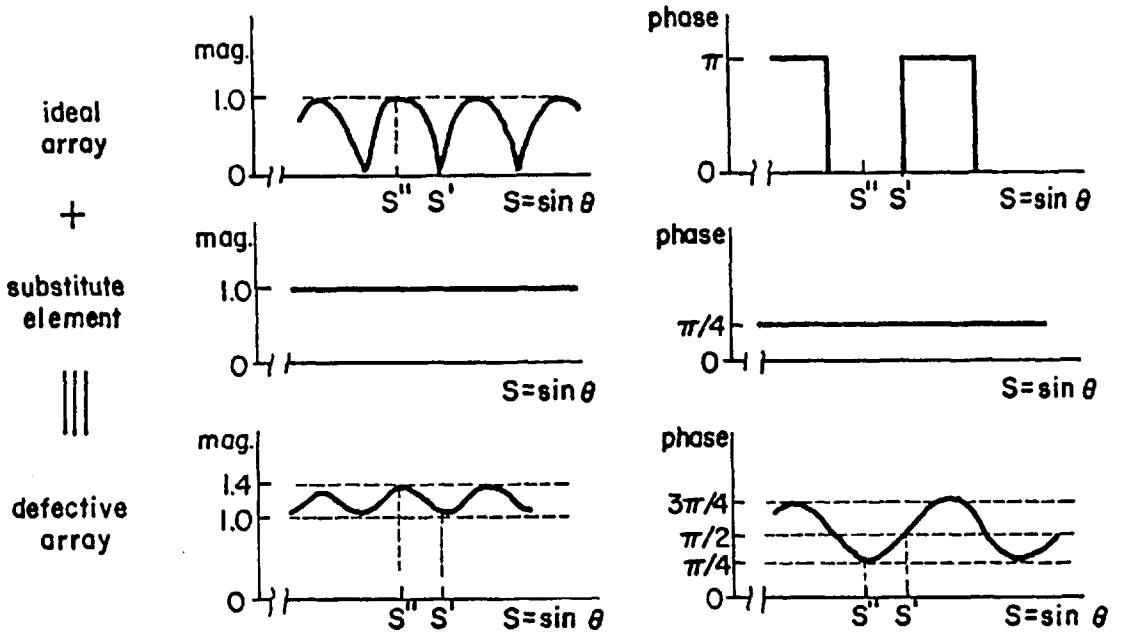


Fig. 2.6 Array pattern for case 2 ; phase and amplitude defects in center element of the array.

Referring to Fig. 2.6 a defect consisting of a $\pi/4$ phase shift and +3db change in amplitude, causes the following changes in amplitude and phase referred to the pattern of the ideal array. The nulls of the ideal array side-lobes are filled in and smoothed with a maximum of 3db between crest and trough. Side-lobe amplitude periodicity does not change. The phase behaviour also changes, from a square wave between π and 0 into a sine wave with the same periodicity but ranging between $\pi/4$ and $3\pi/4$.

From cases 1 and 2, as well as other cases not presented, it appears that the far side-lobe region contains sufficient information for identifying defects, at least in the center element of the array.

Case 3 Defective element located off the centre of the array ; far field, entire angular range

Case 1 and 2 dealt with defects in the center element of the array. If the defect is now located off-centre, the additional phase shift of the substitute element will be superimposed on the phase-line $m \sin\theta$ as described pictorially in Fig. 2.7 : In this drawing the phase-line is given over the whole range of direction angles for two values of m which in turn depend on the position K of the defective element. The relation between m and K is

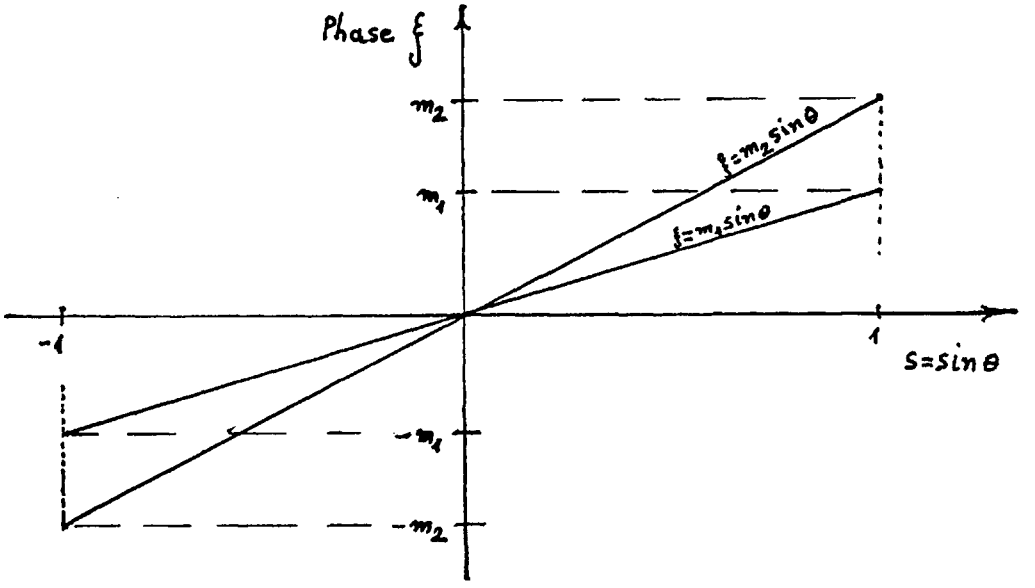


Fig. 2.7 Phase-line for case 3 ; far-field entire angular range

$$m = \frac{2\pi d}{\lambda} \left[K - \left(\frac{N+1}{2}\right)\right] \qquad (2.11)$$

This phenomenon can be used as the basis of a technique for identifying a single defective element, as follows.

2.8 A method to extract the location of a defective element.

From equation (2.11) it is clear that subtraction of the ideal array field from the defective array field yields the field of the equivalent substitute element in the array. A method to extract a defective element location in an array can be performed by the "subtraction method" using the following procedure :

- Measure the amplitude and phase in the far field of the defective array pattern in discrete steps of $\sin\theta_i$:

$$Y_i = Y(\sin\theta_i) , \qquad i=1,2,....M ,$$

where M is the number of samples and Y is complex.

- The corresponding values for the ideal array would be :

$$X_i = X(\sin\theta_i) , \qquad i=1,2,....M.$$

- Subtract, giving :

$$Z_i = Y_i - X_i , \qquad i=1,2,....M. \qquad (2.12)$$

These values will include the required information of the equivalent-substitute (defective) elements in the array and their location. This data will then contain the radiation field pattern of the substitute elements, sampled at M points in the angular range from θ_1 to θ_M. If a single element is missing in the array and the resulting phase ambiguity is resolved, two values Z_1 and Z_M are sufficient to give full identification of the defective element. For more than one missing element additional work will be required. The following example shows how the method is applied.

Example Given an N-element isotropic homogeneous linear array

where element number K is missing, the difference values Z_i will have the magnitudes ($|Z|$) and phases ($\xi_i = \text{Arg } Z_i$) given in Fig. 2.7. From equation (2.11)

$$\frac{2\pi d}{\lambda}\left[K-\left(\frac{N+1}{2}\right)\right] = \frac{\xi_M - \xi_1}{\sin\theta_M - \sin\theta_1} \qquad (2.13)$$

Hence the missing element number will be

$$K = \frac{\lambda}{2\pi d}\left[\frac{\xi_M - \xi_1}{\sin\theta_M - \sin\theta_1}\right] + \frac{N+1}{2} \qquad (2.14)$$

Equation (2.14) although simple, is a powerful tool which is effective for practically any array aperture illumination. As will be shown in chapters 3 and 4 this method can give good results even in cases which are subject to random phase-shift excitation errors and mutual coupling effects.

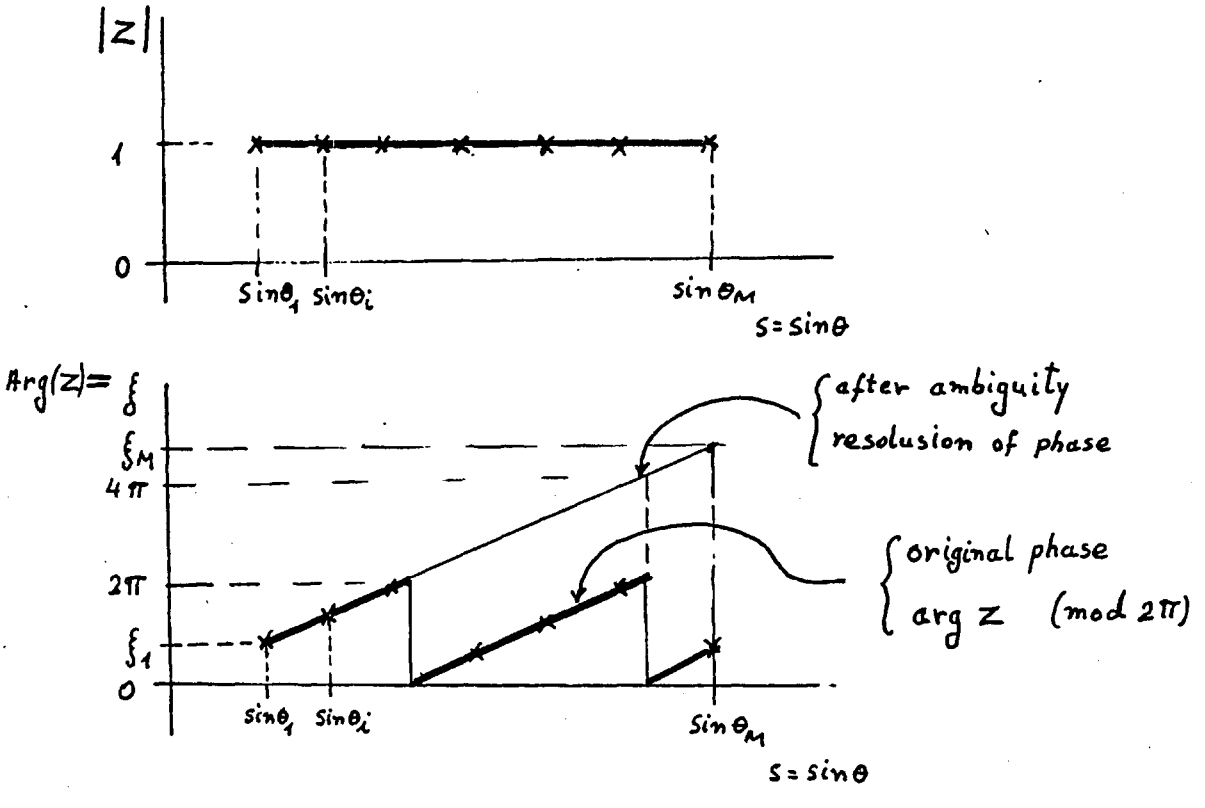


Fig. 2.8 Subtraction method, equivalent substitute element far-field values.

2.9 Identification of type of defect

The type of defect is identified from the values of the phase shift error $\Delta\phi$ and the magnitude ratio a (see Fig. 2.3),which can be derived as follows.

After finding the position of the defective element K, using equation (2.14), the same equation can be modified to find the phase shift δ between the ideal element and the substitute element. It can be seen from equation (2.5) that δ is given by,

$$\delta = \xi_i - [\, K - (\tfrac{N+1}{2}) \,] \sin\theta_i \qquad (2.15)$$

where ξ_i is the phase of Z_i in the direction θ_i .

For example if $\xi_i = \xi_M$ then $\sin\theta_i = \sin\theta_M$. The value b is given by $|Z|$. Inverting equations (2.4), the relative amplitude and phase of the defect are

$$\left.\begin{aligned} a &= (\, 1 + b^2 + 2b\cos\delta \,)^{1/2} \\ \Delta\phi &= \pi - \arcsin(\tfrac{b}{a}\sin\delta) \end{aligned}\right\} \qquad (2.16)$$

Hence a full description of the defective element, namely its location and type, are given by equations (2.14) and (2.16).

2.10 Some computer simulations

Simulation on the computer of two types of defective elements will now be given.

a) A missing element.

An N=99 element linear uniform isotropic array is assumed with $d=.61\lambda$ interelement spacing, where element K = 47 (-3d

distant from array centre) is missing. The far-field far side-lobe patterns (in db) of the ideal, the defective and the substitute array are plotted in Fig. 2.9. The phase-line of the substitute element is shown in fig. 2.10.

b) A phase defect

Element K = 56 (+6d from the array center) is then simulated to have a pure phase defect of $\Delta\phi = \pi/4$. The results are plotted in Figures 2.11 and 2.12, and are similiar to 2.9 and 2.10.

Figures 2.10 and 2.12 give the substitute element phase lines (Arg Z). It can be seen that the linear phase lines are of opposite signs, for defects located respectively to the left and to the right of the array phase center. Also the slope is doubled for doubling the spacing between the defective element and the array centre. Any region can be used, however the far side-lobe region enables the subtraction of magnitudes in the order of 1/N of the main-lobe region (see section 2.3). Hence the expected accuracy in the far side-lobe region will be greatly enhanced, in cases when measurement noise is present, by a factor of about N.

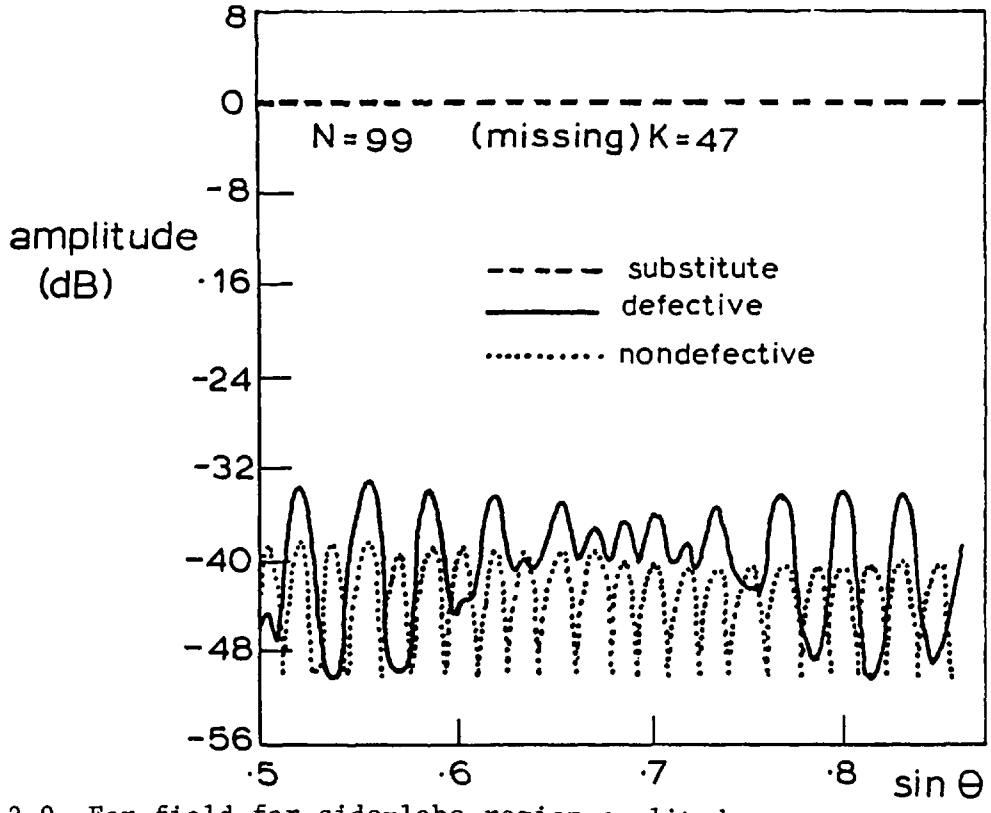


Fig.2.9 Far-field far side-lobe region amplitude patterns N=99 element array, missing element K=47.

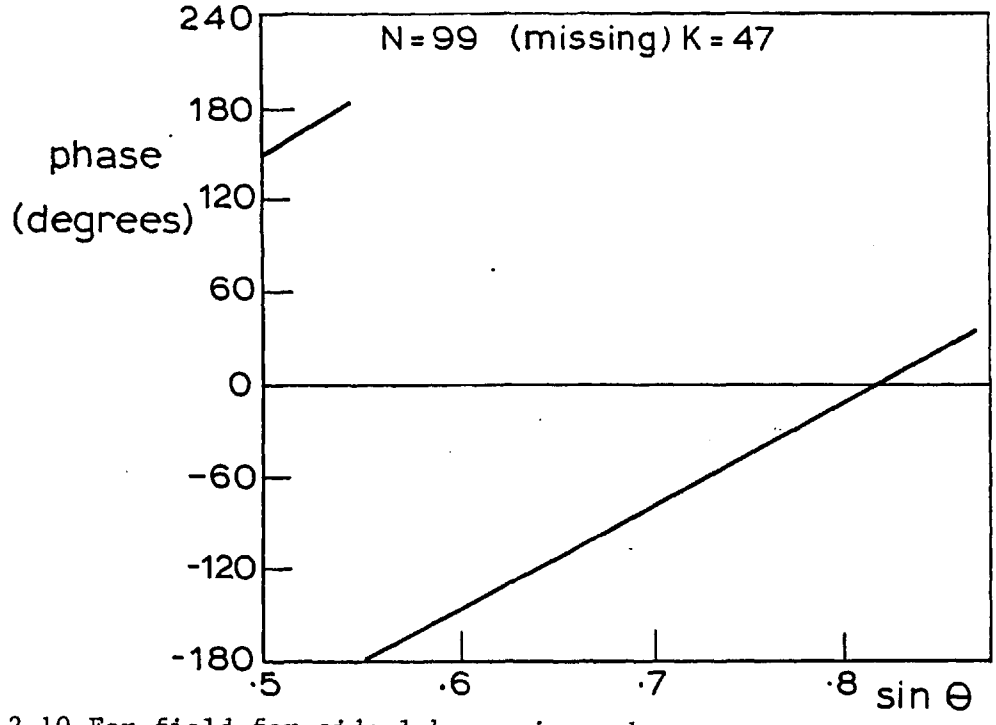


Fig.2.10 Far-field far side-lobe region, phase pattern of substitute element N=99, K=47.

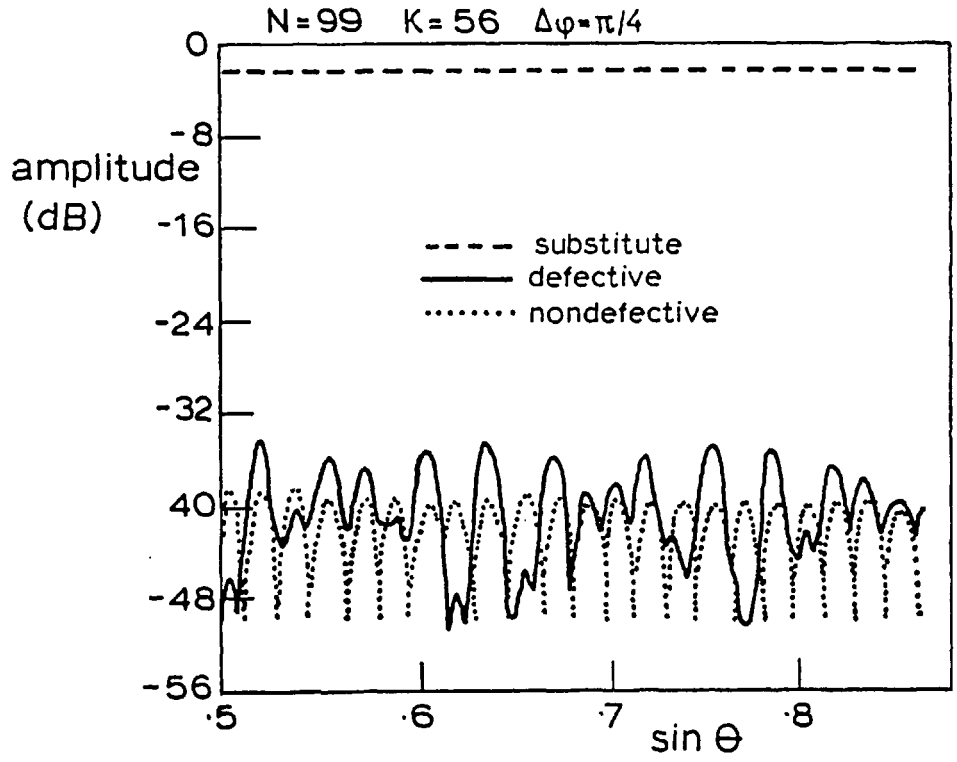


Fig.2.11 Far-field far side-lobe amplitude patterns
N=99 element array, $\pi/4$ phase defect in element K=56

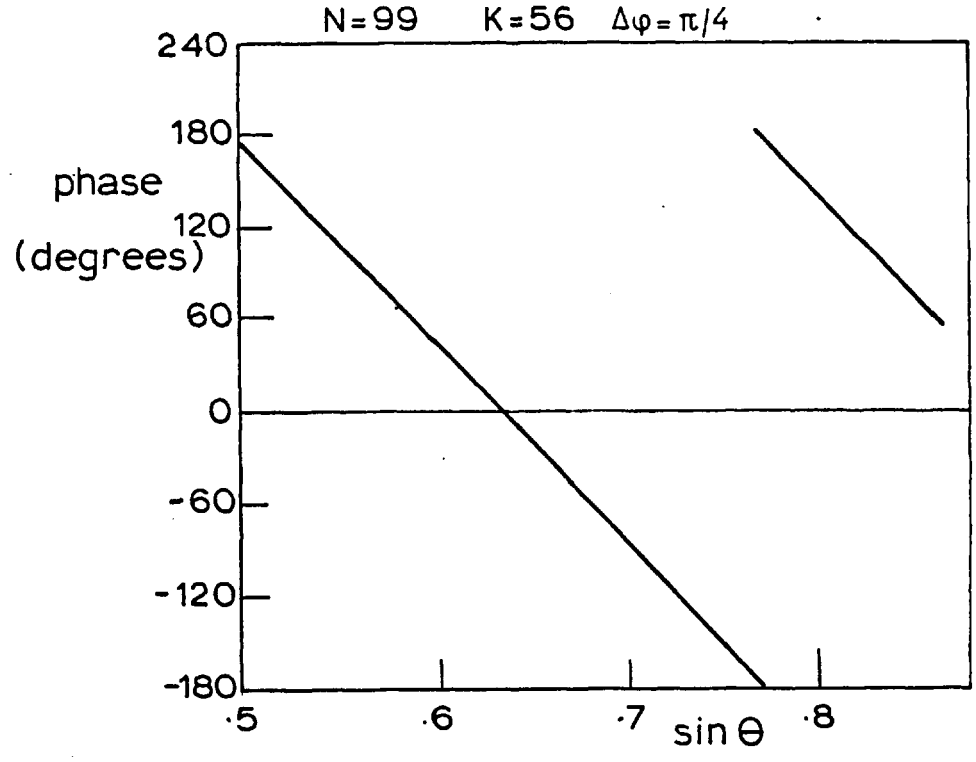


Fig.2.12 Far-field far side-lobe phase pattern of substitute array, N=99 element array, $\pi/4$ phase defect in K=56

2.11 Non necessity of measuring in the far field

In the case of a single defective element, or of a single defective sub-array, the subtraction method does not require the measurement to be performed in the far-field of the complete array. It is merely necessary to be in the far-field of the element or the sub-array (whichever is being sought), since the field due to the complete array is subtracted out.

2.12 Applicability of the subtraction method

The subtraction method gives simple results in cases when a single element of the array is defective.

Due to the expected high reliability of present and future solid state phased-arrays, it is very unlikely that more than one element will fail at any one time. Hence, if the reference pattern is updated, and previously found failures are memorized, this modified subtraction method can be used sequentially for the identification of a sequence of defective elements in the array.

In comparison to the near-field method suggested by Ransom and Mittra [2], based on inverse diffraction, the subtraction method uses simple equations and does not require Fourier transformations. Also, in the subtraction method it is preferable to use the far side-lobe region, hence avoiding obstruction of the array radiation, which is required using Ransom and Mittra's method. The subtraction method, in addition, enables the identification of the type of defect. No such claim is made by Ransom and Mittra.

2.13 Conclusions

The presentation so far has shown that the subtraction method is a simple but efficient tool for the detection of defective elements in antenna arrays. As the far side-lobe region gives the highest sensitivity to the presence of defective elements, it is recommended that this region be used for monitoring. Its importance lies in the additional fact that the monitoring technique does not obstruct the radiation.

The technique is not limited to the far-field region of the array ; only to the far field of the (equivalent) substitute element or substitute array.

The technique is so simple that in the case of defects in ideal arrays, two non-ambiguous measurements are sufficient to identify a single defective element.

However the high reliability of present and future phased array antennas enables one to use the modified subtraction method (explained earlier in section 2.12) in cases where there are many defective elements in the array. The assumption has to be made that no more than one element fails at a time.

The applicability of the method to more realistic arrays, including measurements in the presence of random phase excitation errors and mutual coupling effects, is considered in chapters 3 and 4.

CHAPTER 3

APPLICATION OF THE SUBSTITUTE ELEMENT TECHNIQUE

The analysis has so far dealt with static defects in ideal arrays. It is the purpose of this chapter to analyze more realistic models of arrays by the introduction of random phase excitation errors. The subtraction method will then be examined in the presence of these random excitation errors.

In the second part of this chapter defects of a dynamic nature will be analyzed where an unintetional stuck phase-shifter is introduced into the array. Two cases will be examined. The first is a stuck phase-shifter in a fully filled array, where each phase-shifter drives a single element of the antenna. The second case will be that of a thinned array where each phase-shifter drives a subarray of the array. The subarray beam is then further controlled by a beam switching network if a wider angle coverage than the subarray beam-width is required. The last case should be applicable to the Plessey MLS phased-array, where present design proposes to use switchable input ports to a Rotman lens.

3.1 Performance of an array of isotropic elements with random phase errors.

The far field pattern E(s) of a unity amplitude illuminated isotropic linear N-element phased-array antenna can be written in the form (see equation (2.1))

$$E(s)= \sum_{i=1}^{N} \exp\{ j k x_i s \} \exp\{j \phi_i \}. \qquad (3.1)$$

Where $x_i = id$, the displacement of the ith element from the array centre and $s=\sin\theta$. The random phase excitation errors ϕ_i

attributed to the ith element, are assumed to be statistically independent and uniformly distributed over the range $\varphi=\pm b$, as shown in Fig. 3.1.

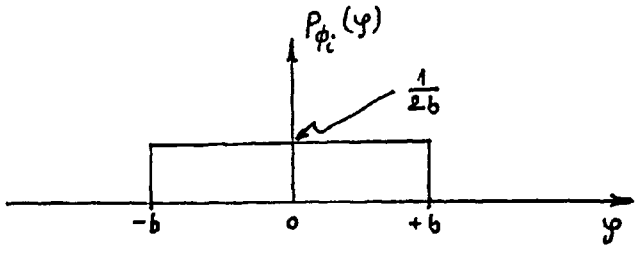


Fig. 3.1 Random phase of the ith element uniformly distributed.

The random phase will reduce the mean, or "coherent", far-field radiation pattern at the same time introducing a variance representing the fluctuating, or the "incoherent", radiated power [21]. The far-field pattern can therefore be regarded as composed of the sum of its coherent and incoherent components. These will now be described.

3.1.1 The mean far-field radiation

The mean far field will be given by the expectation of the ensemble of realizations as follows

$$\langle E(s)\rangle=\langle \exp\{j\,\phi_i\}\rangle \sum_{i=1}^{N} \exp\{jkx_i s\} \qquad (3.2)$$

where $\langle\ \rangle$ designates the expectation. For a uniformly distributed phase $\langle \exp\{j\,\phi_i\}\rangle$ is given by

$$\begin{aligned}\langle \exp\{j\,\phi_i\}\rangle &= \int_{-\infty}^{\infty} p_{\phi_i}(\varphi)\, \exp\{j\,\varphi\}\, d\varphi \\ &= \int_{-b}^{b} \frac{1}{2b} \exp\{j\,\varphi\}\, d\varphi \\ &= \operatorname{sinc} b \end{aligned} \qquad (3.3)$$

where sinc b = sin b /b.

The term $\sum_{i=1}^{N}\exp\{jkx_i s\}$ in equation (3.2) equals the N element array factor $A_N(s)$. Hence,

$$A_N(s) = \exp\{jkx_i s\} \tag{3.4}$$

$A_N(s)$ equals N for the direction of the main-lobe maximum, and approximates 1 in the far side lobe region. Hence the coherent far-field pattern is given by

$$\langle E(s)\rangle = A_N(s)\ \text{sinc}\ b \tag{3.5}$$

3.1.2 The variance of the far-field radiation

The variance of the incoherent radiated power, is

$$\text{Var}[\,E(s)] = \langle|E(s)|^2\rangle - |\langle E(s)\rangle|^2 \tag{3.6}$$

where

$$\langle|E(s)|^2\rangle = \langle E(s)\,E^*(s)\rangle$$

$$= \sum_i \sum_\ell \langle\exp\{j(\phi_i - \phi_\ell)\rangle\exp\{jks(x_i - x_\ell)\} \tag{3.7}$$

The complex conjugate of E(s) is designated by $E^*(s)$. The term $\exp\{j(\phi_i - \phi_\ell)\}$ can be divided into two parts : the first N terms for which i=1, and the remaining (N^2-N) for Which $i\neq 1$, Giving,

$$\langle|E(s)|^2\rangle = N + \langle\exp\{j(\phi_i - \phi_\ell)\rangle \sum_{i=1}^{N}\sum_{\ell=1}^{N}\exp\{jks(x_i - x_\ell)\} \tag{3.8}$$

where $\langle\exp\{j(\phi_i - \phi_\ell)\rangle$ is given by

$$\langle\exp\{j(\phi_i - \phi_\ell)\}\rangle = \left(\frac{1}{2b}\int_{-b}^{b}\exp\{j\varphi\}d\varphi\right)\left(\frac{1}{2b}\int_{-b}^{b}\exp\{-j\varphi\}\}d\varphi\right)$$

$$= \text{sinc}^2\, b \tag{3.9}$$

Since ϕ_i and ϕ_ℓ are assumed to be independent. Rearranging equation (3.8) will give (see also [21]) ;

$$\langle|E(s)|^2\rangle = N(1-\text{sinc}^2\, b) + \text{sinc}^2 b \sum_{i=1}^{N}\sum_{\ell=1}^{N}\exp\{jks(x_i - x_\ell)\} \tag{3.10}$$

where the double summation equals the array factor squared, namely,

$$\sum_{i=1}^{N}\sum_{\ell=1}^{N}\exp\{jks(x_i-x_\ell)=\sum_{i=1}^{N}\exp\{jksx_i\}\sum_{\ell=1}^{N}\exp\{-jksx_\ell\}$$
$$=|A_N(s)|^2 \qquad (3.11)$$

Therefore

$$\mathrm{Var}[E(s)]=N(1-\mathrm{sinc}^2 b) \qquad (3.12)$$

where Var[E(s)] is radiated isotropically (for an isotropic array).

3.1.3 The incoherent to coherent far field radiation power ratio

Two regions will be considered : the main-lobe and the far side-lobe regions. In the main lobe maximum (s=0 for broadside array)

$$|A_N(0)|^2 = N^2 \qquad (3.13)$$

In the far side lobe (s≈1 for broadside array)

$$|A_N(1)|^2 = 1 \qquad (3.14)$$

Hence the main-lobe incoherent to coherent ratio will be given by

$$\frac{Var[E(s)]}{|<E(0)>|^2}=\frac{1}{N}\,\frac{(1-\mathrm{sinc}^2 b)}{\mathrm{sinc}^2 b} \qquad (3.15)$$

The far side-lobe incoherent power ratio will be given by

$$\frac{Var[E(s)]}{|<E(1)>|^2}=N\,\frac{(1-\mathrm{sinc}^2 b)}{\mathrm{sinc}^2 b} \qquad (3.16)$$

The results of equations (3.15) and (3.16) for several values of b are given in Table 3.1 and described pictorially in Fig 3.2.

Table 3.1

Incohernt to coherent power ratios in main lobe and far side lobe, as a function of the phase error range b, for N=100 element array

phase error range: $\pm b$(rad)	Incoherent to coherent power ratios	
	Main-lobe (%)	Far sidelobe (db)
0 (no phase error)	0	$-\infty$
$\pi/16$	$1.3\ 10^{-2}$	1.1
$\pi/8$	$5.3\ 10^{-2}$	7.2
$\pi/4$	0.2	13.7

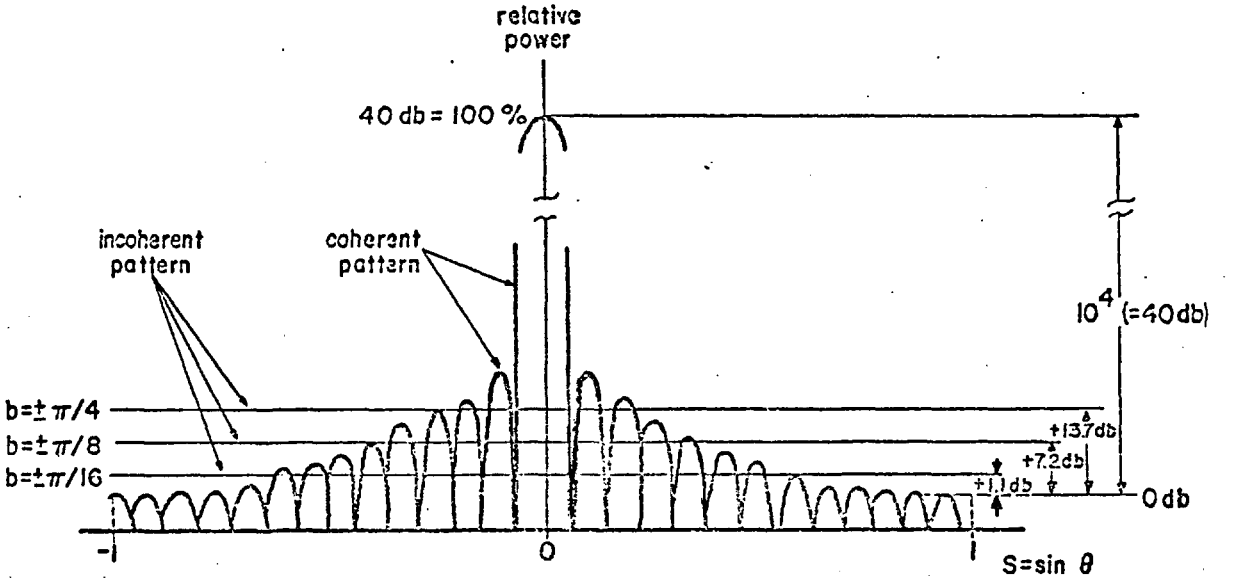


Fig. 3.2 Uniformly distributed phase-shift excitation errors in N=100 uniform array; incoherent and coherent patterns (qualitative)

A conclusion of this analysis is that a major effect of phase-shift errors is to mask and distort the side-lobe region of

the array pattern, threrby complicating the monitoring method considered previously.

3.2 Use of the proposed subtraction method in the presence of random phase-shift errors

In spite of the deterioration of the side lobes of the array in the presence of random phase excitation errors, the proposed subtraction method seems to be efficient for identifying a defective element in the array. Two cases will be discussed as representatives of the types of random-phase excitation: the "static" and the "dynamic" case (see also section 2.4).

3.2.1 The static case

Here the set of random phase fluctuations is fixed over the array elements and independent of the pointing angle of the array beam. This could be the case of a non-scanning linear array, or it could be a case where ideal phase shifters are used with non ideal radiation elements. The resulting Z_i values will now contain the information on the location of the defective element, derived from the phase slope-line according to equation (2.14). The phase slope would be a non-fluctuating line but will include an additional constant phase equivalent to the phase excitation error attributed to the defective element. The type of defect will not be known (unless the excitation error of the defective element is known) but the location of the defect can be identified with no error (see for example Fig. 3.3), since the slope is unchanged .

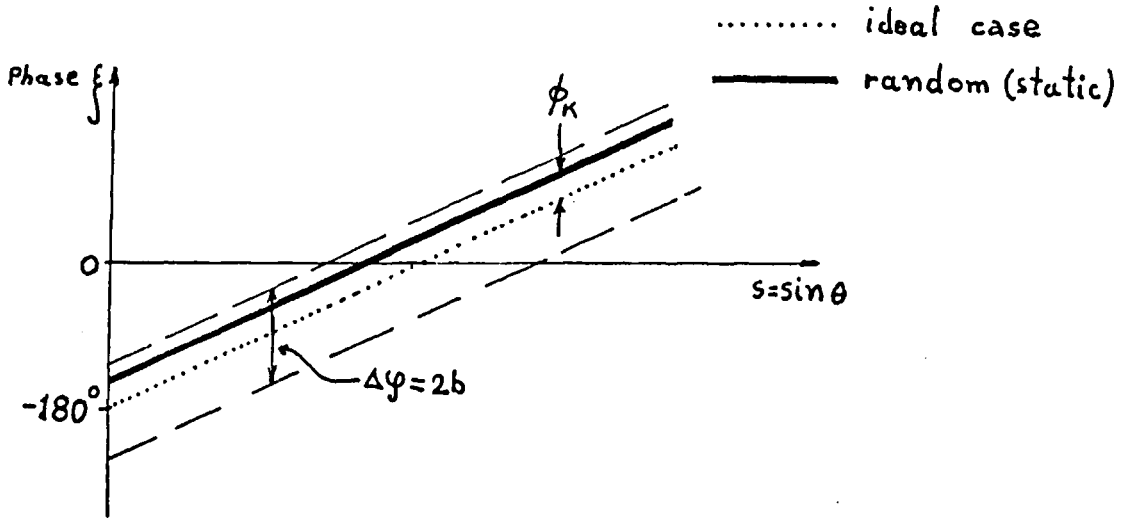


Fig. 3.3 Phase pattern, static case.

The phase slope-line for a missing element K, whose phase shift was ϕ_K, before it became defective, is parallel to that of the ideal array (with no phase excitation errors) and seperated from it by $\approx \phi_K$ (in section 3.3 it will be shown to be within $\pm b/N$ of ϕ_K). The range of ϕ_K will be limited by the phase distribution range of $\pm b$.

3.2.2 The dynamic case

The set of phase excitation errors attributed to the array elements will now be allowed to change with every monitored direction angle of the array. This could be the case of a scanning phased-array, where all the phase shifters are changing for each angle increment introducing different sets of random phase-errors in all the elements. The difference values Z_i will result in a fluctuating phase around the ideal phase slope line. The range of these fluctuations will be $\pm b$, as shown schematically in Fig. 3.4. In this case a statistical estimation of the regression line will be required. The regression error will depend on b and on the number of statistically independent

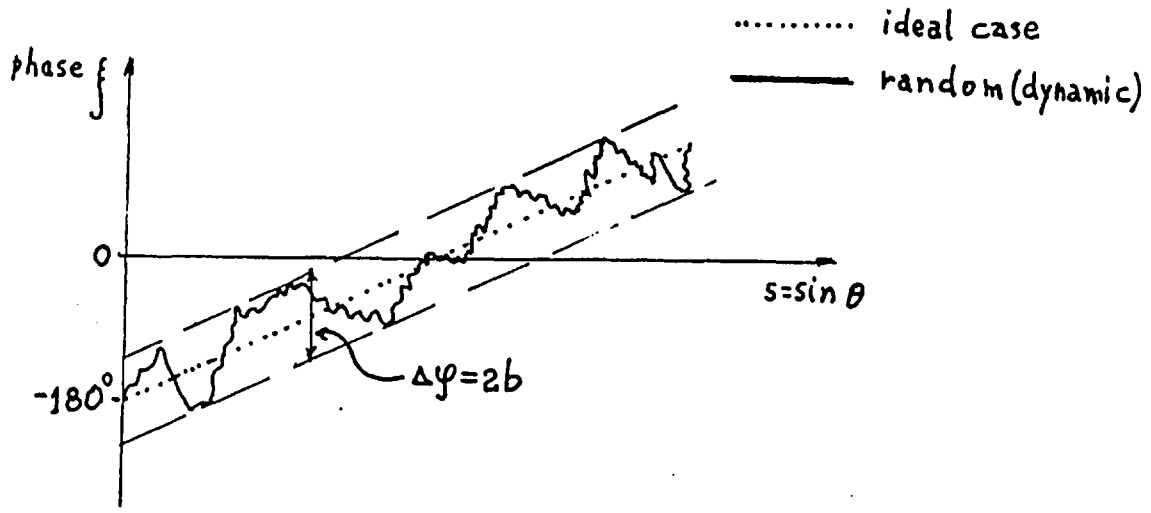


Fig. 3.4 Phase pattern, dynamic case.

samples used for the estimation. Consequently, the linear phase variation used for the identification of a defective element in the array (using the subtraction method), is found to be a very efficient tool even in the presence of random phase excitation errors.

3.3 Array centre reference phase for defective and non-defective arrays

A phase reference is required for the proposed monitoring system. Reception of the main beam by the monitoring system is one way of supplying the phase reference without a physical connection between the phased-array system and the monitoring system. The difference in phase between the main beam of an ideal array (with no random phase errors) and that of an actual array (with random phase errors) is very small, being of the order of a fraction of a degree for large arrays. This is due to the assumption of a zero mean for the phase-error distribution. Provided b is small, the error will be of the order of b/N(see Appendix b). So for $b=\pi/4$ and N=100 the error is less than a

degree. The same applies to the phase difference between the actual array before and after a defect in a single element has happened. It also applies to the extent of the shift in phase-slope fluctuations in the "dynamic" and "static" cases already discussed in 3.2.

Consequently, the main beam received by the monitoring antenna could supply the reference phase, provided a suitable technique for memorizing this phase is available.

3.4 Computer simulation of defects in presence of random phase excitation error.

Simulation on the computer of arrays with the two types of excitation errors will now be given.

a) A missing element in the presence of dynamic phase excitation errors.

The same parameters as in 2.10 example a will be used. In addition a non-reset pseudo-random number generator will produce dynamic phase errors in the range $b=\pm\pi/8$.

The far field patterns (in db) of the non-defective, the defective and the substitute array are shown in Fig. 3.5. The phase line is given in Fig 3.6.

b) A missing element in the presence of static phase errors.

The same parameters as above will be chosen but here a reset random number generator will produce static phase errors in the range $b=\pm\pi/8$. The results are shown in Figures 3.7 and 3.8, which are similiar to Figures 3.5 and 3.6.

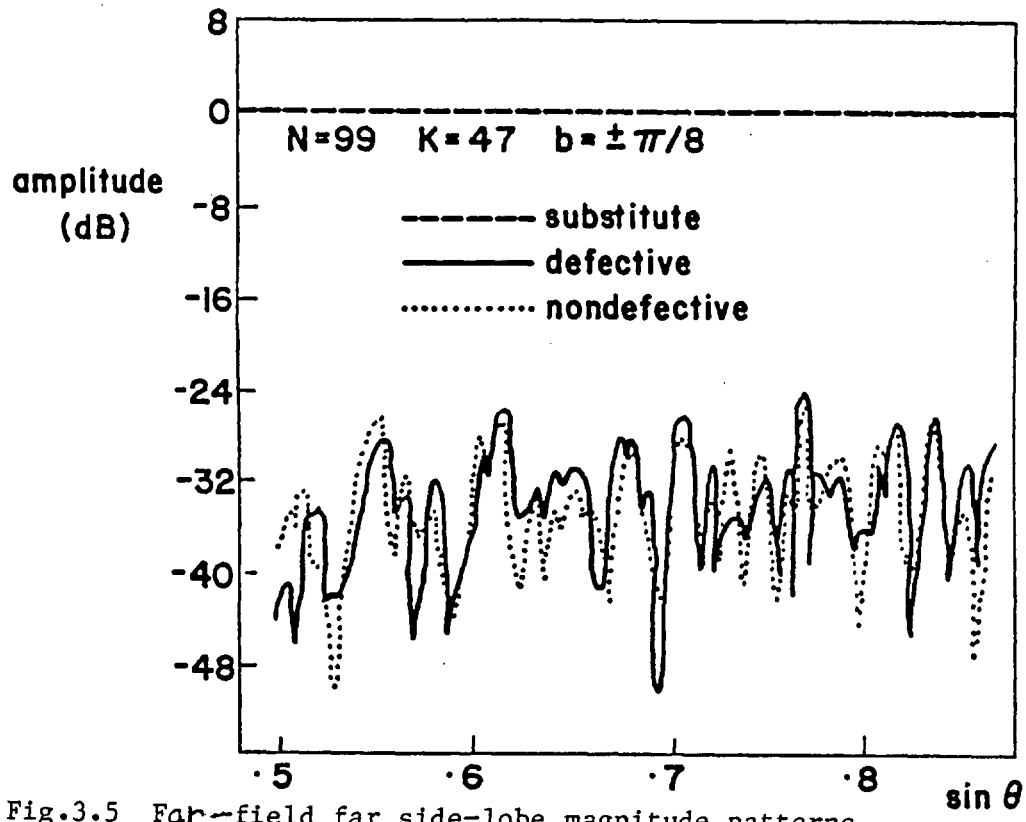


Fig.3.5 Far-field far side-lobe magnitude patterns in presence of random phase excitation (dynamic case)

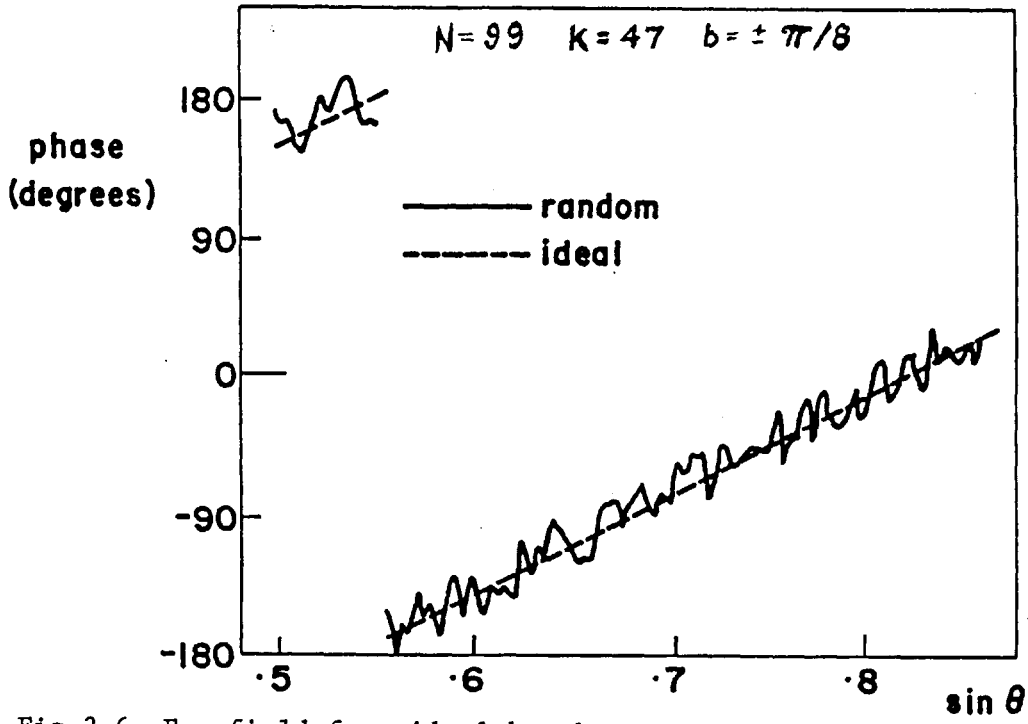


Fig.3.6 Far-field far side-lobe phase pattern of substitute element in presence of random phase (dynamic case)

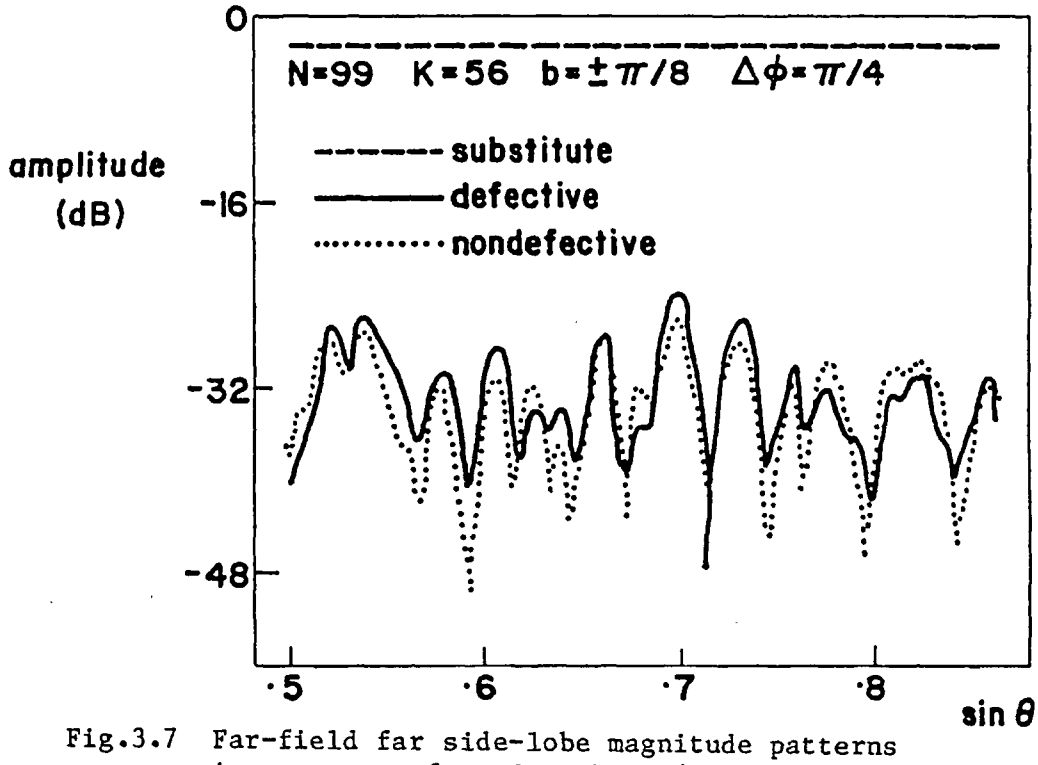


Fig.3.7 Far-field far side-lobe magnitude patterns in presence of random phase (static case)

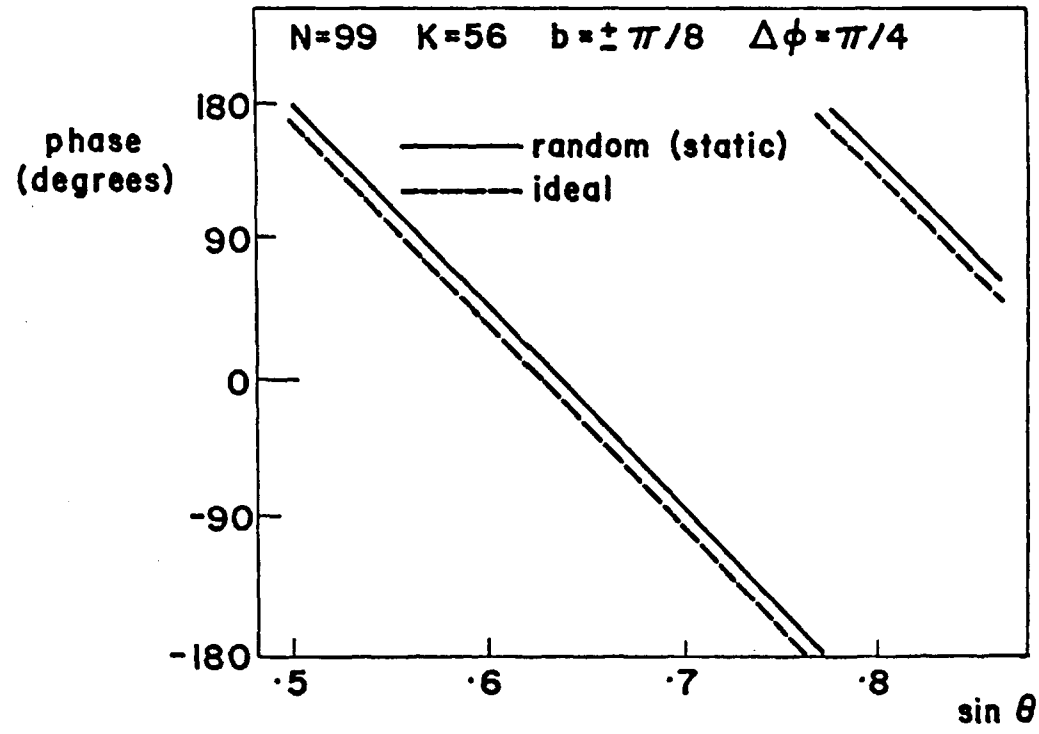


Fig.3.8 Far-field far side-lobe phase pattern of substitute element in presence of random phase (static case)

Figures 3.6 and 3.8 give the substitute-element phase lines. It can be seen that, as expected from section(3.2.2) the phase line in Fig. 3.6 fluctuates around the correct mean slope line (dashed line) which is reproduced from Fig. 2.10. Using equation (2.14) the "missing" element location can be deduced very precisely (to be within ~ 10% of the element spacing). In Fig. 3.8, however, the phase line gives no variation around the mean slope-line but a parallel line to it as described in section (3.2.1).

These promissing, and quite stable, results have been examined in circumstances where the good and defective arrays both exhibit apparently indistinguishable erratic behaviour in their far fields (see Figs. 3.5 and 3.7; also compare with Fig. 2.9). The results demonstrate that the method can be used with phased arrays in the presence of the quantized phase-shift errors.

This concludes the first part of the chapter dealing with application of the subtraction method in presence of random phase excitation errors.

Next a dynamic defect of a stuck phase shifter will be discussed.

3.5 Inadvertently latched (stuck) phase-shifter feeding a single element.

Having analyzed defects of a static nature in the presence of static and dynamic phase-excitation errors, it is now intended to deal with the important practical case of a stuck phase shifter. As explained previously this type of defect is of a dynamic nature since the relative phase shift between the required and the available excitation phasor changes dynamically

with the beam scanning. In the present section the effect of a stuck phase shifter feeding a single element of the array will be discussed. This is followed in section 3.6 by an investigation of a stuck phase-shifter feeding a sub-array of the antenna.

3.5.1 The equivalent substitute element of a stuck phase-shifter feeding a single element.

It has been shown (section 2.5) that the equivalent substitute element of a defect with constant amplitude and phase in a single element is given by

$$b\exp\{j\tilde{\delta}\}=[\ a\exp\{j\Delta\phi\}-1\ ]\exp\{j\phi_0\} \tag{3.17}$$

Designating $\phi_2=\tilde{\delta}$ and $\phi_1=\Delta\phi+\phi_0$ where

$$\phi_0=\frac{2\pi}{\lambda}d\sin\theta \tag{3.17a}$$

we could write the following

$$b\exp\{j\phi_2\}=a\exp\{j\phi_1\}-1\cdot\exp\{j\phi_0\}. \tag{3.18}$$

Now, ϕ_1 is constant for a stuck phase shifter while ϕ_0 changes as a function of the scan angle θ (equation 3.18 above). Therefore b and ϕ_2 will also change with the scan angle. The previous case of a missing element could be represented as a special case of a stuck phase-shifter feeding a missing element, where a=0 , resulting in b=-1 and $\phi_2=\phi_0$, as before. For $a\neq 0$ and a stuck phase-shifter three cases will be discussed corresponding to the different value of a; namely, a=1, a<1 and a>1. The phasor representation for all three cases is given in Fig. 3.9.

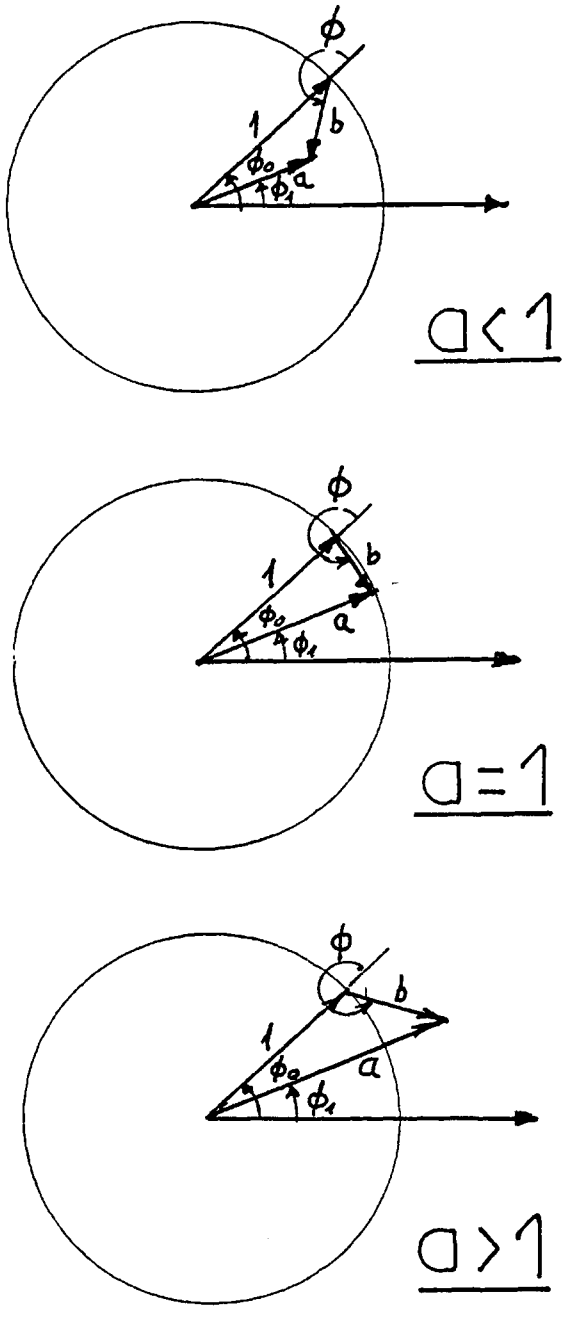


Fig. 3.9 A phasor representation for three cases of a stuck phase-shifter feeding a single element

The resulting amplitude and phase patterns are shown in Fig. 3.10 in comparison with the missing-element case.

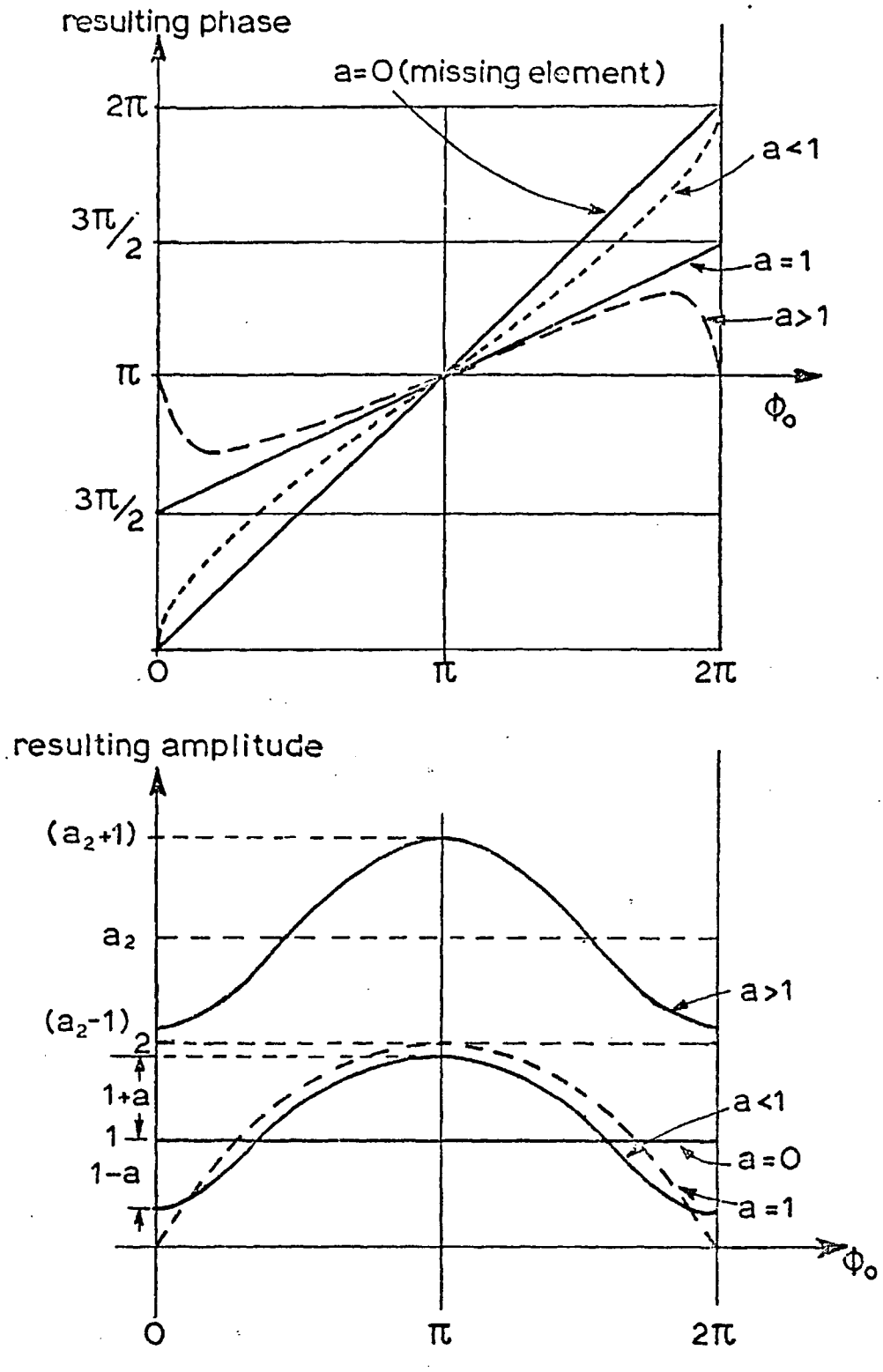


Fig. 3.10 Resultant amplitude and phase of the equivalent substitute element for $a \lessgtr 1$ and $\phi_1 = 0$.

It is to be noticed that if $\phi_1 \neq 0$ then the only additional effect will be a shift in the location of the zero crossing of the phase and in the accompanying amplitude maxima and minima.

3.5.2 A modification in the subtraction method for a stuck phase-shifter.

From Fig. 3.10 it is still possible, although with somewhat greater difficulty, to decide on the type of defect and its location, using a modification of the subtraction method formula (equation 2.14). One possibility is to measure the periodicity of the phase curve, thus a modified formula like the following one can be used.

$$K = \pm \frac{\lambda}{2\pi d} \frac{2\pi}{\Delta s} - \frac{N+1}{2} \qquad (3.19)$$

The sign is that of the phase slope, Δs is the direction-cosine difference for one period (cycle) of the phase variation. However, when a=1 a linear phase variation results, but with half the slope. Hence, use could be made of equation (2.14), but doubling the values of the calculated phase difference between the two samples measured at $\sin \theta_1$ and $\sin \theta_M$. The modified equation will then be in the form of

$$K = \frac{\lambda}{\pi d}\left[\frac{\xi_M - \xi_1}{\sin\theta_M - \sin\theta_1} \right] + \frac{N+1}{2} \qquad (3.19a)$$

Therefore equation (3.19) or (3.19a) can be used to derive the location of the (defective) stuck phase shifter.

3.6 The equivalent substitute array of a stuck phase-shifter feeding a single subarray

The main difference between the resulting equivalent substitute element and the equivalent substitute subarray for a stuck phase shifter, is in the amplitude and phase dependence of the subarray factor to that of a single element. A modification of equation (3.18) will be used as follows

$$b \exp\{j\phi_2\} = a \exp\{j\phi_1 - A \exp\{j\phi_o\} \tag{3.18a}$$

with the following different meaning of the factors a and b. The factor a is the normalized defective subarray factor, and b is the resulting normalized equivalent substitute (sub) array factor. The ideal M element subarray factor A is given by,

$$A = \frac{\sin[kMd(s-s_o)/2]}{\sin[kd(s-s_o)/2]} \tag{3.20}$$

where $s_o = \sin\theta_o$, is the direction cosine of the monitoring antenna to the array broadside direction. The normalized defective subarray factor a in the case of a stuck phase-shifter, is given by

$$a = \frac{\sin[(kMds_o - \phi_1)/2]}{\sin[(kds_o - \phi_1)/2]} \tag{3.21}$$

where ϕ_1, as before, is the phase of the stuck phase-shifter. While A changes with the scan angle, the factor b is fixed for a given value of ϕ_1 and of the direction-cosine s_o (if no beam switching is used).

Example A stuck phase shifter feeding an M element subarray, the case of $s_o=0$, $\phi_1=0$

The factor a behaves differently in the main-lobe region and in

the far side-lobe region. In the main-lobe region, A and a tend to the same amplitude value of M hence the result will be similiar to the case of a stuck phase-shifter feeding a single element for a=1 (see Fig. 3.10). In the far side-lobe region, $|A| \lesssim 1$, while $|a| \cong M$ (which is assumed >>1), hence the appropriate case of a>>1 will apply (see Fig. 3.10).

The resulting phase of the equivalent substitute array will be sketched in Fig. 3.11,

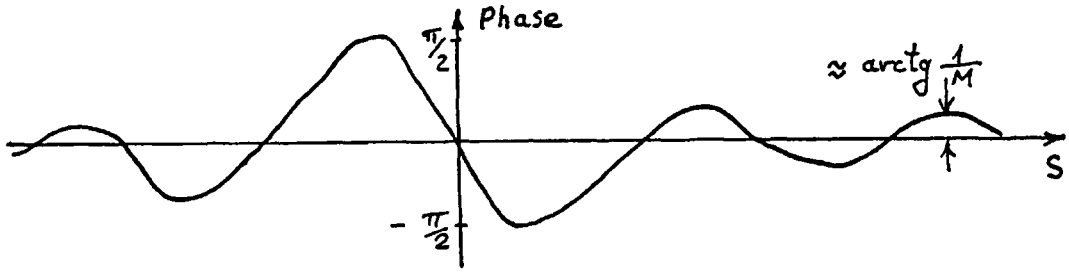


Fig. 3.11 Phase pattern, stuck phase shifter feeding subarray (qualitative)

It should be noticed that the resulting mean phase in the far side-lobe region gives the value of the phase at which the defective phase-shifter was stuck (for $s_0=0$). This result could be used as part of the defect detection algorithm. However the location of the defective sub array is best decided from the main-beam region with a correction equivalent to that of a single element stuck phase-shifter in the case of a=1 (see equation 3.19a). It should be noted that the assumption in the above discussion was of perfect phase-shifters connected to each element of the array, but stuck phase-shifters of equal value of phase ϕ_1 were assigned to the defective subarray elements.

An additional more complex case where a stuck phase shifter is feeding a beam switched sub-array will be investigated next.

3.7 A stuck phase-shifter feeding an M element subarray with a switched beam-forming network (B.F.N.)

This case applies to a real phased-array such as the MLS phased-array using switched Rotman lenses [8,22].

If both the switch and the phase-shifter are stuck the anslysis given in subsection 3.6 will apply. But if the switch is functioning properly and only the phase-shifter is stuck, then, depending on the location of the monitoring antenna, a case similiar to a=1, a<1 or a>1 of a single element stuck phase shifter will be appropriate for the resulting phase. However the resultant b can be approximated by a stair case amplitude with angle, due to the sampling of the subarray factor (see Fig. 3.12).

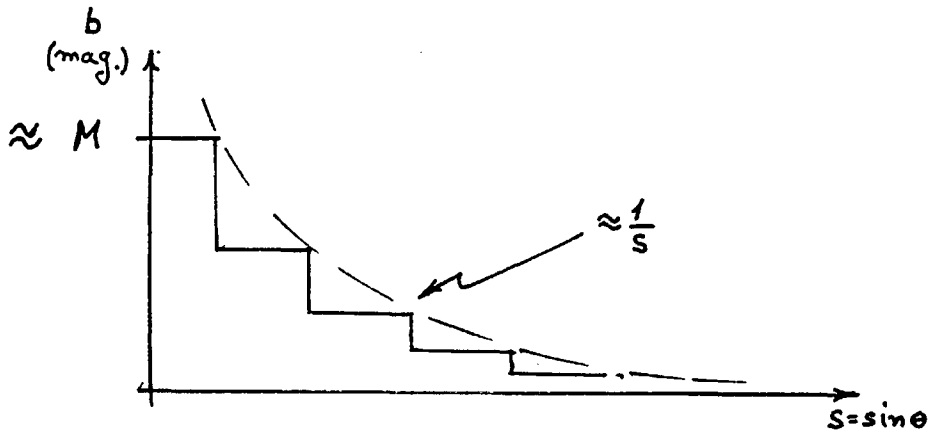


Fig. 3.12 Sketch of the amplitude pattern of a stuck phase-shifter and a good switching B.F.N.

Simulation on the computer for several cases of stuck phase-shifters will be given next.

3.8 Simulation of stuck phase shifters in ideal arrays

Several examples of defects will be simulated.

An N=100 element array is assumed in the following five examples.

a) A single element defective in amplitude, stuck phase-shifter with the following parameters.

K=44 (i.e., defective element number 44).

a=0.8 (i.e., a<1 amplitude defect).

pl=0 (i.e., phase shifter stuck to 0 phase value).

the far field patterns are shown in Fig. 3.13a and the resulting phase line in Fig. 3.13b. The same notation as in previous simulations is used for the patterns and their phase variations.

b) Single element with a larger amplitude defect with stuck phase-shifter.

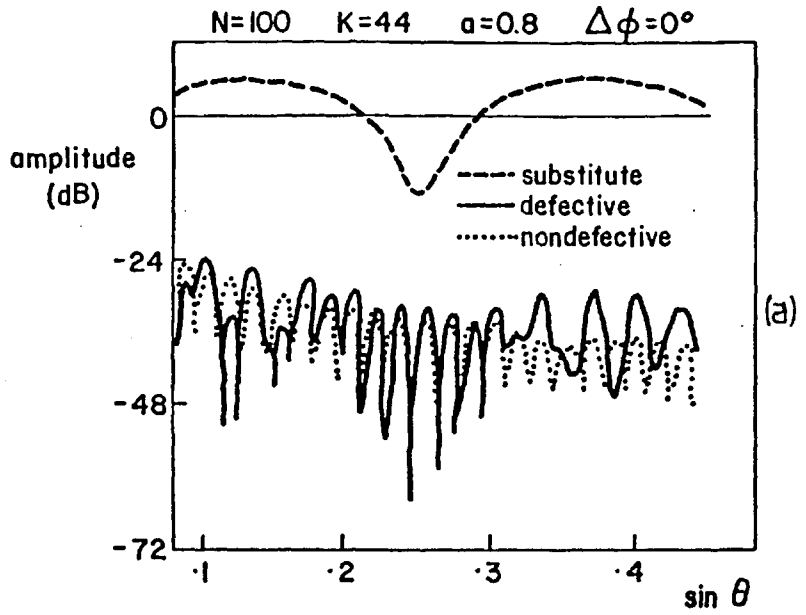
K=44 , a=1.2 (i.e. a>1) and pl=0.

The far field patterns are shown in the side lobe region in Fig. 3.14a. The resulting phase-line is shown in Fig.3.14b.

c) Single element defective in phase, stuck phase-shifter with the following parametrs.

K=35 , a=1 (i.e., no amplitude defect) and pl=0.

The far-field patterns are given in Fig. 3.15a. The resulting phase-line is given in Fig. 3.15b.



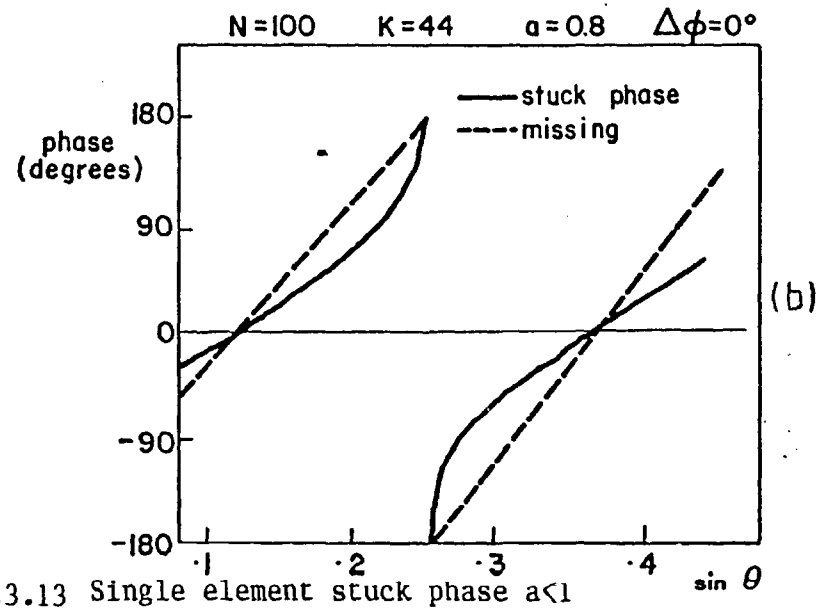
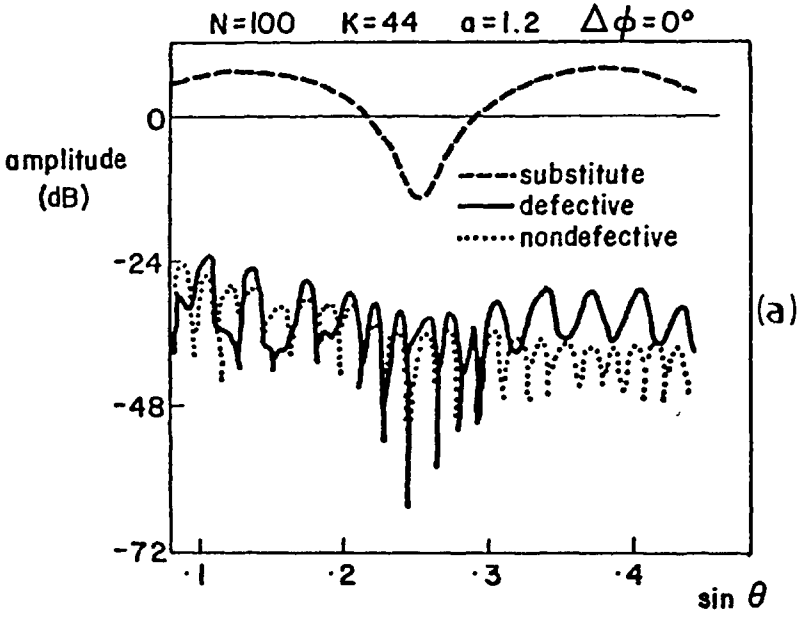


Fig.3.13 Single element stuck phase a<1 patterns a) Magnitude b) Phase



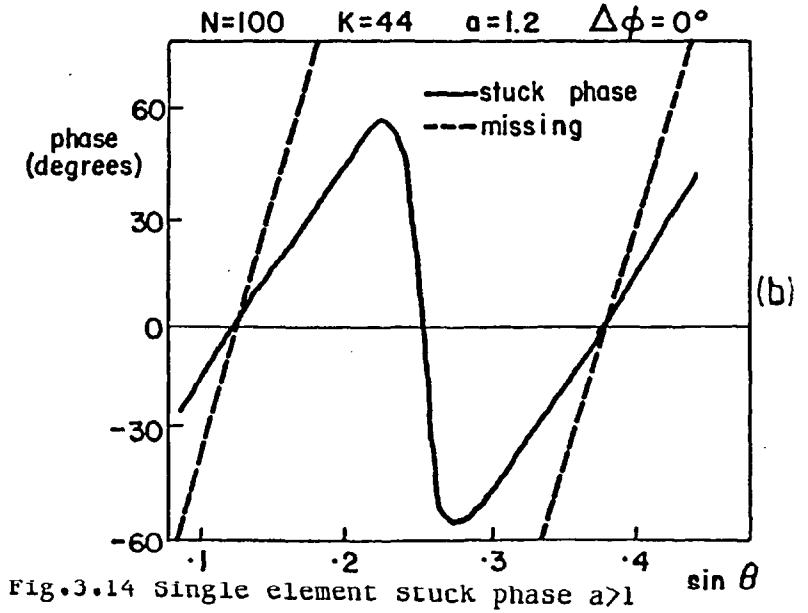


Fig.3.14 Single element stuck phase a>1 patterns a) Magnitude b) Phase

d) A stuck phase-shifter feeding a sub-array (no beam switching).

The parameters are as follows

NSUB=10, i.e., a ten element subarray.

K1=40, i.e., first element of the subarray is No 40.

a=0.8

p1=0

In Fig. 3.16 three phase lines are shown on the same graph. The solid line shows the resulting phase-line of the subarray, the dotted shows the slope-line that would have occured if the center element of the sub array was simply missing (k=44.5), and the dashed describes a slope line that would have been measured if a stuck phase-shifter feeding the center element of the sub array had an amplitude defect, a<1. It should be noted that $s_o=0$ and for this case the asymptote of the resulting sub array phase-line (solid) equals the stuck phase value P1=0.

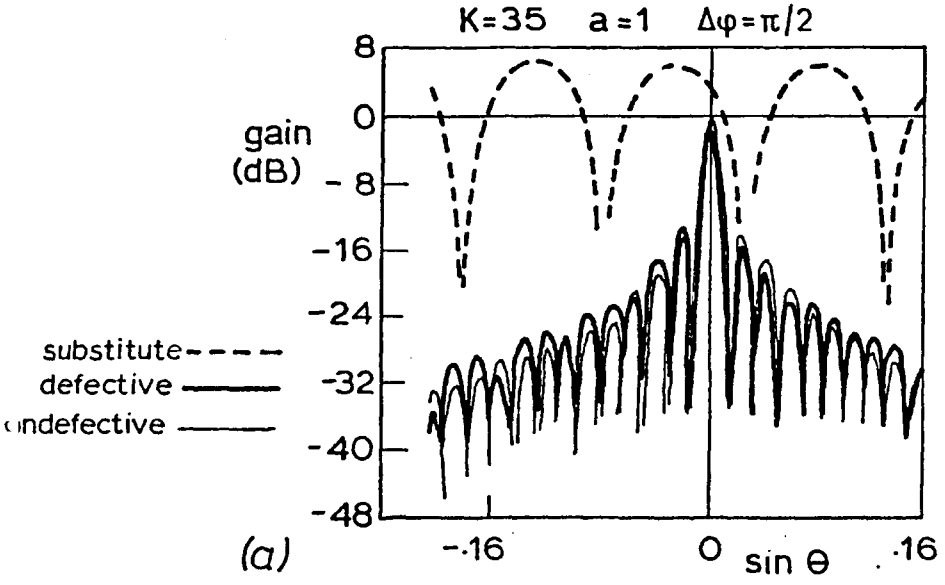
e) A stuck phase-shifter feeding a subarray (no beam switching).

The same parameters as in (d) but with

a=1 and p1= $\pi/2$

The scan direction cosine variation includes the main beam as well as the side-lobe regions (see Fig. 3.17). The same designation for the curves as in Fig. 3.16 are used for Fig. 3.17.

It should be noticed that in the main beam region the resulting sub-array phase line coincides with the single element stuck phase-shifter phase line (dashed), as expected. In addition, as exlained previously, the asymptotic value of the resulting phase-line of the sub-array tends to the p1= $\pi/2$ value.



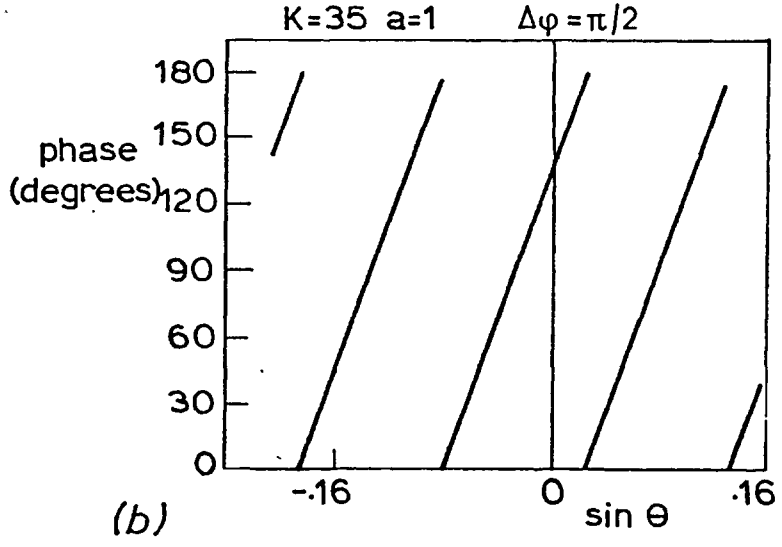


Fig.3.15 Single element stuck phase a=1 patterns a) Magnitude b) Phase

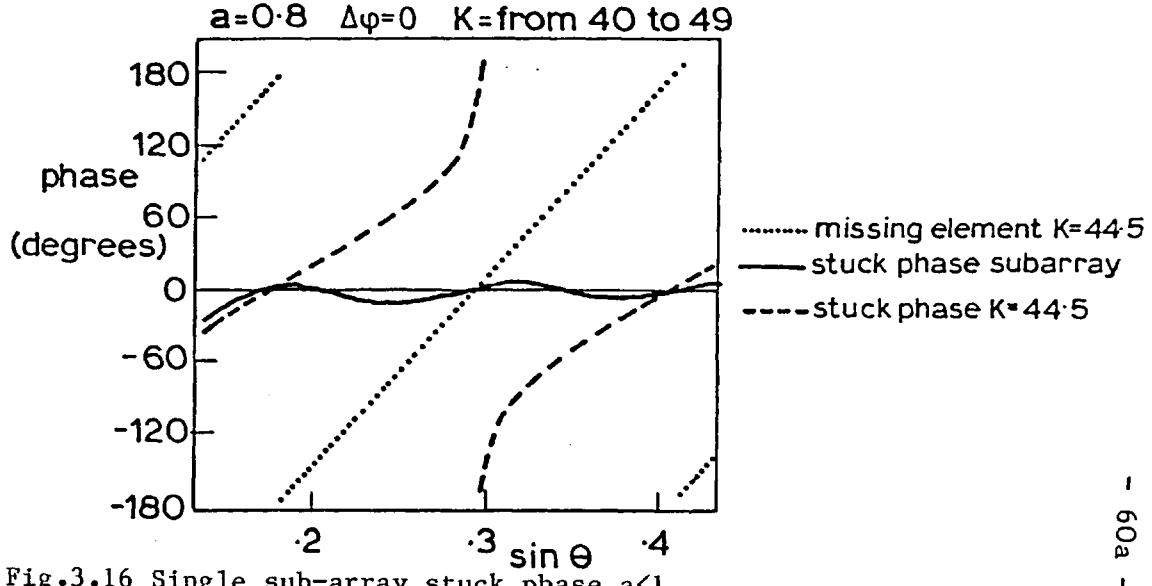


Fig.3.16 Single sub-array stuck phase a<1 phase patterns.

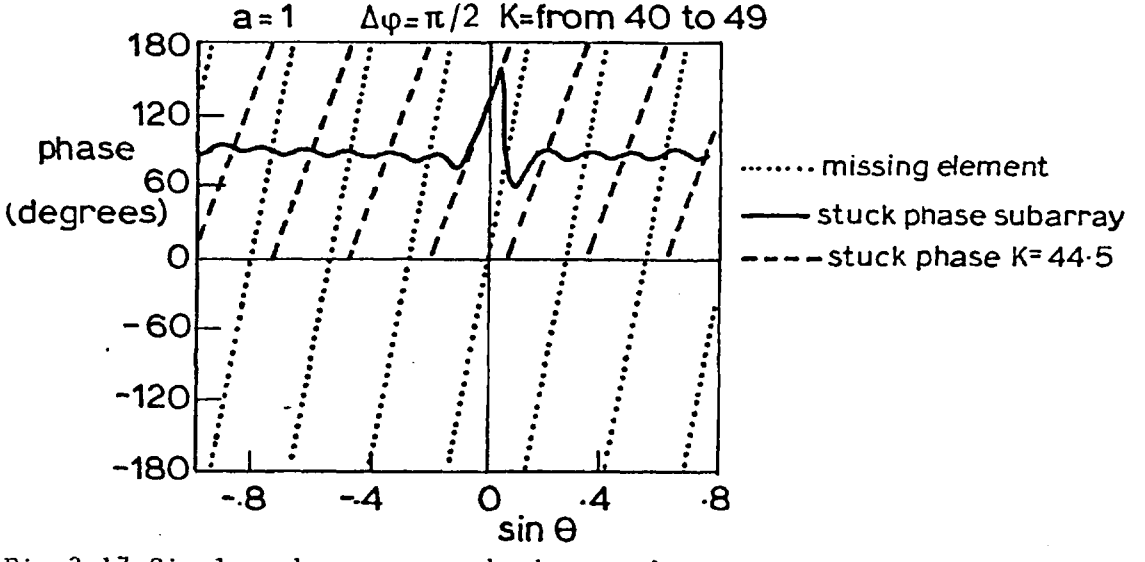


Fig.3.17 Single sub-array stuck phase a=1 phase patterns.

Summarizing these simulation results, it can be said that the modified formula for the subtraction method can be used in the main-lobe region (equations 3.19 and 3.19a) for a stuck phase shifter feeding a single element or a single subarray. Also the value of the stuck phase-shifter can be found in the case of an unswitchable beam forming sub-array. The phase line asymptote in the far side-lobe region points out the value of the stuck phase if only the monitoring antenna is placed in direction cosine $s_o=0$(the broadside direction).

3.9 Discussion

The substitute element technique has been shown to be a very useful tool for analyzing defects of a dynamic nature as well as defects of static nature.

The subtraction method has been found to be an efficient monitoring method for realistic models of antennas in the presence of random-phase excitation errors.

A modification to the subtraction method has been suggested for several cases, of stuck phase-shifters, using analysis and simulation on the computer.

A further important aspect of realistic modelling of phased-array antennas will be investigated in chapter 4, where mutual coupling effects will be considered.

CHAPTER 4

MUTUAL COUPLING EFFECTS

In the previous chapter a more realistic model of antenna arrays has been sought, by the introduction of defects in the presence of random excitation errors. The present chapter will lead to a further more realistic antenna model by the inclusion of coupling effects (in an actual array), and will examine their influence on the performance of the monitoring method suggested. Coupling effects could, broadly, be divided into two categories, the first which is dependent on the separation between elements and the second which is independent of the separation. The mutual coupling effect is due to the proximity of the elements and, hence, is dependent on the separation. Power reflected from an element affecting other elements of the antenna, through the antenna feed network, is independent of the distance. The last statement is made assuming a lossless feed network (this independence ignores periodic changes of coupling along the feed network). As the ultimate interest is to judge the major effects of coupling, with a minimum disturbance of unimportant details, simplified cases will be demonstrated based on known formulas [9,10,11]. A simplified model of an "actual" array available in the laboratory [23] will be simulated on the computer . In a later part of this thesis (chapter 7), results of the present chapter will be compared to those of the experimental investigation.

The next section will deal with the effect of mutual coupling.

4.1 Mutual coupling effects between array elements

One convenient way to describe the effects of mutual coupling, is through the impedance matrix network representation

$$V = Z\ I \tag{4.1}$$

or in its general form given below

$$\begin{vmatrix} V_1 \\ V_2 \\ \cdot \\ V_i \\ \cdot \\ \cdot \\ V_N \end{vmatrix} = \begin{vmatrix} Z_{11} & Z_{12} & \cdot & \cdot & \cdot & Z_{1N} \\ Z_{21} & Z_{22} & \cdot & \cdot & \cdot & \cdot \\ \cdot & \cdot & \cdot & \cdot & \cdot & \cdot \\ \cdot & \cdot & \cdot & Z_{ii} & \cdot & \cdot \\ \cdot & \cdot & \cdot & \cdot & \cdot & \cdot \\ \cdot & \cdot & \cdot & \cdot & \cdot & \cdot \\ Z_{N1} & \cdot & \cdot & \cdot & \cdot & Z_{NN} \end{vmatrix} \begin{vmatrix} I_1 \\ I_2 \\ \cdot \\ \cdot \\ I_j \\ \cdot \\ I_N \end{vmatrix} \tag{4.2}$$

Here, V_i are the impressed voltages, and I_j are the resulting currents. The latter are functions of Z_{ii} the self impedances, and Z_{ij} $(i \neq j)$ the mutual impedances. For reciprocal networks $Z_{ij} = Z_{ji}$.

In the ideal arrays described previously no mutual coupling was present, hence $Z_{ij} = 0$ for $i \neq j$. There, the only impedances present were Z_{ii}, giving

$$\begin{aligned} V_1 &= Z_{11} I_1 \\ V_2 &= Z_{22} I_2 \\ \cdot &= \cdot \quad \cdot \\ \cdot &= \cdot \quad \cdot \\ V_N &= Z_{NN} I_N \end{aligned} \tag{4.3}$$

Hence, any defects in one or more of the elements did not interact with other elements. But in actual antennas mutual coupling effects will be present, and hence array elements are affecting and are influenced by other elements. For simple element configurations such as that of the broadside dipole array, formulas for the mutual impedance have been developed by Carter [9] and have been used by Kraus[10] and Oliner and Malech [11].

In the following section a simple case of mutual coupling will be described for a two element $\lambda/2$ broadside array, using these coupling formulas.

4.2 Mutual coupling effects in a two element array

One of the simplest cases of mutual coupling, occurs in a two element $\lambda/2$ broadside array. It is, therefore, best to summarize some known results on this model befor getting to a more complex case of a multi-element array.

The impedance matrix representation for a two element array, from equation (4.2), is given by

$$V_1 = Z_{11} I_1 + Z_{12} I_2$$
$$V_2 = Z_{12} I_1 + Z_{22} I_2 \qquad (4.4)$$

The geometry is described in Fig. 4.1.

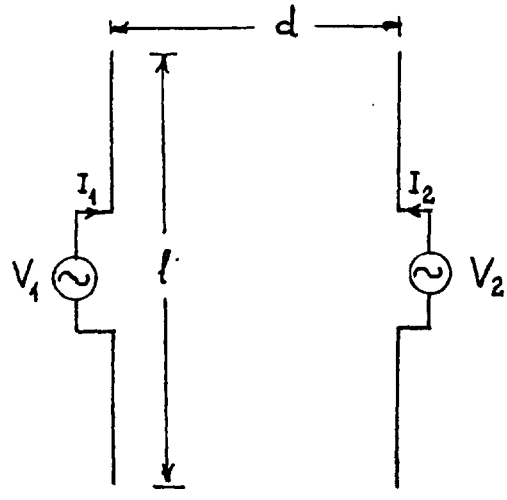


Fig. 4.1 Two element $\lambda/2$ dipole array geometry

The equivalent network description of (4.4) is given [11] in Fig. 4.2

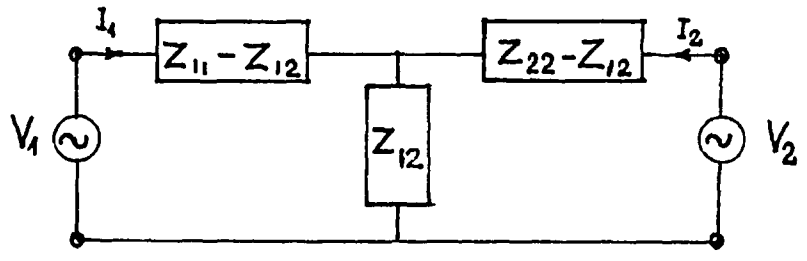


Fig. 4.2 Equivalent network description of mutual coupling in a 2 element array

For a case where both antennas are symmetrical $Z_{11}=Z_{22}$. The effect of mutual coupling will then depend on the input impedances of the dipoles and hence on the resulting currents. However, the current ratio I_1/I_2 will remain unchanged and therefore the normalized radiation patterns will be the same as those of the ideal array (i.e., for which there is no mutual coupling).

The input impedance of element 1 in the presence of element 2, when the latter is passively loaded with impedance Z_2, may be written as [11]

$$Z_1 = Z_{11} - \frac{Z_{12}^2}{Z_{22}+Z_2} \qquad (4.5)$$

So the value of Z_1 is dependent on Z_2 through the mutual impedance Z_{12}. The following two extreme, but simple, cases of defects could occur in such an array. The first is when one voltage source is open circuited (o.c.). Assuming element 2 is o.c., then, $Z_2=\infty$, and $I_2=0$. The result will be

$$Z_1 = Z_{11} \qquad (4.6)$$

i.e., the input impedance equals that of a single element. The radiation pattern will also be that of a single element radiation, due to $I_2=0$, but with $I_1=V/Z_{11}$ due to equation (4.6).

The other extreme case would be that of a short circuit replacing the voltage source then $V_2=0$ and $Z_2=0$. However $I_2 \neq 0$ due to the mutual coupling. The input impedancee will be given by

$$Z_1 = Z_{11} - \frac{Z_{12}^2}{Z_{22}} \qquad (4.7)$$

putting $V_2=0$ in equation(4.4) the resulting current ratio will be given by

$$\frac{I_2}{I_1} = \frac{Z_{12}}{Z_{22}} \qquad (4.8)$$

instead of $I_2/I_1=1$. For a given array the value of Z_{11} is known by the dipole configuration. The Z_{12} is given through known formulas due to Carter [9] for some simple configurations. Formulas for the self and mutual impedances between two broadside (parallel) dipoles, as in Fig. 4.3 ,

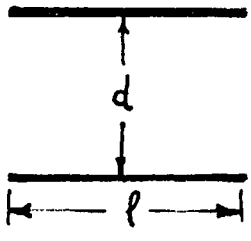


Fig. 4.3 Geometry of parallel dipoles

is described (for infinitely thin dipoles) by the following expressions

$$Z_{ii}=30[\ \ln(\gamma kl) - C_i(2kl) + jS_i(2kl)] \qquad (4.9)$$

where 1 and d as described in Fig. 4.3 , $k=2\pi/\lambda$ and $\gamma=1.781$

$C_i(\ )$ and $S_i(\ )$ are the cosine and sine integral defined by

$$C_i(u) = \int_{\infty}^{u} \frac{\cos x}{x} dx$$

$$S_i(u) = \int_{\infty}^{u} \frac{\sin x}{x} dx \qquad (4.10)$$

These functions are tabulated in various places [25,26]. The mutual impedance is given by

$$Z_{ij} = 30\left[2C_i(kd) - C_i(g+kl) - C_i(g-kl)\right]$$
$$-j30\left[2S_i(kd) - S_i(g+kl) - S_i(g-kl)\right] \qquad (4.11)$$

where, $g = \frac{2\pi}{\lambda}(d^2 + l^2)^{1/2}$. Expressions for other simple configurations, such as collinear dipoles, and parallel dipoles in echelon, are also given in the literature [11]. Expressions for the mutual coupling of finite size ratios of element shape is also given in the open literature [19].

The above formulas for mutual coupling will now be used to find the equivalent substitute array in the case of mutual coupling in a two element array.

4.3 The equivalent substitute array in a two element array

The expressions given in the previous section will now be used to describe the equivalent substitute array, for those defects.

The non-defective array is given (for voltage source generator), by

$$I_1 = V/Z_1 \qquad (4.12)$$

and due to symmetrical elements

$$I_2 = V/Z_2 = V/Z_1 \qquad (4.13)$$

Hence the current ratio for the non-defective array equals

$$I_2 / I_1 = 1$$

In the case of a defect, this ratio changes to

$$I_2 / I_1 = a \exp\{j\Delta\phi\} \qquad (4.14)$$

For the case of v_2 short circuited, the input impedance to element 1 will remain unchanged (following the assumption of voltage source generators), and

$$I_2 / I_1 = Z_{12} / Z_{22} = Z_{12} / Z_{11} = |Z_{12}/Z_{11}| \exp\{j(\phi_{12} - \phi_{11})\} \qquad (4.15)$$

where $\phi_{11} = \arg(Z_{11})$ and $\phi_{12} = \arg(Z_{12})$.

Therefore the non-defective array current excitation and the defective array current excitation could be described pictorially as in Fig. 4.4 . The subtraction of these will result in the equivalent substitute array current excitation, described in the same figure.

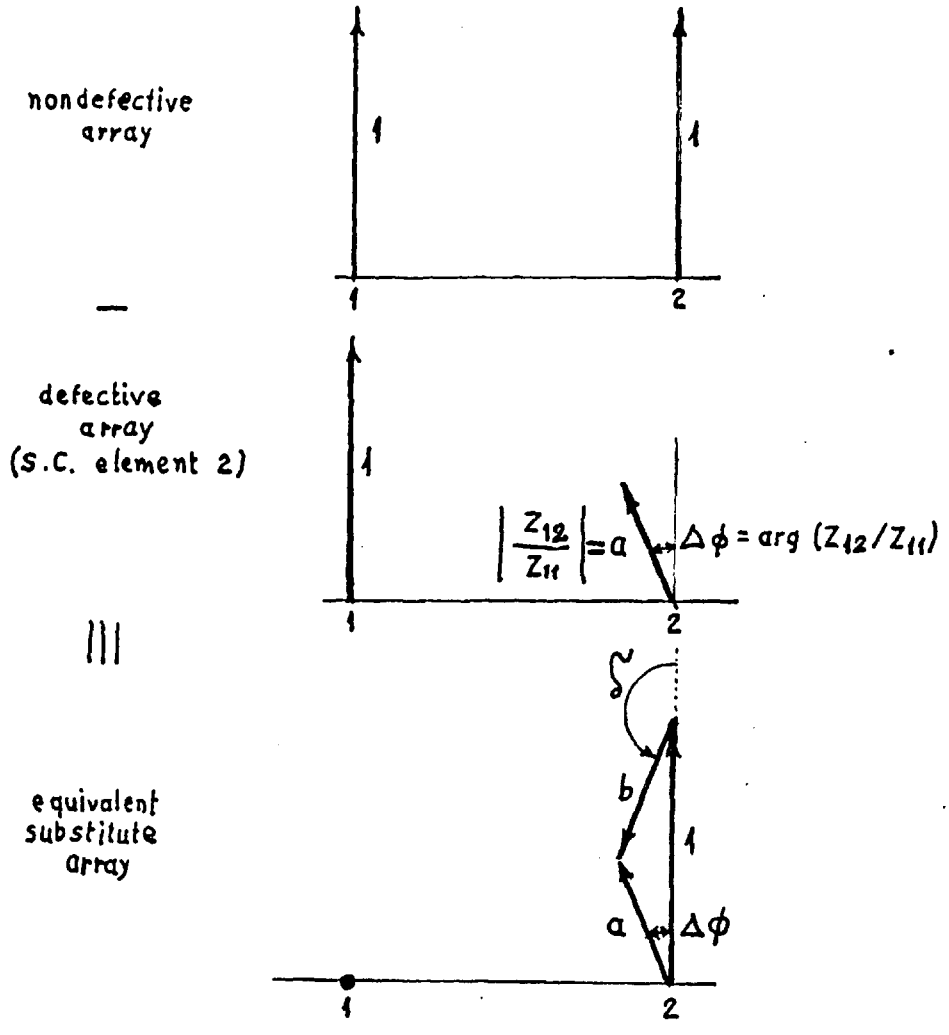


Fig. 4.4 Description of a s.c. defect in a two element array with mutual coupling

The equivalent substitute array will, therefore, be given by equations (2.3) to (2.5).

where

$$a = |Z_{12}/Z_{22}|$$

and (4.16)

$$\Delta\phi = \arg(Z_{12}/Z_{11})$$

In the case of an open-circuit defect it has been shown already that we are left with a single element radiation pattern. It is best described pictorially as in Fig. 4.5.

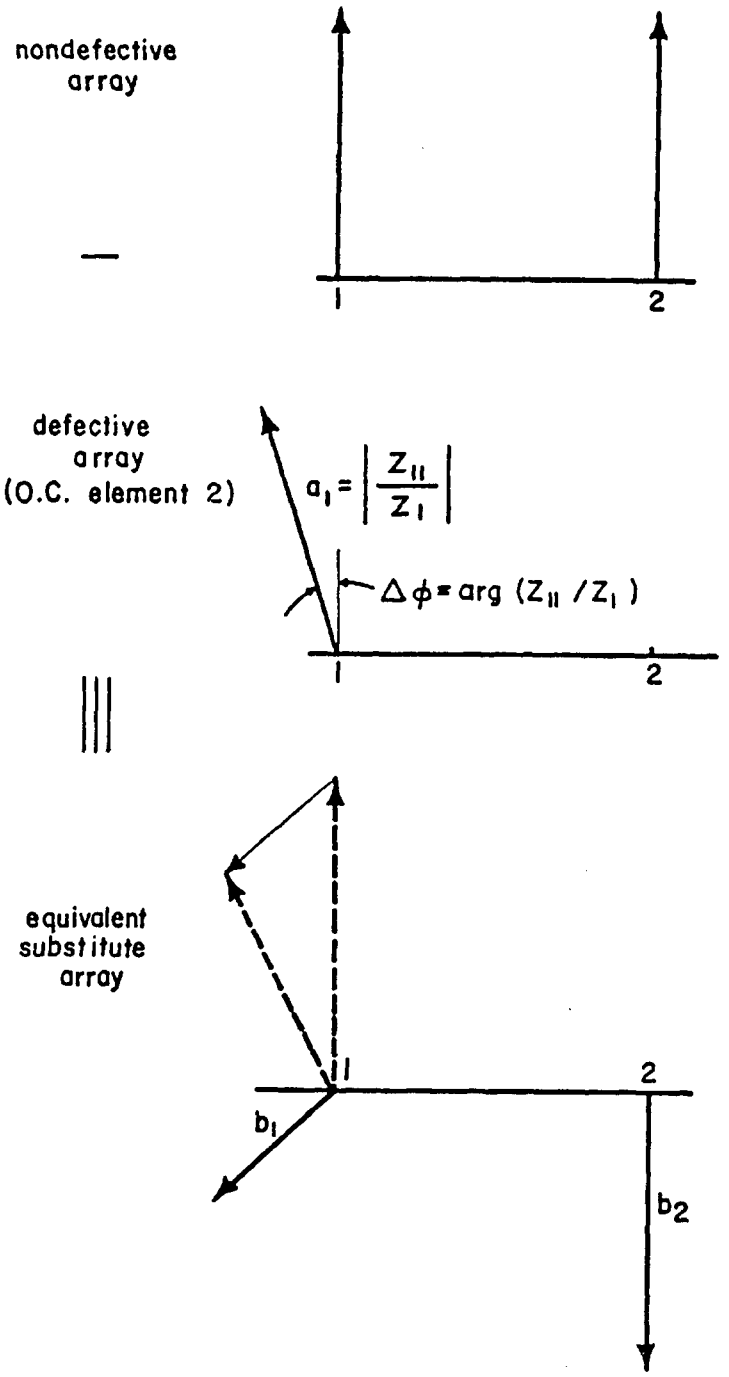


Fig. 4.5 Description of an o.c. defect in a two element array with mutual coupling

The equivalent substitute array for an o.c. defect in element 2 (for voltage source generators) will, therefore, be given by the superposition of two elements, where the equivalent substitute for element 2 equals -1, and the equivalent substitute for element 1 is given by equations(2.3) and (2.4). Here,

$$a = |Z_{11}/Z_1|$$

and (4.17)

$$\Delta\phi = \arg(Z_{11}/Z_1)$$

It is to be noticed that although the excitation and defect demonstrated has been chosen to give a simple description, other types of excitation generators and defects can be analyzed similarly. The example of mutual coupling between broadside (parallel) elements, is important because mutual coupling for this configuration is strongest, and hence will produce the largest effects.

So far, mutual coupling effects between two elements have been discussed. For large arrays, like the MLS array, the present analysis has to be extended, which will be done next. The idea of infinite arrays, as presented by Oliner and Malech [27], will be used.

4.4 Defects in an infinitely long uniform arrays

Large arrays are thought of as consisting of two parts [27] : a "central part" which constitutes the bulk of a large array and the regions near the "edges". Each element in the central portion feels the same environment. Hence the treatment of mutual coupling effects in infinite arrays is suitable for large arrays, if edge effects are ignored. It will be assumed for

simplicity, that only first order effects are important. Hence the effect of changing parameters of a single element (e.g. due to a defect) will be "felt" by the neighbouring elements and will modify their parameters without the chain reaction (second order effects) of each one of the neighbouring elements affecting the others as well. Ignoring these second order effects simplifies the analysis by avoiding the need to solve a large number of simultaneous equations or looking for an infinite series representation.

Following these assumptions, mutual coupling effects due to a defect can be calculated seperately for each element in a manner similiar to the treatment used previously for two elements (equations 4.16 and 4.17).

For example, assume element i is missing. Then the magnitudes a_j of the substitute elements will be given by the following expressions

$$a_j = |Z_{ij}/Z_{jj}|$$

and the phase $\Delta\phi_j$ by: (4.18)

$$|\Delta\phi_j| = |\arg(Z_{ij}/Z_{jj})|$$

A defect in one element of the array will cause symmetrical effects in elements located on both sides of the defective element, i.e.,

$$\left.\begin{aligned} a_{i+\ell} &= a_{i-\ell} \\ \Delta\phi_{i+\ell} &= \Delta\phi_{i-\ell} \end{aligned}\right\} \qquad (4.19)$$

Because of the decrease of mutual coupling, inversely with distance according to equation (4.11), the modification of the mutually coupled elements due to the defect will decrease in the same proportion. The effect is therefore that of a substitute array with an amplitude taper, decreasing sharply and symmetrically with the distance, from the location of the defect. The phase of the coupled element will change in accordance with the argument ratio of the impedance to the original input impedance. Fig. 4.6 demonstrates the case of a missing element in an infinitely long homogeneous array.

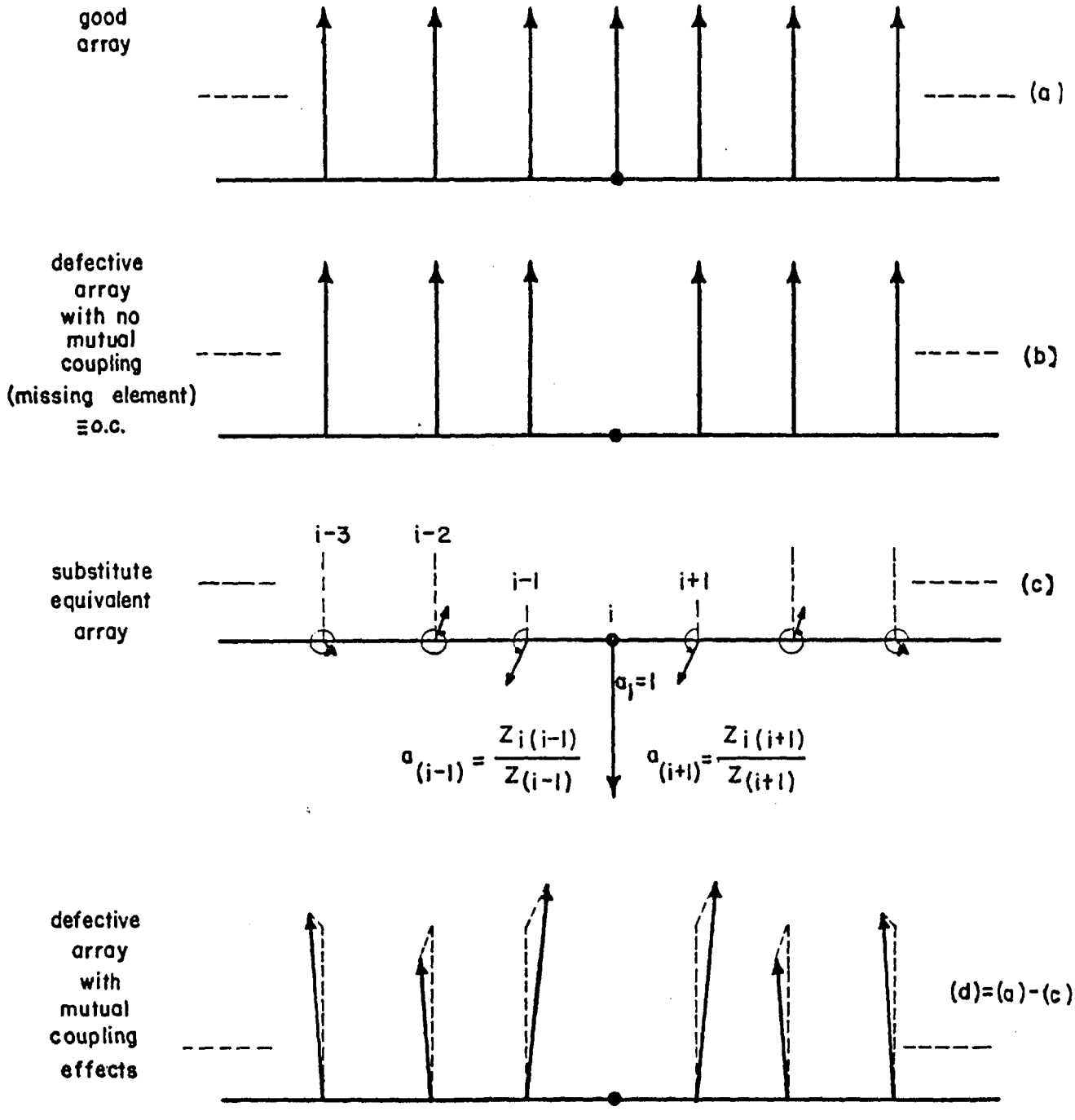


Fig. 4.6 Demonstration of defective element in an infinitely long, homogeneous array incorporating mutual coupling effects

Fig. 4.6 demonstrates qualitatively the substitute subarray of a missing element i due to mutual coupling effects. It is clear that the resultant substitute subarray far-field phase-pattern will now deviate periodically from the ideal phase-line (i.e. if no mutual coupling is included). Also the far-field magnitude pattern will be amplitude modulated. It will be found convenient to use a practical numerical example, which will be presented next.

Example: A missing element i in an infinite $\lambda/2$ parallel dipole array.

The interelement spacing is 0.68λ (the parameters were chosen to fit a similiar experimental linear array investigated in chapter 7). Using equations (4.9) to (4.14) and (4.16), (4.17) the following values are calculated, see table 4.1

Table 4.1

Mutual coupling substitute subarray value for missing elemnt i, infinite $\lambda/2$ parallel array 0.68λ interelement spacing.

l	...	-3	-2	-1	0	+1	+2	+3	...
$a_{i+\ell}$ mag	...	.11	.16	.3	1	.3	.16	.11	...
$\Delta\phi$ phase[°]	...	112	-10	-126	0	-126	-10	112	...

It can be concluded that the expected R.M.S. phase variation is about 30 degrees. These (periodic) phase variations can be smoothed using a statistical regression line, as in the case of random excitation described in section 3.2.2, although less efficiently due to their non-random nature. The values calculated in table 4.1 will be used in a computer simulation in a later section, where the resulting phase (and magnitude) variation will

be given. In order to complete the discussion on interelement coupling effects, the other type of coupling i.e. the reflected power due to a defect in an element array, have also to be included, as follows.

4.5 Effects of reflected power due to a defect in array elements

As explained in the begining of this chapter, reflected power in the feed network, comprises another mechanism of coupling. It was also explained that this effect is not attenuated with distance, if a lossless feed network is assumed. The effect of reflected power is dependent on the configuration of the feed network (e.g., series coupled elements in a waveguide antenna), and whether the feed network is reciprocal (e.g., nonreciprocity could be due to the presence of ferrite isolators). It is assumed that a travelling wave series-fed antenna array will mostly be affected by a forward reflected power from an open-circuited defective element. If all the other elements are matched to the (characteristic) impedance of the feed line network, then open circuiting an element only means a longer transmission line (assumed to be lossless) between the element preceding the defect, and that following it. The original excitation signal experiences the same delay to subsequent elements, as the forward reflected power due to the defect. This is because both signals travel the same path length in the feed network. The main effect will, therefore, be in modifying the excitation of subsequent elements from the defective element. This will introduce asymmetry (a jump) in the excitation of all the elements from the defect onward. The amount of this jump in

excitation, will be related to the expected coupled voltage to the defective element.

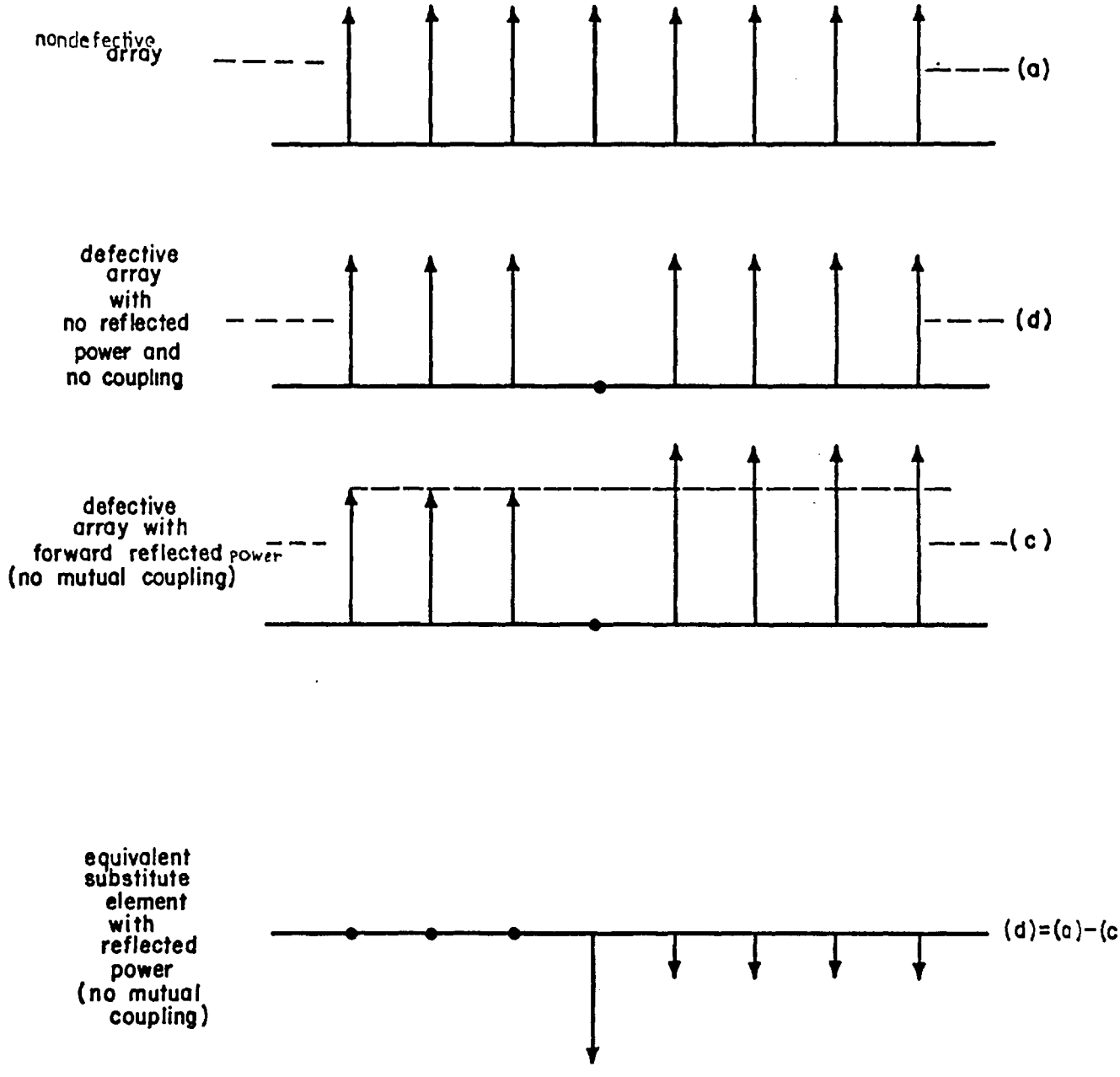


Fig. 4.7 Demonstration of defective (o.c.) element in an infinitely homogeneous array, forward reflected power

Due to asymmetry it is expected that this type of effect, is more severe in its effect when the subtraction method is applied than the mutual coupling effect if a short array is considered. A computer simulation of this type of effect will be demonstrated in the following section.

4.6 Simulation of defective elements in actual arrays (deterministic case).

A simulation of the effect of mutual coupling and forward reflected power due to an open circuited element in an array is demonstrated in Figs. 4.8 to 4.11. The spacing and element dimensions are chosen to apply to the array investigated experimentaly as described in chapter 7. It is seen that the effect of forward reflected power is more severe than that of mutual coupling. The mutual coupling values are taken from table 4.1. The reflected power ratio is taken from the design parameters of a waveguide slot array [23]. These results are compared to those of the experimental investigation in chapter 7.

4.6.1 Simulation parameters

An 8-element $\lambda/2$ slot array with a cosine square over pedestal aperture illumination with 0.68λ interelement spacing is assumed. The mutual coupling effects are given in table 4.1. The forward reflected power is given in table 4.2, obtained from the slot-coupled power calculated from the array design parameters [23].

Table 4.2

Element coupled power in an 8-element slot array with cosine square on pedestal

El No	1	2	3	4	5	6	7	8
Slot coupled power (db)	23	16	9.4	5.6	4.2	5.4	11	17

The following examples are simulated.

a) Missing element No 6: only forward reflected power effects considered.

The results are given in Fig.4.8a for the magnitude patterns and in Fig. 4.8b for the phase patterns. In Fig. 4.8b the dashed lines are the expected phase pattern when no coupling effects are considered.

b) Missing element No 6: with 2 nearby elements ($l=\pm 1$) mutually coupled and forward reflected power considered.

The results are given in Figs. 4.9a and 4.9b.

c) Missing element No 3: only forward reflected power effects considered.

The results are given in Figs. 4.10a and 4.10b.

d) Missing element No 3: with 2 nearby elements ($l=\pm 1$) mutually coupled and forward reflected power considered.

The results are given in Figs. 4.11a and 4.11b.

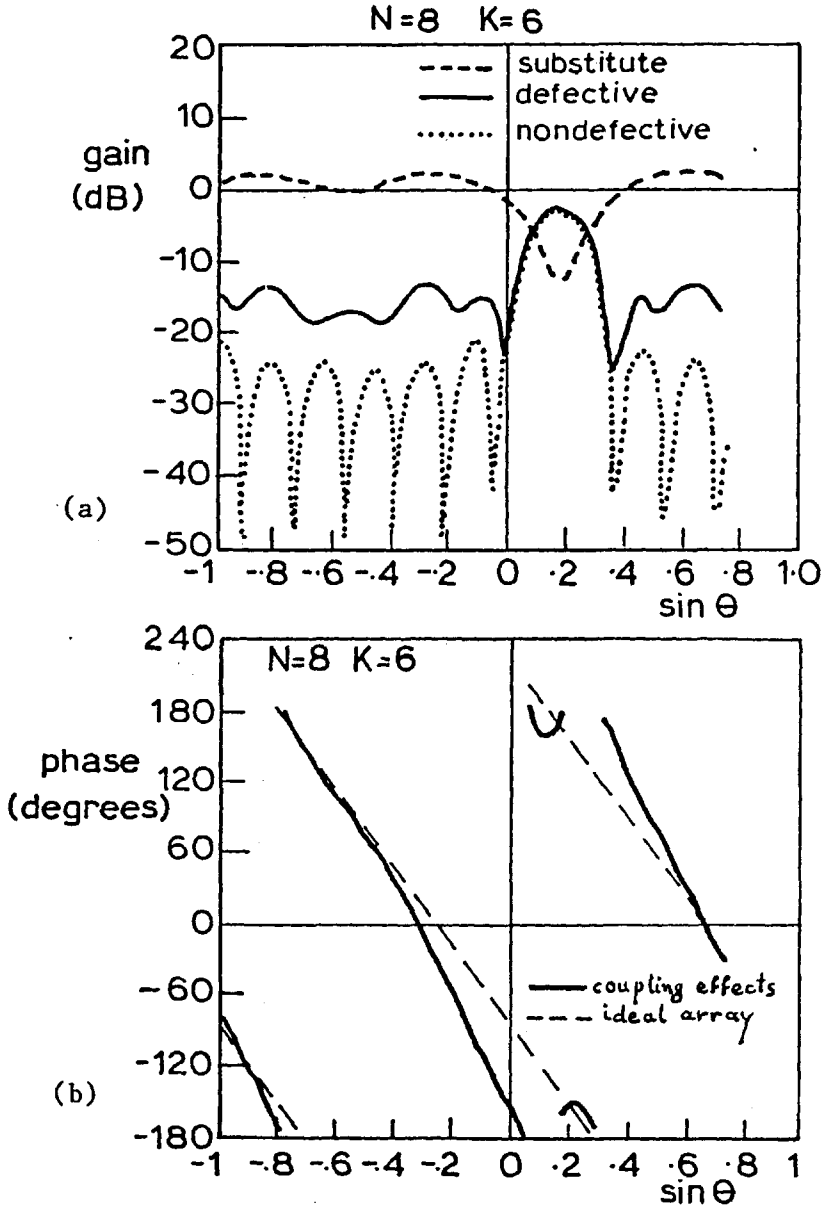


Fig.4.8 Missing element 6: only forward reflected power effects considered. Patterns (a) gain (b) phase.

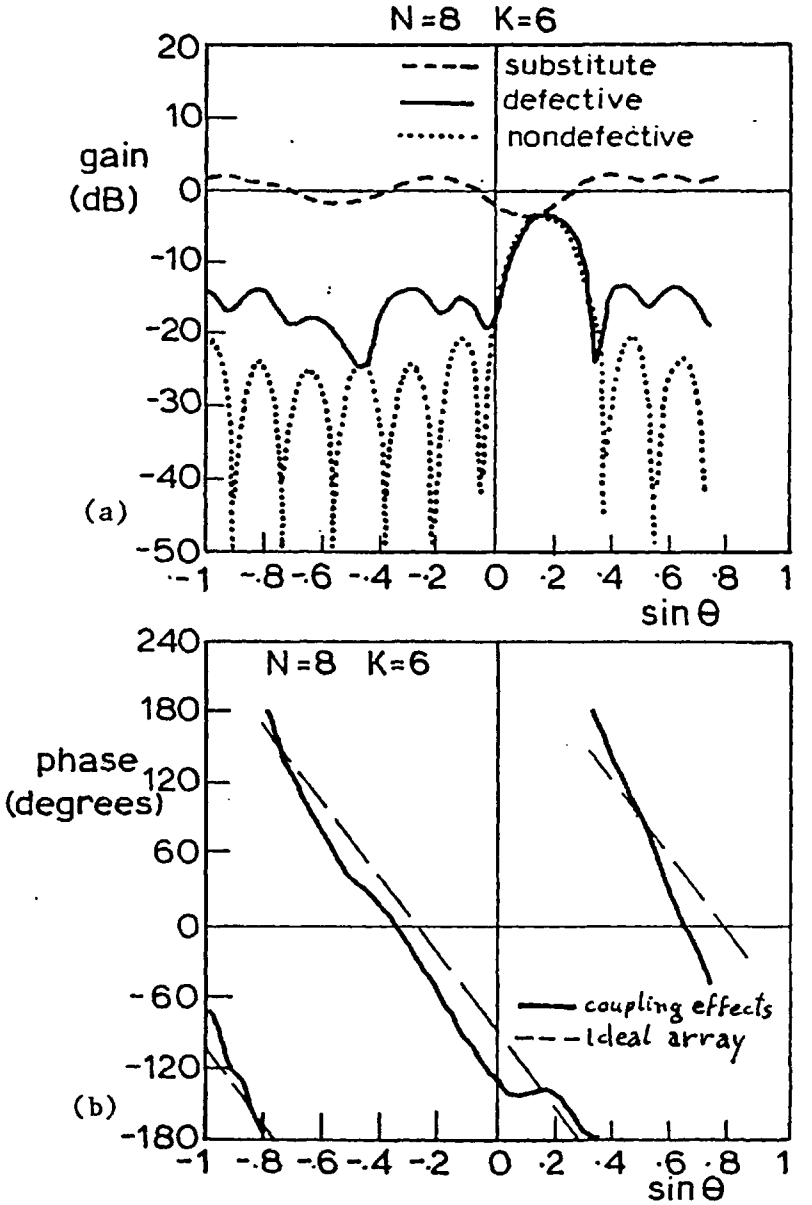
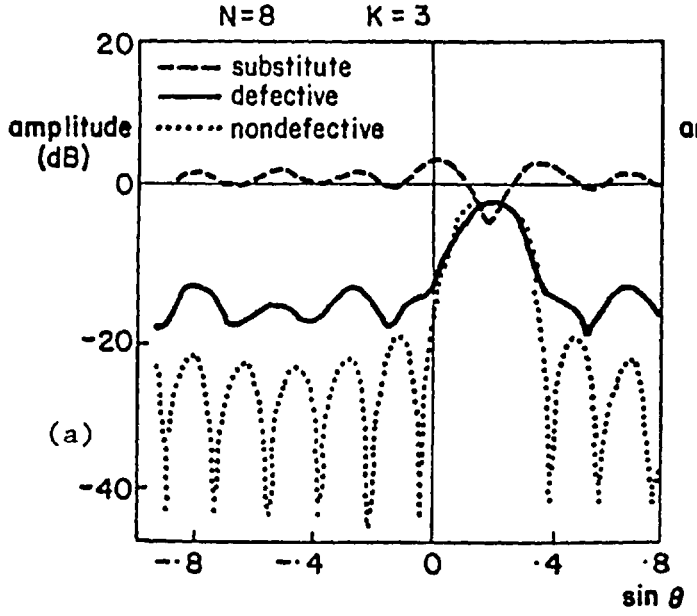
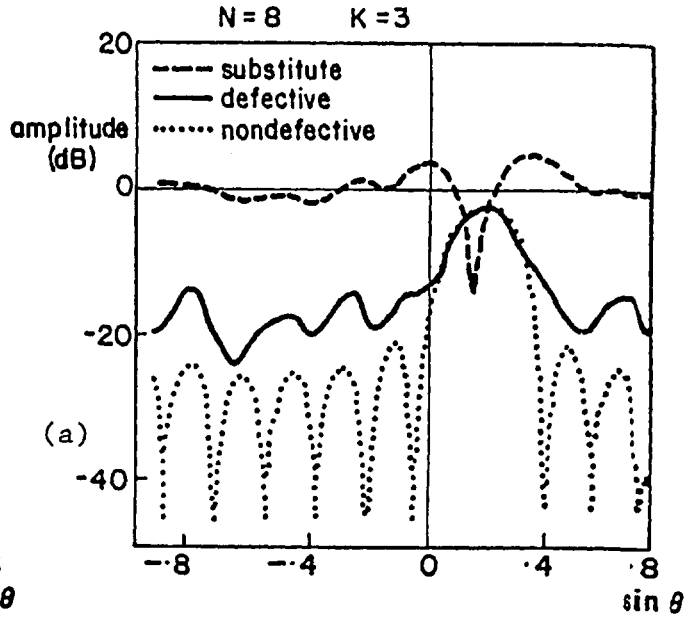


Fig.4.9 Missing element 6: mutual coupling effects and forward reflected power considered. Patterns (a) gain (b) phase.





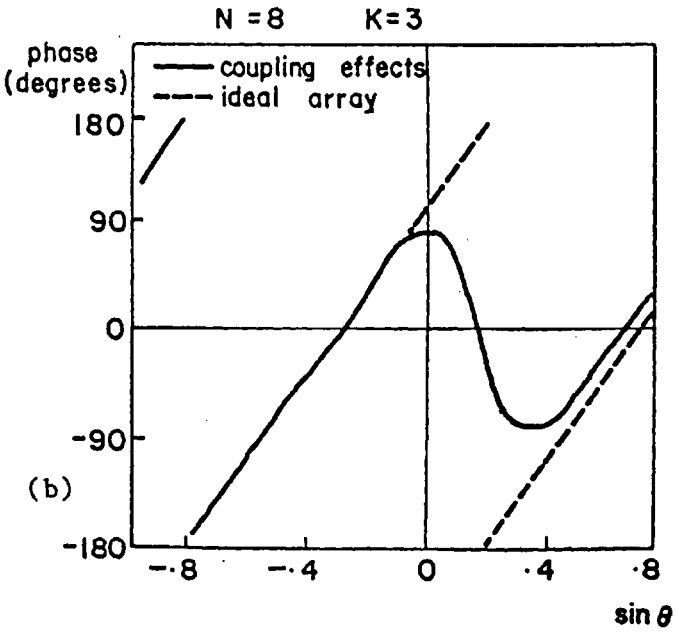


Fig.4.10 Missing element 3: only forward reflected power effects considered. Patterns (a) gain (b) phase.

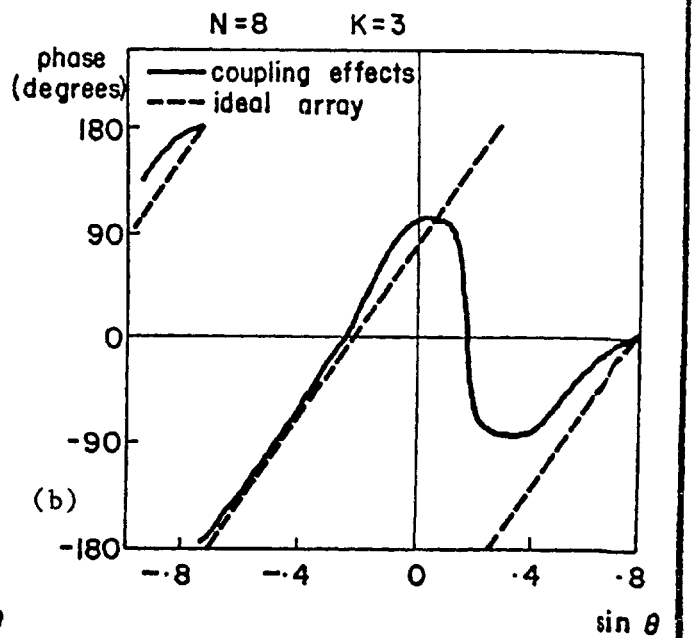


Fig.4.11 Missing element 3: mutual coupling effects and forward reflected power considered. Patterns (a) gain (b) phase.

4.6.2 Assessment of the results

The examples have been chosen such that the missing element will be examined to the left and to the right of the array center, thus introducing different substitute subarrays due to forward reflected power asymmetry. As expected, the forward reflected power with the above parameters causes the maximum phase deviation around the ideal phase-line (dashed), this is in comparison with the small effect of the mutual coupling model. The substitute array when element 3 is defective introduces a larger effect due to the fact that the resulting substitute array (due to forward reflected power) is larger (5 elements) than that modeled when element 6 is defective (2 elements). The resulting phase deviation is about ± 20 degrees (peak) for missing element 6 and about ± 60 degrees (peak) for missing element 3.

These results are to be compared to those of the experimental investigation in chapter 7.

In addition to the phase deviation of the substitute subarray pattern there are magnitude deviations from the expected constant line if no coupling effects are considered.

4.7 Discussion (expected usefulness of the subtraction method in actual arrays - deterministic case)

The analysis in this chapter, combined with simulation on the computer has shown that coupling effects of the two types, namely: the mutual coupling and feed network coupling (forward reflected power) can cause deviations of the resulting phase around the expected phase-line. It is instructive to deduce the phase deviation by examining the amplitude variations of the

substitute array pattern (the upper curve in Figs. 4.8a to 4.11a). There the amplitude pattern shows periodic variations around the "correct" (constant) value of the substitute element pattern when no mutual coupling effects are present. If a statistical regression line is constructed then the ideal array substitute element amplitude pattern can be derived (i.e. when no mutual coupling effects are present). Similarly for the phase variation pattern which accompanies the amplitude pattern. It is therefore believed that a statistical regression line, constructed from the phase data points, is able to resolve a defective element in actual arrays in the presence of coupling effects. (It should be noticed that the smoothing in this case is expected to be less effective than in the case of random phase examined in section 3.2.2, due to its non random nature.) In a seperate chapter (chapter 7) experimental investigation of actual arrays with similar parameters will be demonstrated, in order to test the present analysis and simulations.

The present chapter concludes the first part of this work which investigated the concept of the equivalent substitute element and the proposed subtraction method, based on this idea. The subtraction method, first analyzed with defects in ideal arrays, was then examined in the presence of random phase excitation errors in chapter 3 and in the presence of mutual coupling effects in the present chapter. Simulations on the computer have shown that the subtraction method is a powerful tool for use in monitoring defects in actual arrays.

It has also been found that the substitute element technique is a convenient tool to describe defects of both static

and dynamic nature, and has provided insight into the effects of mutual coupling.

The second part of the work will investigate further monitoring methods based on the angular plane-wave spectrum concept.

CHAPTER 5

APPLICATION OF THE ANGULAR SPECTRUM CONCEPT

In the first part of the work a simple method of monitoring was suggested, called the subtraction method, based on the equivalent substitute element technique. The method was found efficient for the detection of defects in a single element or in a single subarray of the antenna. This technique has also been found to be applicable for the detection of defects in many elements if elements fail one at a time. The present chapter deals with other methods which are more adequate for the detection of many elements failing at one time, although at the price of more complex processing. These methods, based on the concept of the angular plane-wave spectrum, will be referred to as "the angular spectrum direct method" and the "autocorrelation function (a.c.f.) method". The basic angular spectrum concept will first be summarized.

5.1 Summary of the angular spectrum concept

It has long been known that Huygens' principle, which states that each point on a propagating wavefront can be considered as a secondary source radiating a spherical wave, is only one way of describing fields diffracted from apertures, using Fresnel's formulation based on the principle of superposition. An alternative way is to represent fields by the superposition of a discrete set or a continuum of plane waves travelling in different directions. This is what is meant here by the concept of the "angular spectrum of plane waves" or, in its abreviated form, "the angular spectrum" concept. The theory of this approach has been

covered by several authors, see for example, Booker and Clemmow [12], Ratcliffe [14] and Clarke and Brown [13]. The basic idea is that the radiation from an aperture can be considered as a superposition of an infinite number of plane waves propagating in different directions into the half space in the direction of propagation. The amplitude and phase of each plane wave depends on the aperture field distribution. A demonstration of this representation is given in Fig. 5.1.

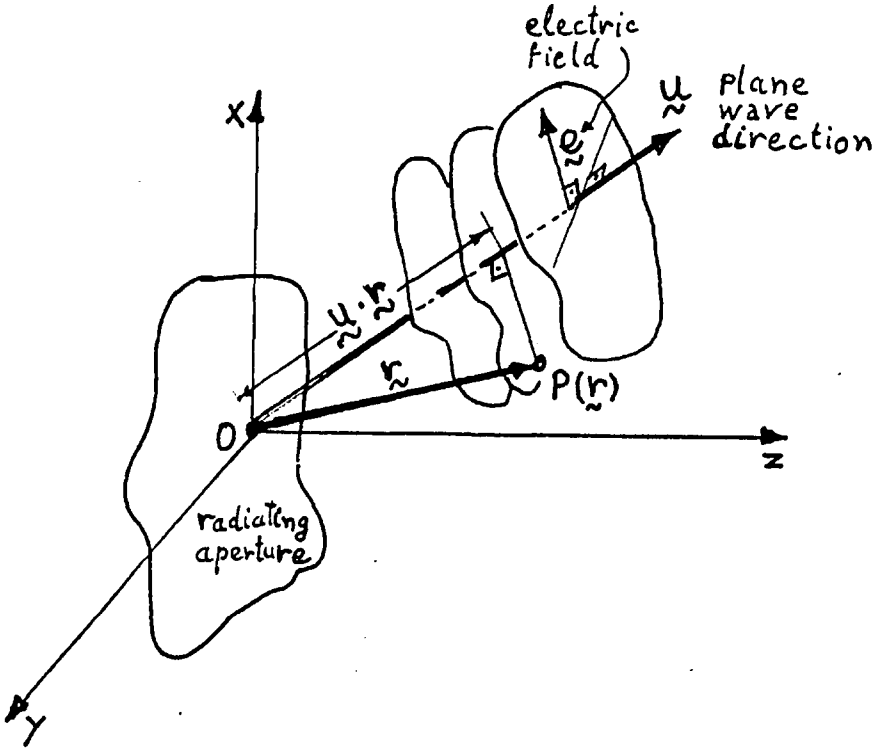


Fig. 5.1 A representative plane wave in the field radiated by an aperture

The field radiated from the aperture can be considered as a superposition of an infinite number of plane waves radiating into the half space $z>0$. A representative incremental plane wave propagating in the $\underset{\sim}{u}$ direction is shown to have an electric field

$\underset{\sim}{e}$ (a phasor vector) that is constant throughout all space and for all time (For a purely sinusoidal field the time dependence of exp{jωt} will be suppressed). Since the field of plane waves are wholly transverse, we have

$$\underset{\sim}{e}\cdot\underset{\sim}{u}=0 \ .$$

For a set of plane waves travelling in different directions, their individual phasor-vector amplitudes can be written as $\underset{\sim}{e}(\underset{\sim}{u})$. The vector function of direction $\underset{\sim}{e}(\underset{\sim}{u})$ is related to the angular spectrum function $\underset{\sim}{F}(\underset{\sim}{u})$ by $\underset{\sim}{e}(\underset{\sim}{u})=\underset{\sim}{F}(\underset{\sim}{u})\ d\underset{\sim}{u}$. Hence $\underset{\sim}{F}(\underset{\sim}{u})\ d\underset{\sim}{u}$ is the amplitude of the elemental plane wave. (Note that $\underset{\sim}{F}(\underset{\sim}{u})$, being a function of direction has two independent variables, such as (θ,ϕ), so that $d\underset{\sim}{u}$ would in that case be $d\theta d\phi$.) The phase of this elemental plane wave at some point $P(\underset{\sim}{r})$ at vector distance $\underset{\sim}{r}$ from the origin 0, will be retarded by an amount corresponding to a distance $\underset{\sim}{u}\cdot\underset{\sim}{r}$, which is the projection of $\underset{\sim}{r}$ on the direction $\underset{\sim}{u}$ as shown in Fig. 5.1. Hence the electric field at the point $p(\underset{\sim}{r})$ will be given by

$$\underset{\sim}{E}(\underset{\sim}{r}) = \int \underset{\sim}{F}(\underset{\sim}{u})\ \exp\{-jk\underset{\sim}{u}\cdot\underset{\sim}{r})\}d\underset{\sim}{u} \qquad (5.1)$$

and the corresponding magnetic field $\underset{\sim}{H}(\underset{\sim}{r})$ will be given by

$$\underset{\sim}{H}(\underset{\sim}{r}) = \frac{1}{Z}\int \underset{\sim}{u}x\underset{\sim}{F}(\underset{\sim}{u})\ \exp\{-jk\underset{\sim}{u}\cdot\underset{\sim}{r}\}\ d\underset{\sim}{u} \qquad (5.2)$$

where Z the characteristic impedance of the medium.

The tangential component $\underset{\sim}{E}_a(\underset{\sim}{\rho})$ of the aperture field is given by putting $\underset{\sim}{r}=\underset{\sim}{\rho}$ in equation (5.1), as

$$\underset{\sim}{E}_a(\underset{\sim}{\rho})= \int \underset{\sim}{F}(\underset{\sim}{u})\ \exp\{-jk\underset{\sim}{u}\cdot\underset{\sim}{\rho}\ )\ d\underset{\sim}{u} \qquad (5.3)$$

where $\underset{\sim}{\rho}$ is confined to the aperture plane and defined by two

independent variables. Hence equation (5.3) can define a Fourier transform from the direction domain $\underset{\sim}{u}$ into the position domain $\underset{\sim}{\rho}$. The inverse transform yields the angular spectrum

$$\underset{\sim}{F}(\underset{\sim}{u}) = \frac{1}{\lambda^2}\int \underset{\sim}{E}_a(\underset{\sim}{\rho}) \exp\{+jk\underset{\sim}{u}\cdot\underset{\sim}{\rho}\}\, d\underset{\sim}{\rho} \qquad (5.4)$$

Therefore the angular spectrum can be found from the aperture field using equation (5.4), and the field anywhere to the right of the aperture can be deduced using equation (5.1). In general the solution of equation (5.1) is not simple. However a simple result is achieved for the far field using the method of stationary phase.

The far field of an antenna can be resolved by an approximation to equation (5.1) for kr>>1. The phase term in the integrand of equation (5.1) can be written as

$$k\underset{\sim}{u}\cdot\underset{\sim}{r} = kr\cos\psi \qquad (5.5)$$

where $\cos\psi = \underset{\sim}{u}\cdot\underset{\sim}{r}/r$.

Since in the far field kr is very large, the phase term will undergo large variations (through many multiples of 2π) for only small changes in the direction $\underset{\sim}{u}$ relative to the direction $\underset{\sim}{u}_r$ (which now coincides with $\underset{\sim}{r}$), except when $\cos\psi$ is stationary. This "stationary-phase" condition occurs when $\cos\psi = 0$ and $\underset{\sim}{u}=\underset{\sim}{u}_r$. Then it can be said that the contributions from the integrand will tend to cancel one another except in the region $\underset{\sim}{u}\cong\underset{\sim}{u}_r$. Hence the result will be that

$$\underset{\sim}{E}(\underset{\sim}{r}) \sim \underset{\sim}{F}(\underset{\sim}{u}_r) \ . \qquad (5.6)$$

Therefore the far field amplitude depends directly on the angular

spectrum function.

To be specific, an x-polarized component of the radiated electric field in Cartesian coordinates is

$$E_x(x,y,z) = \iint_{-\infty}^{\infty} F_x(\alpha,\beta)\, \exp\{-jk(\alpha x+\beta y+\gamma z)\}\, d\alpha\, d\beta \qquad (5.7)$$

Where E_x the x component of the field at P(x,y,z), see Fig. 5.2.

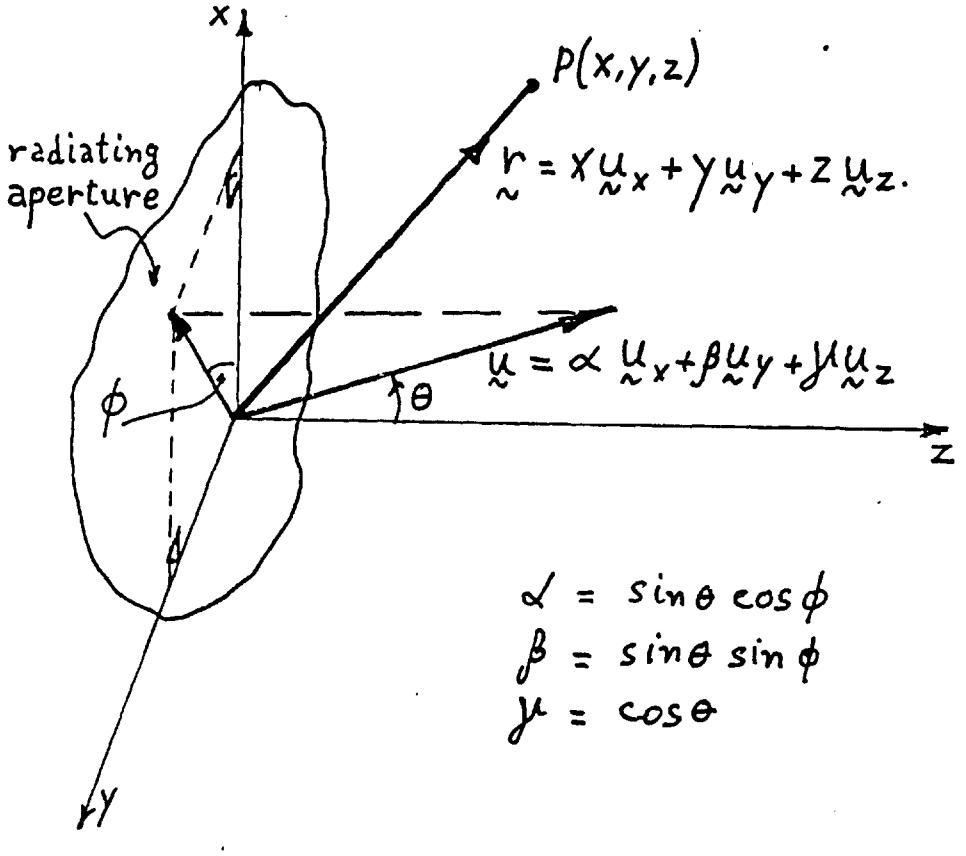


Fig. 5.2 Aperture radiation geometry

The angular spectrum of the x component of the aperture field is $F_x(\alpha,\beta)$, where α,β and γ are the direction cosines to the x,y and z axes (where $\alpha^2+\beta^2+\gamma^2=1$). Similiar expressions can be given for other components (see Clarke and Brown [13]).

In many cases, like the MLS array, physical fields can be

described based on the simpler two dimensional representation provided the radiating aperture is separable (i.e. if the aperture field $E_a(x,y)$ can be expressed as a product of two functions say $E_a(x,y)=f_1(x)\ f_2(y)$). Then the angular spectrum is also separable. Then each function can be treated separately assuming the other is unchanged. Use will be made of the two dimensional representation in discussing the monitoring methods based on the angular spectrum, and so the angular spectrum representation of two dimensional fields will be described next.

5.1.1 The angular spectrum of two dimensional fields

Consider an x-polarized aperture field $E_{ax}(x)$ radiated into the half-space $z>0$ in the two-dimensional geometry of Fig. 5.3 .

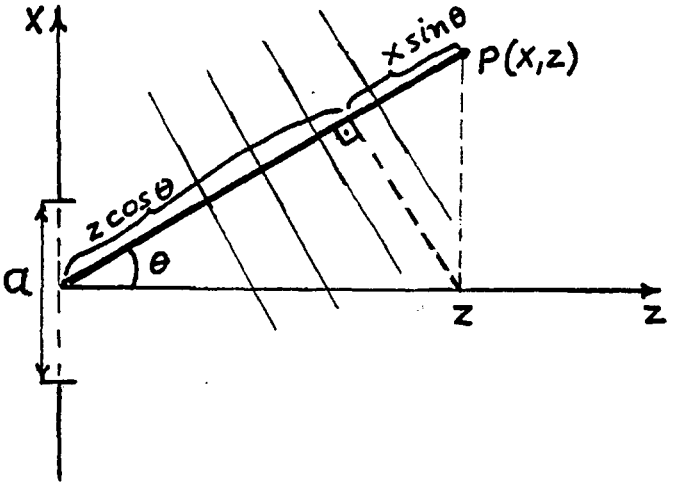


Fig. 5.3 Two dimensional geometry

The field components corresponding to equation (5.1) are then (see Clarke and Brown [13]),

$$\begin{bmatrix} E_x(x,z) \\ E_z(x,z) \\ H_y(x,z) \end{bmatrix} = \int_{-\infty}^{\infty} F(s) \begin{bmatrix} 1 \\ -s/c \\ 1/zc \end{bmatrix} \exp\{-jk(sx+cz)\} ds \qquad (5.8)$$

where $s=\sin\theta$ and $c=\cos\theta=(1-s^2)^{1/2}$. The extended integration limits for $|s|>1$ correspond to evanescent waves which although not propagating are included for completeness of the presentation. The tangential aperture field is

$$E_{ax}(x) = E_x(x,0)$$
$$= \int_{-\infty}^{\infty} F(s) \exp\{-jksx\}\, ds \qquad (5.9)$$

Which is the Fourier transform of the angular spectrum function $F(s)$. The inverse transform then holds, giving

$$F(s) = \frac{1}{\lambda} \int_{-\infty}^{\infty} E_{ax}(x) \exp\{+jksx\}\, dx \qquad (5.10)$$

As an example the x component of equation (5.8) is given approximately by (putting $c \simeq 1-\frac{1}{2}s^2$),

$$E_x(x,z) = \exp\{-jkz\} \int_{-\infty}^{\infty} F(s) \exp\{j1/2\ kzs^2\} \exp\{-jkxs\} ds \qquad (5.8a)$$

This is a Fourier transform of the product of two functions of s having the following Fourier transforms (pairs)

$$F(s) \longleftrightarrow E_{ax}(x)$$

and

$$\exp\{j\ \tfrac{1}{2}kzs^2\} \longleftrightarrow (j\lambda/z)^{1/2} \exp\{-j1/2\ kx^2/z\}$$

where the notation $\longleftrightarrow$ designates the Fourier transform relation. It follows from the convolution theorem of Fourier transforms that

$$E_x(x,z) = (j/\lambda z)^{1/2} \exp(-jkz) \int_{-\infty}^{\infty} E_{ax}(x') \exp\{-jk\frac{(x-x')^2}{2z}\} dx' \qquad (5.8b)$$

which is Fresnel's diffraction formula [13]. Use of this result will be made in chapter 6.

The far field is approximated as explained earlier, by the method of stationary phase to give the following

$$\begin{bmatrix} E_x(r,\theta) \\ E_z(r,\theta) \\ H_y(r,\theta) \end{bmatrix} = \begin{bmatrix} \cos\theta \\ -\sin\theta \\ 1/Z \end{bmatrix} \sqrt{\frac{j\lambda}{r}}\, f(\sin\theta)\, \exp\{-jkr\} \qquad (5.11)$$

or in polar form

$$E_\theta(r,\theta) = ZH_y(r,\theta) = \sqrt{\frac{\lambda}{r}} F(\sin\theta)\, \exp\{-j(kr - \pi/4)\} \qquad (5.12)$$

A similar set of equations hold for a y-polarized one-dimensional aperture field.

The inverse process, i.e the determination of the aperture field from the far field measurement will be used as a basis for the monitoring methods suggested later in this chapter.

The determination of far-field from near field measurements will be described next.

5.1.2 Determination of far-field from near-field measurements

The planar near field measurement technique now in extensive use is only a straight-forward use of the angular spectrum concept. Consider the system in Fig. 5.4

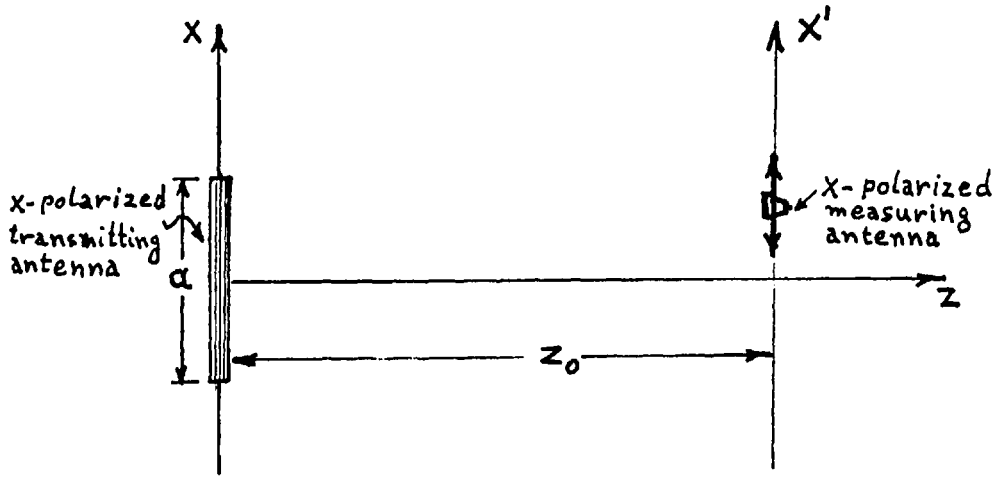


Fig. 5.4 Geometry of near field measurement

The far field of an x-polarized aperture is to be determined from near field measurements. An x-polarized isotropic antenna (in practice possibly a low gain open waveguide) is traversed over the plane $z=z_o$. From equation (5.8) it follows that:

$$E_x(x,z_o)= \int_{-\infty}^{\infty} F(s)\ \exp\{-jk(sx+cz_o)\}ds \qquad (5.13)$$

and since z_o=constant,

$$E_x(x,z_o)= \exp(-jkcz_o) \int_{-\infty}^{\infty} F(s)\ \exp(-jksx)\ ds \qquad (5.14)$$

Inverting, gives

$$F(s) = \frac{\exp\{jkcz_o\}}{\lambda} \int_{-\infty}^{\infty} E_x(x,z_o)\ \exp(jksx)\ dx\ . \qquad (5.15)$$

This means simply that measuring the field over z_o=constant, then taking its Fourier transform yields the angular spectrum function of the transmitting antenna (multiplied by $\exp\{-jkcz_o\}$). According to the far-field theorem mentioned previously, the far field is also determined using equation (5.12). In practice however the measurement range is finite, and hence also are the integration limits in equation (5.15). This means a truncated

near-field measurement which, again, modifies the results. According to the convolution principle only a smoothed finite range of the angular spectrum and hence the far field is, thereby, determined. A further practice is to apply the discrete Fourier transform (DFT), using available computer subroutines. The sampling then needed is done in equal Δx samples, which must comply with the spatial Nyquist criterion, given by

$$x \leqslant \lambda/(2|s_{max}|) \tag{5.16}$$

where $|s_{max}| = |\sin \theta_{max}|$. In practice however about $1/3\,\lambda$ is used. The above technique was extensively used in the experimental investigation described in chapter 7.

Having summarized the angular spectrum concept and some of its applications it is now possible to present the monitoring method, based on that principle. This will be done in the next section.

5.2 Use of the angular spectrum method to locate defects in antenna arrays

The angular spectrum concept enables one to resolve the aperture illumination of an antenna, if its angular spectrum is known. The far-field of an antenna is asymptotically equal to its angular spectrum, and the angular spectrum is the Fourier transform of the aperture field. Hence the measurement of the far-field of an antenna can, in principle, yield the aperture field illumination. It is therefore suggested that the angular spectrum concept be used as an alternative method for the detection of defects in antenna arrays.

The monitoring method is based on a procedure for the detection of defective elements through their effect on the aperture illumination field, as follows:

- Measure the far field over the range $-\pi/2<\theta<\pi/2$.

- Using equation (5.12) solve the angular spectrum function F(s).

- Perform a Fourier transform of the angular spectrum functions equation (5.9) to yield the aperture field distribution.

Any anomaly in the aperture distribution is due to defects in the antenna elements excitation.

In practice, however, this procedure is not fully applicable, due to the finite measurement range of the far-field. Hence, a modification is needed.

- Measure the far field, with the same polarization of the transmitted signal, in the direction cosines $s_1<s<s_2$. This will approximate the angular spectrum function of the radiating aperture.

- Perform a Fourier transform of the truncated angular spectrum function. This yields the smoothed aperture distribution.

- Identify defects by checking for anomalies in the calculated aperture field distribution.

It should be noted that the modified calculated aperture distribution could have a different shape than the unmodified one. It depends strongly on the range of the direction cosines chosen for measurement. Broadly, this could be chosen in the two extreme cases: The far side-lobe region and the main-lobe region. Both

ranges give information on defects in the antenna aperture distribution. It will be demonstrated with the aid of simplified examples that, as with the subtraction method, the angular spectrum method also gives superior information in the far side-lobe region for monitoring purposes.

5.2.1 Demonstration of the angular spectrum method

An ideal linear uniform broadside array of $\lambda/2$ spaced isotropic N elements is assumed, with missing elements in the antenna. The far side-lobe region of an ideal array pattern can be approximated by $\sin(\pi Nds/\lambda)$, (see equation 2.1). This is equivalent to the interference pattern of the two edge elements of the array, with a distance (measured in wavelengths) of Nd/λ in between, where all other elements have zero illumination.

The Fourier transform of this angular spectrum is given by two delta functions located at $\pm(Nd/\lambda)/2$ (i.e. $E_a(x)=E_o[\delta(x-a/2) + \delta(x+a/2)]$, thereby representing the edges of the aperture. Missing elements in the array will be represented according to equation (2.5) and Fig. 2.9 by additional delta functions in accordance with their relative location in the array aperture. The magnitude ratios of the spectral components of the angular spectrum is given by their normalized amplitude ratio. Therefore the magnitude ratio is given by

$$E_m/E_e = 2\sin(\pi ds_a/\lambda) \qquad (5.17)$$

where E_m/E_e the missing to edge-element illumination amplitude ratio, s_a is the mean direction-cosine and $\sin(\pi ds_a/\lambda)$ is the reciprocal of the mean side-lobe level magnitude (e.g. in the far

side lobe region $E_m/E_e \cong 2$).

If measurements are performed in a region symmetrical about the main lobe then the Fourier transform of the angular spectrum will give approximately constant illumination over the aperture range. Missing elements will be identified by holes in the calculated illumination. Due to the finite direction-cosine range used the resulting illumination will spread outside the theoretical aperture range and the theoretical delta functions will be replaced by $\sin[k(x-x_i)L]/k(x-x_i)$ functions, where 2L=direction range, and x_i the location of the peaks in the aperture plane. Qualitative results, when use is made of this technique, are presented in Fig. 5.5 for two cases: a the far side-lobe region (Fig.5.5a) and b the main lobe region (Fig. 5.5b).

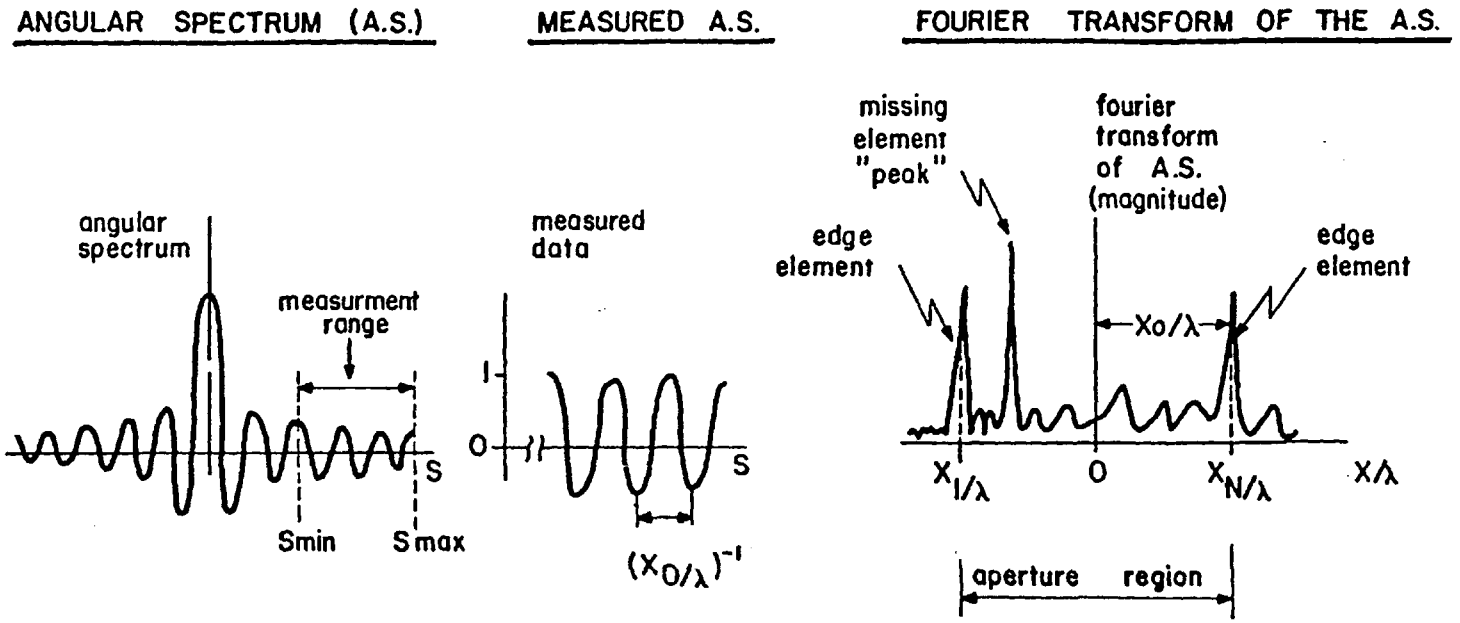


Fig.5.5a The angular spectrum method, far side-lobe region.

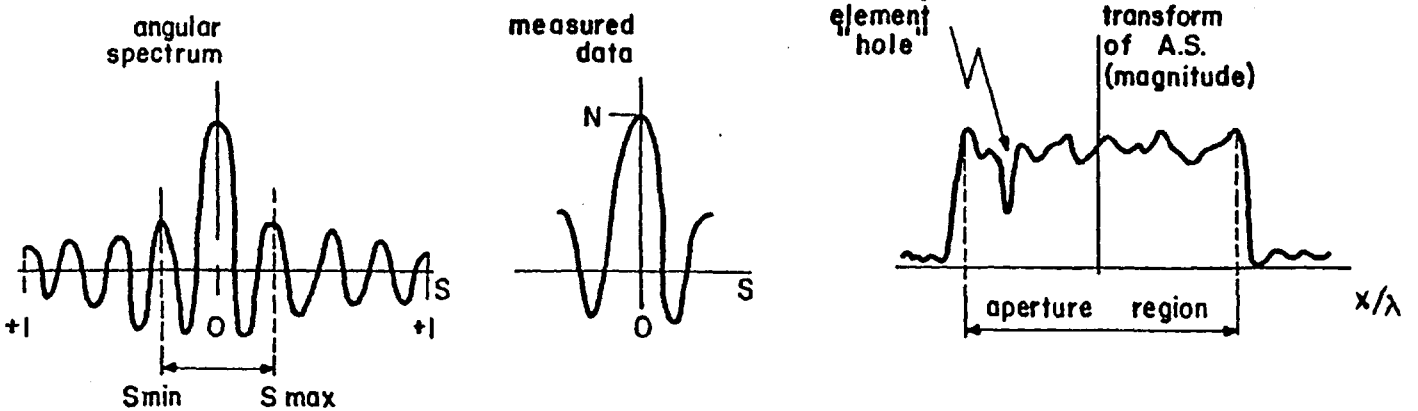


Fig.5.5b The angular spectrum method method, main-lobe region.

In Fig. 5.5 λ/x_o is the range of the direction-cosine for one period of $\sin(\pi Nds/\lambda)$ given by $\lambda/x = (2\lambda/Nd)$, 2L is the measurement range of the direction-cosine given by $2L=(s_{max}-s_{min})$. The location of the edge element will be given after Fourier transformation by x_o/λ and the width of the $\sin[k(x-x_i)L]/k(x-x_i)$ function by $\Delta x/\lambda = 1/L$.

As an example:

Assume that a 100 element array with 0.61λ between elements has element number 35 missing, and the phase error range is $\pm\pi/16$. The following procedure is used for the identification of the defective element:

- The angular spectrum (a.s.) of the defective array is measured in the range of about 30° to 90° degrees in M=100 equal direction-cosine steps, i.e., in the far side-lobe region.

- The first 44 (out of 100) a.s. values are Fourier transformed by a standard DFT (using the computer NAG-routine C06ADF) to yield the array aperture illumination. These results are demonstrated in Fig. 5.6 .

- The results are compared to those of the ideal array (not shown in this report), to check for any anomaly representing a defective element.

As seen in Fig. 5.6 the missing element is made prominent and the ratio E_m/E_e is about 1.5, close to the value of 2, as predicted at the end of the paragraph containing equation (5.17).

From the comparison of the qualitative examples in Fig.5.5 (and Fig. 2.9), it is evident that the results of the far

side-lobe region are superior to those obtained in the main-lobe region. This is because the higher peaks of the F.T. of the a.s. magnitude are all relevant as they point out the antenna edge elements and the corresponding missing elements. In addition the peaks of the missing element is pointed out more clearly and with a larger magnitude ratio to the edge element illumination than in the main-lobe region.

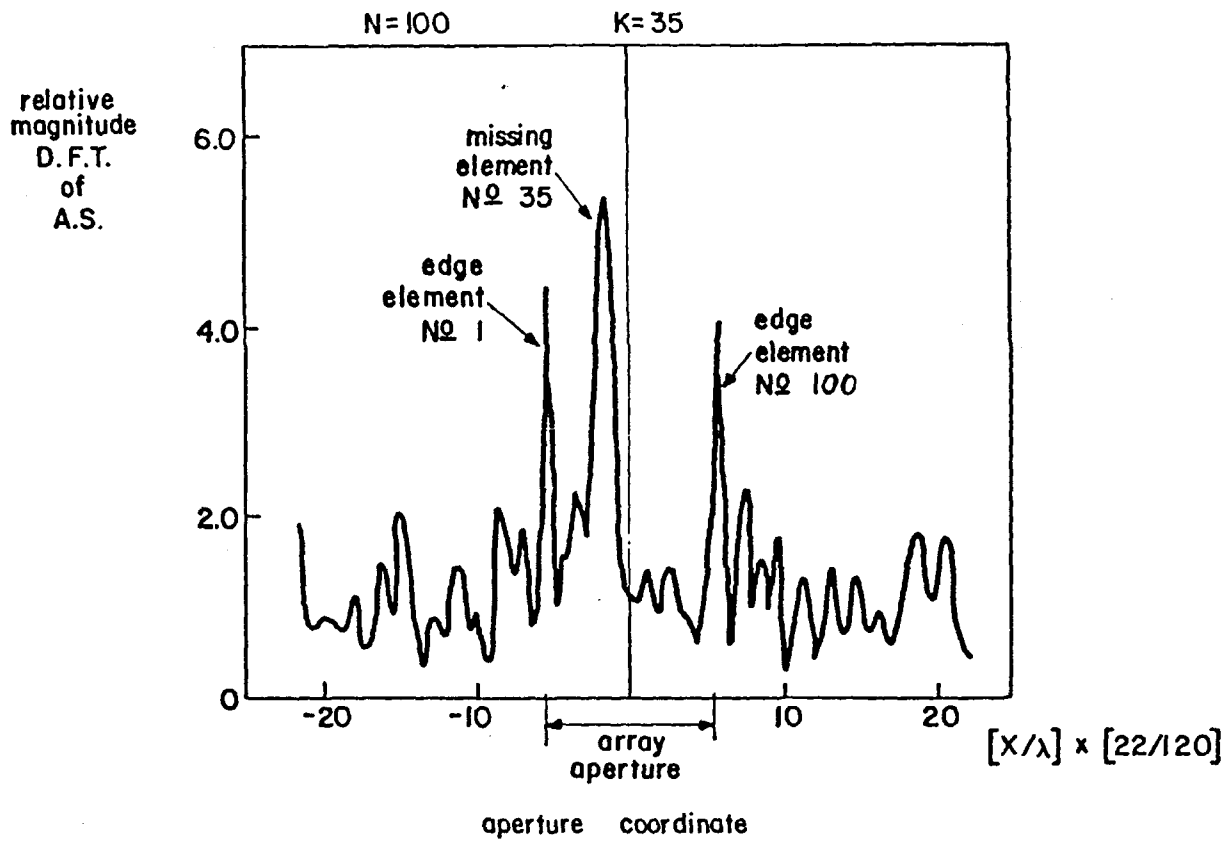


Fig.5.6 Simulation of detection of a missing element by the angular spectrum method.

5.3 Use of the angular autocorrelation function of the angular spectrum to locate defects in the presence of random errors

The autocorrelation function (a.c.f.) is a very useful function for treating random data. It has the properties of smoothing the data and extracting sinusoidal components buried in the fluctuating data points.

It has already been shown that the effect of a defective element is broadly to introduce oscillations in the pattern. The essence of the autocorrelation technique is to extract these oscillations and hence identify the position of the defect. Utilization is made of Ratcliffe's work [14], based on the Van Cittert - Zernike theorem [18], on the dual Fourier transform pair: the a.c.f. of the angular spectrum and the aperture power illumination, a description of which is also given in Appendix C and is summarized here.

5.3.1 The a.c.f. and the aperture illumination.

It can be shown that the Fourier transform of the a.c.f. of the angular spectrum yields the aperture power illumination function (see Appendix C). Designating $\rho(\sigma)$ the a.c.f. for the direction-cosine displacement σ, then

$$|\mathcal{F}[\rho(\sigma)]|=f(x)\, f^{*}(x) \tag{5.18}$$

Where $\mathcal{F}[\ ]$ the Fourier transform and $f(x)\, f^{*}(x)$ is the aperture power illumination over the aperture axis x. The a.c.f. is given by

$$\rho(\sigma)=\int_{-\infty}^{\infty} F(s)\, F^{*}(s+\sigma)\, ds \tag{5.19}$$

and its Fourier transform is given by

$$\mathcal{F}[\rho(\sigma)] = \int_{-\infty}^{\infty} \rho(\sigma) \exp\{-jk\sigma x\} d\sigma \qquad (5.20)$$

A demonstration of the method will now be given.

5.3.2 Demonstration of the a.c.f. method.

A simplified description is given below for results anticipated when utilization is made of this technique. The explanation given in section 5.2.1 is also relevant here. As before the far side-lobe region of an ideal pattern (equation (2.1)) is equivalent to the inteference pattern of the two edge elements of the array, where all other elements are of zero illumination. The a.c.f. of this interference pattern function is a sine-wave of the same argument. The Fourier transform of the a.c.f. is given, as explained earlier, by two delta functions located at $\pm\frac{1}{2}Nd/\lambda$, thereby representing the edges of the aperture. Missing elements in the array will be represented by additional delta functions (equation (2.5)) in accordance with their relative location in the array aperture. The magnitude ratios of the spectral components of the a.c.f. is given by their normalized powers. Therefore, the magnitude ratio is given by

$$I_m / I_e \cong 4 \sin^2(\pi d s_a / \lambda) \qquad (5.21)$$

where I_m / I_e the missing to edge-element illumination power ratio; s_a is the mean direction-cosine and $\sin^2(\pi d s_a / \lambda)$ is the reciprocal of the mean side-lobe level (e.g., in the far side-lobe region

$I_m / I_e \cong 4$).

If measurements are performed in a region symmetrical about the main-lobe, rather than in the side-lobe region, then the Fourier transform of the a.c.f. will give approximately constant power illumination over the aperture range. Missing elements will then be identified by holes in the calculated power illumination. Due to the finite direction-cosine range utilized the resulting power illumination will spread outside the theoretical aperture range and the theoretical delta functions will be replaced by $\sin[\, k(x-x_i)\, L]/k(x-x_i)$ functions. Qualitative results when use is made of this technique are presented in Fig. 5.7 for two cases: a the far side-lobe region (Fig. 5.7a), and b the main-lobe region (Fig. 5.7 b).

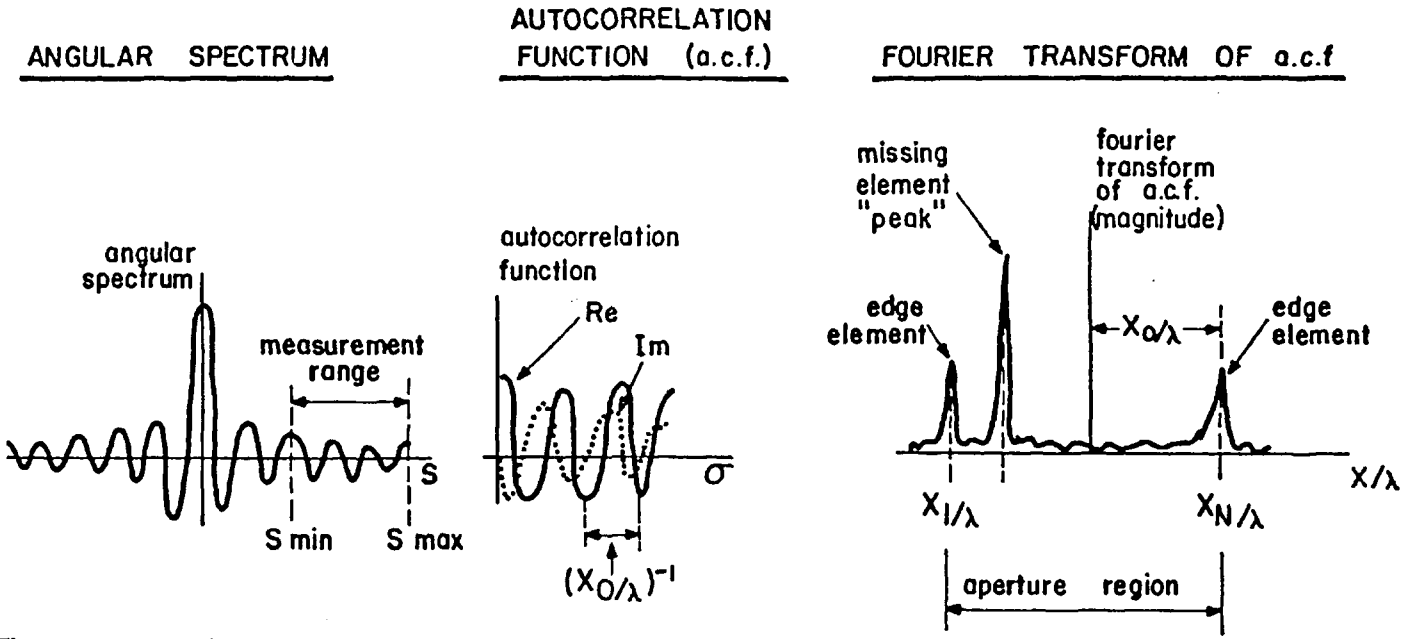


Fig.5.7a The autocorrelation function method, far side-lobe region.

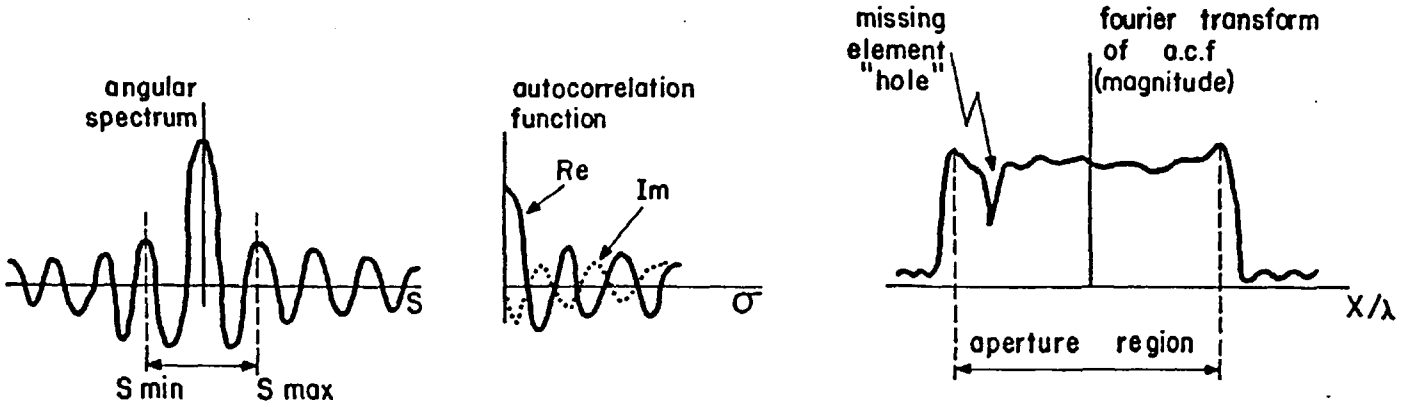


Fig.5.7b The autocorrelation function method, main-beam region.

In fig. 5.7 the variables are designated similar to those in Fig. 5.5. Attention should be paid to the a.c.f., where the imaginary part (I_m) will be in a quadrature phase, +ve or -ve depending on whether the location of the defective element is to the right or to the left of the array centre ($\frac{x}{\lambda}=0$).

The same example as explored with the angular spectrum method is used here. The procedure used for the identification of the defective element is the same, with the following changes:

- After measuring the angular spectrum in equal direction-cosine steps, the complex a.c.f. of these values is then calculated (Subroutine COREL03)

- Then the first 44 (out of 100) a.c.f. values are Fourier transformed by the same NAG-routine, to yield the array aperture power illumination.

- The results are compared, as before, to those of the ideal array, to check for any anomaly representing a defective element.

As seen in Fig. 5.8 the missing element is revealed and the ratio I_m/I_e is about 4, as predicted at the end of the paragraph containing equation (5.21).

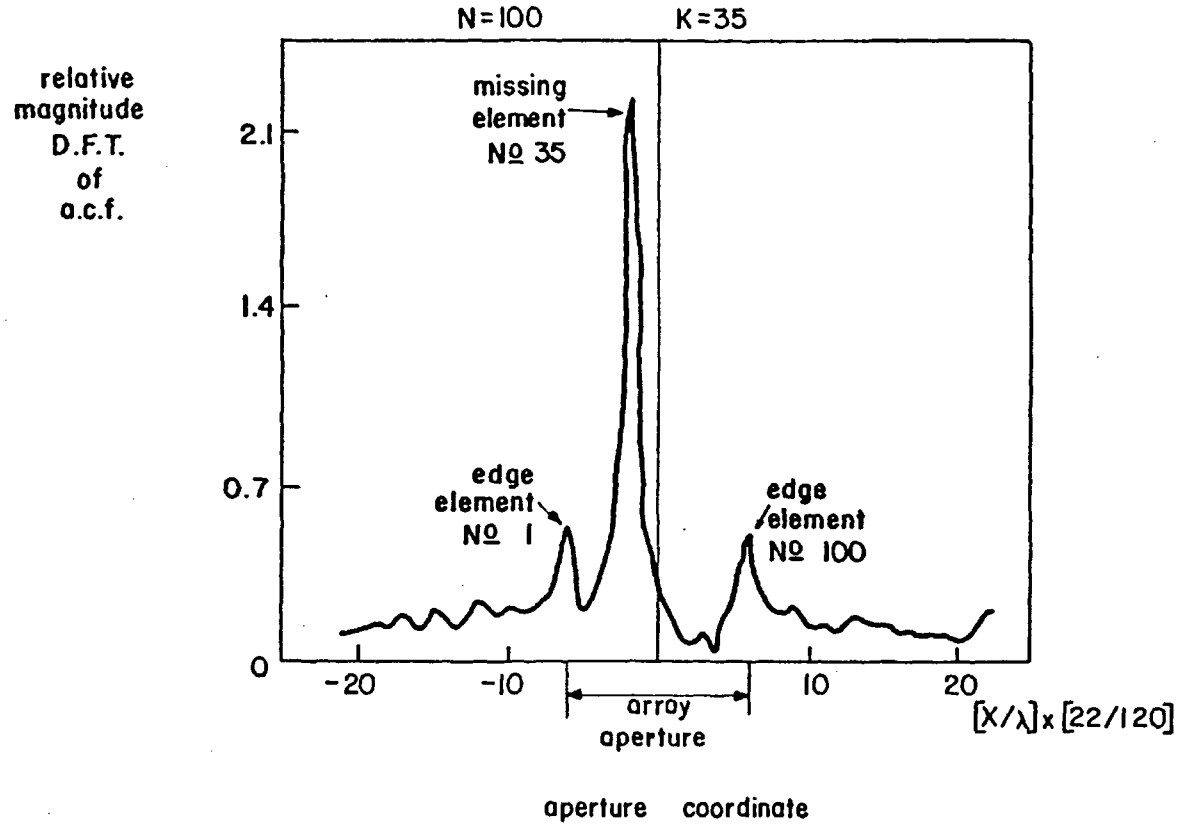


Fig.5.8 Simulation of detection of a missing element by the autocorrelation function method.

5.4 Discussion

The three methods suggested so far, the subtraction method, the angular spectrum method and the autocorrelation function method (a.c.f.), have all been shown to be capable of detecting defective elements in antenna arrays. The preferred region of monitoring has been demonstrated to be in the side-lobe region for all three methods.

In comparing the methods, the subtraction method uses the phase variation of the far-field substitute element to determine a defective element, employing a simple linear equation. The angular spectrum method, however, uses the relation between the far field, the angular spectrum function and the aperture field to yield the aperture illumination modified by the presence of defects in the array. However, the method requires the computation of a Fourier transform of the angular spectrum, which complicates the processing in comparison with the subtraction method. The a.c.f. of the angular spectrum makes further use of the angular spectrum concept. Using the a.c.f. method the aperture power illumination is determined, which when modified by the presence of defective elements can be used to resolve defects in the array. The a.c.f. method is expected to give superior results compared to the angular spectrum method, due to its properties of smoothing the data, as already explained. However, this advantage is at the cost of additional computation of the a.c.f., which makes this method more demanding from the processing aspect.

The subtraction method is particularly appropriate for the detection of a single defective element in the array. As

explained, it can also be used in the case of many defective elements provided defects do not occur in more than one element at a time. This assumption is justified by the expected high reliability of present and future solid-state phased-array antennas. The other two methods can be used for a single as well as for many simultaneous defects, but at the cost of more computational complexity than the subtraction method.

For systems like the MLS where real time processing is needed it seems that the subtraction method is the only one that is adequate. However, for maintenance purposes or where longer delays can be tolerated, a combination of two or even of all three methods is recommended.

This chapter concludes the analysis of far-field monitoring methods. Near-field methods will be discussed next.

CHAPTER 6

MONITORING IN THE NEAR FIELD

In the previous chapters far-field analysis was used in the main for the derivation of the recommended methods of monitoring, as normally the antenna array is to perform in the far-field. However, to minimize uncontrolled multipath effects between the transmitter and the monitor antenna, a near-by positioning of the monitor antenna is most favorable, provided measurements can be processed to overcome the inevitable defocusing effects. The present chapter is therefore concerned with near-field analysis for the derivation of further monitoring applications.

This chapter deals with the two aspects of near field monitoring. The first is concerned mainly with monitoring of the array main beam pointing, and the second with the application of the monitoring techniques described earlier to very near field monitoring. The first part of this chapter is dealing with monitor antenna focusing for the monitoring of main beam pointing, based on the properties of Fresnel integrals [25]. These are followed by simulation experiments with a near field monitoring antenna. The last part of this chapter will describe an internal/integral monitoring technique based on a beam forming network of the Blass [29] type.

6.1 A focused near field monitoring antenna

The technique of focusing a transmitter antenna into the near zone, to determine its far field pattern, is widely used [3]. However this technique requires modification of the

transmitting array phase excitation from linear to parabolic. This means a monitoring in real time, which is not practical in some cases, such as MLS. The present section is concerned with the problem of monitor antenna focusing without the need to modify the transmitting antenna phase excitation, and hence enabling real-time main-beam monitoring on a non-interference basis. The analysis is based on the Fresnel diffraction formula which gives the field in the radiating near zone. A technique is specified and examined with simulation on the computer.

6.1.1 Fresnel diffraction in the near-field

Consider the system in Fig. 6.1.

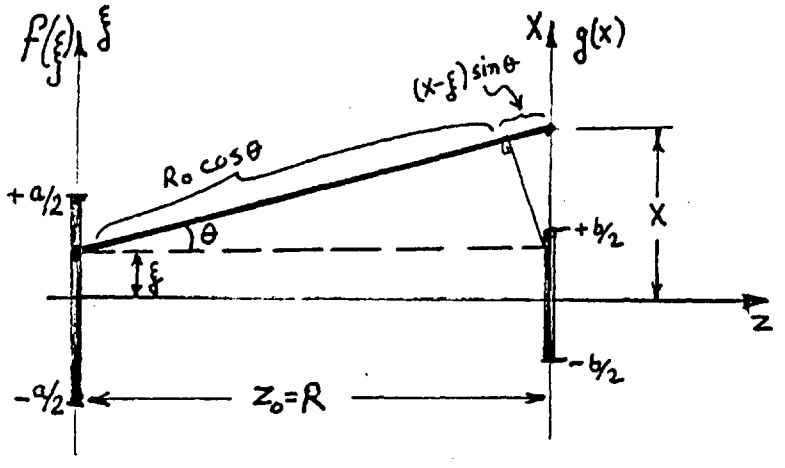


Fig. 6.1 The geometry of near field monitoring

The aperture field distribution $f(\xi)$ of the transmitting antenna, assumed to be composed of y-polarized dipoles, hence is isotropic in θ, extends over the aperture a. The monitoring antenna of aperture b is parallel to the transmitting antenna, is assumed to have the same polarization, and senses the field distribution g(x) diffracted from the transmitting antenna. The parabolic phase approximation is assumed. Hence,

$$s=\sin\theta,\quad c=\cos\theta=(1-\sin^2\theta)^{1/2}\simeq 1-\tfrac{1}{2}s^2 \tag{6.1}$$

The signal V received by the monitor antenna is given by

$$V=\int_{-b/2}^{b/2} g(x)\,dx \tag{6.2}$$

where the received field distribution g(x) is

$$\begin{aligned} g(x)&=E_y(x,R)\\ &=\exp\{-jkR\}\exp\{-jkx^2/2R\}(j/\lambda R)^{1/2}\int_{-\infty}^{\infty} f(\xi)\exp\{jk(\tfrac{x}{R}\xi-\tfrac{\xi^2}{2R})\}d\xi \end{aligned} \tag{6.3}$$

as described in section 5.1.

Assume now that the transmitting antenna is of uniform illumination f(0), and has a linear phase scan corresponding to propagation in the direction s. Hence

$$f(\xi)=f(0)\exp\{-jks\xi\} \tag{6.4}$$

Designating the integral of equation (6.3)

$$\begin{aligned} g'(x)&=\int_{-a/2}^{a/2} f(\xi)\exp\{jk(\tfrac{x}{R}\xi-\tfrac{\xi^2}{2R})\}d\xi\\ &=f(0)\int_{-a/2}^{a/2}\exp\{jk[(\tfrac{x}{R}-s)\xi-\tfrac{\xi^2}{2R}]\}d\xi \end{aligned} \tag{6.5}$$

This integral can be evaluated in terms of Fresnel integrals [25], after completing squares. Hence

$$\begin{aligned} g'(x)=\exp\{jk\tfrac{R}{2}(s-\tfrac{x}{R})^2\}\{&\mathcal{F}[\sqrt{\tfrac{2}{R\lambda}}\tfrac{a}{2}+\sqrt{2\tfrac{R}{\lambda}}(s-\tfrac{x}{R})]+\\ &+\mathcal{F}[\sqrt{\tfrac{2}{R\lambda}}\tfrac{a}{2}-\sqrt{2\tfrac{R}{\lambda}}(s-\tfrac{x}{R})]\} \end{aligned} \tag{6.6}$$

where $\mathcal{F}[\ ]$ is the Fresnel integral. The implication of this formula will now be examined.

6.1.2 Several properties of the Fresnel integral and the recommended monitoring technique

The expression of equation (6.6) is composed of the product of two terms: the phase term and the Fresnel integral term.

The Fresnel integral term Fl, is given by

$$Fl=\{\int_{H}[\cdots+\cdots]+\int_{H}[\cdots-\cdots]\}\ . \qquad (6.7)$$

The phase term Pl, is given by

$$Pl=\exp\{jk\frac{R}{2}(s-\frac{x}{R})^2\}\ . \qquad (6.8)$$

opening first the brackets in the phase term we get

$$Pl=\exp\{\underset{(I)}{jk\frac{R}{2}s^2}+\underset{(II)}{jk\frac{x^2}{2R}}-\underset{(III)}{jkxs}\} \qquad (6.9)$$

The first term (I) of equation (6.9) is dependent on s^2 but is independent of x.

The second term (II) is the parabolic phase term which is independent of s. However it is cancelled by the parabolic phase term outside the integral in equation (6.3).

The third term (III) is a typical expression for the phase term of a linear phase scanned antenna to an angle $s=\sin\theta$.

If for a moment the term Fl, equation (6.7), is assumed to be approximately constant (which will be justified later), the following recommendation could have been stated:
based on the above discussion it will be possible to get the approximate far-field main-beam width of the transmitting antenna, if the monitoring antenna has the following characteristics.

1) The length of the monitoring antenna is equal to the transmitting antenna,

$|x_{max}|=a/2$.

2) A linear response to the field g(x) is assumed.

With the above assumptions the received signal V which will be the integral, equation (6.2), of this modified phase term performed over $|x|\leqslant b/2$ will result in

$$V=C\int_{-b/2}^{b/2}\exp\{-jkxs\}dx$$

where C is a constant, hence

$$V=Cb\frac{\sin(\frac{1}{2}kbs)}{\frac{1}{2}kbs} \qquad (6.10)$$

Putting b=a according to our assumption gives,

$$V=Ca\frac{\sin(\frac{1}{2}kas)}{\frac{1}{2}kas} \qquad (6.10a)$$

It should be emphasized that s in these expressions is the pointing direction cosine, s_p say, of the main antenna. The pointing s_p can thus be determined, since λ and b are known.

It now remains to discuss our first assumption that has not been justified yet, of supposing that Fl of equation (6.7) is approximately a constant.

The asymptotic value of the Fresnel integral $\mathcal{F}(v)$, as $v\to\infty$, is [13,24]

$$\mathcal{F}(v)\simeq (1-j)-\frac{1}{j\pi v}\exp\{-j\frac{\pi v^2}{2}\} \qquad (6.11)$$

The behaviour of the Fresnel integral for a large positive argument is therefore of small oscillations which are inversly

proportional to the (πv), where v is the argument. The period of the oscillations is $v^2/4$. The phase has a similiar behaviour: it oscillates around the asymptotic value of $-\frac{3}{4}\pi$ with decreasing phase proportional to ($\pi v^2/2$). For values of v larger than o.5 the amplitude oscillations are less than about 2.5 db. The phase magnitude oscillation is about 15 degrees or less, for arguments ≥ 1. For a value of $v \geq 0.5$ this phase magnitude could reach about 40 degrees. The numerical values are given in Fig. 6.2.

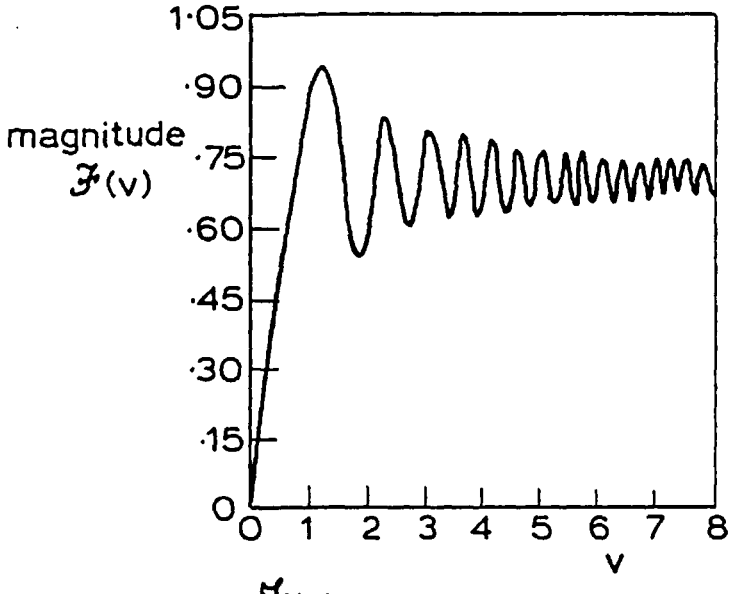


Fig. 6.2a Magnitude of $\mathcal{F}(v)$

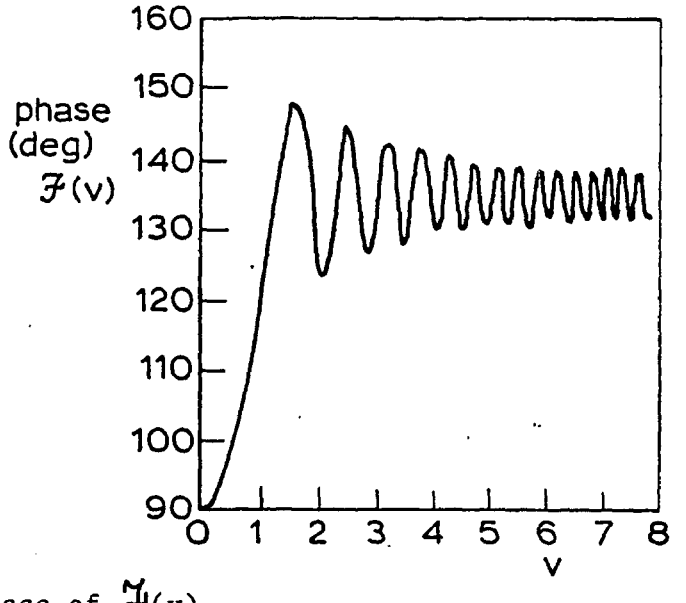


Fig. 6.2b Phase of $\mathcal{F}(v)$

Fig. 6.2 The Fresnel integral magnitude and phase

The discussion so far on the properties of the Fresnel integral might be summarized as follows:

The Fresnel integral could be approximated by its asymptotic phase

and magnitude values, with errors of

~2db and ~15 degrees

(or 40deg if arguments$\geq$0.5 are sought).

The term F1 of equation (6.7) which is a difference of two Fresnel integrals shifted by the argument value of

$$\pm\sqrt{\frac{2}{R\lambda}}\, a/2 \qquad (6.12)$$

could similiarly be approximated by a step function of magnitude and phase extended parallel and over the approximate edges of the radiating aperture. This approximation to the term F1 holds for cases of R~a or where R is a small multiple (or subdivision) of the aperture a, and where $a/\lambda >> 1$ which is adequate for the MLS phased arrays.

This concludes the discussion on the technique recommended for monitoring the main-beam of uniformly illuminated scanning arrays. One possible implementation of the monitoring system is sketched in Fig. 6.3.

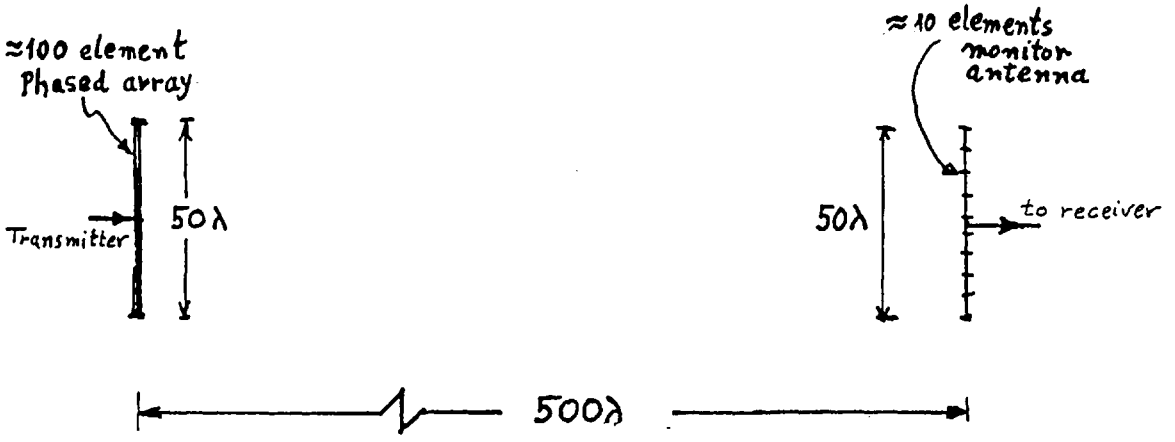


Fig. 6.3 The geometry of main-beam near-field monitoring

6.1.3 The near field monitoring technique

Summarizing, a technique for near field (Fresnel region) monitoring of the main beam pointing of an array has been proposed. The technique, based on approximations to Fresnel integrals is a simple one, it consists of a uniformly illuminated monitor antenna positioned in parallel with the transmitting antenna. It has been shown that the radiated beam is focused with no necessity of changing its illumination phase function. No additional transformations are required beyond the linear response to signals of the sampling elements which are sparsely distributed over the monitoring aperture (see Fig. 6.3). A numerical confirmation of the method will be described next.

6.2 Simulation experiments with a near-field monitoring antenna

Aperture fields $f(\xi)$, over the transmitting antenna of width a, of uniform, half-cosine, raised cosine over a pedestal and half-sine form were tested. The Fresnel field over the plane

of observation (see Fig. 6.3), a distance R from the transmitting antenna, was simulated for aperture fields

$$f(\xi)\exp\{-jks_\rho\xi\}$$

Which is the basic aperture field $f(\xi)$ with a linear phase superimposed in order that it will radiate in the direction making an angle $\sin^{-1} s_\rho$ to the transmitting aperture.

The Fresnel field is then sampled at points seperated by Δx along a line of length b, parallel to the aperture plane. A rough idea of the required sample spacing can be obtained from equation (5.16) with $s_{max} \sim 5\lambda/a$, say, which gives $\Delta x \sim a/10$. In the following simulations the spacing was varied between a/6 and a/99 (i.e., between 7 and 100 sampling elements).

The width of the linear transmitting phased-array antenna was kept constant at $a=50\lambda$. The width b of the monitoring antenna and its distance R were varied.

A comparison of equations (6.8) and (6.9) shows that a replica of the transmitted far-field beam shape is reproduced in the monitor antenna when choosing its aperture b=a. However due to the nature of Fresnel diffraction a sharp (exponential) decrease is expected for fields in $|x|>a/2$. Hence choosing b>a is expected to measure main-beam shape and first side-lobes with reasonable precision. The wider the monitor antenna aperture the larger amount of the field radiated into wider direction cosine is intercepted. Hence a better reconstruction of the focused beam for farther side-lobes is expected. This last assumption is also left to be confirmed by the simulation experiments.

The numerical simulation uses the cosine and sine integrals available as computer NAG library functions S20ADF and S20ACF. These are used in the precise evaluation of the Fresnel integrals in their complex form

$$\mathcal{F}\{v\}=C(v)-jS(v)$$

where $\mathcal{F}\{v\}$ is the Fresnel integral, and C(v) and S(v) are the cosine and sine Fresnel integrals which are widely tabulated [25].

6.2.1 Uniform transmitting antenna aperture field

In the simulation the focused near-field and the far-field normalized patterns of a 50λ transmitting aperture are calculated. To aid comparison a 10db constant magnitude-ratio is added to the near field pattern in the figures. The far-field pattern is generated from the expected sinc function. The near field (focused) pattern is dependent on R/a the distance to aperture ratio, and N the number of isotropic sampling elements equispaced over a planar monitoring aperture. The superposition of these N signals results in the near field reconstruction of the far-field main-beam pattern. Samples of the simulation results are given in Figs 6.4 to 6.9, the near-field patterns are shown as the upper pattern in each simulation, with the 10db added artificially.

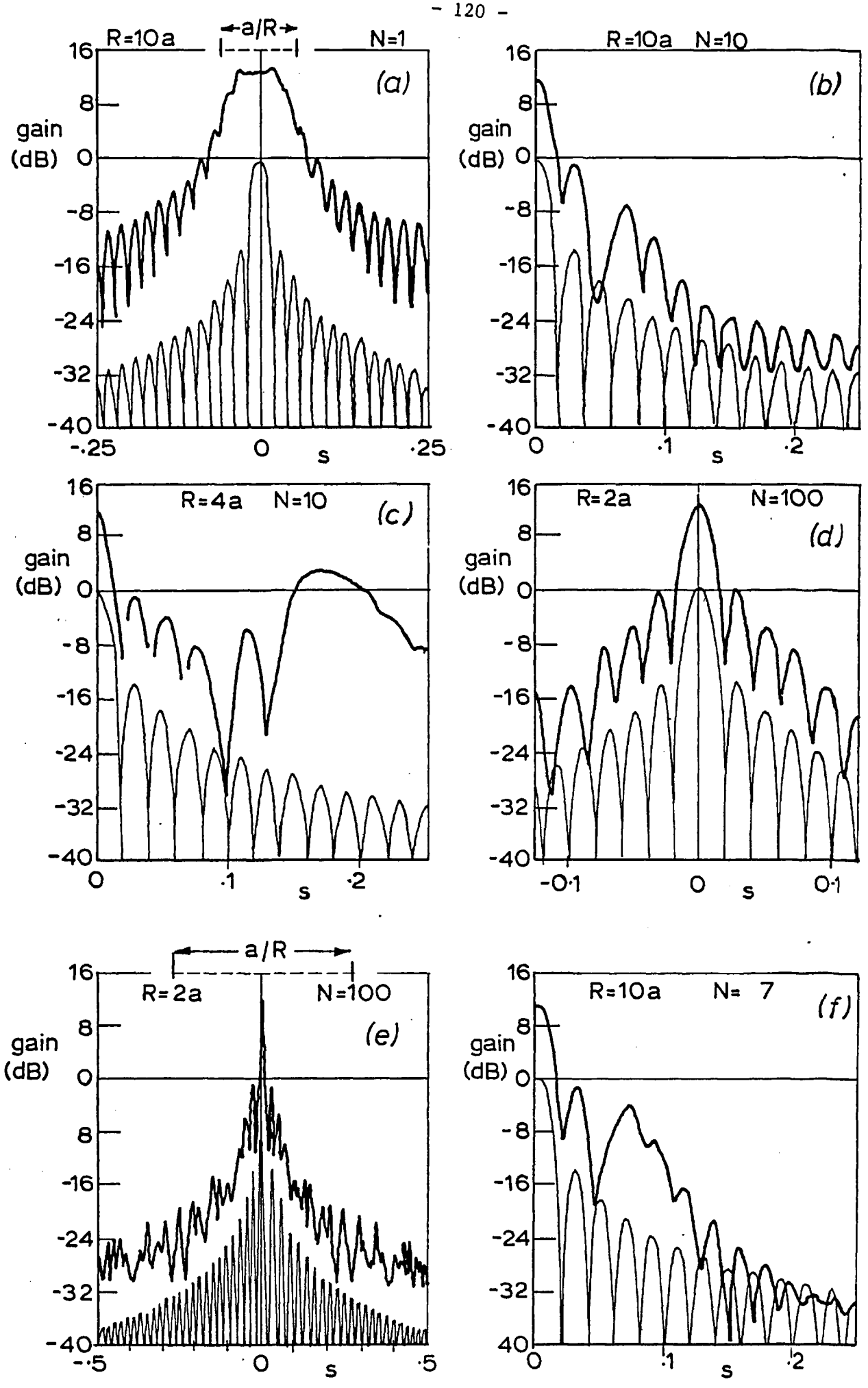


Fig.6.4 Computer simulation of near field monitoring uniform illumination.

In Fig. 6.4a R/a=10 which is one tenth of the Rayleigh distance ($R = 2a^2/\lambda$), and N=1, i.e., the signal received is given by the normalized magnitude of the Fresnel integral with no corrections. Two areas are noticed in the near-field; the on-axis region where most of the radiated energy is concentrated giving an almost constant magnitude over 3 to 4 beam-widths in the region parallel to the radiating aperture designated by |----------| on the graph. The other region is in the side-lobe region which becomes pronounced and more like the far-field side-lobe region, as the scan angle increases.

In Fig. 6.4b with the same R/a=10 as before, the near field is sampled over ten isotropic elements, (N=10), equispaced about 5.5λ apart, over a parallel planar aperture. It is noticed that the reconstructed main-beam now resembles the far field main-beam up to about the 10 db point. A better than 0.5 db difference is achieved up to the 3 db points, and up to 2 db difference is achieved up to the 10 db points.

In Fig. 6.4c with R/a=4 keeping the same number of sampling elements the main beam is still reconstructed properly, but a grating lobe starts to be pronounced (at $s \simeq .175$) as anticipated. This is due to the fact that x was arbitrarily chosen to be about 5λ, therefore s_{max} is limited roughly to $s_{max} \sim 1/10$ (for $a=50\lambda$). Hence (ambiguous) reconstruction of grating lobes can be produced for s>smax. The maximum value for these grating lobes depends on the side lobe level (peaks) and the number of sampling elements used. For example, for 10 sampling elements the grating lobe is expected to be about 20 db higher than the side lobe level monitored by a single sampling element

(see Fig. 6.4a), which is very close to the value noticed on the graph.

In Fig. 6.4d and 6.4e a further decrease is used in the distance of the monitor antenna, now at R/a=2. But, a N=100 elements is used for sampling, hence the grating lobe in Fig. 6.4c, now disappeared. The wide scanning angle is shown in Fig. 6.4e while the main-beam region is shown in Fig. 6.4d.

In Fig. 6.4f The R/a=10 value as in Fig. 6.4b are used but now with a reduced number of sampling elements N=7. The result seems to be quite practical as the grating lobe (in $s \sim 0.07$) is only 2--3 db above the side-lobe level. However, the main beam is reproduced quite well. The small number of sampling elements used in the last example show the potential feasibility of a practical monitoring antenna.

As explained earlier, it is expected (arguing heuristically) that the wider the receiving aperture the better the reproduction of the focused main-beam and first side-lobes. A demonstration of the "performance" of the monitor antenna for various b/a aperture ratios, from 0.8 to 3, is given in Figs. 6.5a to f.

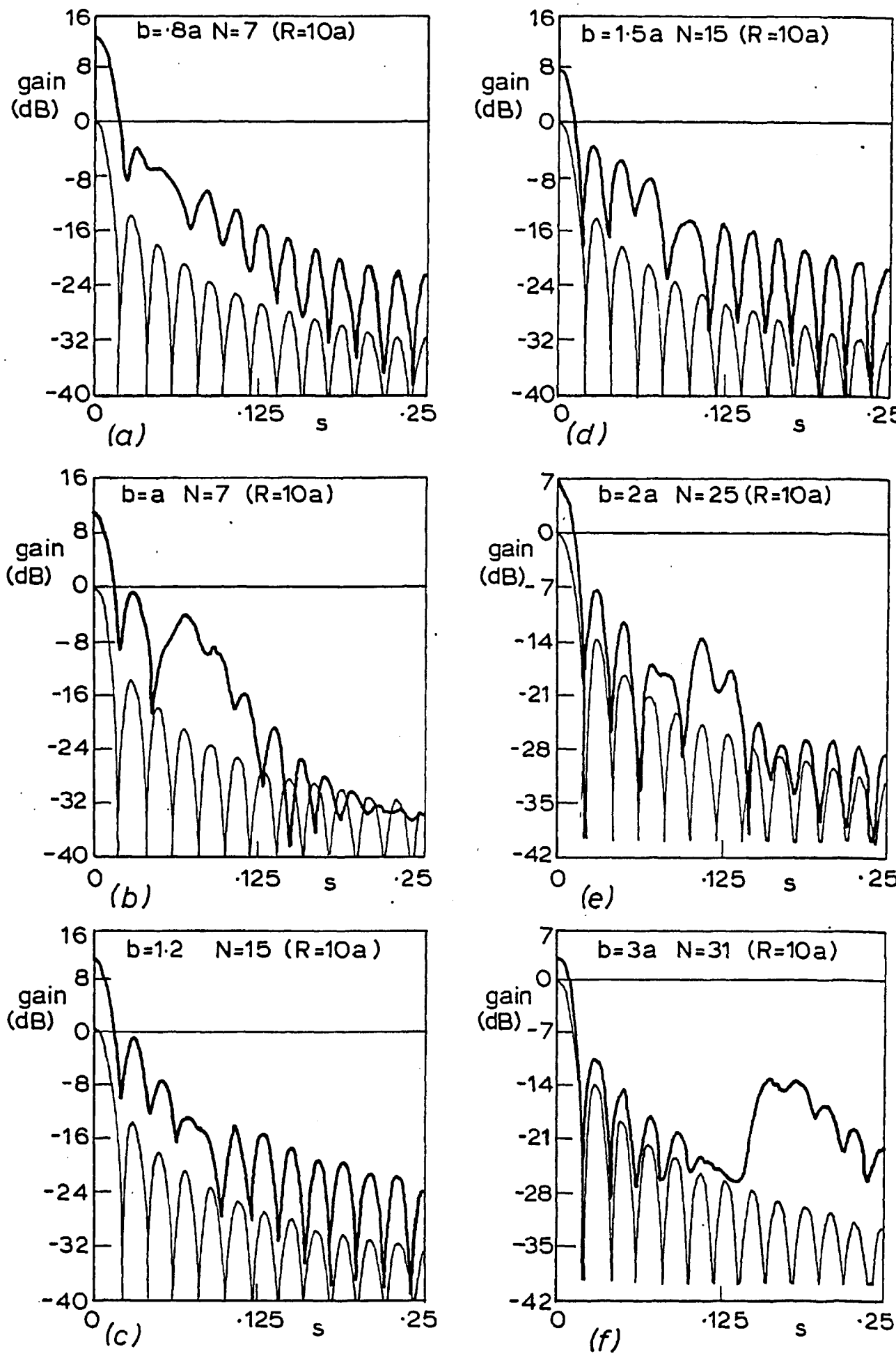


Fig.6.5 Simulation of near field monitoring uniform illumination: $0.8 \leqslant b/a \leqslant 3$.

Figs. 6.5a to f show the results for the focused beam and the first side-lobes, for various values of b/a. It is seen that for b$\geq$a (fig. 6.5b to f) the focused main beam is reasonably similar in shape to the far-field beam. However for b=0.8a in Fig. 6.5a the main beam slope is reproduced less faithfully than in the previous cases (b$\geq$a). Checking the focused first side lobes it is clearly seen that the wider the monitor antenna aperture the better the reconstruction of additional side-lobes. This means that the resolution between main lobe and first side-lobes is improved for wider apertures, which was to be expected intuitively.

The simulation of near field focusing of uniformly illuminated apertures has shown some promising results. The focused main-beam shape has been reproduced quite faithfully for monitor apertures equal to or larger than the radiating antenna aperture. This, while only a few sampling elements have been used for monitoring. it now remains to show that the uniform illumination function is not a singular case where this method can be applied. Hence, other practical illumination functions will be examined in a similar way. These will be the half cosine and the sine (i.e., monopulse). As explained earlier almost any wanted illumination can be decomposed into a series of uniform, cosine and sine illumination functions. A demonstration of a useful illumination function, the cosine square over a pedestal [23] will be given later based on such a decomposition. First the half cosine will be examined next.

6.2.2 Half-cosine aperture field

Following similar stages to those used in deriving

equations (6.2) to (6.5), the diffraction field of a cosine aperture illuminated scanning antenna can be shown to be equal to;

$$g(x)=\exp\{-jkR\}\exp\{-j\frac{kx^2}{2R}\}I(s) \qquad (6.13)$$

The term I(s) is given by

$$I(s)=\int_{-a/2}^{a/2}[\exp\{+j\frac{\pi}{a}\xi\}+\exp\{-j\frac{\pi}{a}\xi\}]\exp\{-j\frac{k\xi^2}{2R}\}\exp\{jks\xi\}d\xi \; . \qquad (6.14)$$

Where I(s) the normalized near field over the z axis. The far-field will be derived after ignoring the parabolic phase term in (6.14). Hence,

$$I(s)_{\infty}=\int_{-a/2}^{a/2}[\exp\{+j\frac{\pi}{a}\xi\}+\exp\{-j\frac{\pi}{a}\xi\}]\exp\{jks\xi\}\,d\xi \qquad (6.15)$$

where $I(s)_{\infty}$ the far-field normalized field pattern. It can be shown that the far field is given by

$$I(s)_{\infty} \propto \frac{\cos(\frac{\pi as}{\lambda})}{(\pi/2)^2-(\pi as/\lambda)^2} \qquad (6.16)$$

This expression will now be used for comparison with the reproduced far -field pattern, described below. Approximations to equation 6.15 have been derived in a similar way to those derived previously for uniform illumination. This analysis is represented in appendix D. The results may be summarized as follows:

The cosine illumination leads to the production of two functions which can be approximated to yield the normalized field over the monitoring aperture as :

$$\exp\{j\pi(-\frac{2sx}{\lambda})\}\cos[\pi(-\frac{sR}{a}+\frac{x}{a})] \qquad (6.17)$$

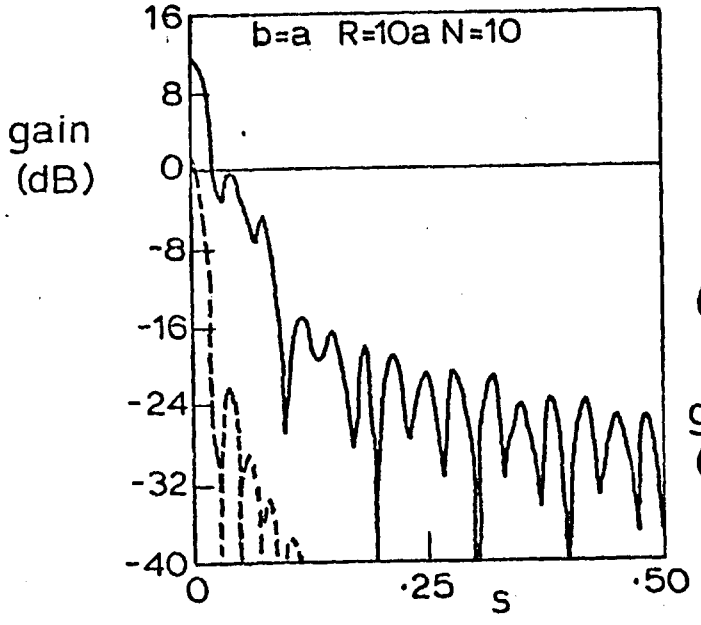
This should be integrated over $-b/2<x<b/2$ to yield the monitoring signal. This is to be compared with the integrand of the far

field expression which is of the form

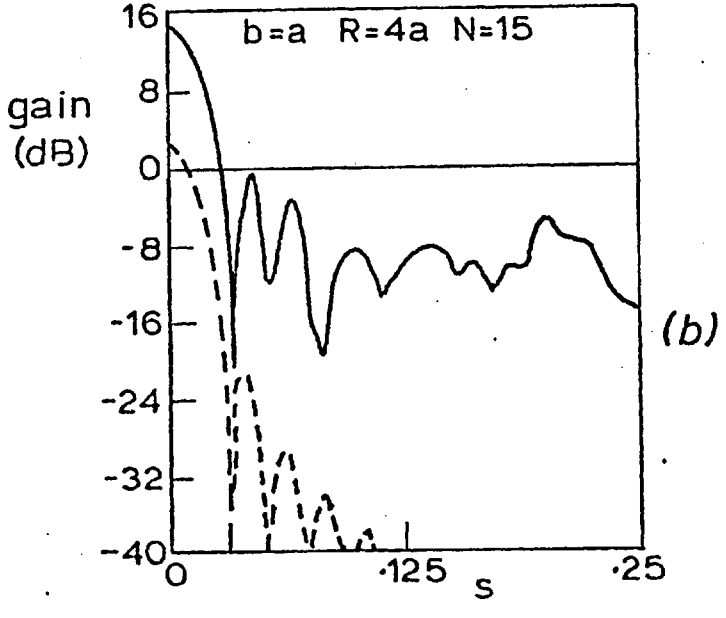
$$\exp\{j\pi(-2\frac{sx}{\lambda})\}\cos(\frac{\pi x}{a}). \qquad (6.18)$$

The term $\pi sR/a$ (in equation (6.17)) is therefore causing the difference between the expression for the "correct" far field and that approximated using the focusing technique. This additional term can be ignored for $s \to 0$ (i.e., the main beam direction) provided R/a is not large (i.e. $R/a \lesssim 1$). With this additional restriction the monitoring system described earlier for the uniform illumination (Fig. 6.3) will also be adequate for the half-cosine illumination.

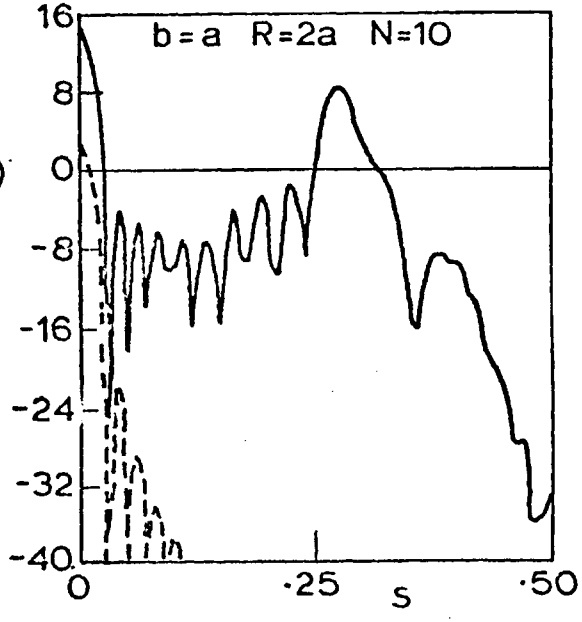
Simulation results are given in Fig. 6.6.



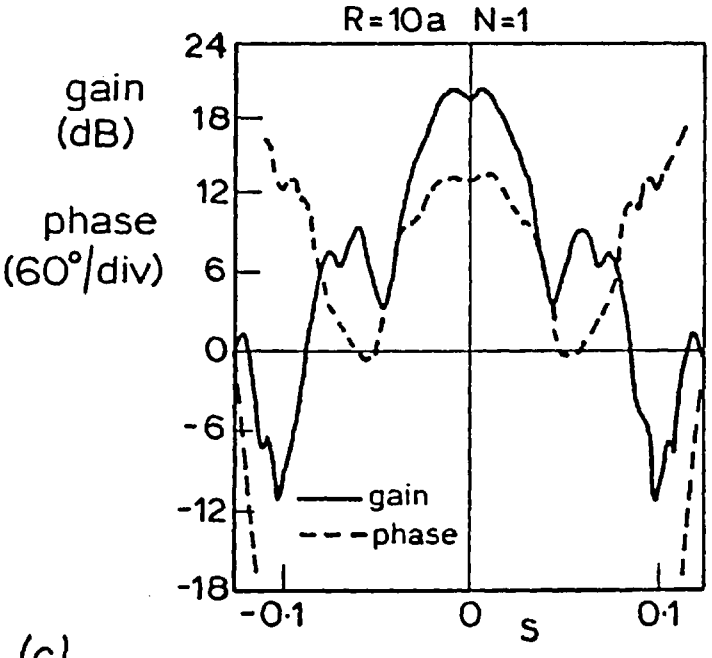
(a)



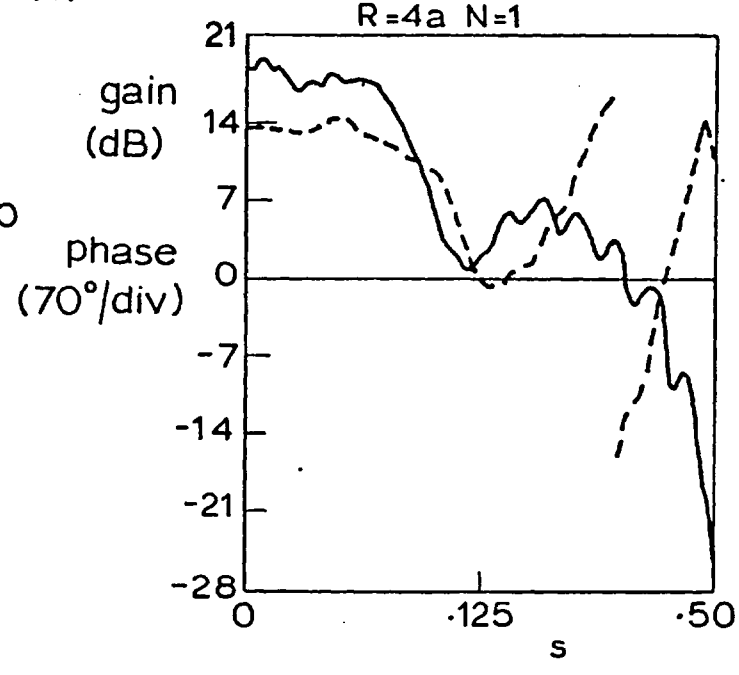
(b)



(c)



(d)



(e)

Fig.6.6 Simulation of near-field monitoring, cosine illumination.

Fig. 6.6 a,b,c describe the following simulation results:

$a=50\lambda$ transmitting antenna. R/a distance ratios of 10, 4, 2. Reception with 10-15 sampling elements equispaced over the monitor antenna aperture. The following points should be noted:

1) The accuracy of reproducing the main-beam is improved the closer the monitor and receiving antennas are located.

Example, the -2 db points are within 0.17 db at all 3 distances. However the -9.5 db points are within 0.7 db for R/a=2, within 1.8 db for R/a=4, and within 4.5 db for R/a=10.

2) However, due to the finite number of samples, interelement spacing (of almost 3.5λ) grating lobes start to appear at the closer seperations. Hence the side-lobes are improved with increasing R/a, as expected.

From points (1) and (2), optimal value could be achieved for the monitoring system, if adequate weights are given to the above parameters. The phase and magnitude expected to be received in a single element monitor antenna, are given in Figs. 6.6d and 6.6e. This justifies the previous assumption, that the changes in amplitude and phase due to the four Fresnel integral terms are comparatively small.

In all the simulations of Fig. 6.6 use has been made of available computer NAG-Routines for the evaluation of all four Fresnel integrals arising from equation (6.14) (see Appendix D).

The results so far show that both aperture illuminations investigated, namely, the uniform and the cosine, enable near field reconstruction of the far-field main-beam scanning patterns.

Both illumination functions may use the same type of monitoring system. The relatively small amount of sampling elements needed for monitoring makes the monitoring technique an attractive one.

In the following subsections the sine and cosine square over pedestal illuminations will be investigated and simulation results presented.

6.2.3 Sine aperture field

Following the previous stages for the cosine illuminated aperture, the sine function will follow. Use will be made of results obtained previously.

A sine aperture illuminated scanning antenna can be shown to be equal to:

$$I(s)=\int_{-a/2}^{a/2}\left[\exp(+j\frac{\pi}{a}\xi)-\exp(-j\frac{\pi}{a}\xi)\right]\exp(-j\frac{k\,\xi^2}{2R})\,\exp(jks\xi)\,d\xi \qquad (6.19)$$

which is similiar to equation (6.14) but with a minus sign for the second term in [ ]. The far field is given by:

$$I(s)\underset{\infty}{\propto}\frac{\frac{\pi as}{\lambda}\cos\left(\frac{\pi as}{\lambda}\right)}{\left(\frac{\pi}{2}\right)^2-\left(\frac{\pi as}{\lambda}\right)^2} \qquad (6.20)$$

This expression has odd symmetry in s, in contrast with the even symmetry in equation (6.16) of the cosine illumination. Hence, a "difference" rather than a "sum" pattern is expected from the sine function.

The analogous equation to (6.17) for the field diffracted over the parabolic phase corrected aperture will be

$$\exp\{j\pi(-\tfrac{2sx}{\lambda})\}\sin[\pi(-\tfrac{sR}{a}+\tfrac{x}{a})] \qquad (6.21)$$

While the far-field, analogous to equation (6.18) will now be

given by

$$\exp\{j\pi(-\frac{2SX}{\lambda})\}\sin(\frac{\pi X}{a}) \qquad (6.22)$$

opening the brackets of the sine function in equation (6.21)

$$\sin\{\pi(-\frac{SR}{a}+\frac{X}{a})\}=-\sin\frac{\pi SR}{a}\cos\frac{\pi X}{a}+\cos\frac{\pi SR}{a}\sin\frac{\pi X}{a} \qquad (6.23)$$

As before for small scanning angles s<<1 hence the first r.h.s. term can be ignored and $\cos(\frac{\pi SR}{a})\rightarrow 1$. Hence we remain with the approximated near field of the form

$$\exp\{j\pi(-\frac{2SX}{\lambda})\ \sin\frac{\pi X}{a} \qquad (6.24)$$

which is the required form as in equation (6.22). Therefore the same recommendation given for monitoring the cosine illuminated aperture apply also to the sine illuminated aperture.

Simulation results are given in Fig. 6.7a,b,c,d.

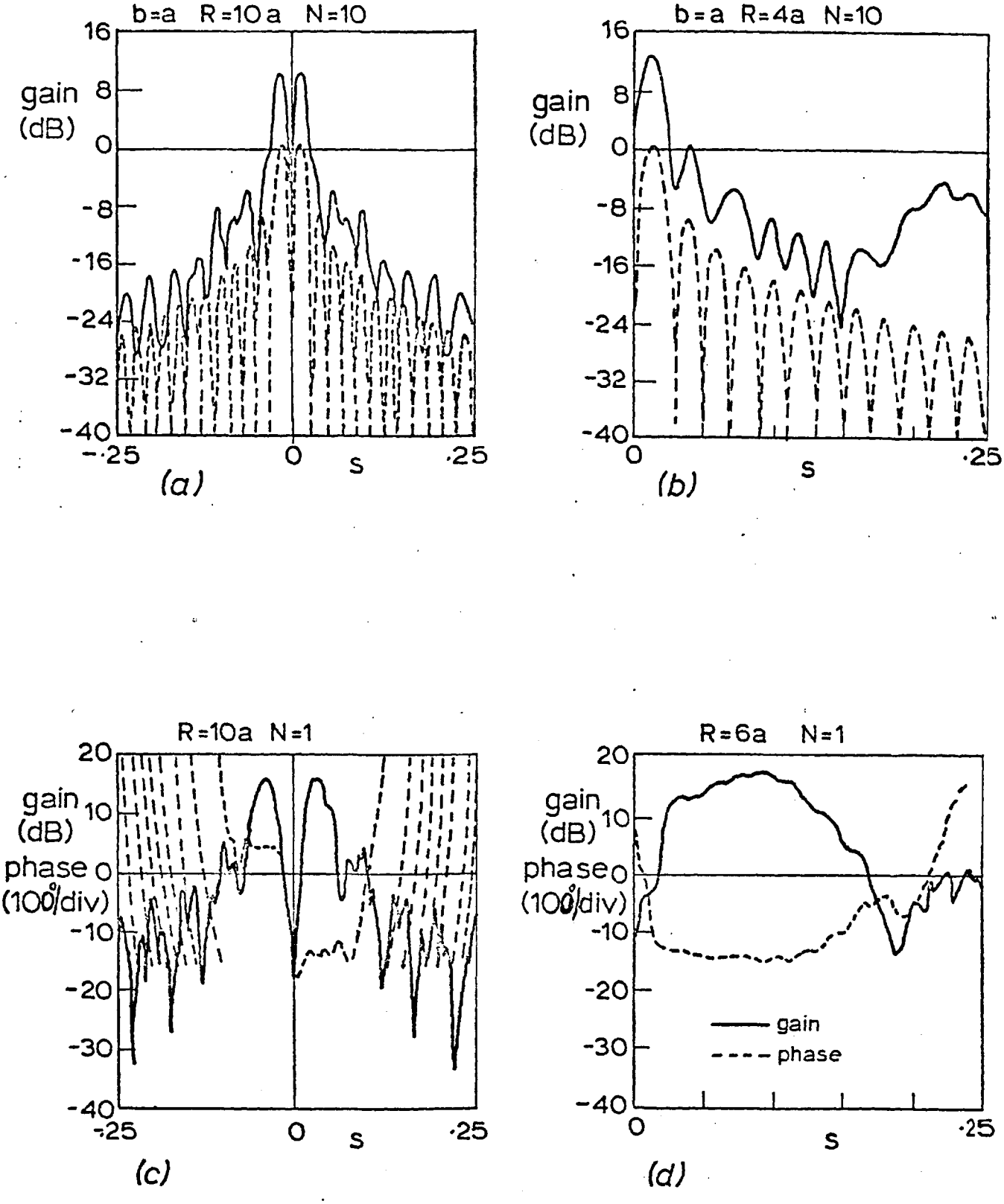


Fig.6.7 Simulation of near field monitoring,

sine illumination.

Fig. 6.7a,b give the following simulation results :

$a=50\lambda$ transmitting aperture.

R/a distance ratios 10 and 4, respectively.

Reception with 15 sampling elements equispaced over the monitoring antenna aperture.

The following results are noted:

1) The reproduced main-beam pointing is more precise with closer receive and transmit antennas. When farther apart the beam tends to squint towards the center (the z axis).

2) The accuracy of the reproduced level is within 0.25 db for the range of -5.1 db (through the peak at 0.0 db) to the -2.0 db point, for R/a=4. While for R/a=10 the accuracy in the same range is reduced to about 1.0 db.

3) Due to the finite number of sampling elements for R/a=4 the grating lobe is about 1 to 2 db higher than for R/a=10, as expected.

The phase and magnitude expected to be received in a single element monitoring antenna are given in Fig. 6.7c and d for R/a=10 and 4, respectively.

The magnitude shows the expected null in the direction s=0 due to the phase inversion. Besides this region the magnitude and phase behave quite smoothly over the region parallel to the transmitting aperture. This justifies the approximations made in the analysis.

Having analayzed the uniform, cosine and sine illumination functions, the practical example of cosine square over pedestal illumination will now be analyzed in the following subsection.

6.2.4 Raised cosine (cosine square over pedestal) aperture illumination

It was proposed by Chignell [23] that a cosine square over pedestal illumination is optimal where the function is given by

$$1/7+6/7\cos^2(\phi) \qquad (6.25)$$

where the argument $\phi=\pi x/a$. The geometrical identity is used

$$\cos^2(\phi)=1/2(1+\cos 2\phi) \qquad (6.26)$$

Therefore the illumination of equation (6.25) could be described by the following expression

$$1/7+6/7[1/2(\cos 2\phi+1)]=4/7+3/7\cos(2\phi)$$

$$=0.5714+0.4286\cos(2\phi) \qquad (6.27)$$

From previous cosine and uniform illumination functions, the present expression is a superposition of the above functions with the weights given by equation (6.27).

Designating I_1 ( ) the uniformly illuminated aperture and I_2 ( ) the cosine(2ϕ) illumination, the following can be written down directly. Attention is drawn to the fact that the cos(2ϕ), rather than cos(ϕ), is now to be used.

The far field given by $I_1(s)$ and $I_2(s)$ are

$$I_1(s) \propto \frac{\sin\pi\left(\frac{2s}{\lambda}\right)\frac{a}{2}}{\pi\left(\frac{2s}{\lambda}\right)\frac{a}{2}} = \frac{\sin(\pi sa/\lambda)}{(\pi sa/\lambda)} \tag{6.28}$$

and

$$\begin{aligned} I_2(s) &\propto \frac{\sin\pi\left(\frac{2s}{\lambda}+\frac{2}{a}\right)a/2}{\left(\frac{2\pi s}{\lambda}+\frac{2\pi}{a}\right)a/2} + \frac{\sin\pi\left(\frac{2s}{\lambda}-\frac{2}{\lambda}\right)\frac{a}{2}}{\left(\frac{2\pi s}{\lambda}-\frac{2\pi}{a}\right)\frac{a}{2}} \\ &= \frac{\sin\pi\left(\frac{sa}{\lambda}+1\right)}{\pi\left(\frac{sa}{\lambda}+1\right)} + \frac{\sin\pi\left(\frac{2s}{\lambda}-1\right)}{\pi\left(\frac{sa}{\lambda}-1\right)} \\ &= \frac{\pi sa}{\lambda}\,\frac{\sin(\pi sa/\lambda)}{\left(\frac{\pi sa}{\lambda}\right)^2-\pi^2} \end{aligned} \tag{6.29}$$

The last expression like that of the sine illumination has an odd symmetry and therefore introduces a null on the direction s=0 (the z-axis). The difference between expressions for cos(ϕ), cos(2ϕ) and sin(ϕ) is evident physically from the difference of illumination, see Fig. 6.8

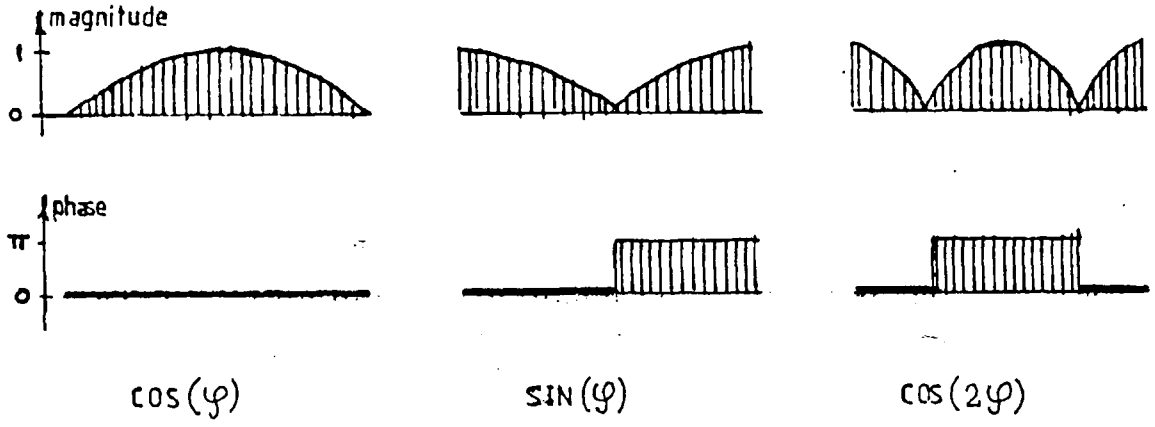


Fig. 6.8 Demonstration of the differences in the three illumination functions $\cos\phi$, $\sin\phi$, $\cos 2\phi$

It is clear from Fig. 6.8 that while the $\sin(\phi)$ and $\cos(2\phi)$ have nulls in the direction s=0 the $\cos(\phi)$ has a maximum in that direction. Designating CF1=0.5714 and CF2=0.4286, we can write the following for the total far-field

$$I(s)=CF1\ I_1(s)+CF2\ I_2(s)$$

$$=CF1\left[\frac{\sin(\pi s a/\lambda)}{(\pi s a/\lambda)}\right]+CF2\left[\frac{\sin\pi\left(\frac{sa}{\lambda}+1\right)}{\pi\left(\frac{sa}{\lambda}+1\right)}+\frac{\sin\pi\left(\frac{sa}{\lambda}-1\right)}{\pi\left(\frac{sa}{\lambda}-1\right)}\right] \qquad (6.30)$$

The near field will be given by the following expressions

$$I_{N1}(s)\propto \exp\{j\pi(s-\tfrac{x}{R})^2\tfrac{R}{\lambda}\}\left[\mathcal{H}\left\{\sqrt{\tfrac{2}{\lambda R}}\tfrac{a}{2}-\tfrac{2(s-\frac{x}{R})}{\lambda}\sqrt{\tfrac{\lambda R}{2}}\right\}+\right.$$

$$\left.+\ \mathcal{H}\left\{\sqrt{\tfrac{2}{\lambda R}}\tfrac{a}{2}+\tfrac{2(s-\frac{x}{R})}{\lambda}\sqrt{\tfrac{\lambda R}{2}}\right\}\right]$$

$$=\exp\{j\pi(\overset{(1)}{\tfrac{s^2R}{\lambda}}+\overset{(2)}{\tfrac{x^2}{\lambda R}}-\overset{(3)}{\tfrac{2sx}{\lambda}})\}\left[\mathcal{H}(\cdot-\cdot)+\mathcal{H}(\cdot+\cdot)\right] \qquad (6.31)$$

and

$$I_{N2}(s)\propto \exp\{j\pi(\overset{(1)}{\tfrac{s^2R}{\lambda}}\pm\overset{(2)}{\tfrac{sR}{a}}+\overset{(3)}{\tfrac{\lambda R}{a^2}}+\overset{(4)}{\tfrac{x^2}{\lambda R}}\mp\overset{(5)}{\tfrac{2x}{a}}-\overset{(6)}{\tfrac{2sx}{\lambda}})\}*$$

$$*\{\mathcal{H}(\cdot-\cdot)+\mathcal{H}(\cdot+\cdot)\} \qquad (6.32)$$

where $I_{N1}(s)$ due to the uniform and $I_{N2}(s)$ due to the $\cos(2\phi)$.

As before, analysis of the effects of the phase terms in the two equations (6.31) and (6.32) will follow

Term (1) in $\exp_{I_{N1}}$ and $\exp_{I_{N2}}$ are equal.

Term (2) of $\exp_{I_{N1}}$ and term (4) of $\exp_{I_{N2}}$ are the parabolic phase terms which are cancelled out as before.

Term (3) of $\exp_{I_{N1}}$ and term (6) of $\exp_{I_{N2}}$ are the linear phase scanned array term.

Terms (2) and (5) of $\exp_{I_{N2}}$ comprise the $\cos\pi(sR/a-2x/a)$ result of the cosine illuminated aperture, but this time the $(\pm 2x/a)$ rather than the $(\pm x/a)$ is used.

Term (3) of $\exp_{I_{N2}}$ is to be included this time due to the fact that it does not appear in $\exp_{I_{N1}}$.

Discussion on the effect of term (3):

Term (3) is introducing additional phase-shift between the linear and the $\cos(2\phi)$ illuminated aperture. It is assumed that its effect is negligible in the near field where

$$\lambda R/a^2 \ll 1 \quad , \text{ given } a \gg \lambda \text{ and } R/a \approx 1 \, . \tag{6.33}$$

Example 1 $a=50\lambda$, $R=a=50\lambda$ and $\lambda=1$, giving $\lambda R/a^2 = 1/50$ hence $\Delta\phi = \pi/50 \approx 3.5$ deg.

Example 2 what is R where this term introduces a π radian phase shift.

Giving $R=100a=5000\lambda$.

The above example only demonstrates why term (3) in $\exp \imath_{N2}$ can be ignored in the near field approximations and simulation.

The simulation results of near field monitoring for cases of R/a=10 and 4 when sampling with 15 elements, is presented in Fig. 6.9 a and b accordingly.

The first point to be noticed is that as with the sine and cosine illumination the closer the distance between transmit and monitoring antenna the better tracking is achieved. While in Fig. 6.9 b there is good tracking between the far field and near field main-lobes, the pattern of Fig. 6.9a is noticeably squinted.

The differences between the near field reconstruction and the far field pattern is about 0.3 db to the 1 db point and 1.2 db to the -2.5 db point in the R/a=4 case. For the R/a=10 case the -2.5 db point gives a larger difference of about 1.9 db as expected.

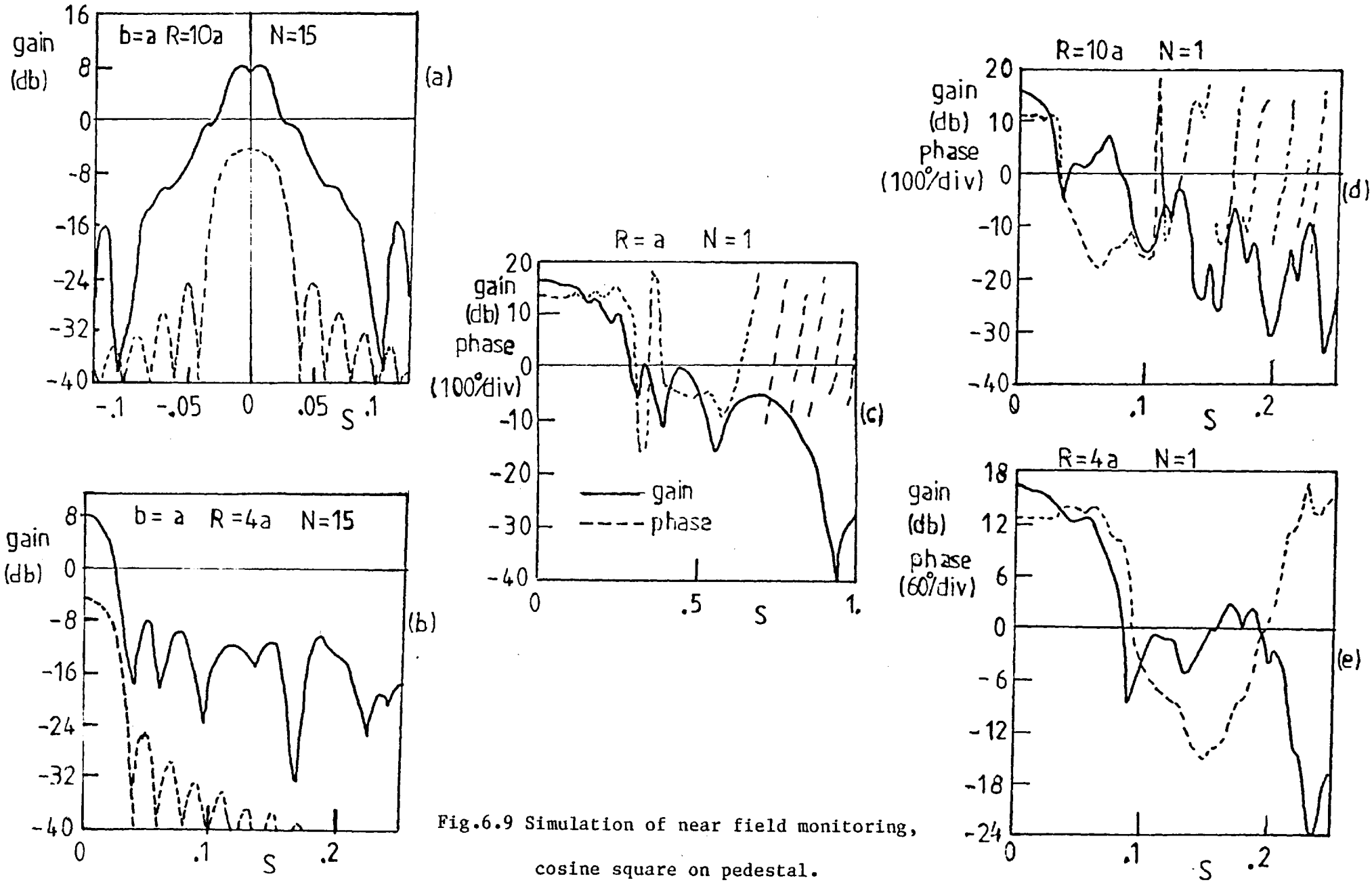


Fig.6.9 Simulation of near field monitoring, cosine square on pedestal.

In Figs. 6.9 c, d and e the magnitude and phase received at the point x=0 of the monitoring aperture is simulated by sampling with a single element on the z-axis. This gives an additional justification for the assumption of almost constant amplitude and phase in the region parallel to the radiating aperture.

6.2.5 Summary of the near-field simulation experiments

Approximations based on the properties of Fresnel integrals led to a proposal of a novel technique for monitoring in the near-field (Fresnel region) of the field radiated from the antenna aperture to yield its far-field pointing and beam shape. The technique is quite simple, it consists of a monitor antenna of the same size, or larger than, the radiating antenna, with only a few sampling elements whose signals are linearly combined, to produce the output signal. This output signal is a reproduction of the far-field main-beam shape.

The first step taken in order to get some confirmation of the idea based on the above approximations was a computer simulation. The technique, based on these approximations could be "tested" against precise representation for the Fresnel integral expressions, using very accurate Computer NAG-Library Functions.

In the simulation various aperture fields were examined, namely, the constant (uniform), 1/2 sine, 1/2 cosine, and cosine, which are the first few basis functions of a complete Fourier analysis of the aperture field.

The output of the simulation was in the form of computer (line printer) graphics which replace (at least in its early

stages) a more precise but difficult analysis or actual experiment. This output was used to asses the technique and to vary the parameters of such a monitoring system, and gives a useful assessment of some of the capabilities and limitations of the proposed technique.

Initial conclusions are:

For a 50λ radiating antenna aperture, the monitor antenna can be placed anywhere from a fraction of an aperture to about 10 apertures. The accuracy of the reproduced beam shape is improved the closer the monitor antenna. However this requires a larger number of sampling elements to avoid excessive grating lobes from being generated in the monitor antenna. No optimization has been made and only "good" engineering sense has used for selecting the number of sampling elements. The effect of increasing the size of the monitoring aperture improves the reproduction of the first side-lobes. However, the unavoidable increase in the number of sampling elements occurs. The following points are to be stressed.

The first is that the technique proposed so far should be regarded as the first steps in putting forward the basic idea. Secondly, that a fuller and more general analysis should eventually be carried out. And thirdly that this type of simulation forms a very valuable substitute (at least in the early stages) for what could be quite a difficult analysis in conventional terms.

Having analyzed the near-field monitoring, the following section deals with a closer distance monitoring technique of

internal/integral monitoring, based in part on the results obtained in the earlier part of this chapter.

6.3 Internal/integral monitoring of phased array antennas

Having dealt with monitoring in the far-field (the Fraunhofer region) and in the near-field (the Fresnel region), the present topic of internal monitoring, can be regarded as monitoring in the very near-field of the antenna.

Internal monitoring may be classified broadly into two main types. One type which involves radiation, although to very short distances, and the other that does not involve radiation. The ultimate concern of internal monitoring as presented in this study is to extend the techniques analyzed so far to apply them to this type of monitoring. Therefore, the direct performance measurements of the individual components of the array, like radiators, phase-shifters, beam switches, etc., are not dealt with here.

The two types of sampling, one external and the other internal to the radiating aperture, will be described in the following subsections.

6.3.1 Sampling the aperture field of the array

From the presentation of the Huygens-Fresnel diffraction analysis, in the previous section, it is clear that sampling the field at a very short distance from the aperture, $R/a \ll 1$ this field is only negligibly different from the aperture field. Hence the far-field pattern can be obtained, using the angular spectrum concept, as the inverse Fourier transform of this aperture field.

For practical implementation, it is only necessary to sample the aperture field with the number of samples that comply with Nyquist's spatial criterion. As before this number depends on the maximum direction-cosine for which the reconstructed far-field pattern is to be monitored, giving, for a linear antenna, the value of

$$N \geq 2a/\lambda \tag{6.34}$$

where N is the number of equispaced sampling points required, and a/λ is the aperture width measured in wavelengths (for the one dimensional spectrum).

In practice it is necessary to avoid obstruction of the aperture field. Therefore, the idea of mutual-coupling can be used to give the very near-field, using appropriate geometry. The superposition of the above samples will then produce a signal that, if normalized, will represent the far field pattern of the scanning array. In a practical system, the superposition and sampling, could be done with the aid of an equally long and adequately polarized linear array, located parallel and inclined to the aperture of the antenna, thereby eliminating obstruction. As an example, a slot waveguide array mutually coupled to the antenna aperture and mounted, as explained above, could be used, and is shown in Fig. 6.10.

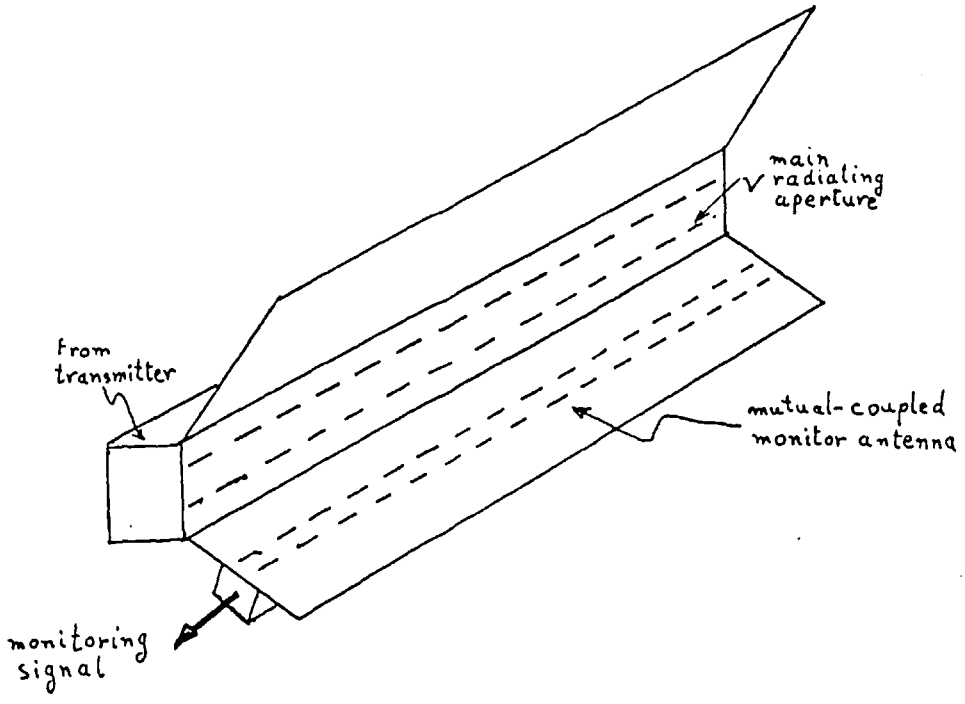


Fig. 6.10 Schematic arrangement for integral monitoring

For a very long array, as in the case of the MLS phased array, edge effects can be ignored and the scanning beam could be monitored. A monitoring of a similar type was proposed by Bendix [4] (see section 1.1), and was supported by an experimental demonstration of the method's capability of reproducing the normalized far-field pattern. The composite signal output from the monitor array will then enable use of the previously described far-field methods for the detection of defects in the array. However, defects due to misalignment of the phased-array structure cannot be detected, as they could be with the real far-field monitoring.

6.3.2 Internal sampling of the radiating elements

An approach which is similiar to the above is to sample the radiating elements or the feed lines to these elements.

As before, superposition of these samples will result in an artificial far-field pattern that has to be normalized. Here radiation is not monitored at all, as the process is completely internal.

One possibility is to use a single beam-forming network of the Blass type [29], which uses a manifold waveguide sampler internally coupled to all the radiating elements. It can be shown that the superposition of these samples will result in a signal that represents the far-field pattern of the scanned phased-array. In the case of a series-fed waveguide manifold coupler (see Fig. 6.11), an additional effect will be, that the main-beam direction is apparently shifted by

$$\sin \theta_o = \lambda_o/\lambda_g \quad . \tag{6.35}$$

Where $\sin\theta$ is the shifted direction-cosine, λ_o the free space wavelength and λ_g the waveguide wavelength of the radiated signal.

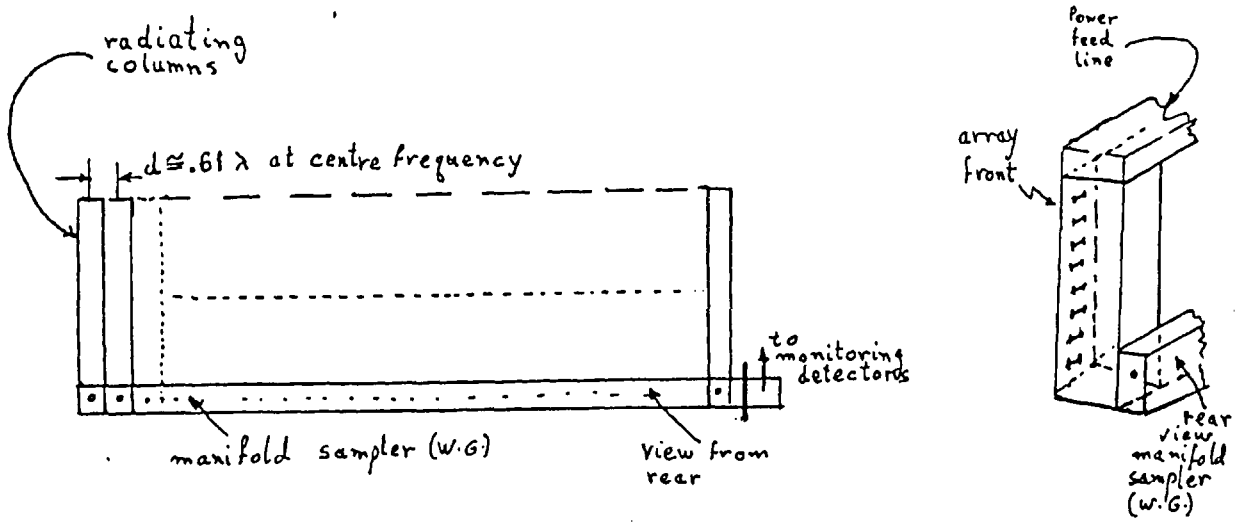


Fig. 6.11 Demonstration of a serial manifold waveguide sampler to be used in the MLS phased-array

Example : For a standard C-band waveguide working in the MLS frequency range, the location of the shifted beam is about 51.5 deg to the boresight. The shift with frequency is given in table 6.1 below.

Table 6.1

The shift of the reproduced main bean in a series manifold waveguide coupler in the frequency band of the MLS

freq. (GHz)	5.031	5.060	5.090
$(f_c/f_o)^2$	0.3925	0.388	0.3833
$[\ 1-(f_c/f_o)^2]$	0.6075	0.612	0.617
$\sin\theta = \lambda_o/\lambda_g = [\ 1-(f_c/f_o)^2\ ]^{\frac{1}{2}}$	0.7794	0.7823	0.7855
θ (deg)	51.206	51.472	51.767

In monitoring of main beam pointing other values of shift angle may be required. As an example, if a special size waveguide (I.D.: 1.27"x0.59", see section 7.1.2) is being used it can be shown that 21.75 rather than the above 51.5 deg will be obtained. Similarly if a XN-band waveguide (a Narda company designation, I.D.: 1.372"x0.622"), is used, then a shift of 33.3 deg is obtained. Also, if sampling slots of "opposite hand" rather than of the "same hand" (which was assumed before) are used, then, very small shifts can be obtained. As an example, if the above special size waveguide with opposite hand slots is used, then, a shift of about 2.9 deg can be obtained. These results will be used in proposing a monitoring system for the MLS, in section 8.5.

According to the above description, either type of internal monitoring scheme could be used in practical applications.

6.4 Discussion

The analysis has so far dealt with monitoring techniques in the near-field and in the very near-field regions of the transmitting antenna aperture.

Near field monitoring

The investigation of near-field monitoring was mainly concerned with the far-field main-beam reconstruction of a scanning array. A technique based on focusing the receiving antenna is suggested as an approximation to the expected far-field scanned main-beam.

Using an approximation to the Fresnel integral and the

spatial sampling Nyquist citerion, a relatively small number of sampling elements on a planar aperture give the required recommendation. It was found that for monitoring a uniformly illuminated aperture size 50λ; ten sampling elements on an aperture seperated a 10 apertures distance from the radiating antenna reproduce the main-beam shape with an accuracy of about 0.5 db to the 3 db points and better than 2 db to the 10db points.

If, however, the far-field far side-lobe pattern is required, an even simpler solution could be used. A single sampling element located at large R/a (distance to aperture ratio) can give a satisfactory answer, at least in the case of a uniformly illuminated aperture (this must be left to be investigated further by a future more precise analysis). It is clear that this method does not need any additional transformation or processing besides the linear combination of the signals sensed by the sampling elements.

Very near-field monitoring (internal monitoring)

The analysis of internal-integral monitoring, although more limited with regard to actual radiation, can give an even better approximation than that of the near-field technique. Here, a good approximation to the far-field main-beam and side-lobe pattern is reconstructed. This is because only a negligible part of the aperture field (edge effects) is ignored. Hence, the recommended technique of sampling the aperture field internally or through the aid of mutual coupling is the answer. This probing could be done using a linear array of sampling elements located in parallel and edequately polarized, of the same length aperture, assuming, of course, that the internally monitored field is

eventually radiated.

Therefore, the far-field techniques analyzed and recommended in the first part of the thesis could successfully be utilized for internal-integral monitoring. The simulation results for a single sampling element in the near field (Fresnel region) show its potential capability to reproduce quite nicely the normalized far-field side-lobe pattern of the radiating antenna (see Fig. 6.4a), hence, if this will be proved to be the case, it could also be used for application of the far-field monitoring techniques in the near-field (Fresnel region) of the antenna.

Incidentally, the simulation on the computer to derive the expected response from a focusing monitor antenna in the near-field (Fresnel region) of the radiating antenna has proved itself to be a useful and cheap replacement for a detailed analyzis (at least in its earlier stages), enabling the user to gain familiarity with, and apreciation of, the advantages and limitations of this monitoring method.

The next chapter is devoted to the experimental investigation to support, where possible, the recommendations and techniques so far suggested. As the investigation was conducted indoors, near-field methods have mainly been used.

CHAPTER 7

EXPERIMENTAL INVESTIGATION

The monitoring theories and their simulation presented up to now need to be tested in practice. The following experimental investigation goes some way towards providing such a test.

7.1 The experimental set-up

7.1.1 The geometry

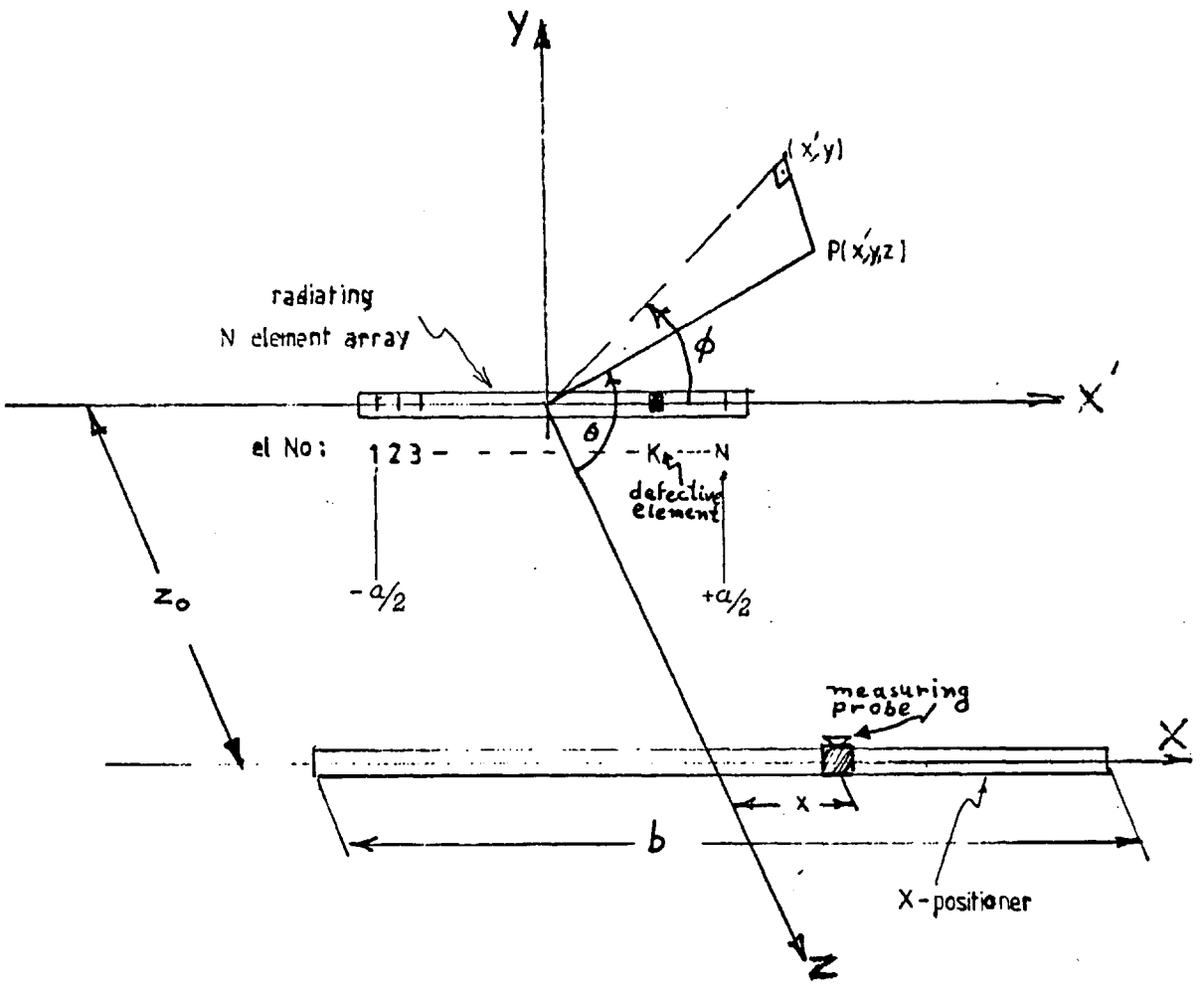


Fig. 7.1 Simplified geometry of the experimental set-up

As shown in Fig.7.1 the linear N-element radiating test array is located along the x'-axis with its aperture, width a, symmetrical about the y-axis. The input to the array is fed from the direction of element number 1 and a matched load terminates the array beyond element N. Element K is the defective element (usually by blocking with a piece of metal tape). The near-field measuring probe is at a distance z_o from the array and is moved in parallel to it, over a linear aperture of width b along the x-axis. For linear arrays the two dimensional case (see section 5.1) holds, hence, the x-z plane (y=0) solely is used for the experiments. When the main beam region is to be probed the measurement aperture is positioned symmetrically about the z-axis. When the side-lobe region is to be investigated, the measuring aperture center is moved to the left (x<0) or to the right, an adequate distance. The polarization of the test array is mainly horizontal (x-polarized). The probe polarization is therefore normally x(horizontal)-polarized unless cross polarization effects are sought, or when the $\phi = \pi/2$, rather than the $\phi=0$ plane characteristics are investigated.

7.1.2 Antenna arrays and probes

The antenna arrays

The test antennas are samples of linear waveguide slot arrays investigated earlier by Chignell [23] in the department's microwave laboratory. The antennas are an open ended waveguide and 8, 16 and 30 slot arrays (see plate 7.1).

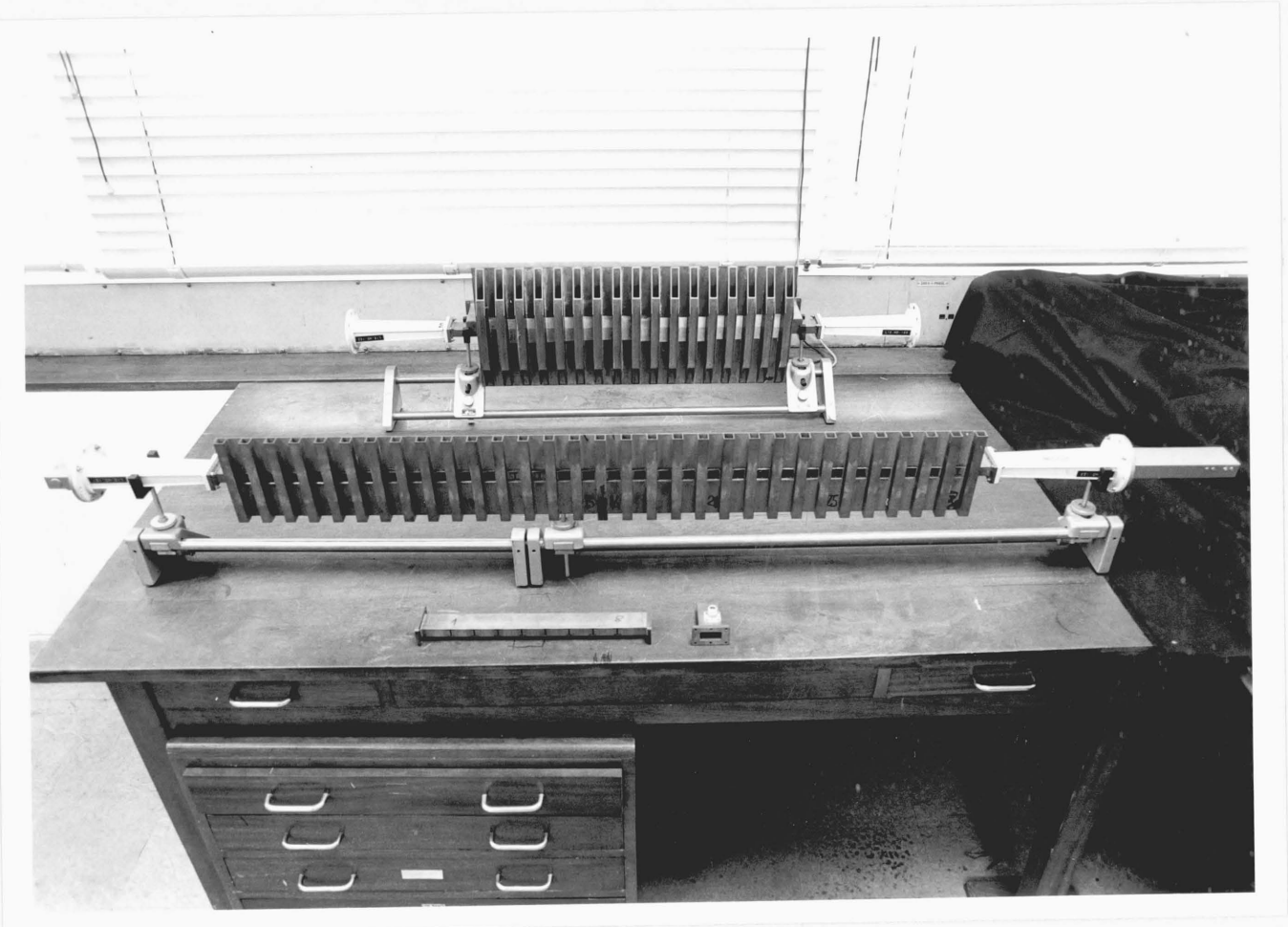


Plate 7.1 The antennas

The probe

The probe is an open ended waveguide to coax adaptor (also shown in plate 7.1 on the right, in the front). Like the other antennas it is made up of a special size waveguide (I.D.:1.270"x0.590", O.D.: 1.350"x0.670"; with a TE_{10} mode cut off frequency of about 4.7 GHz) and operating frequency of 5.7 GHz. In the measurements the E-plane of the waveguide (beam width ~140 deg.) coincides with the x-polarized radiation from the slot arrays.

The 8-slot array

The 8-slot test array is shown in plate 7.1 (on the left in the front row). The array is fed from the left through a

tapered section and is terminated from the right through a similar taper (the tapers to the standard C-band waveguide and termination are shown connected to the 30-slot array in the middle row). The array length (from element 1 to 8) is 25.3 cm with interelement spacing of about 3.6 cm (0.69λ). Different I-shaped slots cut in the narrow wall of the waveguide were designed by Chignell [23] to approximate an aperture field illumination of the form $1/7+6/7\cos^2$ giving a 3db beamwidth of about 10 degrees. The above interelement spacing which was optimized for matching also causes the beam to squint from the broadside direction by about 8.5 degrees towards the load. Similiar illumination and beam squint was noticed in all the test arrays.

The 16-slot array

The 16-slot test array (in the rear row of plate 7.1) is shown with the matching tapers to the standard C-band waveguide (WR-187). This array incorporates a grid of crosspolarization suppression baffles. The array length is 58cm with interelement spacing of .73λ. The 3db beam width is about 6 degrees.

The 30-slot array

The 30-slot test array (in the middle row of plate 7.1) is shown with the waveguide tapers and the matched load termination (right) and the input waveguide to coax adaptor (left). As with the 16-slot array the crosspolarization suppression baffles are incorporated. The array length is 110 cm with interelement spacing of .72λ. The 3db beam width is about 4 degrees.

Additional details on the slot arrays can be found in

Chignell's work [23].

7.1.3 The near field set-up

An experimental set-up was used for near-field measurements of antenna characteristics before and after the antenna has been subjected to defects.

It was decided to experiment with available C-band linear arrays described earlier operating at the center frequency of 5.7 GHz. These were the probe and 8, 16, and 30-element slot waveguide arrays with about 0.7λ interelement spacing.

The required linear motion of a probe to measure the near-field radiated from the antenna under test, was carried out with an x-positioner available in the microwave laboratory.

The schematic diagram is given in Fig. 7.2.

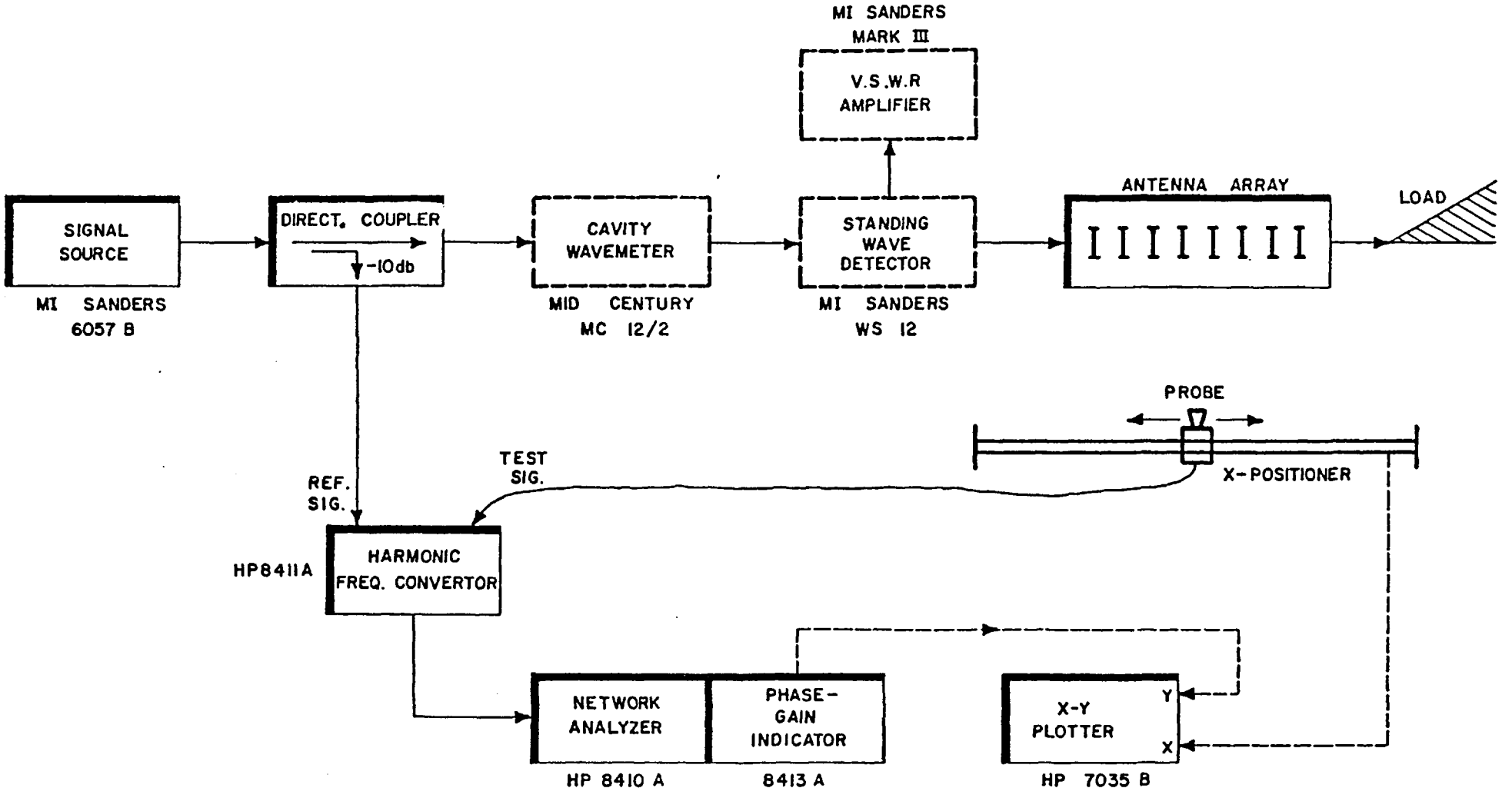


Fig.7.2 Schematic diagram of the experimental set-up.

In Fig. 7.2 a Gunn oscillator signal source is used to feed the antenna under test, which is terminated in a matched load. The field transmitted from the antenna array is sensed by a receiving probe, normally an open waveguide, which is moved transversally on the x-positioner placed in parallel with the array. The received signal gain (db) and phase is measured by a network analyzer, whose output is connected to the Y input of an X-Y plotter. The reference for the network analyzer is taken from a directional coupler placed between the signal source and the transmitting array. A voltage proportional to the transversal motion of the probe, is taken from an helical potentiometer linked to the chain drive mechanism of the x-positioner. When conducting V.S.W.R. tests of the antenna or when the signal source frequency is to be checked, a cavity wavemeter is connected through a slot waveguide standing wave detector (shown dashed in Fig. 7.1), to the array input.

The actual set-up is shown in plates 7.2 and 7.3 for two different sets of measurements. In plate 7.2 the set-up is prepared for near field measurements in the ($x<0$) side-lobe region of the 30-slot array. The absorbing material is purposely removed to give a clear view of the signal source and the directional coupler power splitter. These are normally covered by the absorsing material in order to minimize their stray radiation.

In plate 7.3 the system is shown ready for V.S.W.R. and frequency tests.

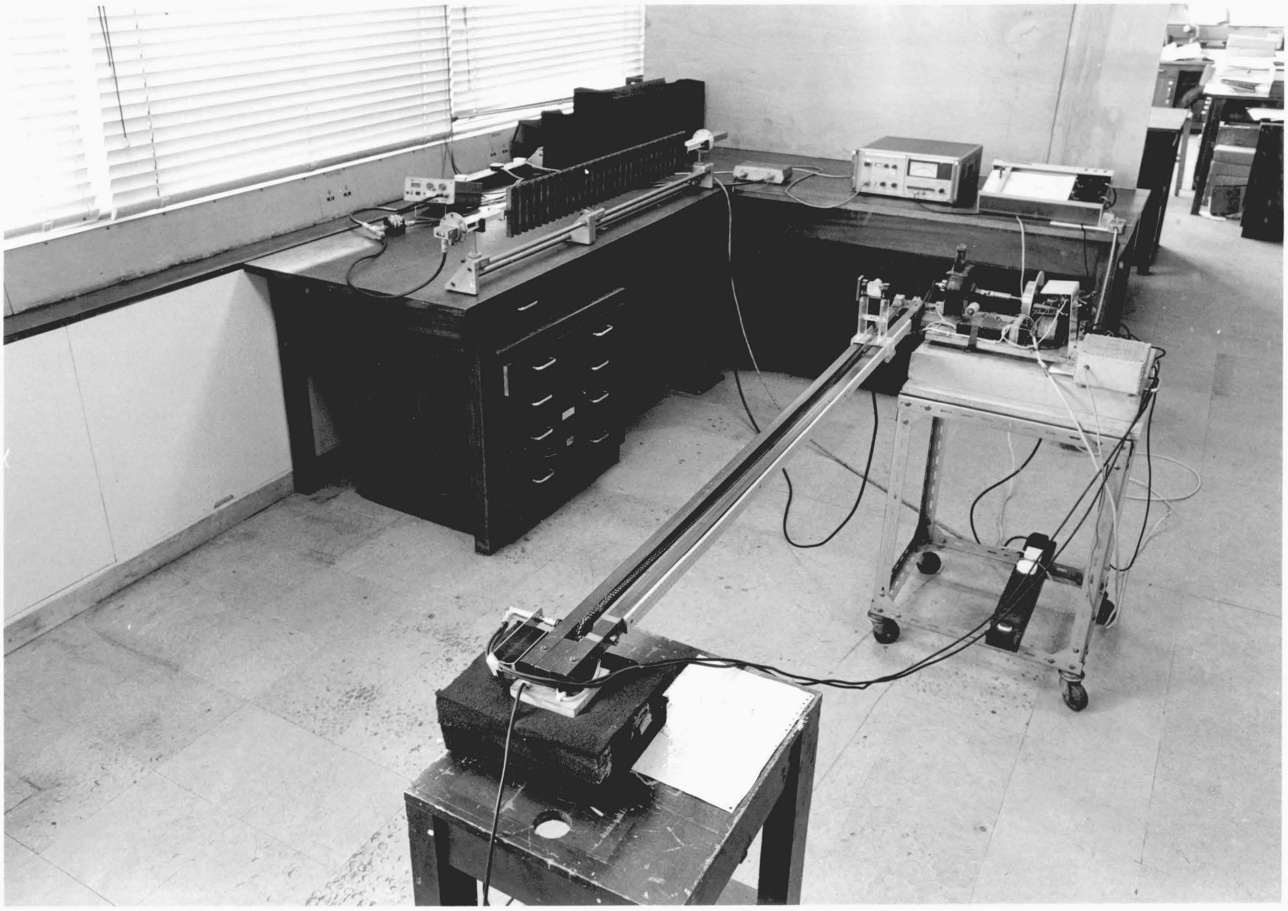


Plate 7.2 Experimental set-up for near field measurements.

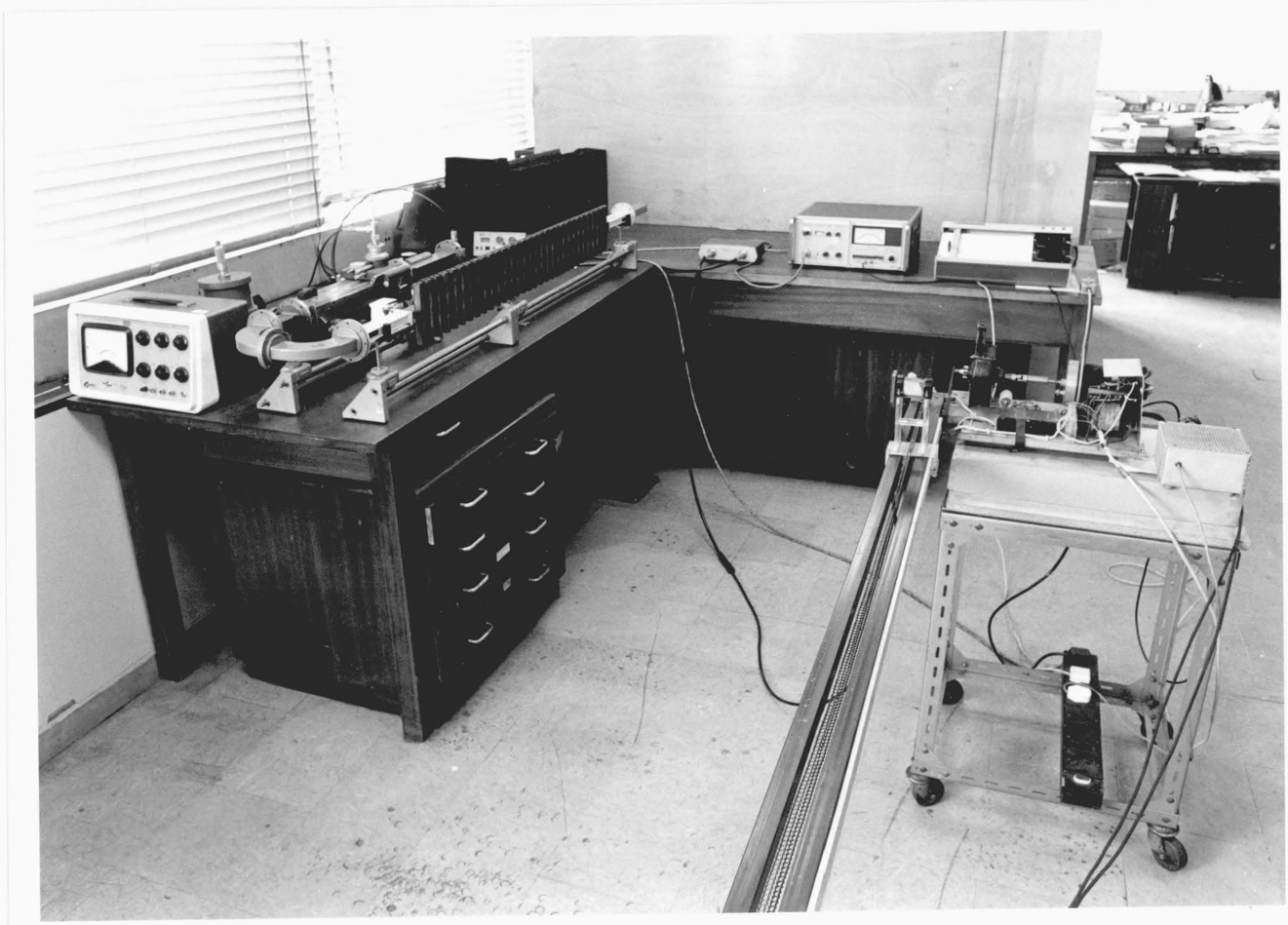


Plate 7.3 Set-up for V.S.W.R. and frequency tests.

7.2 Data collection and processing

7.2.1 Recording and preprocessing

With the set-up installed according to Figures 7.1 and 7.2 the phase and magnitude (db) of the near field measurements are recorded on an analog X-Y recorder. First the non defective array near field magnitude (db) and phase are recorded by repeatedly scanning the probe over the near field aperture, and changing the Y-input of the recorder to the phase or amplitude (db) outputs of the network analyzer (the ink colours are also changed accordingly). The same procedure is repeated after the antenna has been subjected to defects. To minimize mechanical backlash the measurement scans are always taken in the same direction (in the positive x direction). The maximum scan width possible with the x-positioner and the linked helical potentiometer is about 110 cm, similiar to the length of the 30-slot array. The Y-recorded measurements in centimeters are then sampled manually every 0.4 wavelength (0.5 cm of the calibrated x ordinate of the X-Y recorder output) to conform with the Nyquist criterion. An auxiliary program DBPMES1 (see Appendix E) is used to change the measurements recorded in cm into db and degrees according to the calibration formulas (linear calibration formulas give sufficient accuracy). The digital output of the program for the nondefective and defective array is put on a permanent file (MES...) with a format appropriate for use with the main program for near-field to far-field transformation. The test parameters like z_o (the distance of the near-field aperture from the array) and the defective element number are also memorized in the same file.

7.2.2 Near field processing

The near field program JACK30 (see appendix E) calls data from a permanent file (MES...), to a local file (FINX-TAPE7). The near field to far field transformations, according to equations (5.15) and (5.12), are then carried out using a discrete Fourier transform algorithm for the "reference" and "defective" arrays. The "subtraction method" equations (2.12) to (2.14) are then applied to resolve equivalent substitute element array far field pattern over the appropriate angular region, according to the measurement geometry. The results are then displayed against $s=\sin\theta$, numerically and graphically. In addition the "angular spectrum method" is applied using a computer NAG routine (C06ADF) for F.F.T. of the normalized angular spectrum (which is asymptotically proportional to the far field pattern) to derive the aperture field illumination function via equation (5.9). If the "a.c.f. method" is implemented then subroutine COREL03 (see Appendix E) is used to find the autocorrelation function of the angular spectrum before application of the F.F.T., as explained earlier (see section 5.3). The aperture power illumination rather than the aperture magnitude illumination, is then derived and displayed.

7.2.3 Simulation of near field measurements

Subroutine EJIX (see Appendix E) could be used with program JACK30 before the actual measurements have taken place. The subroutine simulates the near field measurements of a $\cos^2$ + pedestal or a uniformly illuminated ideal N-element array with or without defects. It can also be used as a comparative check on the experimental results.

7.3 The near-field experimental results

7.3.1 Open waveguide patterns

The single element near field phase ϕ pattern is given by the hyperbolic parametric equation

$$R^2 - x^2 = z_o^2 \tag{7.1}$$

$$\phi = -R2\pi/\lambda \tag{7.2}$$

where R, x and z_o as given in Fig. 7.3

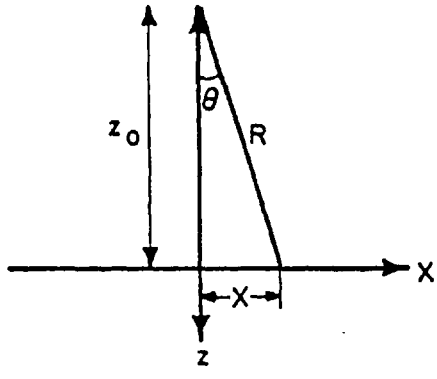


Fig. 7.3 Simplified geometry of near field measurement

The amplitude A (assuming isotropic radiators) is inversly proportional to R. Hence

$$A \propto 1/R = 1/(x^2 + z_o^2)^{1/2} = \cos\theta/z_o \tag{7.3}$$

These functions are described in Fig. 7.4 and 7.5

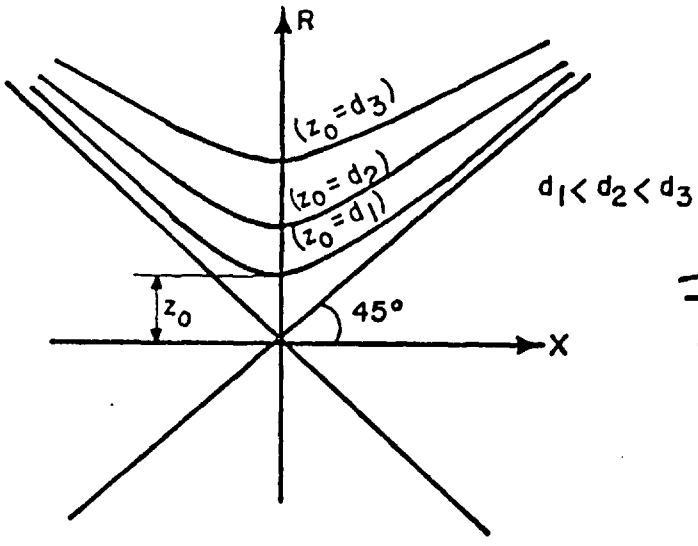


Fig.7.4 Phase representation

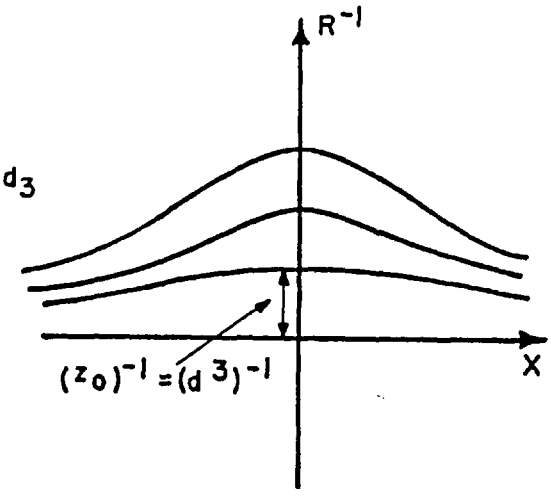


Fig.7.5 Amplitude representation

The amplitude function for two horizontal dipoles is further modified by the factor $\cos^2\theta$. However when the E-plane of two open waveguides is concerned then a $[\mathrm{sinc}(\pi Ws/\lambda)]^2$ (where W the waveguide width in the E-plane) modifies the expression of equation (7.3) (uniform illumination) and hence the modified near field amplitude function will be given by

$$A \propto \cos\theta\,[(\sin\pi Ws/\lambda)/\pi Ws/\lambda)]^2$$

$$= (1-s^2)^{1/2}(\mathrm{sinc}\,\pi Ws/\lambda)^2 \qquad (7.4)$$

Near field measurement results for two open waveguides, one transmitting and the other receiving are shown in Fig. 7.6

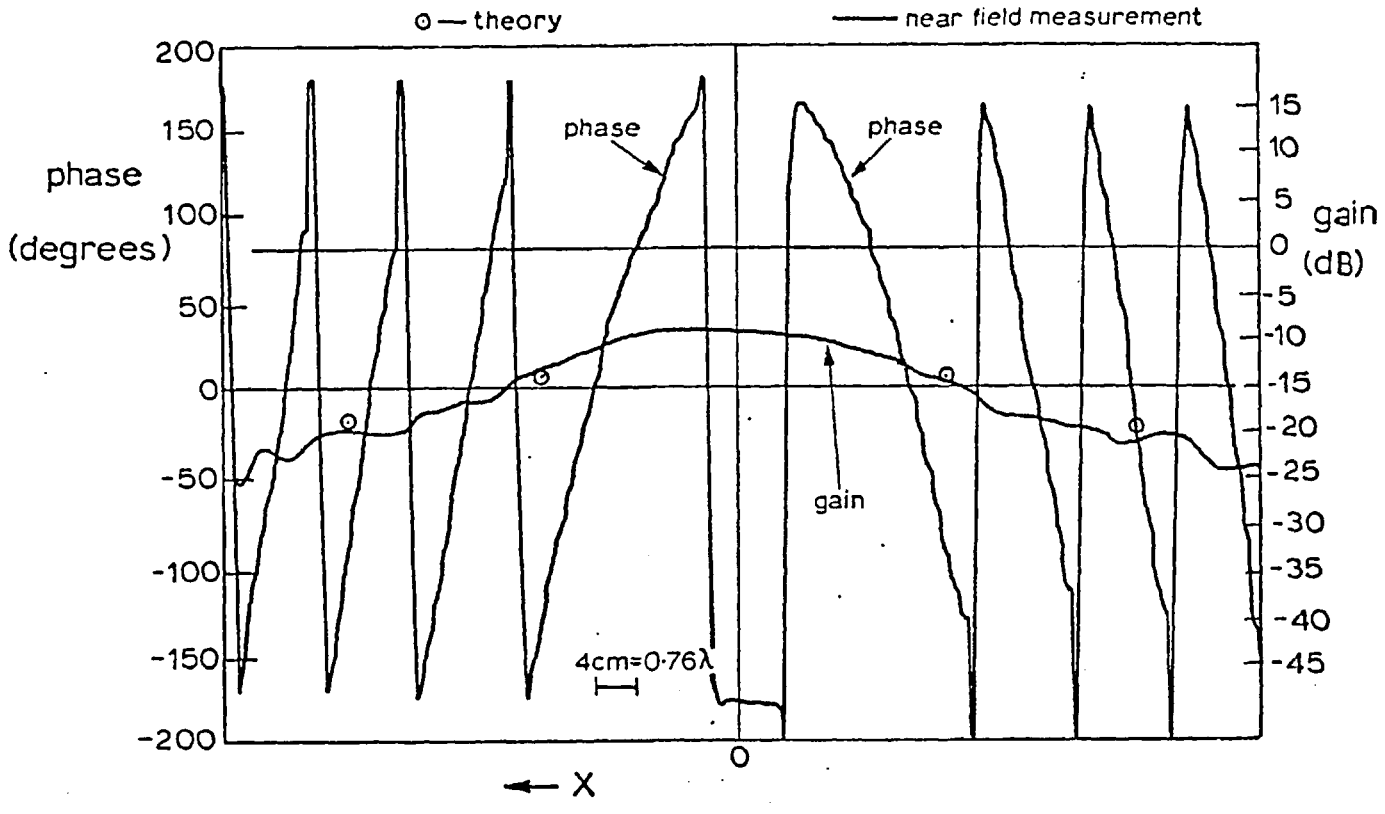


Fig. 7.6 Near field measurements of an open ended waveguide radiator at 5.7 GHz z =19.5cm

Fig. 7.6 gives the amplitude and phase as a function of x, in the near field measurement with z_o=19.5cm. The phase curve behaves according to the hyperbolic function expected from equations (7.1),(7.2). The discontinuities occuring at multiples of 2π. The amplitude curve behaves close to that given by equation (7.4) the differences are less than 1db at ±45 degrees and less than 3db at ±65 degrees, which is reasonable because the sinc^2 form is only a rather crude estimate. The importance of these measurements lies in the fact that the equivalent substitute element is expected to give a similiar result in the near field. The difference should be in the location of the axis of symmetry that is expected to be located opposite the location of the

defective element.

The direct measurements of single elements radiating from an 8-slot array (where all the other elements are covered by metal tapes) are demonstrated in Figures 7.7 and 7.8.

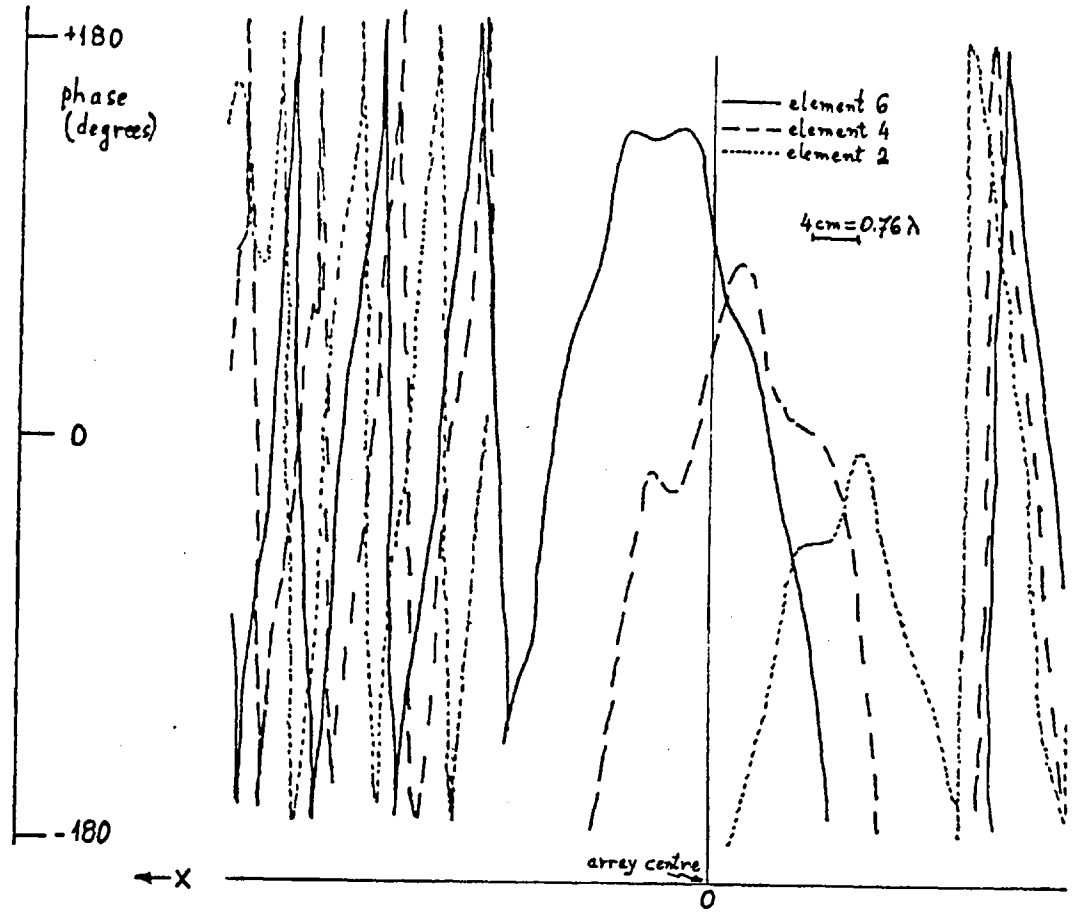


Fig.7.7 Near field measurements of single elements radiating, phase patterns.

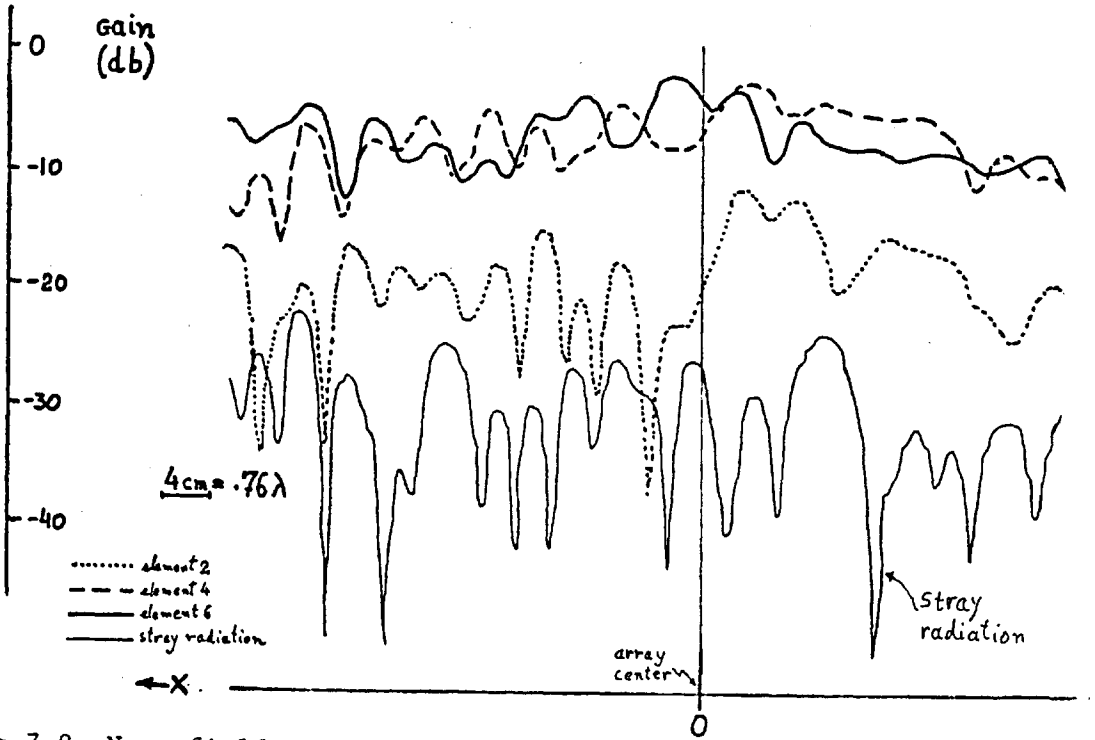


Fig.7.8 Near field measurements of single elements radiating, magnitude patterns.

Fig. 7.7 shows the phase curves of elements 2, 4 and 6 radiating. The curves show an hyperbolic variation similiar to those described by Chignell [23] for a dipole affected by the baffle wall, although no such walls are present.

The amplitude curves are described in Fig. 7.8. Element 2 amplitude is lower than element 4 or 6 as expected, due to the $\cos^2$ + pedestal illumination. The tendency of the mean amplitude curve is similiar to that of Fig. 7.6 (open ended waveguide). However it has a higher ripple, which is caused by interference with stray radiation. The amount of stray radiation present in these measurements can be judged from the near field measurements where all elements are covered (the lower curve of Fig. 7.8). The stray radiation is superimposed and therefore affects the radiation from element 2 more than 4 or 6, due to the lower illumination of 2 compared to 4 or 6.

The far-field transformation of the radiation from element 6 is shown in Figs. 7.9 and 7.10.

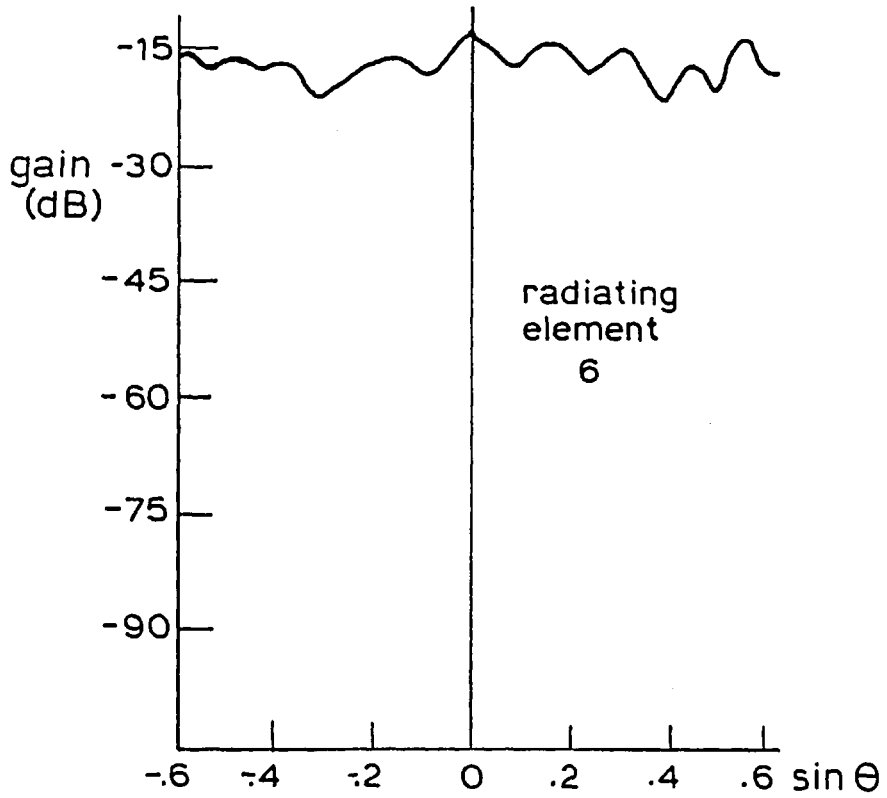


Fig.7.9 Far field pattern (db) of a single element radiating.

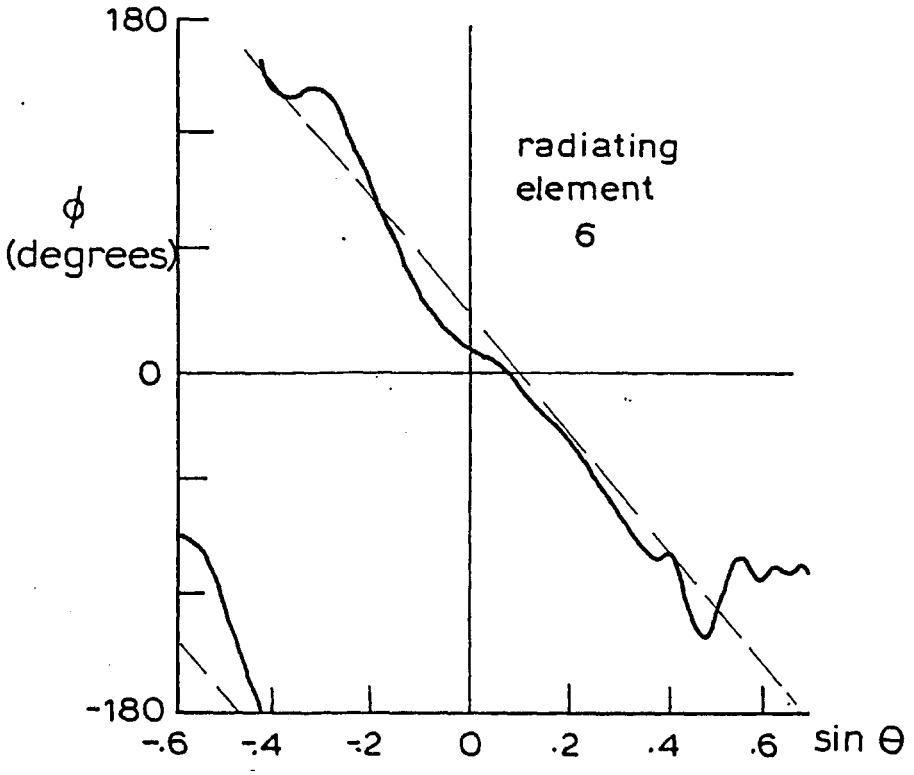


Fig.7.10 The far field phase pattern of a single element radiating.

Fig.7.9 shows the magnitude in db of the far field pattern of element 6 radiating. Use is made of the near-field to far-field transformation of program JACK30 (as explained earlier), but without using the subtraction method algorithm. The amplitude shows a fairly constant amplitude, with variations of less than about $\pm$5db over the direction range which applies to the measurements. The phase curve shows the expected correct slope, according to equation (2.14), arising from the location of element 6 with respect to the array center and to the measurement centre ($x'=x=0$). The phase variation around the mean ideal slope-line is about $\pm$15 deg over most of the range $|s| \lesssim .5$ with about $\pm$50 deg close to $s=\pm 0.6$. It is to be noted that the nature and size of the phase variation enables a correct decision to be made in practice concerning the defective- element number.

7.3.2 The subtraction method

The detection of missing elements will be demonstrated on an 8 element array. It will be recalled that elements at equal distances put on opposite sides of the array center are expected to result in slope-lines of opposite sense. The comparison between the case of an ideal array and the actual array will be based on slope-lines rather than on the absolute phase-lines. (As the subtraction method, equation (2.14), needs the slope and not the absolute phase-line).

A demonstration of missing elements 3 or 6 (by covering the appropriate element with metal tape) is given in Figures (7,11) to (7.14).

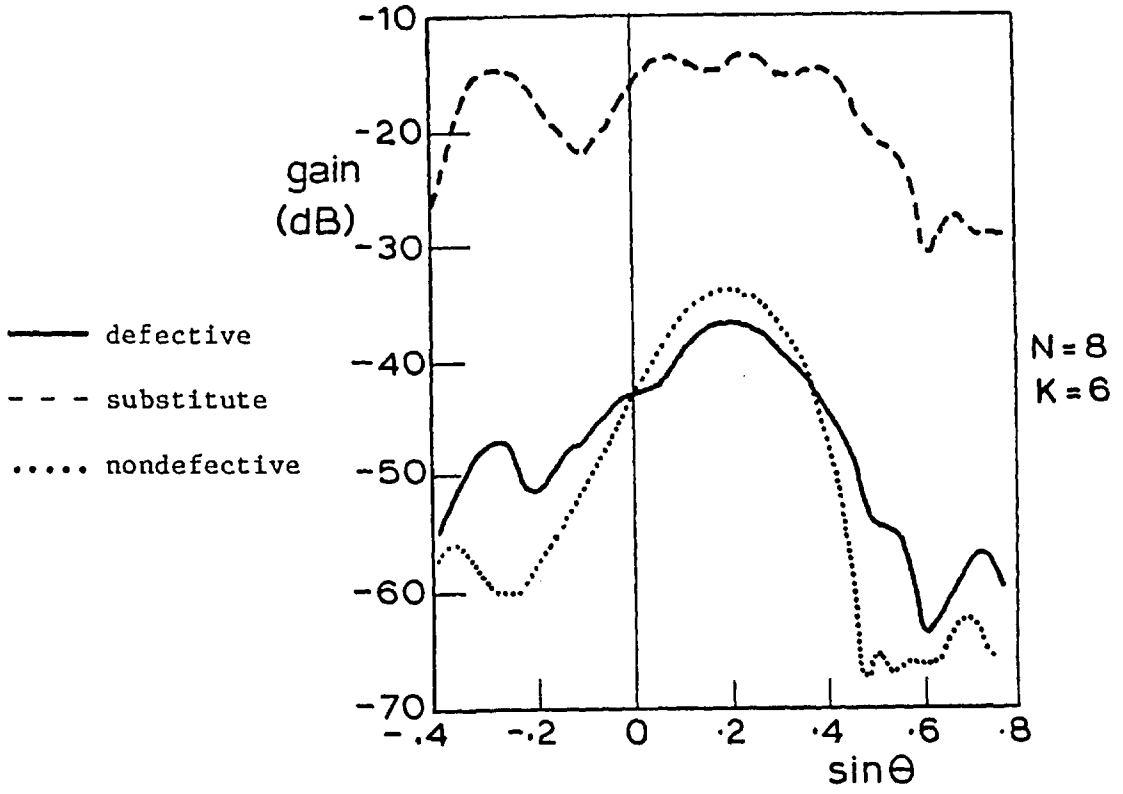


Fig.7.11 The subtraction method: missing element 6 , gain patterns.

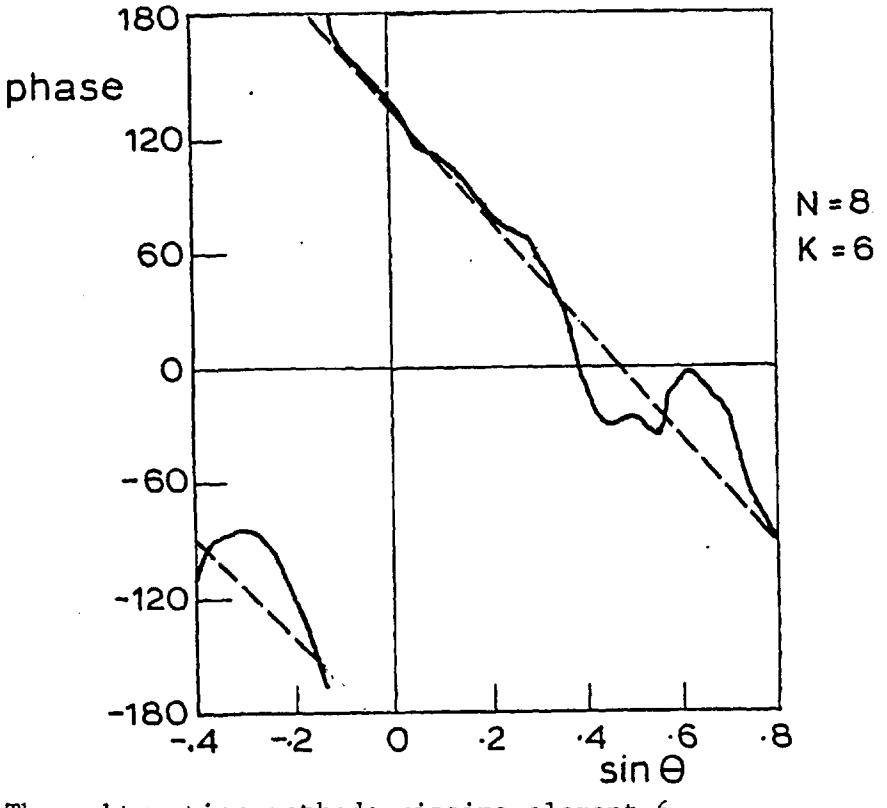


Fig.7.12 The subtraction method: missing element 6, substitute element phase pattern.

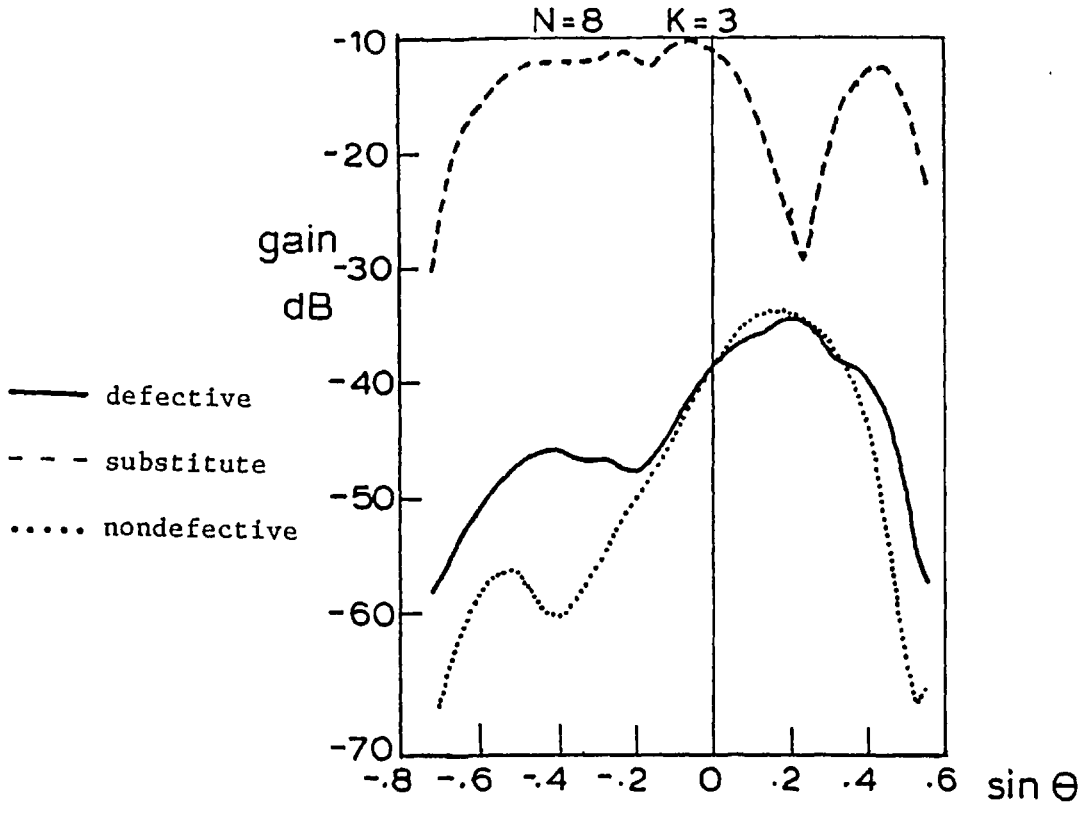


Fig.7.13 The subtraction method: missing element 3, gain patterns.

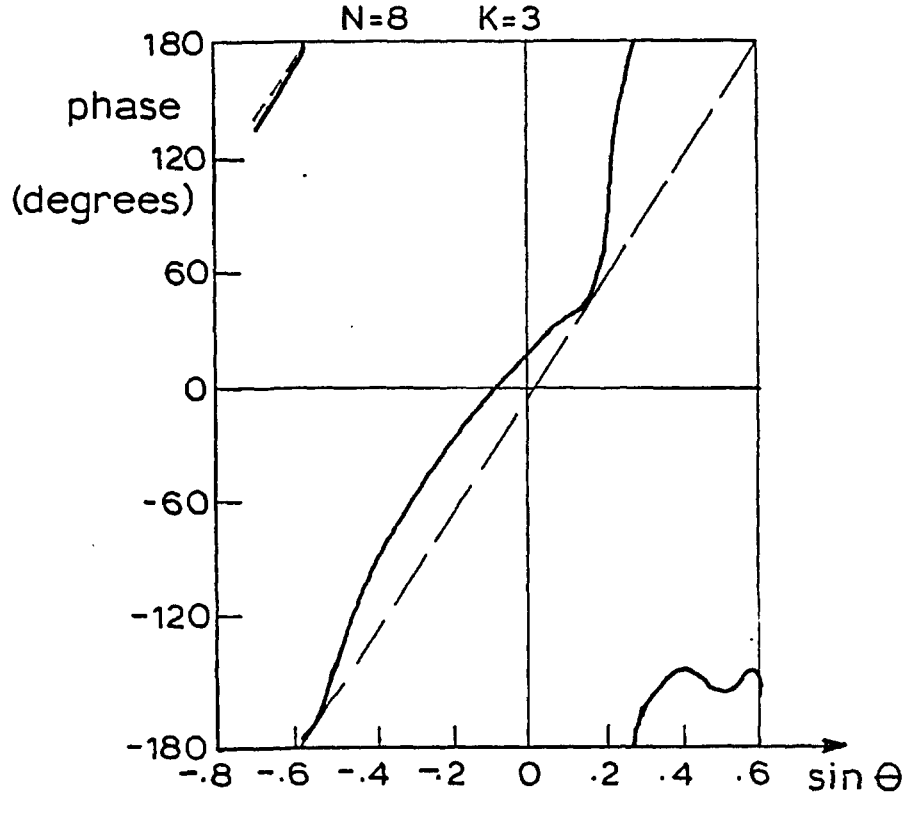


Fig.7.14 The subtraction method: missing element 3, substitute element phase pattern.

Figs. 7.11 and 7.13 show the amplitude (in db) of the non defective 8-element array, the defective array, and the equivalent substitute element pattern magnitude where element 6 (Fig.7.11) or element 3 (Fig. 7.13) are covered by pieces of metal tape. In Fig. 7.12 and 7.14 the phase patterns are shown of the equivalent substitute element of the defective element 6 (Fig. 7.12) and element 3 (Fig. 7.14). The ideal slope lines, give the phase variation of the computed values using the subtraction method.

Both measured patterns show the correct mean slope value. The phase variations when element 6 is missing are ±15deg at most (apart from ±30deg at the edges). The phase variations for element 3 missing are much larger and reach about 120deg close to the edges. However it should be noted that the agreement between the theoretical and experimental slopes for the phase variation is excellent when the amplitude of the equivalent substitute element is roughly constant. The amplitude curves, Fig.(7.11) and(7.13), also show lower ripple for the equivalent substitute magnitude pattern of missing element 6 compared to that when element 3 is missing .

These results are in accord with the mutual coupling effect model outlined in chapter 4, Figs. (4.8) to (4.11). There the main reason for excessive variation is related to the asymmetry caused by forward reflected power due to the metal tape cover of the radiating element. Hence element 3 causes higher asymmetry than element 6.

It can therefore be concluded that the subtraction method of monitoring can be applied to actual arrays, based on the promising results of this test. Other aspects, such as the set-up

instability and thresholds proposed for the subtraction method will be given in section 7.3.5.

7.3.3 The angular spectrum method

The 30-slot array was subjected to defects in either element 13 or element 18. The detection of these will now be examined with the angular spectrum method algorithm. The technique is described in subsection 7.2.2; the results are given in Figures 7.15 and 7.16, which show aperture illumination deduced from the angular spectrum in the main beam region. A smooth curve similiar to the $\cos^2$ + pedestal illumination can be imagined for the non-defective array. The aperture illumination of the defective array has an anomaly (a "hole") in the vicinity of the missing element 13 or 18 respectively.

In these same figures the derived aperture field for the equivalent substitute element is given. It can be seen that in both cases a clear indication of the location of the missing element is given. It can therefore be concluded that the angular spectrum method is also a practical monitoring method that can usefully be applied to actual arrays.

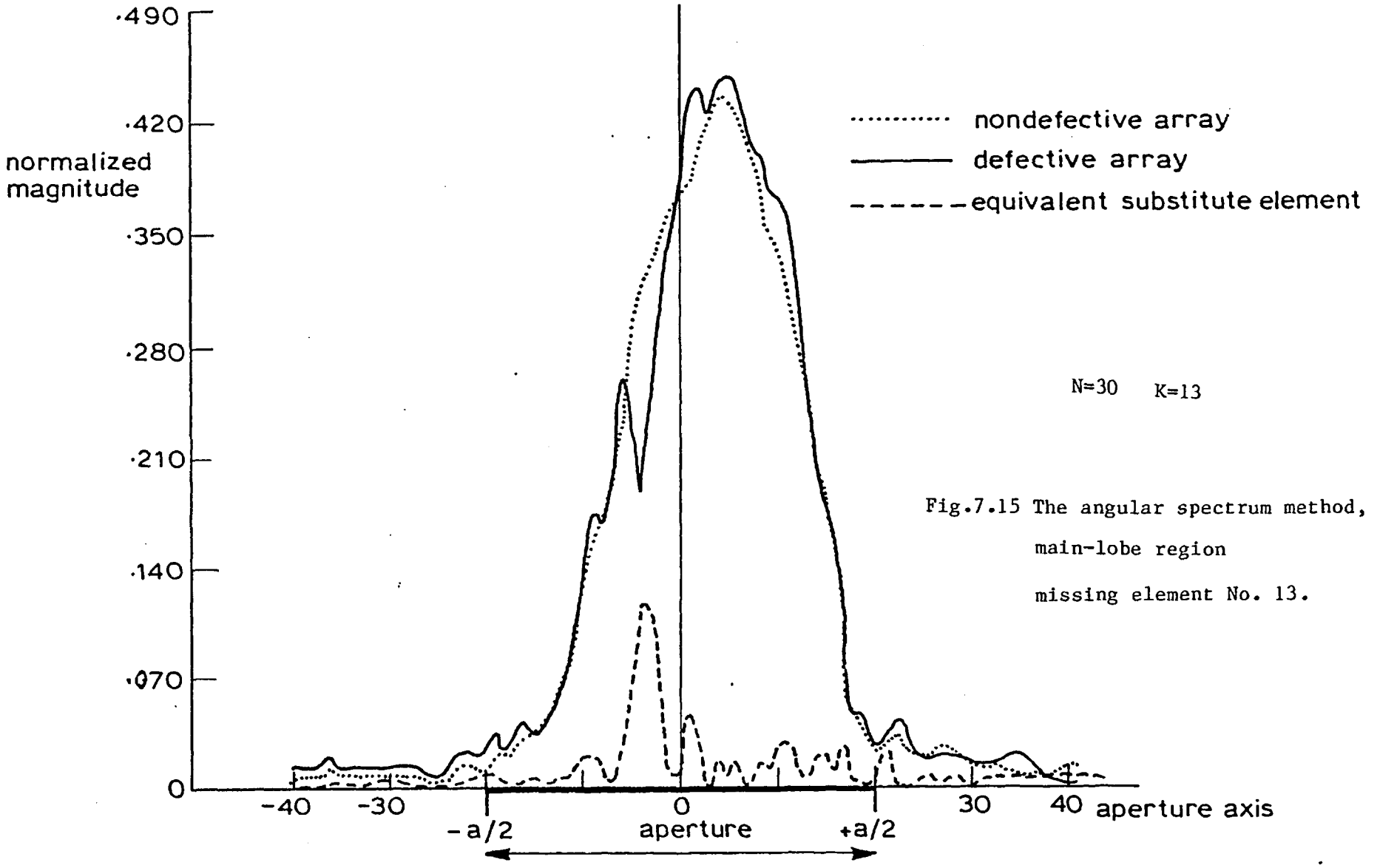


Fig.7.15 The angular spectrum method,
main-lobe region
missing element No. 13.

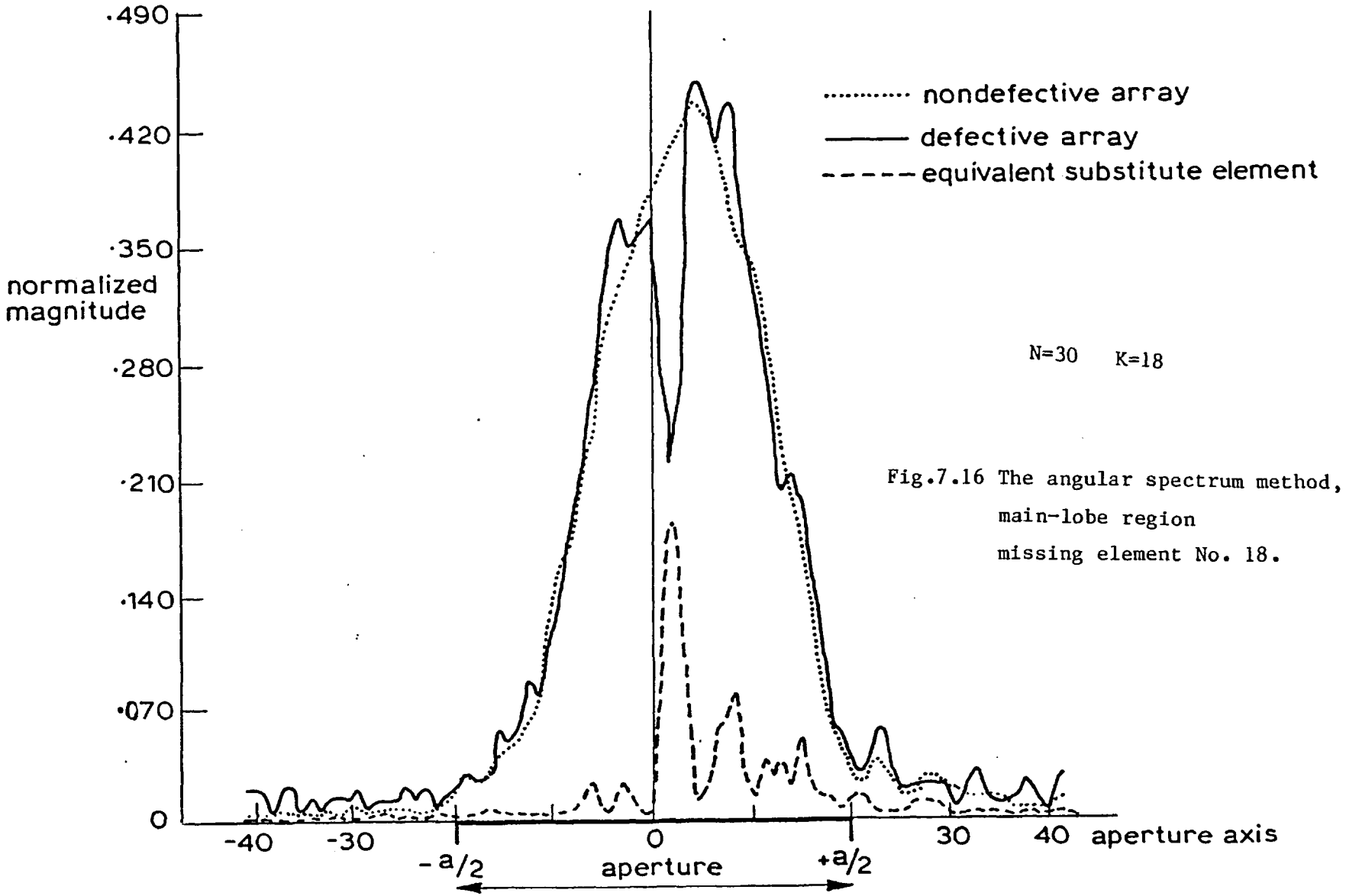


Fig.7.16 The angular spectrum method, main-lobe region missing element No. 18.

7.3.4 The autocorrelation (a.c.f.) method

The autocorrelation function method will be demonstrated in the side lobe region of the 30-slot array. The array will be subjected to the same defects as before. The measurements are now taken from x_{min}=-165cm to x_{max}=-55cm (x_{max} is opposite element number 1). The measurement aperture is placed at z_0=110cm, hence the direction cosines s≃.45 to 0.8 are covered.

Attention should be paid to the fact that the 1/7+6/7 $\cos^2$ rather than the uniform illumination (which was demonstrated in subsection 5.2.2 is now present. Therefore the power peaks of the edge elements are now expected to be fainter by about $(1/6)^2$ if a center element of the array is missing. The results are demonstrated in Figs. 7.17 to 7.20.

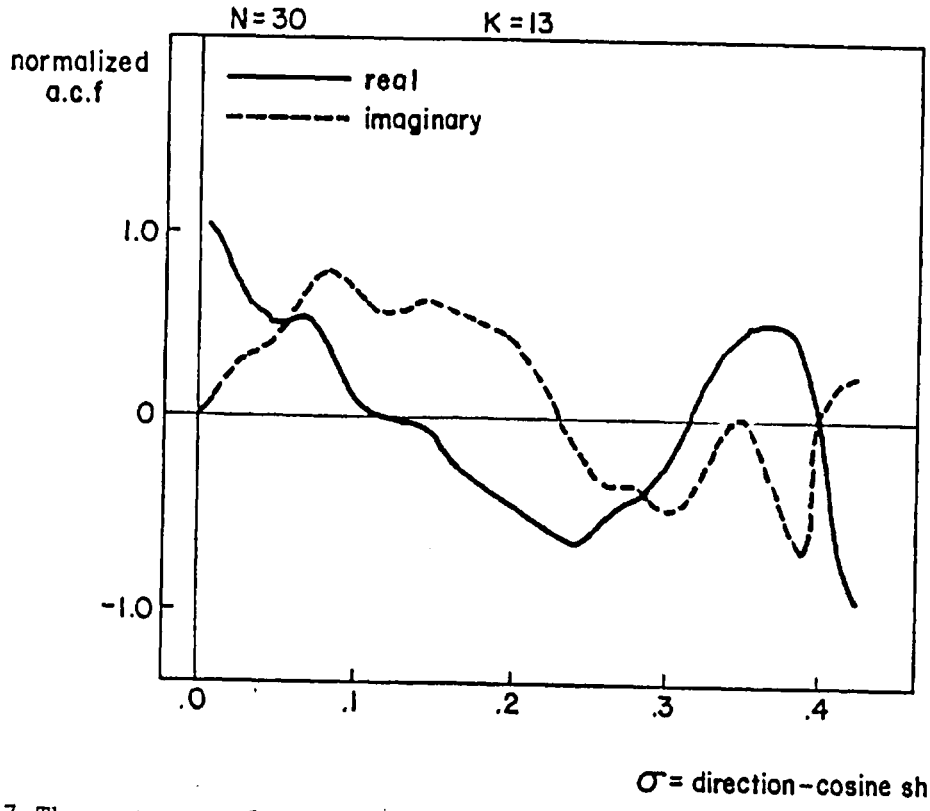


Fig.7.17 The autocorrelation function of the angular spectrum: side-lobe region, missing element 13.

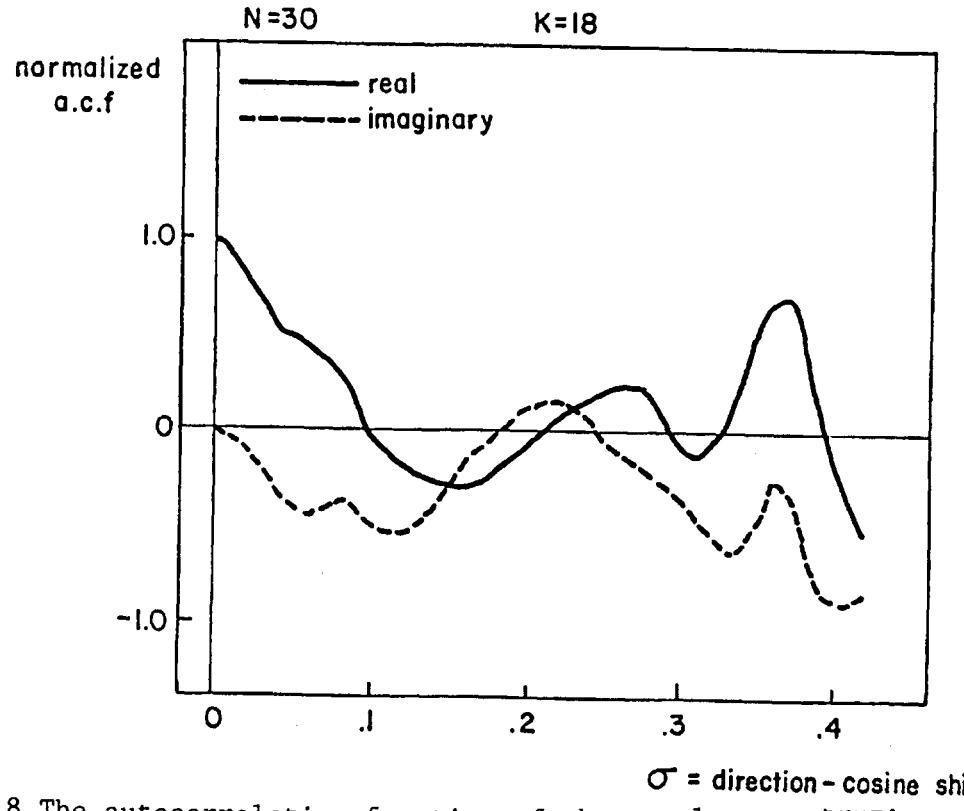


Fig.7.18 The autocorrelation function of the angular spectrum: side-lobe region, missing element 18.

Figs. 7.17 and 7.18 show the real and imaginary components of the autocorrelation function for missing elements to the left and to the right of the array centre. Attention should be paid to the imaginary component of the a.c.f. which is of opposite polarity for defects to the right and to the left of the array center.

The Fourier transform of the a.c.f. of the angular spectrum, in the side-lobe region is approximating the modified aperture power illumination as explained in subsection 5.2.2 (but with a fainter edge-element response, as explained earlier, due to the $\cos^2$ +ped illumination). The modified aperture power illumination derived from side-lobe region measurements is given in Figs 7.19 and 7.20.

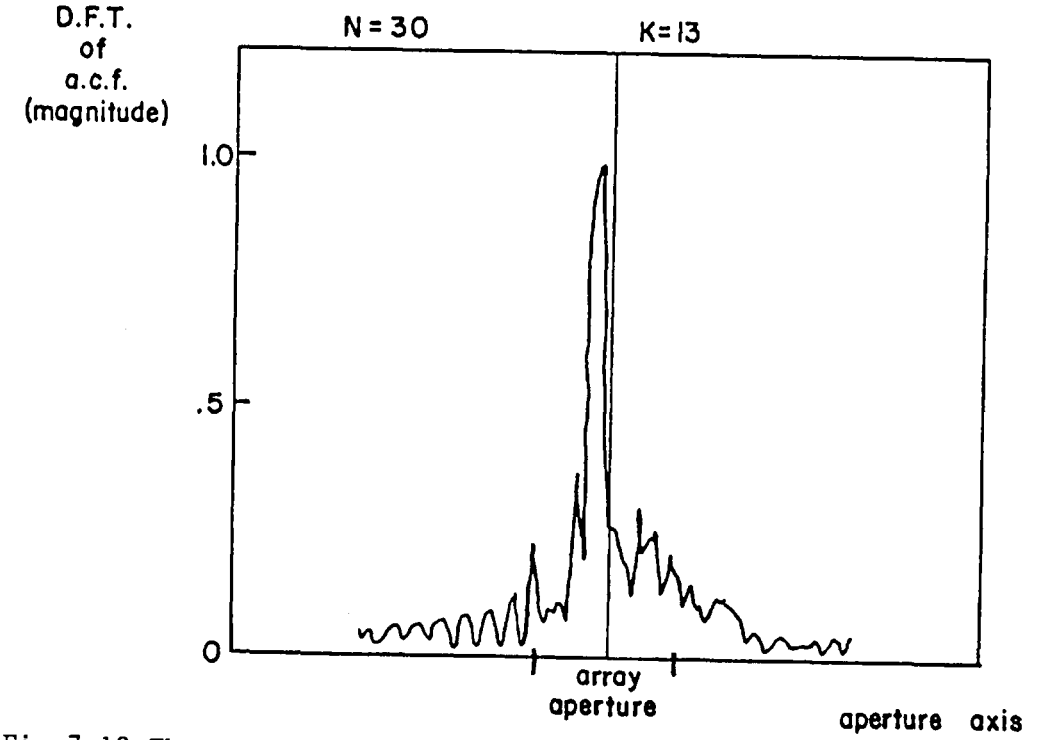


Fig.7.19 The autocorrelation function method (a.c.f.):

side-lobe region, missing element 13.

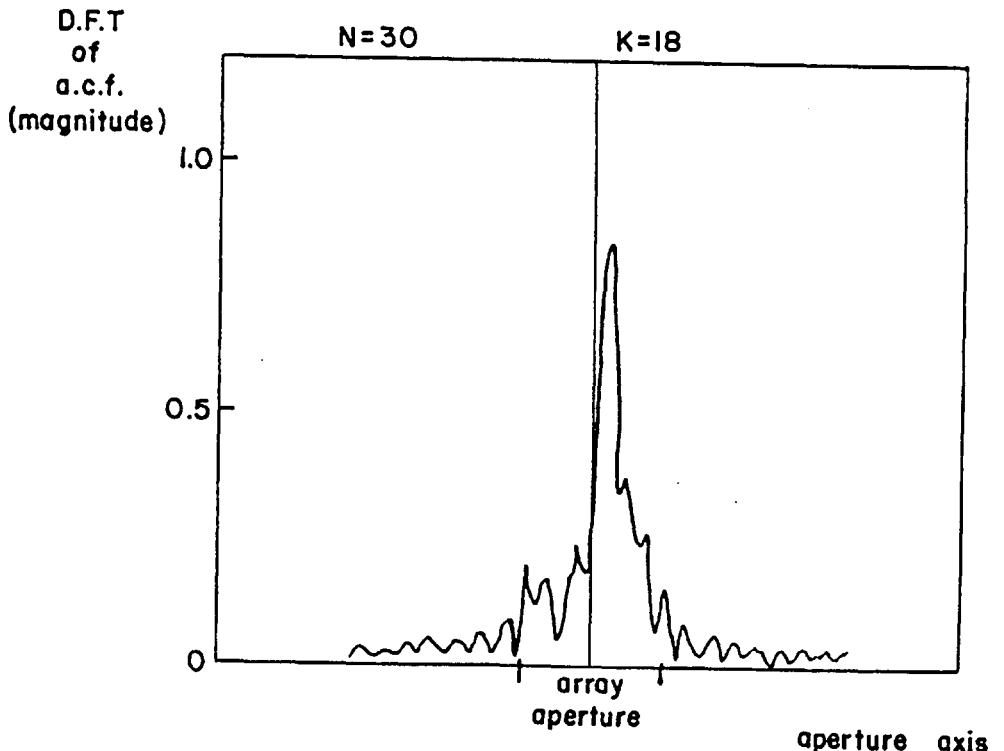


Fig.7.20 The autocorrelation function method (a.c.f.):

side-lobe region, missing element 18.

Figs. 7.19 and 7.20 show the modified aperture power illumination calculated from measurements in the side-lobe region. The illumination due to the equivalent substitute element 13 or 18 missing are pointed out in the relevant figure. Hence it can be concluded that, as with the other two methods, the a.c.f. method can be used with actual arrays.

This concludes the demonstration of the three methods applied to actual arrays. The sensitivity to instability and the problem of thresholds will be discussed next.

7.3.5 Sensitivity to instability (and thresholds)

An experiment has been carried out to examine the effect of instability in the measurements on the performance of the subtraction method.

The angular spectrum method and the a.c.f. method both use absolute magnitudes for comparison in order to identify defective elements by anomalies in the aperture illumination. The subtraction method, however, uses a comparison between complex numbers. Hence it is more important to check the effects of these instabilities with the subtraction method in particular.

It should be noted however that in the case of the angular spectrum and the a.c.f. methods a constant phase drift will have practically no effect on the resulting magnitudes. However a drift in the measured magnitude will result in a proportional change in the aperture illumination function.

The effect on the subtraction method of any drift could introduce an apparent defect. The resulting error pattern is the

phasor subtraction of the two reference patterns measured before and after a drift has been introduced into the measuring instrumentation (i.e. in amplitude and phase). It is expected that the effect will be noticed more severely in the main beam region where the subtraction of two large complex numbers might result in a large error due to a small amplitude or phase error. In the side-lobe region the effect is fainter according to the ratio of the main beam to side lobe levels. There the effect of amplitude or phase drift will be minimal and will, in practice, not affect the phase slope (although the absolute phase can be affected). Therefore the subtraction method is expected to be affected in a similar manner to the other two methods in the side lobe region.

A demonstration of using the near field reference pattern to resolve defects after 5 days with drifts of about 1 to 2 db in magnitude and 40 deg. in phase is given in Figs. 7.21 to 7.25.

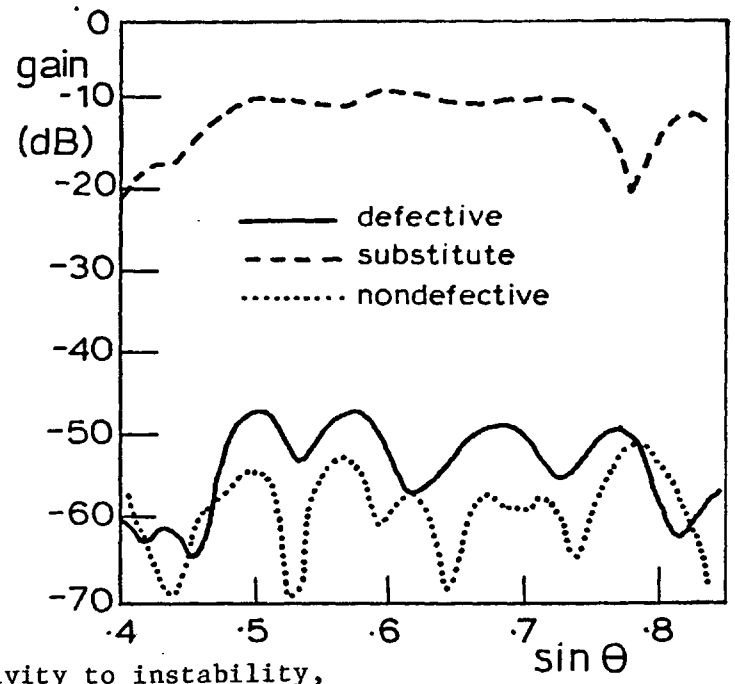


Fig.7.22 Sensitivity to instability, five days difference, gain patterns, missing element No. 13.

N=30 K=13

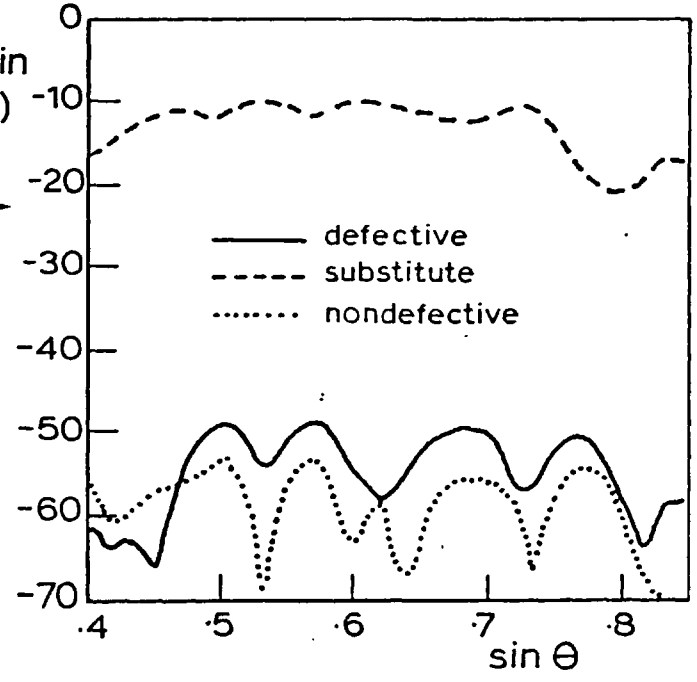


Fig.7.21 Sensitivity to instability, missing element 13, gain patterns.

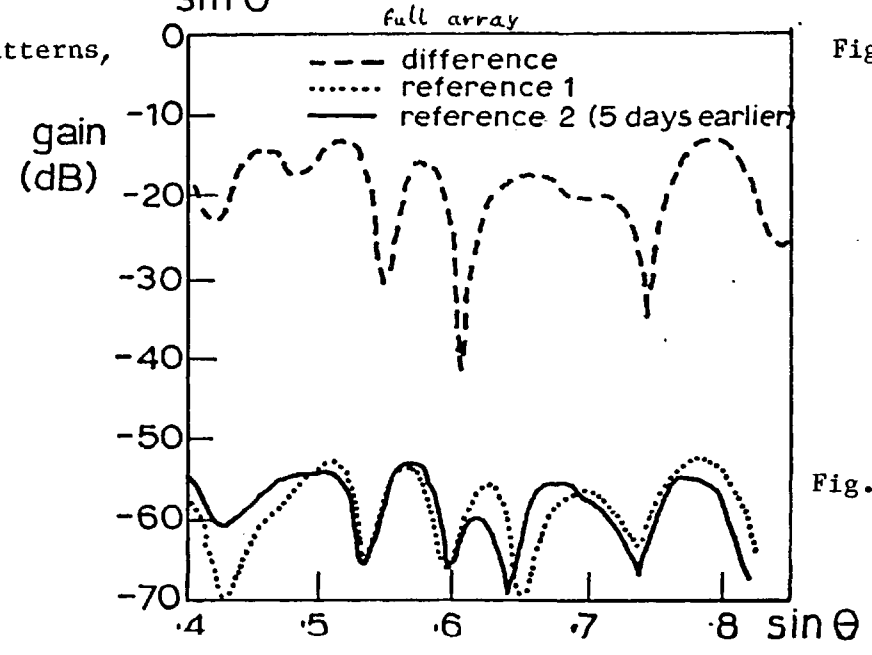


Fig.7.23 Sensitivity to instability, full array, reference measured 5 days earlier.

Figs. 7.21 to 7.23 give the far field patterns derived from near-field measurements. Figs. 7.21 and 7.22 show the far field magnitude patterns of missing element 13. In Fig. 7.21 the reference used is measured shortly before the introduction of the defect, while in Fig. 7.22 a reference measured 5 days earlier is used. Fig. 7.23 shows the far field pattern of the two reference measurements taken 5 days apart, when no defect is present. Comparing the substitute element pattern of a defective array with this non-defective array shows a difference of about 10 db (the pattern of the substitute missing element is 10 db stronger than the non-defective condition). The phase patterns are given in Figs. 7.24 and 7.25.

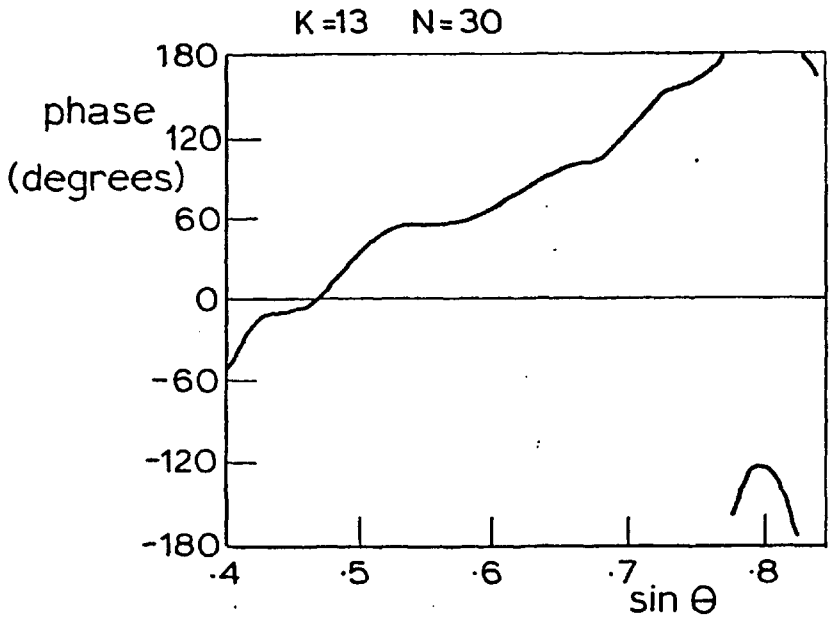


Fig.7.25 Phase pattern, missing element 13, reference measured 5 days earlier.

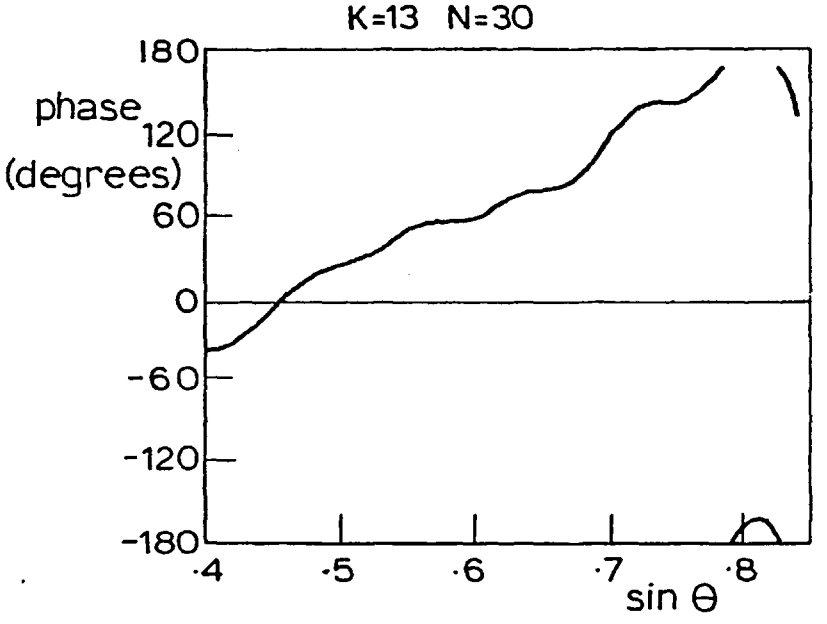


Fig.7.24 Phase patterns, missing element 13, same day reference, gain patterns.

Fig. 7.24 shows the phase patterns of element 13 missing where only a short time has elapsed between the measurements of the reference and the defective array. In Fig. 7.25 the same defective array measurements are compared to a reference measured 5 days earlier. As can be judged from the graphs, the delay has no appreciable affect on the resulting phase slope line.

Another important result is derived by checking the previously mentioned 10 db difference between an apparent defect (due to drift between two reference patterns) and an actual defect. A recommendation is therefore made to use a -6db level threshold to differentiate between an actual defect and an apparent one.

Summarizing the results of sensitivity to instability:

The preferred region for all three methods is in the side lobe region. The subtraction method is expected to be the most vulnerable of the three methods if it is used in the main lobe region in the presence of unstable measurements.

A threshold level of about 6 db can be used in the side-lobe region to distinguish between an apparent defect and an actual one, and ignoring the phase line deviations in the direction cosine regions , below that threshold. For higher instabilities or for a greater delay in taking the reference patten measurements other values for the threshold could be found adequate. Hence using the monitoring methods in the side- lobe region enables the use of measurement systems which have inferior qualities. This is another example of the advantage of using the side-lobe region for measurement.

The experimental investigation was preceded by a series of supporting tests. These are described next.

7.4 Details of some supporting tests

Inspection of the equations used in the near-field to far-field transformation, the following variables are to be considered: wavelength, phase, amplitude and geometry. Therefore the first part of the experimental investigation was dedicated to assessing the systematic and dynamic errors in the measurement of these variables.

7.4.1 Static and dynamic errors

The following tests have been conducted:

Long term stability measurements

- Frequency stability of the microwave power source. (Fig 7.26)

- Phase and amplitude stability of the set-up. (Fig. 7.27)

- Stability of x-coordinate reading.

The dynamic tests included

- Phase and amplitude jitter due to bending of the coaxial cable.

- backlash of the drive mechanism related to the helical potentiometer output signal.

- Repeatability of the drive mechanism when motion in the same direction is examined.

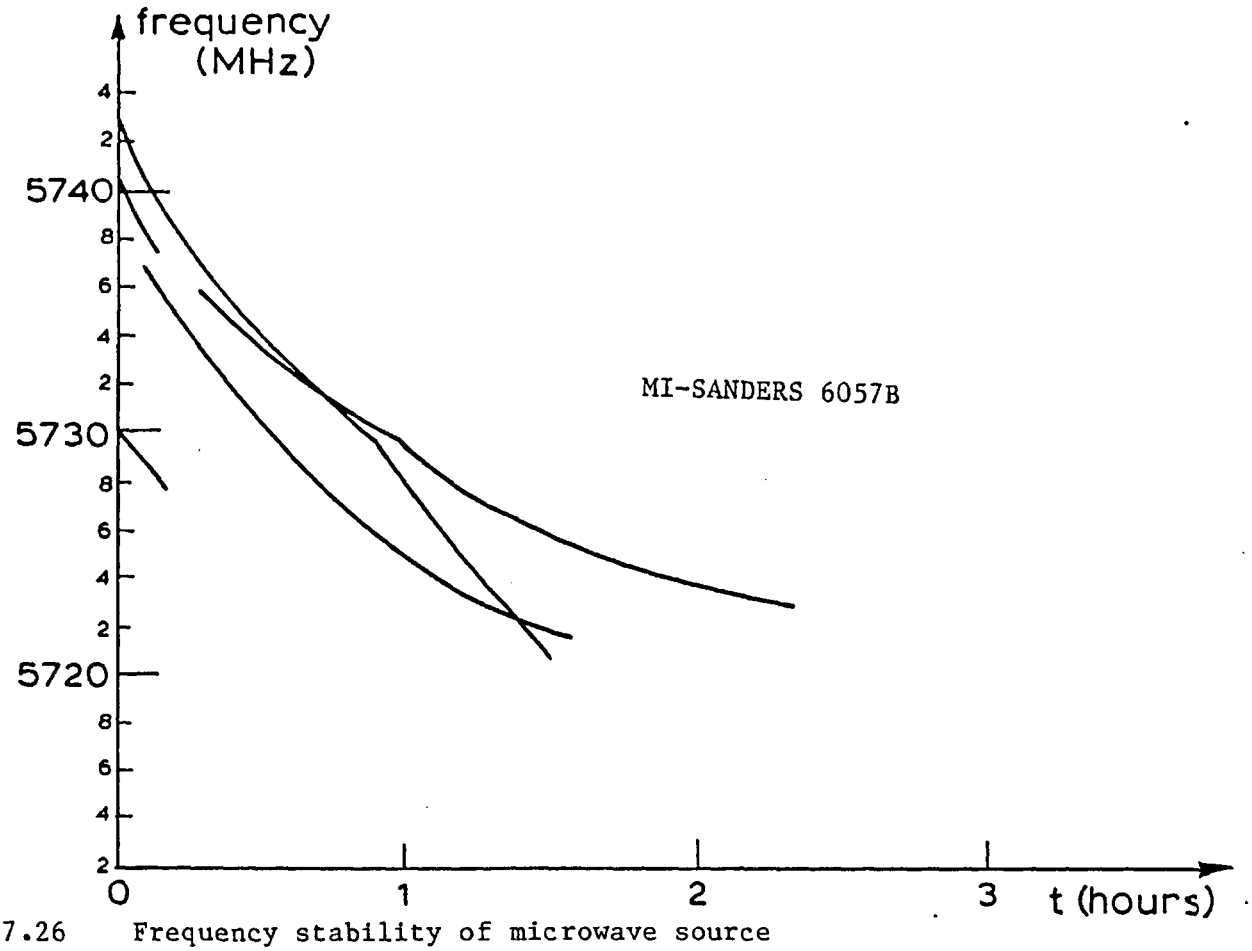


Fig. 7.26 Frequency stability of microwave source

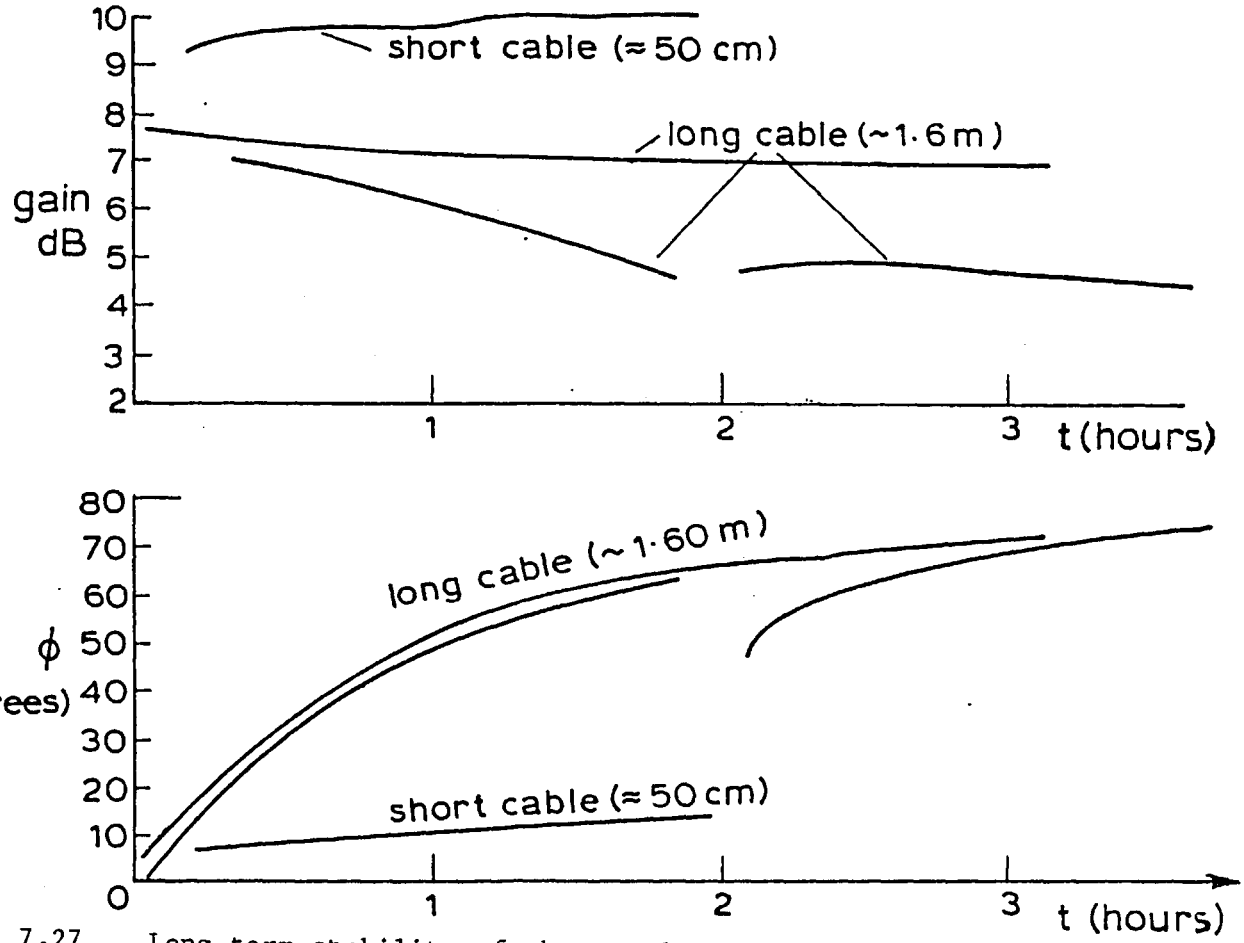


Fig. 7.27 Long term stability of phase and gain of the set-up

Fig. 7.26 shows the frequency of the Gunn source measured over sequences of several hours. The result is about -12MHz/hour frequency drift. In Fig. 7.27 the total phase shift is given as a function of time. Two groups are noticed: small changes of about +4deg/hour and large ones of about +35deg/hour. The reason for these differences was identified with the cable length used between "test" and "reference" channels of the Network Analyzer. Hence the effect is mainly due to the frequency instability of the source (according to Fig. 7.26).

The results of these and of the additional stability tests are summarized in table 7.1.

Table 7.1

Set-up instability errors

Mesured quantities	Error
Bias errors	
Frequency stability	<-12MHz/hour
Gain stability	<+.5 to-2.0 db/hour
Phase stability (3m cable)	<+35deg/hour
Phase stability (1.3m cable)	<+4deg/hour
Stability of x-positioner	<±0.5cm/hour Parallelism
	<±0.5cm (estimate)
Translation orthogonality	< ±2deg (estimate)
Dynamic errors	
Phase jitter due to bending (radius>10cm)	< ±10deg
Backlash of x-positioner	< ±0.5cm
Repeatability of x-positioner (same direction)	<±0.2cm

Note Set-up tests at 5.7GHz measured after 15 minutes warm up time.

7.4.2 Antenna tests (and stray radiation)

The following tests have been made in addition to those previously described, to find out the effect of blocking a radiating slot with metal tape (used to introduce artificial

defects in the array). These are the V.S.W.R. test (results are given for 30 and 8-slot arrays in table 7.2), and aperture illumination (see Fig. 7.28) before and after blocking of a radiating slot by a metal tape.

In addition, the effect of finite screening of available instruments was checked, by measuring the near field radiation level when all the elements were covered by metal tape. The results of this check were mentioned earlier in subsection 7.3.1 and appear in Fig. 7.8.

Table 7.2
Input V.S.W.R. function of radiator blocking

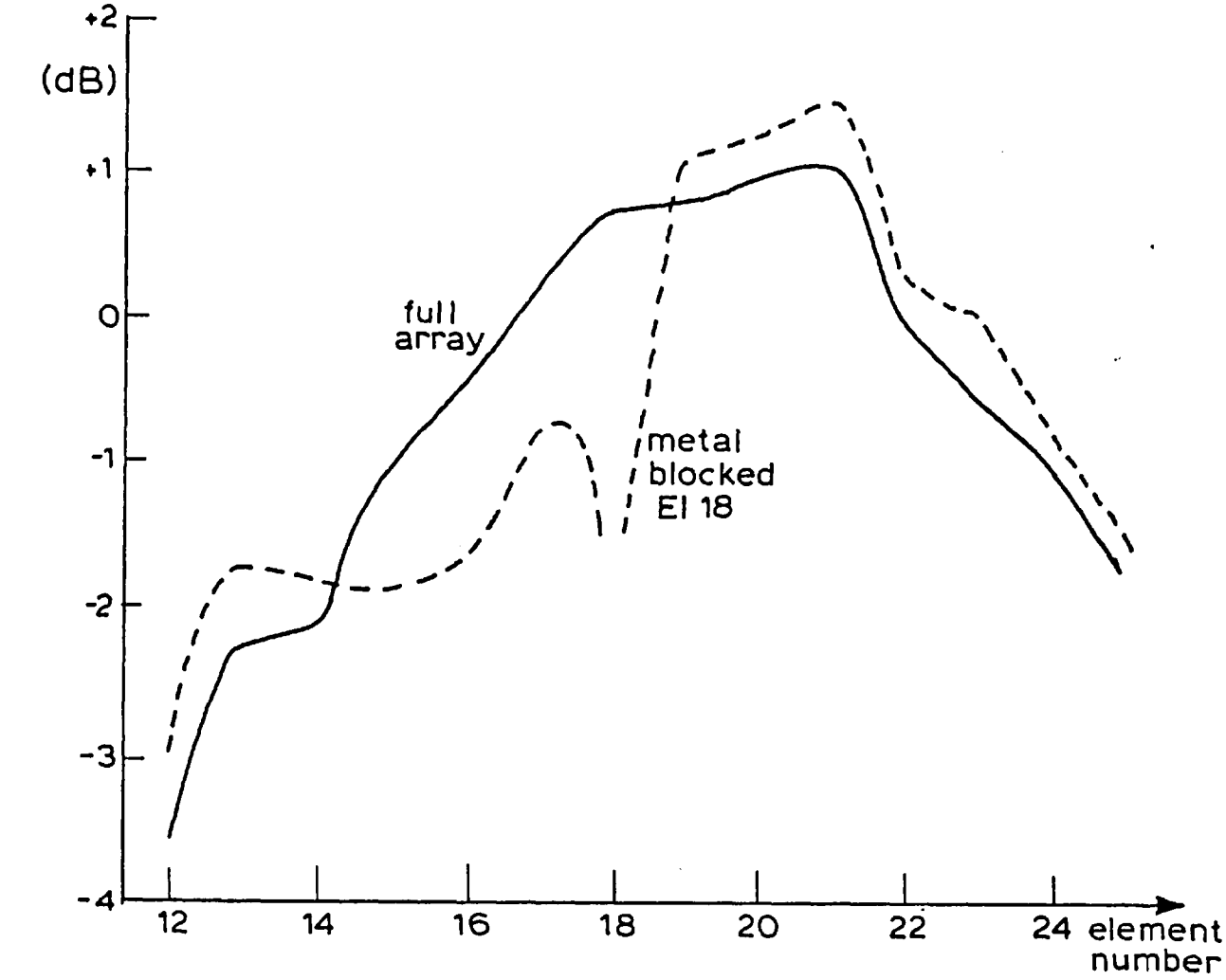
element	V.S.W.R.	element	V.S.W.R.
30-slot array			
no blocking	1.11	17	1.2
1	1.11	18	1.28
5	1.16	19	1.26
11	1.18	20	1.16
13	1.17	26	1.18
14	1.1	13+14	1.21
15	1.05	13+15	1.17
16	1.15	13+18	1.37
8-slot array			
no blocking	1.65	fully blocked	1.035
1 blocked	1.74	1 radiating	1.09
2 "	1.74	2 "	1.1
3 "	1.78	3 "	1.17
4 "	1.27	4 "	1.29
5 "	1.57	5 "	1.48
6 "	1.88	6 "	1.26
7 "	1.71	7 "	1.15
8 "	1.62	8 "	1.09
2+4 "	1.55		

Input V.S.W.R. function of obstruction by probe motion at z_o=25cm of 8-slot array was changed from 1.65 (no obstruction) into 1.58 (with obsruction), when probe was positioned opposite elements 2,3.

Checking table 7.2 the conclusion is reached that the effect of covering the 30-slot array with metal tape has less influence on the input V.S.W.R. than with the 8-slot array. Also covering an

element which has a higher illumination has a larger effect on the input V.S.W.R.

The effect of covering a radiating slot with a metal tape will be given next. (see Fig 7.28)



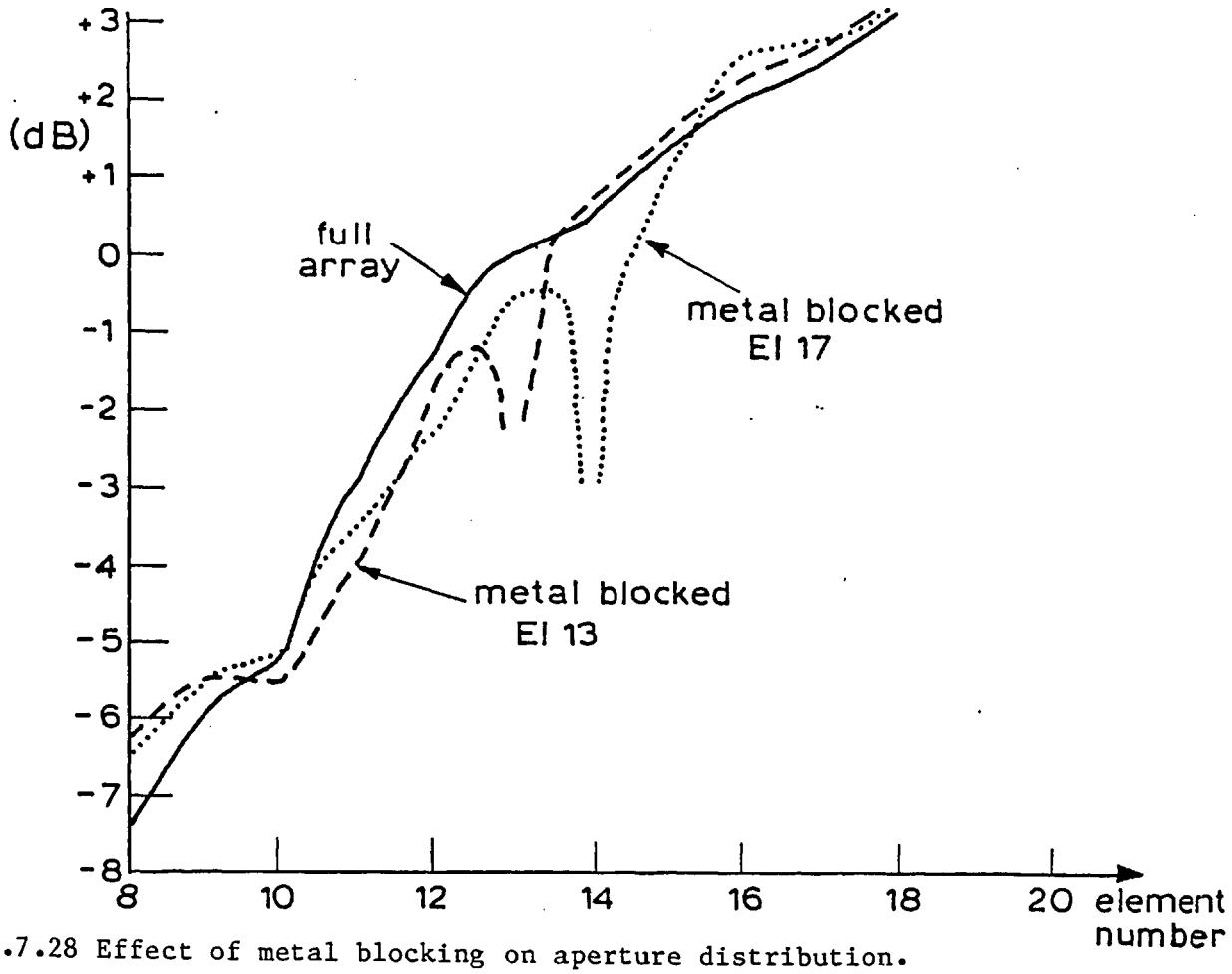


Fig.7.28 Effect of metal blocking on aperture distribution.

The changes in the aperture distribution shown in Fig. 7.28 are as follows.

In the forward direction (towards the load) the amplitude is raised by about 0.2 to 0.5 db . In the backward direction (reflection towards the generator) a decrease by about -1db is noticed (in the 3-4 neighbouring elements). This confirms in part the model used when mutual coupling effects were discussed in chapter 4 (the forward reflected power model).

7.4.3 Comparison of far field measurements

In order to check the applicability of the set up and of the processing (program JACK30), an experiment has been performed to compare the near field measurements transformed to the far field with actual far field measurements. The only antenna that could be checked inside the Microwave laboratory was the 8-slot array, which allows a practical indoors Rayleigh distance ($R=2a^2/\lambda$) of about 2.8 meter.

The 8-slot array near field measurements of subsection 7.3.2 have been compared to the pattern measured at 3.0 meter assumed to be the far field. The "far-field" set-up is shown in plate 7.4. The far-field measurement results are shown in Fig. 7.29.

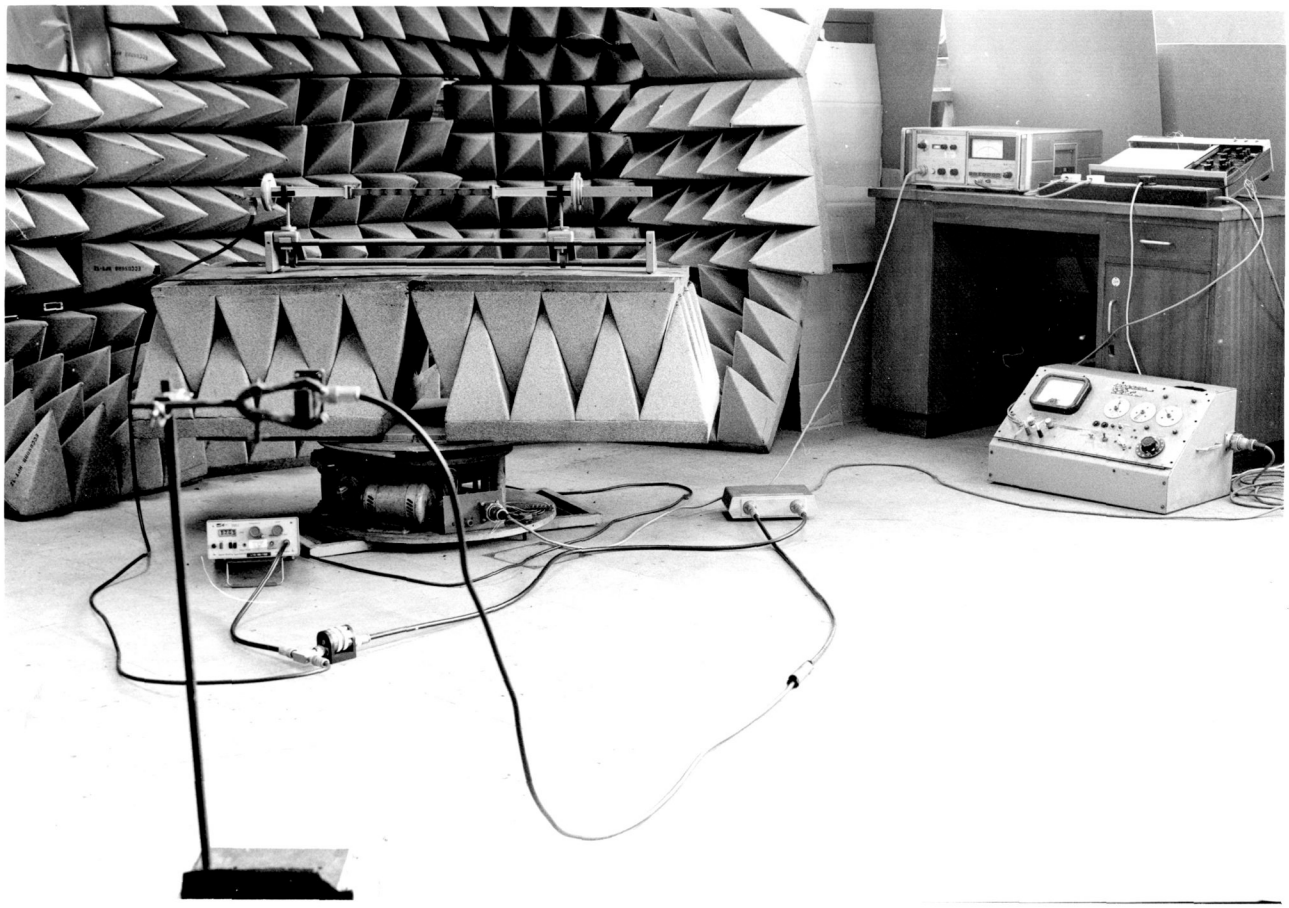


Plate 7.4 Far field measurement set-up of the 8-slot array

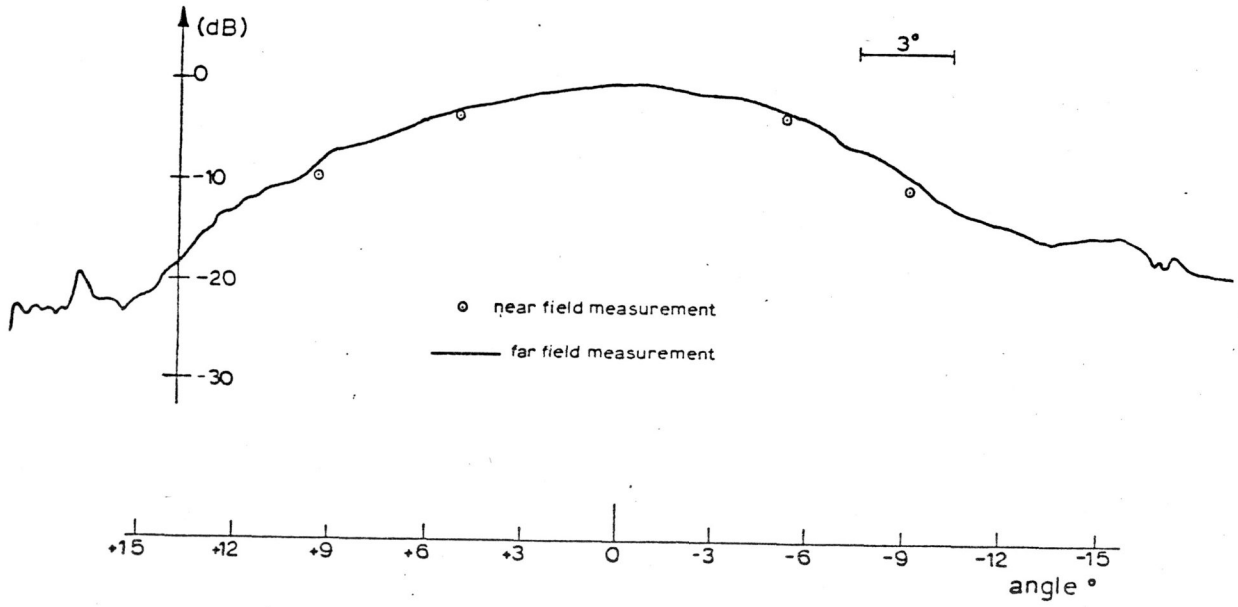


Fig 7.29 Far field measurements of an 8-slot array at 5.7 GHz

The continuous curve in Fig. 7.29 gives the direct measurement of far field in db, using the set-up of plate 7.4. The computed results from near field measurements are marked as circles on the graph. The results show very good agreement : the 3 db beam width and the 10 db beam width of the main beam differ by 0.3 and 0.6db respectively.

7.4.4 Discussion of the results of the preliminary tests

The conclusion that can be drawn concerning the reliability of the monitoring methods that have been recommended are as follows. The frequency change of 0.02% (per hour) has a negligeable effect when the wavelength is considered. However, due to the unavoidable path length differences, this frequency instability might cause a phase change of about 40deg per hour. In addition a second order-effect on the phase slope-line of about 4deg/meter of probe scanning was observed. The effect of phase or gain reference changes using the subtraction method, when two reference patterns are compared, might result in a difference pattern even when no defects are imposed on the array. However, in an actual MLS phased-array this question might not arrise as there the frequency is stabilized. This effect has been discussed already in subsection 7.3.5. The main result from the V.S.W.R. measurement is that blocking of radiating elements having higher illumination has a larger effect on the reflected power, and hence on the aperture illumination, which was rather to be expected.

More meaningful are the measurements of modified aperture illumination due to metal blocking. It was found that similar changes occur in the neighbouring elements, when various locations

were chosen for the imposed defects. The main effect (see Fig.7.28) is the increase in the forward power, apart from the "hole" due to the blocked element. This is similar to the model used in chapter 4 for the internal coupling effects (forward reflected power). This effect is expected to be of second order in actual systems which are not fed in series. The results of the far field measurements comparison to the near field measurements show that the system including the program are of good quality in spite of the errors discussed in the present section.

7.5 Summary and discussion

The monitoring methods recommended in this work have been found to give the expected results, for artificial defects of single missing elements in the array.

Hence a partial verification of the theoretical methods proposed has been achieved. A full verification of the method proposed will be possible only if one-to-one models of actual phased-arrays, with frequency stabilized source, could be checked using the same methods, in particular in the far field. Some conclusions can also be drawn concerning the use of practical measurement system (with phase and amplitude instabilities). In such cases, a threshold should be applied below which results are to be ignored and only results complying with the threshold are to be considered for the methods. This means that the long term instabilities can be tolerated in practice.

The side-lobe region have been found to be preferable for measurement, as being least sensitive to parameter instabilities.

The shape of the phase deviation for differnt locations

of the artificial defect (to the right or to the left of the array centre), justify in part the model of internal coupling (asymmetrical reflections due to a defect, as explained in chapter 4). The shape of the phase deviations also mean that mutual coupling (external) has only a second order effect compared to the internal coupling and hence is not of prime interest in arrays with interelement spacings of about 0.7λ, as used in the experiments. It is believed that MLS arrays (although with $.61\lambda$ interelement spacings) are expected to have lower internal coupling effects due to the power distribution network structure.

The near field to far field comparison shows encouraging results with the laboratory set-up used for these experiments and can be regarded as an overall check on the quality of the experimental system.

CHAPTER 8

COMPARISON OF THE METHODS

In previous chapters several monitoring techniques have been analyzed, and also tested by computer simulation and in part by experiments. A comparison will now be made between the different methods proposed and their applicability demonstrated in a specific example in the form of a proposed monitoring system for the MLS phased-array.

8.1 Analysis tools used

Effectively two analysis tools have been suggested and used in this work. These are the equivalent substitute element technique and the approximations to the Fresnel integral.

8.1.1 The equivalent substitute element technique

This technique proposed the representation of defective elements by their equivalent substitute array (equation 2.4). This representation gives simplified results if a single element is defective in the array, and where defects are of a static nature like a constant amplitude and/or phase defects. In the dynamic case of a stuck phase-shifter, a modified result is expected (see equations 3.19 and 3.19a). This is further modified if a thinned phase-shift network is used, i.e., where single phase-shifters are used to control the phase of a group of elements (a sub-array). An important feature of the equivalent substitute element technique is its inherent normalized phase-line resulting when a single element is defective in the array. This means that the resulting phase-line is independent of the illumination function of array elements. (Hence it is very

attractive for use in practical arrays).

8.1.2 The approximation to the Fresnel integral

Another important tool that has been investigated is an approximation to the Fresnel integral. This representation is specifically helpful in describing the near field (Fresnel region) of a scanning-beam aperture antenna in terms of the antenna aperture illumination and the angle scanning function. The use of this presentation has been described in chapter 6 and will be summarized in a later section dealing with the near-field monitoring technique.

8.1.3 Simulation models used

Simulation on the computer has been found to be a most useful tool as an aid to analysis. Two main tasks have been performed by the simulation. The first was to produce a verification of the analysis, modelling antennas and defective elements in the presence of a variaty of excitation errors, so as to represent actual array performance. The simulation was also used as a kind of "scratch pad" to check and produce ideas leading to new methods. As it is very easy to come to erroneous conclusions, care was taken to check the quality of the simulation and in particular whether any errors were present in the computer programs developed, or in the equations and parameters used in the models. As an example the quality of the random number generator called as a computer function (RANGET), was checked with a subroutine COREL03 (see Appendix E) developed to calculate the autocorrelation function. The computer results have been compared to the expected statistical equations. This comparison then led

to two conclusions. First, that the random number generator is of a good quality of statistically independent numbers, for the sizes used. It also had an accompanying important conclusion that the autocorrelation function subroutine used was correct. Line printer graphics (computer library GRAFIC and GRAFIT), although of insufficient resolution, have been widely used to produce fast and inexpensive displays of selected numerical results, so that spot checks could be used to trace any anomalies in the programs and, also, to enable an immediate assessment of the results. The simulation included programs of the far-field and the near field patterns of N element array of various illumination functions, subjected to defects in single or multiple elements or subarrays, in the presence of random phase excitation errors. The models assumed perfect tracking analogue phase-shifters. Defects of a dynamic nature were examined when, for example, a single phase-shifter was held fixed while the others changed in the prescribed manner. Dynamic phase-shift errors, due to digital quantization of the phase, have been combined in a statistical rather than a deterministic way, which facilitates their modelling. It is also ecconomical, and gives the results neatly in the form of an envelope. A preassigned range of uniformly distributed random phase-shifts are added to the correct calculated values of phase-shift. This range could represent the inaccuracy due to the value of the least significant bit in an m-bit phase shifter. Then, two types of random excitation errors have accordingly been used - static or dynamic, depending on whether the random number generator was reset or not after each sequence of phase settings. Static errors can represent actual phase errors due to production inaccuracies of array elements;

dynamic errors represent, as explained earlier, the built in phase quantization.

Mutual coupling effects were incorporated in the simulation using normalized values of mutual impedances according to Carter's [9] equations, for the external coupling. While internal coupling was represented by a simplified model of forward and/or backward reflected power, due to the supposed defect. These effects were incorporated as an equivalent substitute array, the illumination of which is a function of the values derived from the calculated mutual coupling effects.

Near fields of antenna apertures have been simulated using the Fresnel-Huygens diffraction formula. NAG Routine functions, (S20ADF and S20ACF) given by a series approximation due to Abramowitz and Stegun [25] have been used for the evaluation of the cosine and sine integrals. Near-field to far-field transformation used the discrete Fourier transformation (D.F.T.), using NAG Subroutines (C06ADF). However, D.F.T. programs had to be developed (by the author) in cases when the required number of transformed values was larger than the number of input samples available (the standard procedure which is available as a NAG Routine has equal input and output samples). For example the transformation of near-field to far-field patterns used this technique to achieve small direction increments.

Near-field measurements simulation was helped by an auxiliary Subroutine EJIX (see Appendix E). This subroutine calculated the near-field received over a linear measurement region from an N-element transmitting array. And was used, for example, to find out how critical the near-field sampling

increments were in terms of the resulting far-field pattern. Additional programs are given in Appendix E are DBPMES used for preprocessing to translate data from the X-Y recorder plot into phase and amplitude in the required format for program JACK30. Program JACK20 for mutual coupling between parallel dipoles. Program JACK42 near field focusing of near fields diffracted from a uniformly illuminated aperture. Program JACK37 as before but for half cosine aperture field. Program JACK38 as before but for cosine over pedestal illumination . Program JACK45 for far field radiation from a pyramidal horn antenna with a predetermined phase error.

8.2 A summary and comparison of the monitoring methods

Far-field and near-field monitoring methods have been suggested. The far field methods included:

- The subtraction method.

- the angular spectrum(direct) method, and

- The autocorrelation function (a.c.f.) method.

These three physically distinct methods also correspond to three quite distinct levels of processing, in that they demand an increasing amount of processing time for their implementation.

The near field methods included:

- The near-field monitoring technique.

- The integral and

- Internal monitoring.

These methods will also be compared. Special attention will now be paid to their applicability to monitoring the MLS phased-array antennas.

The subtraction method, based on the representation of defective elements by their equivalent substitute array, has been found to be a most efficient method. Specifically where a single element has become defective in the array. Then in the case of defects in ideal arrays only a few measurement samples are needed to resolve the phase ambiguity and give the equivalent substitute element phase-line, thereby enabling the identification of the location of the defective element and the type of defect. As explained in chapter 3 this method could be used for practically any type of illumination function, including thinned arrays.

This capability, of identifying the type of defect, is not available in the other two methods used, namely, the angular spectrum (direct) method and the a.c.f. method. It is also not available, as explained in the introduction (chapter 1), in the method suggested by Ransom and Mittra [2]. Although those other methods enable the identification of one or of several defective elements occuring at one time in the array. However, with the expected reliability of operational phased-arrays like the MLS, this type of defect occurrence is highly improbable. Hence sequentially memorizing the occurrence of defects in the array could be used instead as an aid to maintenance. A simple criterion can be used for the monitoring and control thresholds. For example, the maximum percentage of defective elements, say 10%, of the array, can be tolerated (see Bendix corporation experimental investigation [4]) before a shut down procedure

(see ICAO [6]) and alarm are to be initiated. Hence, the subtraction method can be used to monitor a multitude of defects in practical antenna arrays. An additional important advantage of the subtraction method arises from the fact that the expected processing time needed is very short, enabling real-time decisions to be made. Incidentally, the time required is far below the 1 second reaction time required by ICAO Standards And Recommended Practices (SARPS) [6].

Alternatively, or in parallel, it is possible to use the other methods to verify the findings of the subtraction method or, if real-time processing is possible, to use them altogether in order to make a decision.

The two other methods, the angular spectrum and the a.c.f. methods, use the aperture illumination magnitude and power, accordingly, for a decision on the presence of defective elements due to anomalies in the aperture distribution. The angular spectrum method requires a longer processing time than the subtraction method, due to the far-field to aperture axis transformation needed. As is evident, this method required many data samples to be Fourier transformed to achieve the normalized aperture illumination function. The resulting illumination function magnitude, is to be compared with a reference aperture illumination pattern of the array, before it became defective. Then, using proper thresholds to minimize false alarms, a decision can be taken on the location of defective elements over the array aperture. As will be shown, in section 8.4, the angular spectrum (direct) method still enables real-time processing, especially if F.F.T. processing is available on the system's already installed

microcomputer.

The autocorrelation method is expected to give results of higher quality (fewer false alarms in a given measurement "noise" background), due to its inherent smoothing capability. This smoothing is a result of correlating many data samples which are used to extract the periodic oscillations, due to elements failure (see section 5.3), before transforming into the aperture plane. This means a longer processing time than that required by the angular spectrum (direct) method.

The near field monitoring methods give the following results. The near field monitoring technique (section 6.2) is expected to give a reconstructed main-beam scanning by near-field (Fresnel region) measurements. The main importance of the near-field monitoring technique, which is based on approximations to the Fresnel integral (chapter 6), is in the non necessity for corrections to be made in the transmitting array and in its real-time (main-beam pointing) monitoring capability. This is due to the fact that no further near-field to far-field (Fourier) transformation are needed. In addition it requires only a few (say 10) sampling elements over the near field monitoring antenna aperture. However, the requirement that this aperture should be extended to the length of the transmitting antenna is a disadvantage. It must be pointed out that the subtraction method could be used in the array near-field if a single element (or a single subarray) is concerned. It is then only necessary for the measurements to be performed in the far-field of the single element (or sub-array), as explained in section 2.7.

In addition it can be speculated, based on the simulation

of the near-field received by a single monitor element (section 6.2.1 and figure 6.4a), that the near field far side-lobe pattern behaves in a manner very similar to that of the far-field. Hence, if this is really the case, the near-field far side-lobe region can be used for the detection of a multitude of defective elements using the far field monitoring techniques, with no need for additional preceding near-field to far-field transformations. However, a modification may be needed to take account of the residual parallax effects.

The other near-field techniques, namely the integral/internal monitoring, are techniques already used for getting the far-field pattern from very near-field monitoring (see Bendix [4]) as explained in section 6.3. The suggestion which was presented, using the serial waveguide sampler, has shown that main-beams scanned to about 51deg, 33deg or 22deg using standard waveguides are detected. Therefore the two main beam locations at $\pm$51, $\pm$33 or $\pm$22 degrees, of the MLS angular coverage ($\pm$60deg.), can be detected if use is made of the two opposite ends of the serial waveguide samplers. This may be found advantageous for simplifying the monitoring of the main beam scan coverage.

Having compared the different methods from an analytical point of view, backed up by simulation, it is instructive to recall the experience using actual arrays.

8.3 A summary of the experimental investigation

The experimental investigation was aimed at getting additional verification, where possible, of the methods suggested, and of their simulation on a computer. The measurements have been

limited to the near-field radiated from linear slot waveguide antennas, operating at a frequency close to that used by the MLS. The array elements were subjected to artificial defects. Far-field monitoring methods have been used for the detection of defective elements in the array, after transforming the measurements to the far-field, using computer programs. The outcome was that these computed patterns have been shown to be similar to those predicted by simulation where mutual coupling effects have been included. Hence, some verification of the far-field monitoring methods has been achieved. Also far field pattern measurements have been made and results very close to those of the near-field measurement after being transformed to the far field have been obtained in the main beam region (see section 7.4.3). Hence a further confirmation of the programs used from near field to the far-field has been reached.

In addition, it has been demonstrated that the far side-lobe region is a preferred region, compared to the main-lobe region, as explained in section 2.3.

An important result was the outcome of the long term stability experiments of section 7.3.5. It was shown that practical measurement systems are sufficiently stable. A shift of about 40 degrees in phase and of about 2 db in magnitude between two such measurements, cuased no significant change in the resulting phase-line of a defective element, using the subtraction method. The two reference patterns in this instance were measured 5 days apart. Also in the calculation of aperture illumination using the angular spectrum methods, no significant difference has been noticed. These stability measurements have shown that a

threshold is important, to distinguish between the case of defective elements and that of an unstable reference. A difference of about 10 db has been observed between the case of a missing element and that due to the subtraction of two unstable reference patterns. Hence a 6db level, below the magnitude expected from a missing element, can be used as a practical threshold.

8.4 Comparison of the required processing

The complexity of processing is dependent on the monitoring method to be used. Hence, there are three main levels of processing, (see section 8.2). The processing is composed of two parts: the preprocessing and the main processing. Preprocessing is necessary to normalize the measured quantities, before the monitoring algorithms can be examined in the main processing. The amount of preprocessing needed is therefore dependent on such factors as the dynamic range and accuracy of measured signal variables. These, in turn, affect the design of the measurement system. Preprocessing and processing will be discussed in the following two sections.

8.4.1 Preprocessing and signal measurements

Magnitude and phase are the variables to be measured. However the quantities used in all the monitoring methods are in effect the real and imaginary parts of the complex signal. Hence, measurement of real and imaginary parts of the complex signal are preferable than the measurement of the signal magnitude and phase.

The necessary dynamic range is dependent on the measurement region. If main-beam and side-lobe regions are to be

included, then about 50db dynamic range is required. However, if only the far side-lobe region is of interest, then a 20 to 30 db dynamic range can be sufficient, enabling linear circuits to be used. This is to be preferred as the circuitry is simplified and becomes cheaper. If a 50db dynamic range is required, then non-linear circuitry, such as logarithmic amplifiers, might be necessary. Due to the non-linear measurements additional preprocessing in order to achieve linearization has to be used, before the monitoring algorithms can be examined. This is in addition to the more complex and expensive circuitry required, like instanteneous logarithmic amplifiers and phase matched limiters.

A block diagram of the above circuits will now be described.

The quadriphase-demodulator widely used in monopulse Radar and data communication, enables one to obtain unambiguous measurements of the phase difference ϕ between two input signals, resolved into two quadrature output bipolar video channels I and Q. A block diagram is describd in Fig. 8.1.

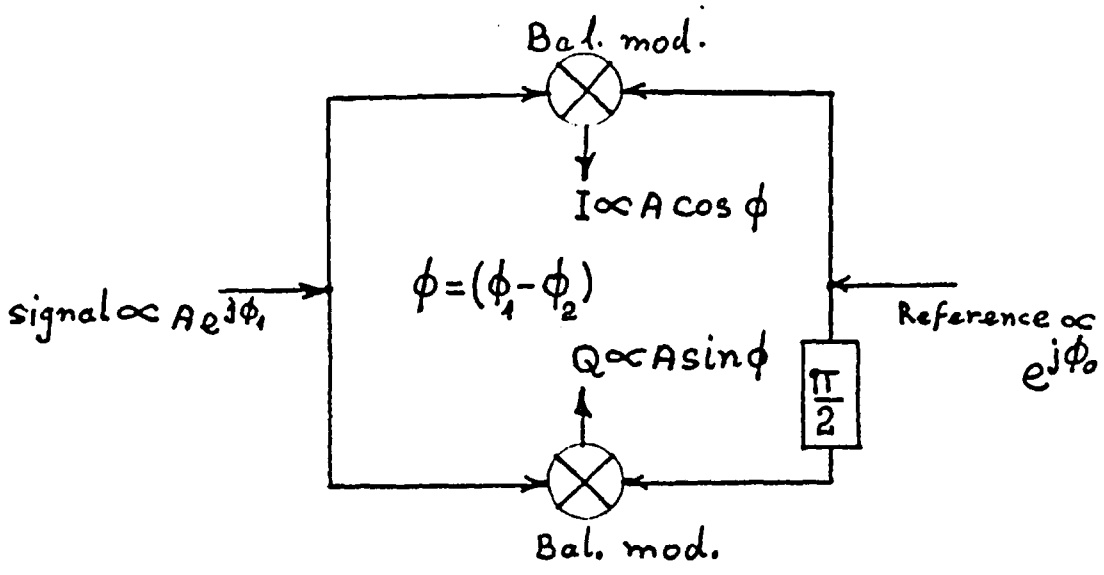


Fig. 8.1 Block diagram of the quadriphase-demodulator

The output signals I∝ Acos ϕ and Q∝ Asin ϕ can be used as long as the expected dynamic range of the input signal does not exceed about 20db. In practice the dynamic range is larger, hence, non-linear circuits should be used. A constant transmission phase-shift limiter can be used to establish a constant input signal for the qudriphase-demodulator. A sample of the input signal before limiting can be detected by a logarithmic video amplifier, as shown in Fig. 8.2.

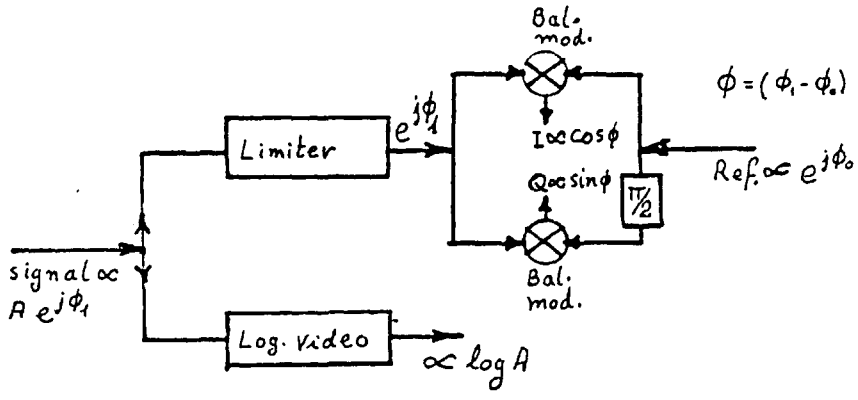


Fig. 8.2 A wide dynamic range quadriphase-demodulator

Here, three data samples are necessary instead of the two needed

in the linear case (Fig. 8.1). As explained earlier in this section an additional translation of log A into A will be needed in the preprocessing. This value will then be multiplied by the I and Q values of the amplitude limited signal, in order to resolve the two orthogonal samples needed for processing. Quadrature-demodulators, limiters and logarithmic amplifiers are available commercially with sufficient accuracies in the I.F. frequencies (see Appendix F). It will, therefore, be recommended that phase and amplitude detection be performed at I.F.

8.4.2 Processing

The approximate number of operations necessary for the processing of the different monitoring methods, will now be discussed. Following section 8.4.1 it will be assumed that normalized real (designated I, i.e., Inphase) and imaginary (designated Q, i.e., Quadrature) signals are to be processed, according to the appropriate algorithms, as follows.

The subtraction method

For ideal antennas, only two complex samples are required in two direction-cosines of the array, for the detecton of defects, using this method. The defect in a single element can be located using the linear equation (see equation 2.14).

$$K = A (\phi_2 - \phi_1) + B \qquad 1 \leq K \leq N . \qquad (8.1)$$

Where, two arctangent functions of the resulting equivalent substitute element ratio Q/I, give the two phase-line points ϕ_1 and ϕ_2, in the two directions θ_1 and θ_2. $A = \lambda / 2\pi d \, [\sin \theta_2 - \sin \theta_1]$, where d is the interelement spacing.

Fixing θ_1 and θ_2, in advance, makes A a constant which could be calculated and placed in memory beforehand. In order to calculate the total phase it is necessary to resolve the phase ambiguity. This can be done by adding one to two more samples, with direction cosines sufficiently closely spaced. From equation (8.1), it is clear that the steepest phase slope-line will occur when an edge element of the array is defective. Then

$$|\sin\theta_1 - \sin\theta_2| = \lambda/\pi a \, |\phi_1 - \phi_2| \qquad (8.2)$$

As an example : for an aperture $a=50\lambda$, and required $\Delta\phi=(\phi_1-\phi_2) \leqslant \pi/2$, then $\Delta\theta=(\theta_1-\theta_2)$ should be $\lesssim 1/4$ deg, near the broadside direction. For actual antennas and measurements this small number of samples might not be sufficient. A statistical estimation of a phase regression-line will then be needed, using tens of data samples.

Summarizing, the number of operations required, each time, using the subtraction method according to equation (8.1) will be

1 addition
2 subtractions
1 multiplication
1 division
1 inverse trigonometrical function

This is assuming an inphase and phase-quadrature (I-Q) representaion of the complex signals. It is self evident that the number of operations required in an actual monitoring system, play an important role in determinating the type of microcomputer to be used for real time monitoring and production of alarms.

The higher levels of processing will now be summarized. It will be assumed, as before, that quadrature channels are used to represent the complex signals.

According to the Nyquist criterion, the number of samples required, using the angular spectrum method, is dependent on the array dimension (a/λ) and the maximum measured scan angle. For example, for $a/\lambda = 50$ and $|\sin\theta| \leqslant 1$, a minimum of 100 samples are required. The resulting resolution in the aperture-axis is dependent on the maximum scan angle (see section 5.1). In order to assess the complexity of processing quantitatively, 128 samples are assumed to be Fourier transformed (D.F.T.), giving the aperture distribution. Using the F.F.T. algorithm it can be shown that about 1800 additions and 1800 multiplications are needed. If F.F.T. processing is not available, than the D.F.T. might require about 18 times more additions and multiplications.

Using the autocorrelation method and assuming M=64 shifted samples and F.F.T. calculated over 128 points, it can be shown that about 75 000 additions and 40 000 multiplications are needed. As before, if F.F.T. processing is not available, then the D.F.T. might require about 105 000 additions and about 70 000 multiplications.

In addition, it should be mentioned that for actual antenna arrays additional criteria, such as thresholds, are to be used which add to the number of operations required.

Summarizing, the first level of processing, the subtraction method, is adequate for real-time processing in actual monitoring systems using microcomputer processing. The second

level of processing, the angular-spectrum method, might still be used for real time processing, assuming F.F.T. processors are available for the monitoring system. The third level, the autocorrelation function method, can only be used in non real-time processing, hence, it is less practical.

Having made a comparison between the monitoring methods, an attempt will now be made to design a system to monitor an MLS antenna. The exercise is admittedly academic, but is nevertheless instructive.

8.5 A tentative proposal for a practical monitoring system (MLS - phased array)

A proposal for a practical monitoring system for an MLS Azimuth phased array will be made based on a hypothetical MLS system specification given in table 8.1 and in Fig. 8.3.

Table 8.1

Hypothetical MLS Azimuth system specification

Frequency range (200 channels)	5.03-5.09 GHz
Beam scanning rate	20000 deg/sec
Scan limits	±40 deg
Beamwidth	1 deg
Polarization	vertical
Array	96 elements
Interelement spacing	.61 λ
Number of phase-shifters	16
Phase quantization	4 bit (22.5deg)
Phase cycling	13.5 Hz
Subarrays (Rotman lens)	
Number of subarrays	16 (of 6 element each)
Lens switched beam ports	16
Aperture distribution	27 db (Taylor taper)

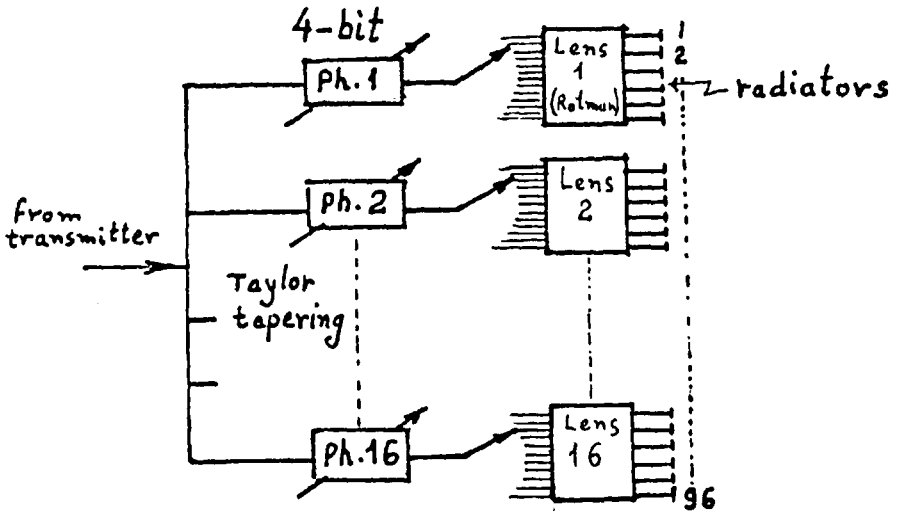


Fig. 8.3 Block diagram of MLS phased array

The monitoring system for the MLS phased-array specified in Table 8.1 and Fig. 8.3 is outlined in Table 8.2. The monitoring is composed of two main tasks. The direct measurements giving the beam pointing error. The indirect measurements giving maintenance alarms in the presence of failed elements in the array. Using a preassigned number, for multielement failure, a downgrade or shut down alarm can be produced (see ICAO [6] or Appendix A)

Table 8.2

Tentative monitoring system specification

Frequency range	4.95-5.2 GHz
Instantaneous frequency band width	5 MHz
Dynamic range	50 db
Accuracy of magnitude measurements	0.5 db
Accuracy of phase measurements	10 deg
Repeatability of phase measurements	5 deg
Proportional angle signals error	(direct measurement)
Beam pointing accuracy	0.01 deg
Side-lobe level and ERP	0.5 db
Number of selected directons in the angle coverage region	
internal/integral monitoring	3
Field monitoring (near field or far field)	1
Indirect measurement of proportional angle signal errors	
Number of preassigned multielement failure	12
Levels of alarms	2
Maintenance alarm	1
Down grade/shut down alarm	1
Reaction time	
proportional angle monitoring	0.5 sec
Element failure processing	0.5 sec

8.5.1 Definition of the monitoring system

A near-field monitoring system is assumed for the detection of defects. This enables minimization of interference and multipath effects.

The monitoring system will be composed of a single monitor antenna, preferably a pyramidal horn, located in the Fresnel region, about 1/10 the Rayleigh distance from the transmitting antenna. (If a near-field real time beam pointing monitoring scheme is required, then a planar monitor antenna should be used (see section 6.1). This or alternatively far-field monitoring might be required as the internal/integral monitoring does not give information on pointing errors due to mechanical or geometrical changes.) Internal or integral monitoring, is to be used for the detection of defects in parallel with the near field

antenna. The near field antenna will enable the determination of any geometrical shift of the array, and will also be used in the subtraction method for the detection of single defective elements in the array. The angular spectrum method (and the a.c.f. method) should only be used with internal/integral monitoring to avoid the additional processing required of near-field to far-field transformations.

The phase detecting system should be composed of two quadrature (I-Q) channels to minimize processing operations (see Fig. 8.1).

The phase reference to the monitoring system will be taken from a single side band (S.S.B.) shifted frequency. The difference between the transmitted frequency and the S.S.B. will be used for the I.F. frequecy of the monitor receiver. The availability of commercial circuits (see Appendx F), leads to the recommendation of using an I.F. centre frequency in the range 30 to 160 MHz. As the required dynamic range is 50 db an instanteneous logarithmic I.F. amplifier should be used for the detecton of amplitude. The phase is to be determined by a quadratic demodulator where its input signal is normalized by a limiter (with a constant transmission phase-shift), as explained in section 8.4.1 and Fig.8.2. This arrangement can achieve the required amplitude and phase accuracies over the dynamic range of the input signal. The I.F. width is given by the expected phase jumps of the scanning array. The MLS specification is an angular scanning rate of 20000 deg/sec, over a range of $\pm$40 deg in azimuth. Using a 4-bit phase-shifter, this leads to an average 4 microsecond period for one phase bit, resulting in a minimum width

of about 240 KHz. Hence I.F. circuitry with a 5 to 10 MHz band-width, which is normally available (see Appendix F), will be adequate.

The instanteneous main-beam pointing angle will be determined from a synchronous timing signal fed from the MLS.

The processing system should include an update memory to record sequentially the presence of all defective elements, using the subtraction method. Periodically, the angular spectrum method will be used for comparison, with the memorized updated defects. An alarm will be given if more than a preassigned number of elements are found to be defective.

8.5.2 A simplified block diagram

Following the system's definition and the explanations in 8.5.1, it is now possible to describe a practical monitoring scheme. The system might be arranged as shown in Fig. 8.4

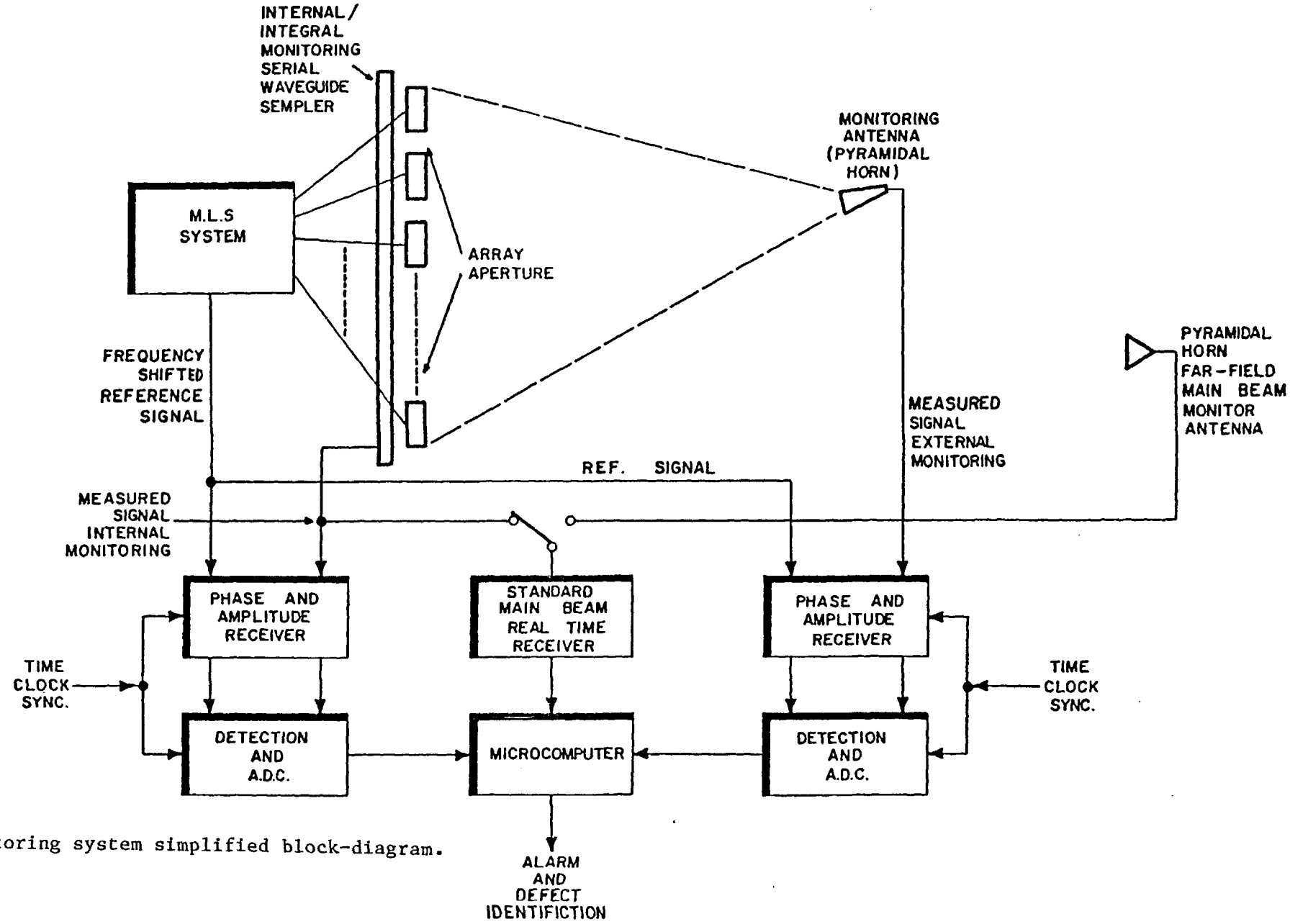


Fig.8.4 Monitoring system simplified block-diagram.

Several of the more important sections of the monitoring system will now be described in detail. These are the phase and amplitude receiver, the internal monitoring serial waveguide sampler and the monitoring near field antennas.

The phase and amplitude receiver has a wide dynamic range, as described in section 8.4.1 and Fig.8.2 . The reference and input signals are shifted to the I.F. as indicated in Fig. 8.5.

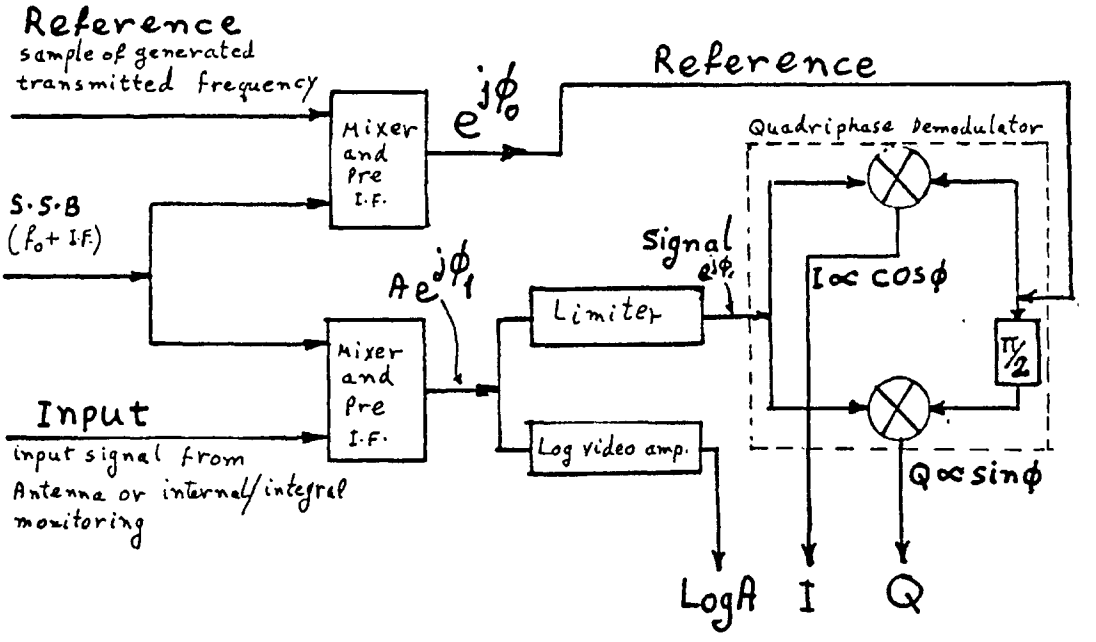


Fig. 8.5 Block diagram of the Phase Amplitude receiver

It is assumed that the S.S.B. frequency is produced in the frequency generation circuitry in the MLS transmitter. A sample of the transmitted frequency is also taken to produce the

reference I.F. channel, using down conversion through a mixer (plus I.F. preamplifier). The signal input from the antenna (or internal) monitoring, is also down converted, similarly. The I.F. signal from the monitor is normalized in amplitude in a limiter, of a constant transmission phase-shift type. It is then fed as the input signal to the quadriphase-demodulator, and its phase compared to the reference signal. the input signal to the limiter is also coupled to an I.F. instanteneous logarithmic amplifier with a wide dynamic range. Three output signals are then available: Log A, I and Q. Example of circuits available commercially are summarized in table 8.3 (for details see Appendix F).

Table 8.3

Examples of commercially available circuits

Circuit	Producer		
	R.H.G. Cat No	OLEKTRON Cat No	M.C.L. Cat No
Quadriphase Demodulator	DPD6010	PC-60	
Limiter (constant phase)	ICSL6010		PLS-1
Logarithmic Amplifier	LST6010		

The internal monitoring system will now be described. It is assumed that three angles of scanned beams are required. Two close to the edges of the angular coverage , between 30 and 40 deg, and one beam close to the boresight inside the range ±3 deg. As explained in section 6.3, for sampler of the same hand (slots) a series waveguide will produce two beams according to the value of $\arcsin(\lambda_o/\lambda_g)$. If a standard wavegude Narda band XN is used

(a=1.372",b=0.622"), then the angles of the reproduced main beam will be at approximately ±33 deg, if the two edges of the waveguide sampler are used. The beam close to the boresight can be reproduced using the standard C-band waveguide (a=1.872", b=0.872") and opposite hand slots are to be used. It can be shown that a beam at an angle of about 2.9 deg, will then be produced. As before the +2.9 or the -2.9 deg can be chosen, according to the waveguide sampler edge used, see Fig. 8.6.

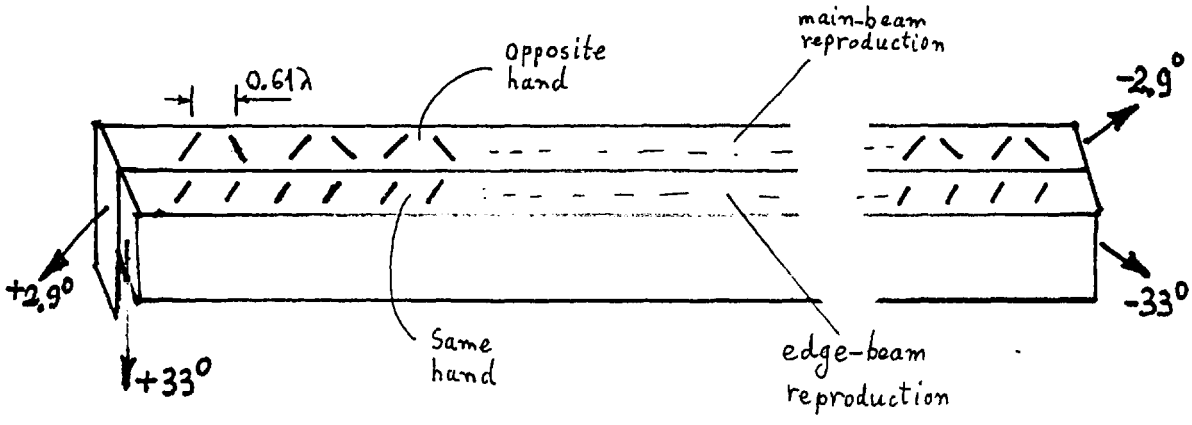


Fig. 8.6 Description of internal monitor waveguide samplers.

Two side by side waveguide samplers of different waveguide cross section are used for internal monitoring.

For the near-field monitor antenna a medium-gain or even a low-gain antenna, can be used. However, in order to minimize the effects of multipath, a medium gain pyramidal horn is recommended; the requirement being that its beamwidth will be sufficient to cover the antenna aperture. A 16 to 20 db gain symmetrical (pyramidal) horn can be used, giving a distance of a few (say 4 to 6) aperture widths from the array, then it will fully

cover the array aperture. The near field horn can be used mainly for the detection of defects in the array elements, in parallel with the internal monitoring, using the subtraction method as explained in sections 2.7 and 8.2. It can also be used, after transformation of near-field to far-field, with the angular spectrum and a.c.f. methods. But as this requires much more processing only non-real-time analysis can be assumed in that case.

The main beam-pointing error is to be detected using a far-field monitor (at the Rayleigh distance). A similar horn can be used. A real-time receiver similar to the airborne one is to be fed to the microprocessor, as a monitor input. As explained, due to expected excessive multipath affects, it is not recommended that the far-field monitoring be used for the identification of defects in the array elements.

The far-field monitoring of main beam pointing errors, is the simplest one. However, as explained in chapter 6, a near field focused monitor antenna can be used instead. This is not justified economically, unless a decision to use a real-time near-field (Fresnel region) monitor antenna is made. Such an antenna can have the followng shape, according to section 6.1 and as described in Fig. 8.7

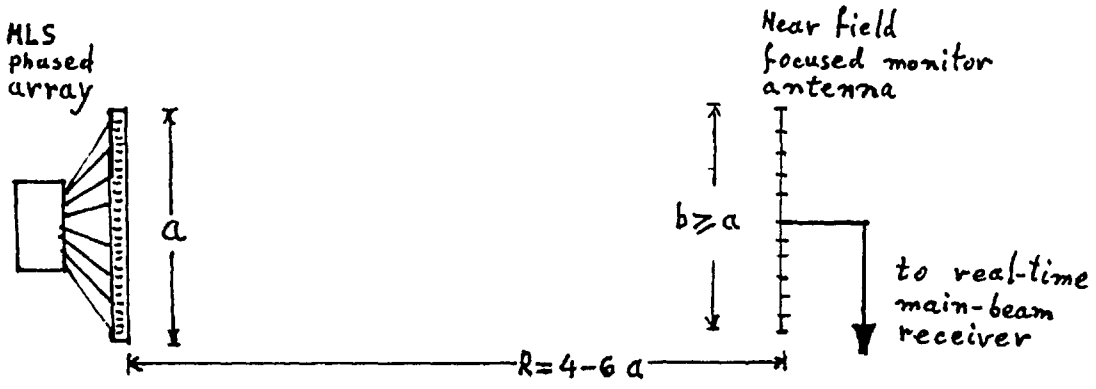


Fig. 8.7 Near field focused monitor antenna

According to sections 6.1 and 6.2 , about 10 to 15 sampling elements are sufficient to comply with the Nyquist criterion, in a distance of 4 to 6 aperture widths. These elements are to be equally distributed over the planar aperture.

CHAPTER 9

CONCLUSIONS

The motivation for the present work arose from the author's discovery of gaps in the solutions which are available to monitor the performance of phased-array antennas. In particular, methods of dealing with the identification of defects in the elements of the array were lacking.

First a method of simplifying the representation of defective elements in antenna arrays was sought. The equivalent substitute element technique, suggested in chapter 2, turns out to be a very efficient tool for this purpose. In this technique the defective array is represented as a superposition of two arrays - the ideal array and the equivalent substitute array. The far-field pattern of the defective array is then given by the superposition of the pattern of the ideal array and that of the equivalent substitute array.

The inverse problem, the detection of defective elements in the array due to anomalies in its far-field pattern, has been solved in several different ways. These are the subtraction method, the angular spectrum (direct) method and the autocorrelation method. In the near field the near-field monitoring technique and internal/integral monitoring have been examined.

The first method, the subtraction method, involves the subtraction of the far-field pattern of the ideal array from that of the defective array. The result is, therefore, the equivalent substitute array far-field pattern. It has been shown that for

the case of a single defective element in the array its identification is straightforward. The location of the defective element is a linear function of the phase of the substitute array pattern. Therefore the process suggested for the identification of a single defective element in the array is quite simple, at least where defects in ideal arrays are concerned.

More realistic array models have been incorporated into the analysis by the inclusion of effects of random phase excitation and mutual coupling into the antenna model. It has been shown that using simple statistical estimation (a linear regression line) of the phase-line a correct identification of a single defective element can be achieved.

It was further suggested that use be made of the far side-lobe region for monitoring. There, the variations due to the presence of defective elements is more pronounced than in the main-beam region. Hence, a higher sensitivity to the presence of defects and a greater immunity to the effect of measurement-noise is achieved. For the same reason the danger of large errors generated by the subtraction of two large numbers, reproducing the substitute element pattern, is minimized in that region. In addition, the analysis and the experimental investigation have shown that thresholds, to minimize false alarms, are easier to implement in the side-lobe region. This is important in cases where long-term instabilities are expected in the measurement system.

A question still remains: could this simple method be used as a general method in the presence of many defective elements in the array ? The answer given to that is in the

affirmative, but with the following assumption, which seems justified, that failures do not occur in more than a single element of the array at any one time. Then, the subtraction method can be implemented sequentially with one modification; an updated reference pattern is to be used rather then the original reference. The process will then be one of memorizing the previously detected elements and applying the modified subtration method sequentially. Taking into account the high reliability of present and future solid-state phased-array antennas, the failure of more than a single element at one time is very unlikely. This assumption is recommended for further investigation.

An additional important feature of the subtraction method is its possible application in near-field monitoring. It has been explained in section 2.7 that in the case of a defective single element or single subarray the subtraction method does not require the measurements to be performed in the far-field of the complete array. It is merely necessary to be in the far-field of the element or the subarray (whichever is being sought), since the field due to the complete array is subtracted out.

Before continuing with the other proposed monitoring methods, the findings on mutual coupling effects on the monitoring will first be summarized. Mutual coupling can be thought of as consisting of two components, one external and the other internal (see chapter 4). The external component can be represented by an equivalent substitute subarray symmetrical, in large arrays, about the location of the defective radiating element. The internal component can in many cases be represented by an odd-symmetrical equivalent substitute subarray (e.g., in a serial waveguide slot

antenna). This odd symmetry causes relatively larger errors in the fault detection process than the symmetrical equivalent substitute array. However, in practical arrays, many of which are using directional feed distribution networks and non-reciprocal phase-shifters, the internal component is expected to have only a second-order effect on the monitoring. The external component is dependent on the interelement separation. For separations greater than 0.5λ , this component is about one order of magnitude less than that of the equivalent substitute element. Hence a ripple is introduced on the resulting phase-line of the substitute element. This can be smoothed using a statistical regression line, as explained previously.

The other far-field monitoring methods, the angular spectrum method and the autocorrelation function (a.c.f.) method are based on the Fourier transform relation between the far-field pattern of the array and the aperture illumination. In comparison to Ransom and Mittra's [2] method the angular spectrum method gives a simpler solution, as only the Fourier transform of the far-field pattern is needed to derive the aperture illumination. In contrast, the method suggested by Ransom and Mittra requires the Fourier transform of two functions. The a.c.f. technique is a method to derive the aperture power illumination, rather than the magnitude illumination which is derived using the angular spectrum method or Ransom and Mittra's method. It is based on the known Wiener-Kinchine [14] transform relation between the autocorrelation and the power spectrum. This method requires the process of deriving the autocorrelation function of the far-field pattern before Fourier transforming onto the aperture axis. This process of autocorrelation has the adventage of smoothing the data

before taking the Fourier transform, where the angular spectrum method does not. However, the disadvantage is that it is a time-consuming process; so that where real-time processing is concerned the angular spectrum method is the preferred one. The application of the angular spectrum method and the a.c.f. method in the far side-lobe region has been shown to give results which are directly applicable to the monitoring of defects. The resulting aperture pattern emphasizes the edge elements and the defective elements of the array. Hence, as in the subtraction method, the far side-lobe region gives results which are directly related to the requirements of the monitoring system in most cases. However, it has been shown that for cases like stuck phase-shifters (chapter 3) measurements which cover the main lobe as well as the side-lobe regions are more useful.

A summary of the far-field monitoring methods will now be given. The simplest method, out of the three investigated, is the subtraction method which requires the minimum number of processing operations out of the three. The method can be used sequentially for the detection of multiple defects, as long as they occur one at a time. It can also be used in real-time monitoring.

The angular spectrum method requires more processing than the subtraction method. However, it can still be used with modern processors in real time monitoring. A dedicated F.F.T. processor would reduce the required processing by an order of magnitude. It therefore seems worthwhile to investigate whether such processing devices can be implemented economically.

The a.c.f. method requires an even larger amount of processing, hence it is recommended only for non real-time processing.

The two methods, the angular spectrum and the a.c.f., can be used periodically to check the detection of defective elements by the subtraction method.

Turning now to the near-field methods, they can be divided into two groups. One group deals with very close-in field monitoring of the array, and the second uses the Fresnel region of the radiation from the array for monitoring.

The two methods of internal or integral monitoring use the very close-in field of the array. The composite field, measured by the internal/integral monitoring system, gives the far-field patterns of the array. Hence the far field methods can be used with the internal/integral monitoring system. However, these methods do not give information on beam pointing errors due to, say, an external mechanical shift of the full array system. Hence, a far-field or a near field (Fresnel region) main-beam pointing error detection is necessary in addition. The far-field main-beam pointing uses a simple antenna. However, uncontrolled multipath errors can be introduced, thus causing uncertainty in the decisions. In order to overcome possible multipath errors, methods for Fresnel-region monitoring can be used. Focusing of the transmitting array is one possibility, as explained in section 1.1. This method is not always acceptable in practice, as it changes the original aperture phase distribution. Hence, the monitor is not measuring the real transmitted wavefront signal.

A near field monitoring technique has therefore been proposed (in chapter 6) to overcome the above problem. It suggests a monitor antenna to be focused onto the transmitting array antenna, with no changes in the transmitting array signal. The idea was developed using the properties of the Fresnel integral to describe the aperture diffraction according to the Huygens-Fresnel formula. Analysis and computer simulation has shown that the main-beam and the near side lobes of a scanning phased-array antenna can be reproduced, with a good quality, in the focused monitor antenna. This requires the monitor antenna to be laid out in parallel to the geometrical aperture of the transmitting array. In this scheme the number of sampling elements required over the monitoring aperture, has been demonstrated by computer simulation to be quite modest. For distances of a few apertures between the transmitting and monitoring arrays the simulations have shown that only few sampling elements (about ten) may be necessary. This proposal makes available an additional technique for near field monitoring, if required.

As explained in chapter 7 the analysis and computer simulation have been accompanied in part by experimental investigation. A near-field measurement set-up has been used with waveguide slot linear arrays. The arrays have been subjected to synthetic defects and the monitoring methods have, in part, been demonstrated and verified. The near-field monitoring technique has not been investigated experimentally and is, therefore, recommended for further experimental investigation.

A final point will be made concerning the experience gained using computer simulations. It was found that computer simulations accompanied by the line printer graphical output are a very important tool for fast but rough analysis with immediate feed back. This can be vital in the early stages of an analysis in gaining familiarity with the subject and leading to new ideas. It can also be used as a replacement for a more precise and difficult analysis (which can follow later), as with the case of the near field monitoring technique (chapter 6). There, the technique proposed, based on an approximation to the Fresnel integral, was later checked against a precise "experiment", using NAG-Functions to represent the Fresnel integral.

APPENDIX A

Reproduced selected sections from ICAO Standards And Recommended Practices (SARPS) for the MLS [6]

1.0 - Definitions

Airborne Subsystem. MLS airborne equipment necessary to obtain, process, and output guidance information.

Auxiliary Data. A feature of the signal format that:

(a) provides data to refine airborne positions calculations;
(b) provides meteorological information;
(c) provides runway status and supplementary information for display in the cockpit.

Basic Data. The required data associated directly with the operation of the landing guidance system and advisory data on the status of the MLS facilities.

Clearance Guidance Sector. The designated volume of airspace which supplements the proportional guidance sector where the proportional guidance sector is less than the coverage sector provided by a function. In this sector, the angular guidance service provided is constant throughout, and not proportionally related to angular displacement of the receiver antenna with respect to (reference).

Control Noise. That portion of the guidance signal error which could affect aircraft attitude and causes control surface, wheel and column motions during coupled flight. Control Noise contains those frequency components of the guidance signal produced by an airborne receiver with an output time constant of 0.1 second which lie above 0.3 radian/second for azimuth data or above 0.5 radians/second for elevation data.

Course Line. The locus of points in the horizontal plane which have the selected azimuth angle.

Coverage Extremes. The boundary of guidance service specified at the maximum range for a particular angular position.

Coverage Sector. A volume of airspace of defined dimensions within which service is provided by a particular function in which the signal power density is equal to or greater then the specified minimum.

Datum point. The origin of the approach and missed approach sector coverages is defined as a point on the runway centerline defined by the intersection of the runway centerline with a vertical plane perpendicular to the centerline and containing the phase center of the elevation antenna.

DME/M. The precision range element associated with the standard MLS. An L-Band Distance Measuring Equipment (DME) is used that is compatible with existing equipment while providing improved accuracy and channelization capabilities.

Facility. The MLS ground equipment necessary to transmit a given function.

Flare Coverage Zone. A zone that extends horizontally between the runway edges and longitudinally from 90 meters (300 feet) - to 760 meters (2500 feet) after runway threshold and vertically from near the runway surface to a height in the order of 45 meters (150 feet).

Function. A particular guidance service (e.g., approach azimuth) provided by the MLS.

Functional Element. The ground and airborne components necessary to achieve the transmission and reception of a given MLS function, e.g., approach azimuth.

Glide Path. The locus of points in the vertical plane which have the selected elevation angle.

Ground Subsystem. MLS ground equipment necessary to provide guidance information at a particular runway.

Missed Approach Reference Datum. The origin of the accuracy requirement for the missed approach azimuth functional element is defined as a point 15 meters (50 feet) above the horizontal plane of the datum point and located above the runway centerline at the runway midpoint.

Out of Coverage Indication (OCI). A signal radiated by certain facilities into those regions which are not within the guidance coverage of the facility.

Path Following Error. That portion of the guidance signal error which could

cause aircraft displacement from the desired course. These perturbations fall within the loop guidance bandwidth of an aircraft. Path Following Error contains those frequency components of the guidance error signal produced by an airborne receiver with an output time constant of 0.1 second which lie below 0.5 radians/second for azimuth data or below 1.5 radians/second for elevation data. Path Following Error includes the error components of both Path Following Noise and mean course alignment.

Path Following Noise. The Path Following Error with the mean course alignment error component removed.

Proportional Guidance Sector. The designated volume of airspace within which the angular guidance service provided by a function is directly proportional to the angular displacement with respect to (reference).

Reference Datum. The origin of the accuracy requirements for the approach functional elements is defined as a point on each operational glide path 15 meters (50 feet) above the horizontal plane containing the datum point and located vertically above the runway centerline.

TDM (Time Division Multiplex). A method of sequencially transmitting a number of functions on a single frequency channel by means of time separation.

[illegible] The first (TO) and second (FRO) scan of a beam from one

2 3 2.0 Add the following:

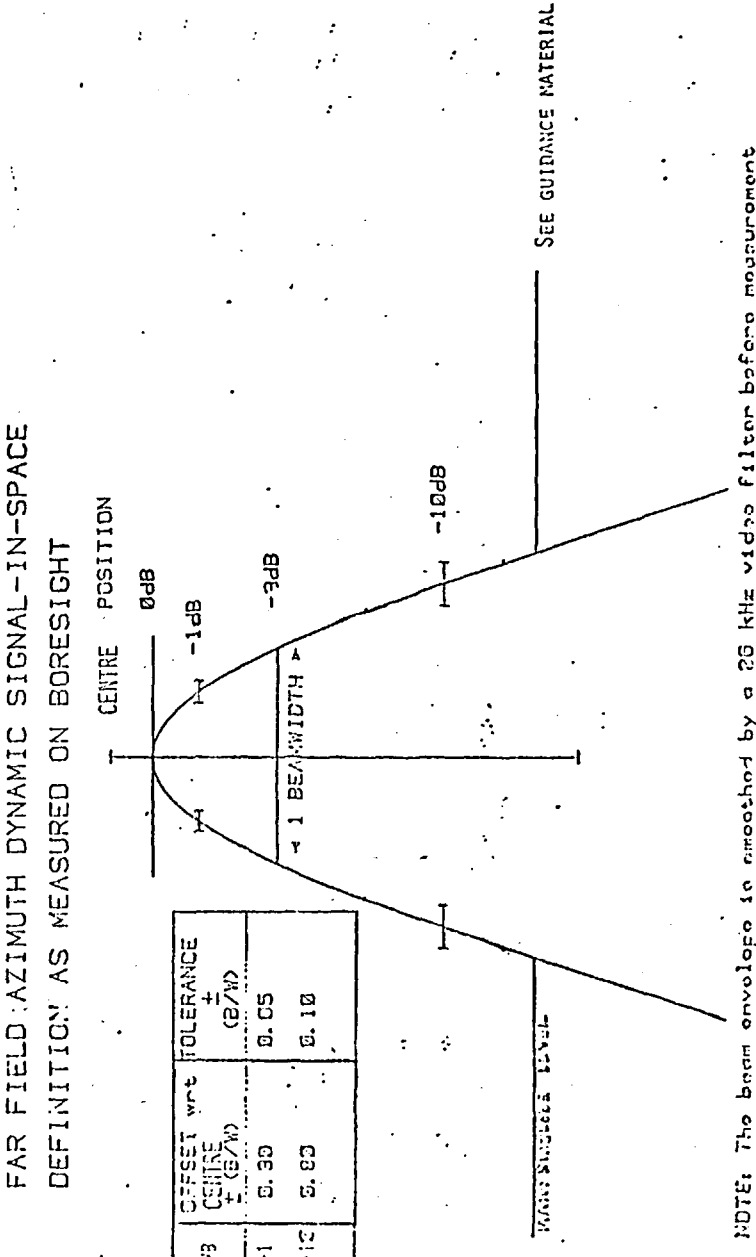
"Specifications in the following paragraphs provide the basic form of a standard Microwave Landing System. This basic system may be modified to suit special needs of individual aerodromes or satisfy particularly stringent requirements. When such changes are made, the systems will be identified as other than a basic MLS, but providing the changes satisfy the following parameters, the system will be deemed to be an acceptable version of MLS:

a. The basic system may be augmented by additional services and wider coverage or be provided with extra redundancy features or monitoring to increase system integrity, for example, more than ±40 degrees proportional guidance for Approach Azimuth, Flare Component, or Missed Approach Azimuth Component.

b. The basic system may be reduced with due regard to operational safety factors, when the competent authority determines that the basic form of the system cannot be fully utilized. (Note that no reduction in angle accuracy is permitted).

c. When MLS installations vary from the basic form, States shall make known the forms of MLS in use, through the medium of Regional Air Navigation meetings."

FAR FIELD AZIMUTH DYNAMIC SIGNAL-IN-SPACE DEFINITION AS MEASURED ON BORESIGHT



dB	OFFSET wrt CENTRE ± (B/W)	TOLERANCE ± (B/W)
-1	0.30	0.05
-10	0.85	0.10

NOTE: The beam envelope is smoothed by a 26 kHz video filter before measurement

FIGURE 2.1

DEFINITION OF SCAN DIRECTIONS AND ANGLES
FOR ELEVATION AND FLARE SYSTEMS

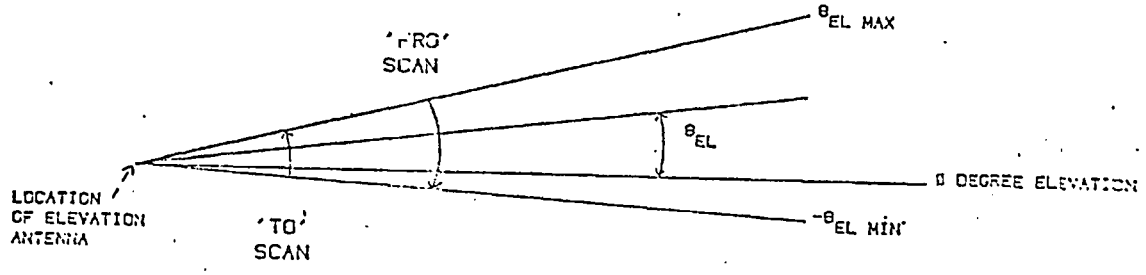


FIGURE 2.3

DEFINITIONS OF SCAN DIRECTIONS AND ANGLES
FOR AZIMUTH AND MISSED APPROACH AZIMUTH SYSTEMS

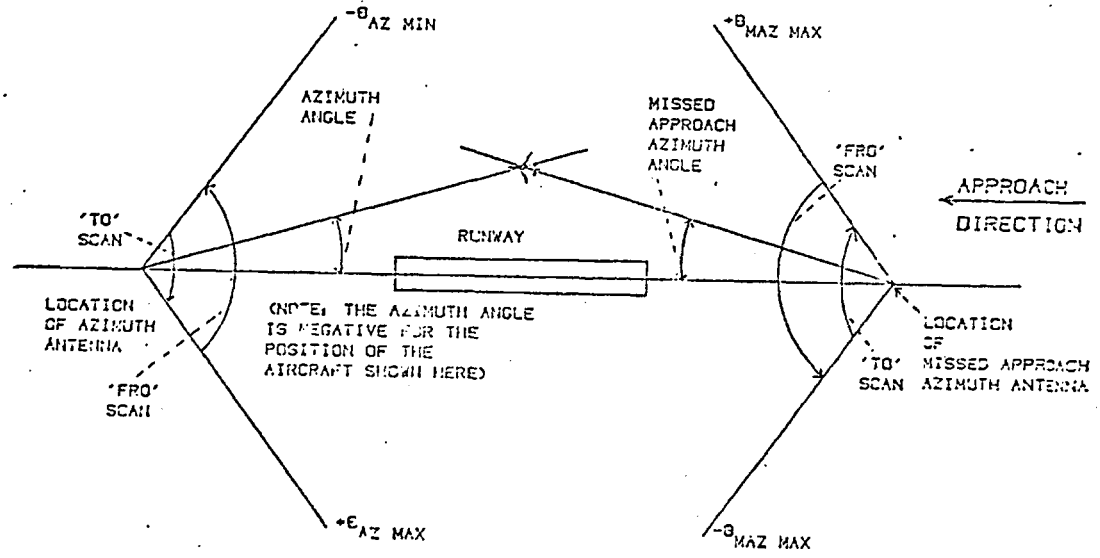


FIGURE 2.4

2.5.2 The DME/M transponder antenna shall be located as close as possible to the approach azimuth element.

2.5.3 The transponder delay shall be adjusted to produce zero range indication at the transponder antenna site.

2.5.4 Distance information shall be provided throughout any coverage volume in which azimuth guidance is available.

2.6 - Coordinate System

The MLS azimuth angle information shall be radiated in conical or planar coordinates. The coordinate system in use shall be indicated by the auxiliary data transmissions. The MLS elevation and flare information shall be radiated in conical co-ordinates.

2.7 - Monitor and Control

Monitor and control equipment shall be associated with each functional element.

2.7.1 Monitors shall assure guidance qualities appropriate to the performance category of operations. When malfunctions occur, the monitors shall initiate action to restore normal operations, downgrade performance categories, or remove the element from service, as appropriate to the situation.

2.7.2 Local and remote controls shall be provided to facilitate maintenance actions and to allow switch over with redundant equipment, downgrading of performance categories, or removal of facilities from service.

3.0 - Signal Format (Angle and Data Functions)

3.1 - General

3.1.1 Both angle and data information shall be transmitted by time division multiplexing (TDM) on a single frequency channel. A Preamble shall identify the particular type of information being transmitted so that each function transmitted is an independent entity, and proper decoding of a function does not depend on its position in the sequence. Data and Preamble shall be modulated using the Differential Phase Shift Keying (DPSK) technique.

3.2 - CHANNELIZATION

3.2.1 The functional elements shall be capable of operating on any one of 200 channels spaced 300 kHz apart with center frequencies between 5031.0 MHz and 5090.7 MHz and numbered 500 to 699 as per Table 3.1.

3.2.2 The pairing of the MLS channel and the channel of the associated ranging equipment shall be taken in accordance with the provisions in Chapter 3.5, Table A (DME Channeling and Pairing).

3.2.3 Initial implementation of MLS shall be in accordance with the stages indicated in 4X, Annex 10, Part II. See CORR-71

3.2.4 Frequency Tolerance. The operating radio frequency of ground facilities shall not vary more than plus or minus 10 kHz from the assigned frequency. The frequency stability shall be such that there is no more than a plus or minus 50 Hz deviation from the nominal frequency during any one-second interval.

3.2.5 Interference. The transmitted signal shall be such that, during the transmission time, the mean power density above a height of 600 meters (2,000 feet) shall not exceed -100.5 dBw/m^2 for angle guidance and -95.5 dBw/m^2 for data, as measured in a 150 kHz bandwidth centered at a frequency of 240 kHz or more from the nominal frequency.

than one-quarter of the allowable path following error applicable at that location.

3.3.3 All system accuracy limits are to be met with the receiving antenna up to twenty degrees from the vertically polarized position.

3.4 - Function Sequence

Each function transmission shall be an independent entity which can occur in any position in the TDM sequence. The time interval between repetitive transmissions of any one function shall be varied in a manner which provides protection from synchronous interference.

Note.--A transmission sequence that satisfied the requirements of 3.4 is described in Appendix X.

3.6.3 - ANGLE SCAN ENCODING

Angular information shall be encoded by the amount of time separation between the centroid of the TO and FRO scanning beam pulses. Angular coding shall be linear with time and given by the formula:

$$\theta = (T_o - t)\,\frac{V}{2}$$

where:

- θ = Receiver angle in degrees
- t = Time separation in microseconds between TO and FRO pulses
- T_o = Time separation in microseconds between TO and FRO pulses corresponding to zero degrees.
- V = Scan velocity in degrees per microsecond.

NOTE.- The timing requirements are illustrated in Figure 3-2.

3.6.3.1 Scan Velocity (V) - The scan velocity shall be as listed in Table 3.5 for each function. The tolerance on the scan velocity shall be sufficient to meet the accuracy requirements.

3.6.3.2 Zero Degree Time (T_o) - The zero degree time for each function shall be as listed in Table 3.5. The tolerance on the zero degree time shall be sufficient to meet the accuracy requirements.

3.6.3.3 Midpoint Time (T_m) - The duration in microseconds between the reference time and the midpoint between TO and FRO pulses is listed in Table 3.5.

3.6.3.4 Ground Radiated Test Time (Tt). The time duration between "TO" and "FRO" pulses of the ground radiated test shall be as listed in Table 3.5.

TABLE 3.5 SINGLE SCAN TIMING CONSTANTS

FUNCTION	ANGLE SCAN RANGE (DEG)	MAXIMUM VALUE OF t (usec)	T_o (usec)	V (Deg /usec)	T_m (usec)	Pause (usec)	T_t (usec)	θ_t (Deg)
AZIMUTH	-62° to +62°	13,000	6,800	0.020	8,300	600	13,133.3	-63.
AZIMUTH (HIGH SITE)	-42° to +42°	9,000	4,800	0.020	6,300	600	9,133.3	-42.
MISSED APPROACH AZIMUTH	-42° to +42°	9,000	4,800	0.020	6,300	600	9,133.3	-42.
ELEVATION	-1.3°to +30.7°	3,600	3,467	0.020	2,600	400	NA	NA
FLARE ELEVATION	-2° to +12.7°	3,333	2,933	0.010	2,467	400	NA	NA

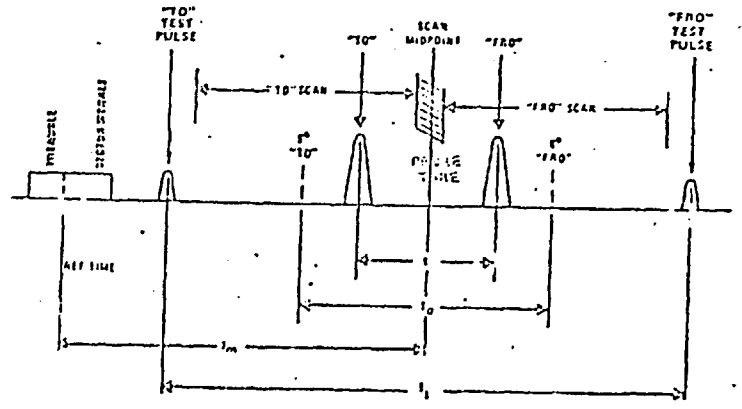


Fig 3-2 Angle Scan Timing

for alphanumeric character data. The content and timing of the Auxiliary Data words are described in Appendix X.

~~4.0 Signal Format (Range Function)~~

Note.-The MLS DME has several technical issued which must be resolved before appropriate draft SARPS can be provided. Proposed draft SARPS for DME should be available late 1979 or early 1980.

5.0 - Ground Subsystem Characteristics

Introduction

The ground subsystem technical and operational characteristics are defined and specified in this chapter. This includes standards on the coverages, power densities, accuracies, monitoring and control and siting requirements for the various facilities.

5.1 - Azimuth

5.1.1 - COVERAGE

5.1.1.1 The approach azimuth facility shall provide guidance in at least the following volume of space:

5.1.1.1.1 Approach Region

(a) Laterally and longitudinally within a sector ±40° about the runway centerline originating at the datum point and extending in the direction of the approach to 20 nm from the runway threshold.

(b) Vertically between

(i) a conical surface originating 8 feet above the runway threshold inclined at .9° above the horizontal, and

(ii) a conical surface originating at the azimuth facility inclined at 15° above the horizontal to a height of 6000 meters (20,000 feet).

Note.-Where intervening obstacles penetrate the .9° surface, guidance need not be provided at less than line of sight heights.

5.1.1.1.2 Runway Region

(a) Laterally and longitudinally within a sector 150 feet each side of the runway centerline beginning at the stop end and extending parallel with

the runway centerline in the direction of the approach to join the approach region.

(b) Vertically between

(i) 8 feet above the runway surface

(ii) a conical surface originating at the azimuth facility inclined at 20° above the horizontal up to a height of 600 meters (2000 feet).

RECOMMENDATION.-The azimuth facility should provide vertical coverage up to 30° above the horizontal.

5.1.1.1.3 The minimum proportional guidance sector shall be ±10° about the runway centerline. Where the proportional guidance sector provided is less than the minimum lateral coverage specified in Paragraphs 5.1.1.1.1 and 5.1.1.2, clearance signals shall be provided to supplement the proportional sector.

5.1.1.2 The missed approach azimuth facility shall provide proportional guidance in at least the following volume of space:

(a) Laterally and longitudinally within a sector ±20° about the runway centerline originating at the missed approach azimuth facility and extending in the direction of the missed approach at least to 5 nm from the runway stop end.

(b) Vertically

(i) Runway region

Between 8 feet above the runway surface and a conical surface originating at the missed approach azimuth facility inclined at 20° above the horizontal up to a height of 600 meters (2000 feet).

RECOMMENDATION: The missed approach azimuth facility should provide guidance to 30° above the horizontal.

Note.-Where obstacles penetrate the lower coverage limits, guidance need not be provided at less than line of sight heights.

(ii) Missed Approach Region

Between a conical surface originating 8 feet above the runway stop end, inclined at 0.9° above the horizontal, and a conical surface originating at the missed approach azimuth facility, inclined at 15° above the horizontal up to a height of 1500 meters (5000 feet).

5.1.1.3 Clearance signals, each band, shall be at least 3 dB greater than any other signal in the appropriate clearance sector.

5.1.1.4 Out of Coverage Indication (OCI) - OCI signals, where used, shall be at least 3 dB greater than any other signal in the appropriate OCI sector (left, right, and rear).

5.1.1.4.1 RECOMMENDATION.-OCI signals should be provided in all lateral

12	23	Add new para 5.1.1.5	New para to read as follows: "5.1.1.5 Ground Radiated Test (GRT) - GRT signals shall be provided throughout the coverages indicated in paragraphs 5.1.1.1 and 5.1.1.2."

FUNCTION/PARAMETER	DPSK	ANTENNA BEAMWIDTH (3 dB) 1°	2°	3°
POWER DENSITY (dBw/m^2) AZIMUTH	-89.5	-88(1)	-85.5(1)	-82 (1)(2)
POWER DENSITY (dBw/m^2) MISSED APPROACH AZIMUTH	-91	-79.5	-77	-73.5

(1) At the reference datum, the power density shall be greater than that indicated in the Table by at least 15 dB. At 8 feet above the run-way surface, the power density shall be greater than that indicated in the Table by at least 5 dB.

(2) For AZ (High Rate) the power density can be reduced as described in the Guidance Material.

5.1.3 - ACCURACY

5.1.3.1 At the appropriate reference datum the AZ functional element shall provide performance in accordance with the error components listed in Table 5-1.

Note.-The overall accuracy limits in Table 5-1-1 include, errors from all causes such as airborne instrumentation, mean course alignment, and multipath propagation effects. Detailed accuracy budgets are included in the guidance material.

TABLE 5-1 - AZIMUTH ACCURACY

TABLE 5-1-1 - SYSTEM ACCURACY

ERROR COMPONENT	APPROACH AZIMUTH	MISSED APPROACH AZIMUTH
PATH FOLLOWING ERROR	±6 METERS (±20 FT)	±6 METERS (±20 FT)

TABLE 5-1-2 - SIGNAL-IN-SPACE NOISE LIMITS

ERROR COMPONENT	APPROACH AZIMUTH	MISSED APPROACH AZIMUTH
PATH FOLLOWING NOISE (95% PROBABILITY)	±3.5 METERS (±11.5 FT)	±3.5 METERS (±11.5 FT)
CONTROL MOTION NOISE (95% PROBABILITY)	±3 METERS (±10 FT)	±3 METERS (±10 FT)

Note.-Control Motion Noise includes both the ground and propagation error components.

Note.-It is intended that the error limits are to be applied over a measurement interval that includes the reference datum. The interpretation of the measurement interval appropriate for flight inspection is discussed in the guidance material.

5.1.3.2 For the approach azimuth facility the equivalent angular Path Following Noise accuracy shall be maintained along the centerline out to a range of 3500 feet from the reference datum point.

5.1.3.3 RECOMMENDATION.-The approach azimuth functional element should provide a path following error not greater than plus or minus 4 meters (13.5 feet).

5.1.3.4 Degradation Allowance

5.1.3.4.1 The linear accuracy specified at the reference datum shall be maintained throughout the runway coverage region defined in Paragraph 5.1.1.4.

Note.-To determine the allowable errors in other regions, the accuracy specified at the reference datum should first be converted from its equivalent angular value with an origin at the antenna.

5.1.3.4.2 The allowable angular path following error calculated for the reference datum shall be allowed to increase linearly to the coverage extremes as indicated in Table 5-X-1.

5.1.3.4.3 At the reference datum, in no case shall the control motion noise exceed 0.1 degree. Furthermore, it shall not exceed 0.1 degree out to a range of 10 nm.

5.1.3.4.4 For the approach azimuth facility, along the centerline from a range of 3500 feet out to a range of 7000 feet from the reference datum point the equivalent path following noise error is permitted to increase linearly. Beyond this point the combined course alignment error and path following error shall be within the overall path following error.

Table 5-X-1, ALLOWABLE AZIMUTH ERROR DEGRADATION

	LINEARLY ALLOWABLE ERROR DEGRADATION		
ERROR COMPONENT	WITH DISTANCE	WITH AZIMUTH ANGLE	WITH ELEVATION ANGLE
PATH FOLLOWING ERROR	TO 0.2 DEGREE AT THE LIMIT OF COVERAGE ALONG THE CENTERLINE	1.5:1	2:1 FROM 9 DEGREES TO 15 DEGREES
CONTROL MOTION NOISE	TO 0.20 DEGREE AT THE LIMIT OF COVERAGE ALONG THE CENTERLINE	1.3:1 OUT TO 40°	NONE

5.1.4 - MONITOR AND CONTROL

5.1.4.1 The monitor system shall cause the radiation to cease if any of the following conditions persist for longer than the periods specified:

(a) There is a shift in the one-second average of the estimates of the zero degree course line of more than 4.8 meters (15.7 feet) at the reference datum.

(b) There is a change in the ground equipment performance which would cause the error, if measured along any radial, to exceed the limits specified in Paragraph 5.1.3.3 for a period of more than one second.

(c) There is a reduction in the radiated power to less than that necessary to produce the requirements of Paragraph 5.1.2 for a period of more than one second.

(d) There is an error in the preamble DPSK transmissions which occurs more than once in any one second.

(e) The timing tolerances specified in X.2 are exceeded for a period of more than one second.

(f) The temporal CMN generated by the ground subsystem, when measured over any 10 seconds, exceeds 0.03 degrees.

5.1.4.1.1 Design and operation of the monitor system shall be consistent with the requirement that radiation shall cease and a warning shall be provided at the designated control points in the event of failure of the monitor system itself.

TABLE 5-2. AZIMUTH MONITOR WARNING LIMITS

FACILITY	MEAN COURSE LINE LIMIT AT THE REFERENCE DATUM
APPROACH AZIMUTH	PLUS OR MINUS 4.8 METERS (15.7 FEET)
MISSED APPROACH AZIMUTH	PLUS OR MINUS 4.8 METERS (15.7 FEET)

5.1.4.2 RECOMMENDATION.-When a path following error of plus or minus 4 meters (13.5 feet) is being maintained per 5.1.3.2, the mean course line limits of Table 5-2 should be reduced to plus or minus 3.2 meters (10.5 feet) at the reference datum.

5.1.4.3 The mean course alignment of the azimuth facility shall be adjusted and maintained to one half the limits shown in Table 5-2.

Note.-It is intended that facilities be adjusted and maintained so that the limits specified in Paragraph 5.1.4.3 are reached on very rare occasions.

5.1.4.4 The period during which erroneous guidance information is radiated shall be as short as practicable and shall not exceed one second. Attempts to clear the fault by resetting the primary equipment or by switching to standby equipment shall be completed within the 1 second period. If the fault is not

cleared within the time allowed, the facility shall be shutdown. After shutdown, no attempts shall be made to restore service until a period of 20 seconds has elapsed.

Note.-Detailed monitoring configurations and information on facility downgrading and shutdown are provided in the guidance material.

5.1.5 - SITING

5.1.5.1 The approach azimuth facility antenna system shall normally be located on the extension of the centerline of the runway beyond the stop end, and the antenna shall be adjusted so that the zero degree course line will be at the reference datum.

5.1.5.2 The missed approach azimuth facility antenna system shall normally be located on the extension of the centerline of the runway at the threshold end, and the antenna shall be adjusted so that the zero degree course line will be at the missed approach azimuth reference datum.

Note.-When siting the approach azimuth or missed approach azimuth antenna along the extended runway centerline is not practical, alternative siting configurations are provided for in the guidance material.

5.2 - Elevation

5.2.1 - COVERAGE

5.2.1.1 The approach elevation facility shall provide proportional guidance in at least the following volume of space.

(a) Laterally within a sector originating at the datum point which is at least equal to the proportional guidance sector provided by the approach azimuth facility.

(b) Longitudinally, from 250 feet from the datum point to 20 nm from threshold.

(c) Vertically within the sector bounded by:

(i) a surface 8 feet above the runway
(ii) a conical surface originating at the datum point inclined at .9° above the horizontal, and

(iii) a conical surface originating at the datum point inclined at 7.5° above the horizontal up to heights of 6000 meters (20,000 feet).

5.2.1.1.1 RECOMMENDATION.-The elevation facility should provide guidance greater than 7.5° above the horizontal where necessary to meet operating requirements.

Note.-Where intervening obstacles penetrate the 0.9° surface, guidance need not be provided at less than line of sight heights.

5.2.1.2 Flare Elevation - The Flare Elevation facility shall provide proportional guidance information in at least the following volume of space:

(a) Laterally and longitudinally over the runway surface and within a sector ±10° about the runway centerline originating at a point on the runway 2500 feet from threshold and extending to 5 nm from threshold in the direction of the approach.

(b) Vertically within the sector bounded by:

(i) surfaces 8 feet and 150 feet above the runway
(ii) a conical surface originating 8 feet above the runway surface at the threshold inclined at .9° above the horizontal
(iii) a conical surface originating on the runway 2,500 feet from the threshold inclined at 7.5 degrees above the horizontal up to 5000 feet.

5.2.1.3 Elevation Antenna Lateral Radiation Patterns.

5.2.1.3.1 RECOMMENDATION - The horizontal pattern of the Approach Elevation and Flare Elevation antennas should gradually de-emphasise the signal away from

antenna boresight. The horizontal pattern of the Approach Elevation should be reduced by 3dB at 20 degrees off boresight and by 6dB at 40 degrees. The horizontal pattern of the Flare Elevation should be reduced as low as practicable beyond 10 degrees off boresight and by at least 12 dB at 40 degrees off boresight.

5.2.1.4 Proportional guidance shall be provided throughout the vertical elevation coverage. Clearance signals shall not be used to supplement the proportional sector.

5.2.1.5 O.C.I. Elevation.

5.2.2 Power Density - The power density for the Preamble transmission shall not be less than -89.5dBW/m^2 under operation weather conditions at any point within coverage. The power density for the angle signal shall be not less than -88.0dBW/m^2 under operational weather conditions at any point within coverage.

5.2.3 - ACCURACY

5.2.3.1 General - The Approach Elevation and Flare Elevation shall provide performance at the reference datum in accordance with the error components listed in Table 5-3. The Flare Elevation accuracy applies throughout the entire flare coverage zone.

Note. ~~The measurement of path following error and control noise is discussed in the guidance material.~~

The overall accuracy limits in Table 5-3 include errors from all causes such as airborne instrumentation, mean course alignment, and multipath propagation effects. Detailed accuracy budgets are included in the Guidance Material.

TABLE 5-3. ELEVATION ACCURACY AT REFERENCE DATUM

ERROR COMPONENT	APPROACH ELEVATION	FLARE
PATH FOLLOWING ERROR (95 PERCENT PROBABILITY)	±0.6 METER (2 FEET)	±0.6 METER (2 FEET)
CONTROL NOISE (95 PERCENT PROBABILITY)	±0.3 METER (1 FOOT)	±0.3 METER (1 FOOT)

22 29 Note (Table 5-3) Delete existing Note and substitute the following Note: "It is intended that the error limits are to be applied over a measurement interval that includes the reference datum. The interpretation of the measurement interval appropriate for flight inspection is discussed in the Guidance Material."

exceed 0.05 degrees.

TABLE 5-X-2 - ALLOWABLE ELEVATION ERROR DEGRADATION

ERROR COMPONENT	LINEARLY ALLOWABLE ERROR DEGRADATION WITH DISTANCE	WITH AZIMUTH ANGLE	WITH ELEVATION ANGLE
PATH FOLLOWING ERROR	TO 0.20° AT 20 NM ALONG THE CENTERLINE	NONE	TO NOT MORE THAN 0.4 DEGREE WITHIN THE VERTICAL COVERAGE
CONTROL MOTION NOISE	TO 0.1° AT 10 NM AND THEN TO 0.2° AT 20 NM ALONG THE CENTERLINE	NONE	NONE

5.2.4 - MONITOR AND CONTROL

5.2.4.1 The monitor and control system shall act to ensure that any of the following conditions do not persist for longer than the periods specified:

(a) There is a shift in the one-second average of the estimates of any commissioned glide path of more than 0.4 meters (1.3 feet) at the reference datum.

(b) There is a reduction in the radiated power to less than that necessary to produce the requirements of Paragraph 5.2.2 for a period of more than one second.

(c) There is an error in the preamble DPSK transmissions which exceed more than once in any one second.

(d) The timing tolerances specified in X.2 are exceeded for a period of more than one second.

(e) The temporal CMN generated by the ground subsystem, when measured over any 10 seconds, exceeds 0.03 degrees.

5.2.4.1.1 Design and operation of the monitor system shall be consistent with the requirement that radiation shall cease and a warning shall be provided at the designated control points in the event of failure of the monitor system itself.

TABLE 5-4. ELEVATION MONITOR WARNING LIMITS

FACILITY	MEAN GLIDEPATH LIMIT AT THE REFERENCE DATUM
APPROACH ELEVATION	PLUS OR MINUS 0.4 METERS (1.3 FEET)
FLARE ELEVATION	PLUS OR MINUS 0.4 METERS (1.3 FEET)

5.2.4.2 The elevation facilities shall be adjusted and maintained to tolerances equal to one half those shown in Table 5-4.

Note: It is intended that facilities be adjusted and maintained so that the limits specified in para 5.2.4.2 are reached on very rare occasions.

5.2.5 - SITING

The Approach Elevation and Flare Elevation shall be located beyond the threshold of the runway being served and offset from the runway centerline. The distance offset from runway centerline shall be consistent with obstruction clearance practices given in ICAO Annex 14. The antenna shall have the minimum height necessary to satisfy the ground clearance requirements necessary to suit local operating conditions.

5.2.5.1 The Approach Elevation shall be sited so that the operationally preferred glide path crosses the threshold at a height of 50 feet above the runway surface. When collocated with an ILS glide path, the same ILS and MLS glide paths should be coincident above the runway threshold.

5.2.5.2 RECOMMENDATION.-The Flare Elevation antenna should be located about 1070 meters (3500 feet) along the runway from threshold.

5.2.5.3 The Siting Coordinates of the Approach Elevation and Flare Elevation antennas shall be transmitted on the Data Channel as defined in 5.3.6.

5.3 - Data

5.3.1 - COVERAGE

5.3.1.1 The Basic and Auxiliary Data shall be radiated throughout any coverage volume in which Azimuth guidance is available.

5.3.1.2 The power density for the DPSK signals shall not be less than the levels indicated in Table 5-X, under operational weather conditions, at any point within coverage.

5.3.2 - ACCURACY

5.3.2.1 The phase imbalance in the DPSK modulation in the 0 degree and 180 degree phase states shall be less than plus or minus 10 degrees.

5.3.3 - SITING

5.3.3.1 Data shall be transmitted from the Approach Azimuth facility where practicable.

5.3.4 - MONITOR AND CONTROL

5.3.4.1 Monitor System - The Monitor system shall provide a warning to the designated control points if the radiated power is less than that necessary to provide the requirement of 5.1.2 or if an error in a data word transmission is detected.

5.3.4.2 Control Actions - If any error is repeated on two consecutive updates in an individual data field, the radiation of this field shall cease within one second.

5.3.5 - BASIC DATA

5.3.5. Basic data shall be transmitted by all ground subsystems. Provision shall be made for the transmission of six Basic Data Words, each with a

5.3.6.3.1 Alphanumeric characters shall be transmitted in the order in which they are to be read. The serial transmission of a character shall be with the lower order bit (b_1) transmitted first and the parity bit (b_8) transmitted last.

~~6.0 DME~~

~~Note.-The MLS DME has several technical issues which must be resolved before appropriate draft SARPS can be provided. Proposed draft SARPS for DME should be available late 1979 or early 1980.~~

7.0 - Airborne Receiver and Associated Data Processing Equipment

The following items shall be defined to the level essential to determine system performance.

7.1 - COVERAGE

In order that the total MLS guidance system shall meet its performance requirements, the overall airborne system performance, allowing for airborne equipment production and in-service tolerances, and under aircraft manoeuvers and attitudes normally encountered within the coverage volume, shall be:

(i) Where the radiated signal power densities are the minimum allowable under paragraph 5.1.2, the airborne equipment shall be able to acquire the signals, and any decoded angle guidance signal shall have a control motion noise component not exceeding 0.2 degrees.

(ii) Where the radiated signal power density is high enough to make the airborne receiver noise contribution insignificant, the airborne equipment shall not degrade the accuracy of any decoded angle guidance signal by greater than ±0.017 degrees (path following error) and ±0.015 degrees (azimuth) ±0.01 degrees (elevation) control motion noise.

(iii) The performance in (i) and (ii) shall be met when, in addition, interference is received at a level not exceeding that specified in paragraph 3.2.3.1.

(iv) The performance shall be met where the radiated signal power density exceeds the minimum specified in (i) above by 20 dB.

7.2 - RECOMMENDATION

The material in Table 7.1 below indicates an acceptable means of satisfying the airborne system accuracy requirements:

TABLE 7.1 - AIRBORNE ACCURACY TOLERANCES (1)

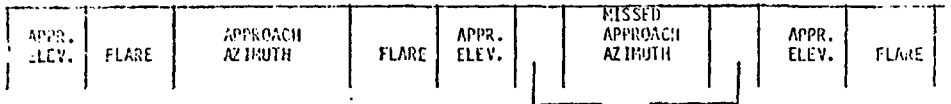
95% Probability

FUNCTION	MEAN ERROR	CMN		
		Instrumentation (3)	SNR (4)	Total (2)
AZIMUTH	±.017°	±.007°	±.013°	±.015°
ELEVATION	0.017°	±.007°	±.007°	±.01°

At the power densities
(1) Specified at Reference Datum. considering only receiver tolerance error.
(2) RSS of Instrumentation and SNR Components.
(3) Instrumentation Error includes all receiver error sources with the exception of SNR components. In general, these components are not beamwidth dependent.
(4) Signal-to-noise ratio error (SNR) is induced by receiver thermal noise.

7.3 - ANGLE ACQUISITION AND VALIDATION LOGIC REACTIONS

7.3.1 The airborne receiver shall be capable of decoding all angles within the appropriate specified coverage sectors. Angle acquisition shall be achieved within 1 second when the minimum power level is received.



(a) SEQUENCE ## 1



(b) SEQUENCE ## 2

5 10 15 20 25 30 35 40 45 50 55 60 63.9

TIME (MILLISECONDS)

DATA RATES:		
	APPROACH AZIMUTH	13.5 HZ
	APPROACH ELEVATION	40.5 HZ
	MISSED APPROACH AZIMUTH	6.75 HZ
	FLARE	40.5 HZ

FIGURE X.1. TRANSMISSION SEQUENCE PAIR INCLUDING ALL FUNCTION.

TABLE X-3 APPROACH ELEVATION FUNCTION TIMING

EVENT	CLOCK PULSE NUMBER	TIME (MS)
PREAMBLE	0-24	0-1.6000
PROCESSOR PAUSE	24-26	1.6000-1.7333
BEGIN OCI PPULSE	26	1.733
BEGIN TO SCAN (-1.3°)	28	1.8667
TO SCAN ANGLE = 0°	29	1.9333
END TO SCAN (+8.0°)	35	2.3333
END TO SCAN (+16.0°)	41	2.7333
END TO SCAN (+30.67°); BEGIN PAUSE	52	3.4667
MID SCAN	55	3.6667
END PAUSE; BEGIN FRO SCAN (+30.67°)	58	3.8667
BEGIN FRO SCAN (+16.0°)	69	4.6000
BEGIN FRO SCAN (+8.0°)	75	5.000
FRO SCAN ANGLE = 0°	81	5.4000
END FRO SCAN (-1.3°); END FUNCTION (AIRBORNE)	82	5.4667
END GUARD TIME; END FUNCTION (GROUND)	85	5.6667

TABLE X-2 APPROACH AZIMUTH FUNCTION TIMING

EVENT	15 kHz CLOCK PULSE NUMBER	TIME (MS)
PREAMBLE	0-24	0-1.6000
BEGIN MORSE CODE BIT	24	1.6000
BEGIN ANTENNA SELECT PULSE	25	1.6667
BEGIN RIGHT GUIDANCE PULSE	31	2.0667
BEGIN LEFT GUIDANCE PULSE	33	2.2000
BEGIN REAR OCI PULSE	35	2.3333
BEGIN LEFT OCI PULSE	37	2.46 7
BEGIN RIGHT OCI PULSE	39	2.6000
BEGIN TO TEST PULSE	41	2.7333
END TO TEST PULSE; BEGIN TO SCAN (-62.00°)	43	2.8667
BEGIN TO SCAN (-42.00°)	58	3.8667
BEGIN TO SCAN (-12.67°)	80	5.3333
TO SCAN ANGLE = 0°	80.5	5.3667
END TO SCAN (+12.67°)	99	6.6000
END TO SCAN (+42.00°)	121	8.0667
END TO SCAN (+62.00°); BEGIN PAUSE	136	9.0667
MID SCAN	140.5	9.3667
END PAUSE; BEGIN FRO SCAN (+62.00°)	145	9.6667
BEGIN FRO SCAN (+42.00°)	160	10.6667
BEGIN FRO SCAN (+12.67°)	182	12.1333
FRO SCAN ANGLE = 0°	191.5	12.7667
END FRO SCAN (-12.67°)	201	13.4000
END FRO SCAN (-42.00°)	223	14.8667
END FRO SCAN (-62.00°); BEGIN FRO TEST PULSE	238	15.8667
END FUNCTION (AIRBORNE)	240	16.0000
END GUARD TIME; END FUNCTION (GROUND)	243	16.2000

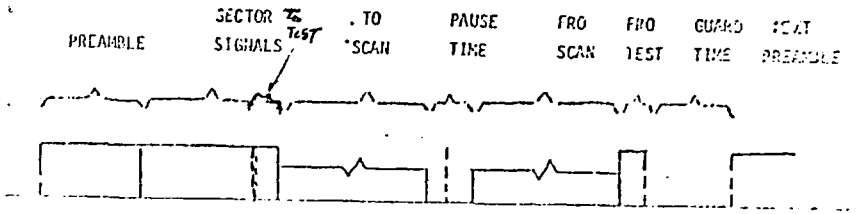


Figure 3-1. Angle Function Organization

APPENDIX B

Expected error in estimating the far-field phase reference (the random case)

The resultant field E_N of an N element array excited with constant amplitude E_0 and random statistically independent phase fluctuation in the range :

$$-b \leq \varphi_i \leq b \quad .$$

The estimated mean field $\hat{E}_N$ equals

$$\hat{E}_N = E_0 \sum_{i=1}^{N} \exp\{j\varphi_i\}$$

in direction of maximum beam (s=0, for broadside array) whose expectation (mean) has been shown to be :

$$\langle E_N \rangle = E_0 \frac{1}{2b} \int_{-b}^{b} \exp\{j\psi\}\, d\psi = E_0 \operatorname{sinc} b \qquad \text{(B.1)}$$

in the direction of maximum radiation (s=0).

Estimated resultant phase of the full array (on beam)

$$\hat{\varphi} = \arg(\hat{E}_N)$$

$$= \arctan \left[\frac{\operatorname{Im}\left(\frac{1}{N} \sum_{i=1}^{N} e^{j\varphi_i} \right)}{\operatorname{Re}\left(\frac{1}{N} \sum_{i=1}^{N} e^{j\varphi_i} \right)} \right]$$

$$= \arctan \frac{\frac{1}{N} \sum_{i=1}^{N} \sin\varphi_i}{\frac{1}{N} \sum_{i=1}^{N} \cos\varphi_i} \qquad \text{(B.2)}$$

Expectation of φ would be (for a full array)

$$\langle \varphi \rangle = \frac{\frac{1}{2b} \int_{-b}^{b} \sin\varphi_i \, d\varphi_i}{\frac{1}{2b} \int_{-b}^{b} \cos\varphi_i \, d\varphi_i} = \frac{0}{\operatorname{sinc} b} = 0 \qquad \text{(B.3)}$$

Estimated resultant phase of an array with missing element K (on beam)

$$\hat{\varphi}_K = \arctan \frac{Im\,(\hat{E_N})_K}{Re\,(\hat{E_N})_K}$$

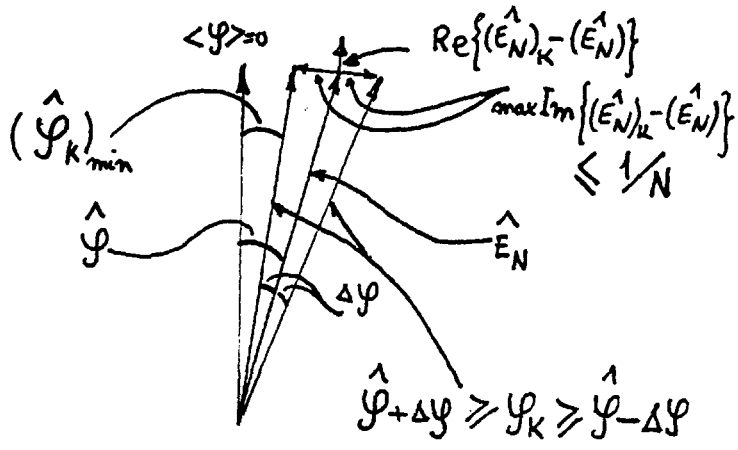
where $Im(\hat{E_N})_K = \frac{1}{N}\sum_{i=1\,(i\neq K)}^{N} \sin\varphi_i + \frac{1}{N}\sin\varphi_K - \frac{1}{N}\sin\varphi_K$

$$= \underbrace{\frac{1}{N}\sum_{i=1}^{N}\sin\varphi_i}_{\text{of full array}} - \underbrace{\frac{1}{N}\sin\varphi_K}_{\text{effect of missing element}} \qquad (B.4)$$

In the same way

$$Re(\hat{E_N})_K = \frac{1}{N}\sum_{i=1}^{N}\cos\varphi_i - \frac{1}{N}\cos\varphi_K \qquad (B.5)$$

Pictorially



where $\Delta\varphi$ maximum phase fluctuation of the resultant of $(\hat{E_N})_K$ in respect to $(\hat{E_N})$. Maximum $\Delta\varphi$ will occur when $\sin\varphi_K \cong \pm 1$, then $Re(\hat{E_N})_K = Re(\hat{E_N})$; (owing to $\cos\varphi_K = 0$), i.e.,

$$\Delta\varphi_{max} \simeq \arctan \frac{\frac{1}{N}\sin\varphi_K}{Re(\hat{E_N})} \qquad (B.6)$$

A good approximation to $Re(\hat{E_N})$ for large N and $b \leq \pi/2$ is the expectation of $Re(E_N)$;

$$Re(\hat{E_N}) \simeq \langle Re(E_N)\rangle = \text{sinc } b \qquad (B.7)$$

hence

$$\Delta\varphi_{max} \simeq \arctan \frac{\frac{1}{N}\sin\varphi_K}{\text{sinc } b} \qquad (B.8)$$

but: max$|\varphi_K|=b$, hence $\Delta\varphi_{max} \simeq \arctan \frac{\frac{1}{N}\sin b}{\mathrm{sinc}\, b}$.

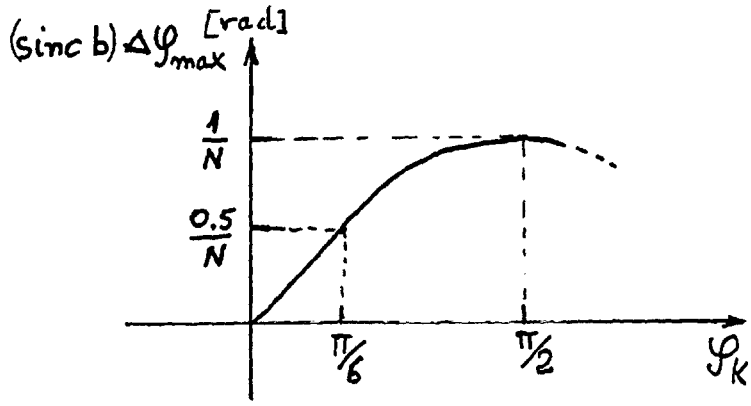
since sincb=sinb/b

$$\Delta\varphi_{max} \simeq \arctan b/N \simeq b/N \qquad (B.9)$$

For other values of $|\varphi_K| < b$

$$\Delta\varphi_{max} \simeq \arctan \frac{\frac{1}{N}\sin\varphi_K}{\mathrm{sinc}\, b} \simeq \frac{1}{N\,\mathrm{sinc}\, b}\sin\varphi_K \qquad (B.10)$$

For $b=\pi/2$ sincb=0.6366 hence for this value of b $\Delta\varphi_{max}$ will be about 60% larger. For $b \lesssim \pi/4$ then sincb is practically equal to 1. This could be represented in the following figure



For example, for N=100 element array and $\varphi_K = \pi/2$, the max difference between estimated resultant phase of the defective array radiation in respect to the non-defective resultant phase will be: $\Delta\varphi_{max} \leqslant 1/100 \simeq 0.6$ degree

for the direction of maximum radiation (i.e., s=0 for broadside antenna array)

Note: The importance of this analysis is the possibility of utilizing the main beam scan as a good phase-reference for monitoring.

APPENDIX C

Angular a.c.f. of the angular spectrum and the aperture illumination

Following Ratcliffe [14], utilization has been made of the dual transform pair of the angular autocorrelation function (a.c.f.) of the angular spectrum and the array aperture power illumination (see section 5.3). Using the relations of the transform pair of angular spectrum and the aperture illumination, expressions for the dual transform pair of angular a.c.f. of the angular spectrum and the aperture power illumination, will be derived.

C1 Angular spectrum and aperture illumination

The dual Fourier transform relation :

$$\left.\begin{aligned} F(s) &= \frac{1}{\lambda}\int_{-\infty}^{\infty} f(x)\,\exp\{jksx\}dx \\ f(x) &= \int_{-\infty}^{\infty} F(s)\,\exp\{-jkxs\}ds \end{aligned}\right\} \qquad (C.1)$$

where $f(x)$ is the aperture illumination, and $F(s)$ is the angular spectrum, with $s=\sin\theta$.

C2 A.c.f. of the angular spectrum and aperture power illumination

The autocorrelation function (a.c.f.) of the angular spectrum can be defined as

$$\rho(\sigma) = \int_{-\infty}^{\infty} F(s)\,F^{*}(s+\sigma)\,ds \qquad (C.3)$$

The Fourier transform of $\rho(\sigma)$ is

$$\mathcal{F}[\rho(\sigma')] = \int_{-\infty}^{\infty} \rho(\sigma') \exp\{-jkx\sigma'\} d\sigma'$$

$$= \iint_{-\infty}^{\infty} F(s)\, F^*(s+\sigma')\, ds \exp\{-jkx\sigma'\} d\sigma' \qquad (C.4)$$

changing the order of integration in equation (C.4) gives:

$$= \int_{-\infty}^{\infty} F(s) \left[\int_{-\infty}^{\infty} F^*(s+\sigma') \exp\{-jkx\sigma'\} d\sigma' \right] ds \qquad (C.5)$$

Integration of $[\int F^*(\ ).....d\sigma']$ after replacing $-s'=s+\sigma'$, will give:

$$\left[\int_{-\infty}^{\infty} F^*(s+\sigma') \exp\{-jkx\,\sigma') \, d\sigma' \right] =$$

$$= \exp\{jksx\} \int_{-\infty}^{\infty} F^*(-s') \exp\{jks'x\}(-)\, ds'$$

Replacing $\xi = -x$, it can be shown (see Papoulis [16], p.16) that

$$\int_{-\infty}^{\infty} F^*(-s') \exp\{-jks'\xi\}(-)\, ds' = (-)\, f^*(\xi) \qquad (C.6)$$

now

$$\int_{-\infty}^{\infty} F(s) \exp\{-jks\xi\} ds = f(\xi) \qquad (C.7)$$

Therefore, multiplying expression (C.6) times (C.7) will give:

$$\mathcal{F}[\rho(\sigma')] = (-)\, f(\xi)\, f^*(\xi)$$

$$= (-)\, f(-x)\, f^*(-x) = -|f(x)|^2 \qquad (C.8)$$

Use of the relation between the inverse Fourier transform of the a.c.f. of the angular spectrum and the aperture power illumination has been made in section 5.3.

APPENDIC D

Approximations to the near field of a half-cosine aperture field

A more detailed derivation of the results given in section 6.2.2 are presented in this Appendix.

Following similar stages for deriving equations (6.2) to (6.5) in section 6.1, the diffraction of a cosine aperture illumination can be shown to be equal to

$$g(x) = \exp\{-jkR\}\exp\{-jk\frac{x^2}{2R}\}I(s) \qquad (D.1)$$

The term I(s) is given by

$$I(s) = \int_{-a/2}^{a/2}[\exp\{+j\frac{\pi}{a}\xi\}+\exp\{-j\frac{\pi}{a}\xi\}]\exp\{-j\frac{k}{2R}\xi^2\}\exp\{jks\xi\}d\xi \qquad (D.2)$$

Where I(s) the normalized near field over the z-axis. The far-field will be derived after ignoring the parabolic phase term in equation (D.2). Hence

$$I_\infty(s) = \int_{-a/2}^{a/2}[\exp\{+j\frac{\pi}{a}\xi\}+\exp\{-j\frac{\pi}{a}\xi\}]\exp\{jks\xi\}d\xi \qquad (D.3)$$

where $I_\infty(s)$ the far-field normalized field pattern.

It can be shown that the far field is given by

$$I_\infty(s) \propto \frac{\cos(\frac{\pi as}{\lambda})}{(\frac{\pi}{2})^2-(\frac{\pi as}{\lambda})^2} \qquad (D.4)$$

This expression will be used for comparison with the reproduced far-field pattern described below.

As before , for near-field monitoring of a scanning phased array, the s(=sinθ) should be replaced by (s-x/R). Where R the distance between the antennas and x the sampling element

location in the x-axis (monitoring aperture). The following is the result

$$I(s-x/R) \propto \exp\{ j\frac{\pi}{4}\lambda R[\frac{2(s-x/R)}{\lambda}+\frac{1}{a}]^2 \}* \\ *\{ \mathcal{H}[\sqrt{\frac{2}{\lambda R}}\frac{a}{2} - \sqrt{\frac{\lambda R}{2}}(\frac{2(s-x/R)}{\lambda}+\frac{1}{a})]+ \\ +\mathcal{H}[\sqrt{\frac{2}{\lambda R}}\frac{a}{2} + \sqrt{\frac{\lambda R}{2}}(\frac{2(s-x/R)}{\lambda}+\frac{1}{a})]\}+ \\ +\exp\{ j\frac{\pi}{4}\lambda R[\frac{2(s-x/R)}{\lambda}-\frac{1}{a}]^2\}* \\ *\{ \mathcal{H}[\sqrt{\frac{2}{\lambda R}}\frac{a}{2} - \sqrt{\frac{\lambda R}{2}}(\frac{2(s-x/R)}{\lambda}-\frac{1}{a})]+ \\ +\mathcal{H}[\sqrt{\frac{2}{\lambda R}}\frac{a}{2} + \sqrt{\frac{\lambda R}{2}}(\frac{2(s-x/R)}{\lambda}+\frac{1}{a})]\} \qquad (D.5)$$

for which, as before, the following assumptions will be made:

The aperture a and the distance R are much greater than the wavelength ($a,R \gg \lambda$), and that $R=n\cdot a$ where n varies from 1 to 10. .....(D.6)

Hence, the term $\pm\sqrt{\frac{\lambda R}{2}}\frac{1}{a}$ in the $\mathcal{H}[\cdots\cdots]$, could be ignored in relation to $\sqrt{\frac{2}{\lambda R}}\frac{a}{2}$. As has been shown, the Fresnel integral is insensitive to small changes of arguments larger than 1. Hence the following approximation is achieved (Attention is drawn to the fact that the 1/a term is not ignored in the exponential phase terms):

$$I(s-x/R) \simeq [\exp\{j\frac{\pi}{4}\lambda R(\frac{2(s-x/R)}{\lambda}+\frac{1}{a})^2\} + \\ +\exp\{j\frac{\pi}{4}\lambda R(\frac{2(s-x/R}{\lambda}-\frac{1}{a})^2\}]* \\ *(\mathcal{H}\{\sqrt{\frac{2}{\lambda R}}\frac{a}{2} - \sqrt{\frac{\lambda R}{2}}[\frac{2(s-x/R)}{\lambda}]\}+ \\ +\mathcal{H}\{\sqrt{\frac{2}{\lambda R}}\frac{a}{2} + \sqrt{\frac{\lambda R}{2}}[\frac{2(s-x/R)}{\lambda}]\}) \qquad (D.7)$$

Opening the brackets in the exp_1 and exp_2 terms, where exp_1 exp_2 the first and second exponential accordingly, we get :

$$\begin{matrix} & & (1) & (2) & (3) & (4) & (5) & (6) \\ exp_1 + exp_2 = & \exp\{j\pi(\frac{s^2R}{\lambda} & + \frac{sR}{a} & + \frac{\lambda R}{(2a)^2} & + \frac{x^2}{\lambda R} & - \frac{x}{a} & - \frac{2sx}{\lambda})\} + \\ & +\exp\{j\pi(\frac{s^2R}{\lambda} & - \frac{sR}{a} & + \frac{\lambda R}{(2a)^2} & + \frac{x^2}{\lambda R} & + \frac{x}{a} & - \frac{2sx}{\lambda})\} \end{matrix} \qquad (D.8)$$

It is instructive to analyze the six terms of exp_1 and exp_2, in equation (D.8)

- Term(1) Is independent of x and affects all elements of the receiving aperture (the monitor antenna).
- Term (2) is dependent on s but has opposite signs in exp_1 and exp_2.
- Term (3) is a constant.
- Term (4) is the parabolic phase term which is cancelled, as with the uniform illumination (shown erlier in section 6.1.1), by the parabolic phase term outside the integral of equation (6.1.3).
- Term (5) is a linear phase term function of the position only, but has opposite signs in exp_1 and exp_2.
- Term (6) is the known linear phase scanned array term.

The other terms in equation (D.7), given by the Fresnel integrals are, again, assumed to be approximated by a constant amplitude and phase over the receiving antenna aperture.

A comparison will be made between the terms given by the expected far-field of a cosine illuminated aperture, and those terms which cause differences between the expected and the reproduced patterns will be discussed. This will lead to the definition of the near field monitoring antenna.

From equations (D.3) and (D.4) the far-field is given by an integral of the form

$$\int_{-a/2}^{a/2} [\ \exp\{j\pi(-\frac{x}{a}-\frac{2sx}{\lambda})\}+\exp\{j\pi(+\frac{x}{a}-\frac{2sx}{\lambda}\ ]\ dx \qquad (D.9)$$

Ignoring terms (1) and (3) in equation (D.8), we are left with the following expression.

$$\exp\{j\pi(+\frac{sR}{a}-\frac{x}{a})\}\exp\{j\pi(-\frac{2sx}{\lambda})\}+$$

$$+\exp\{j\pi(-\frac{sR}{a}+\frac{x}{a})\}\exp\{j\pi(-\frac{2sx}{\lambda})\} \qquad (D.10)$$

This will be used as the field diffracted over the monitoring aperture (the x-axis) from the transmitter, proportional to the expression,

$$\exp\{j\pi(-\frac{2sx}{\lambda})\}\cos[\ \pi(-\frac{sR}{a}+\frac{x}{a})\ ]\ . \qquad (D.11)$$

This expression is to be integrated over $-b/2<x<+b/2$ for getting the monitoring signal. now the far-field, equation (D.9), is given by the integral over $-a/2<\xi<+a/2$ of the expression

$$\exp\{j\pi(-\frac{2sx}{\lambda})\}\cos(\pi x/a) \qquad (D.12)$$

Hence we have to correct for the term $\pi sR/a$ in equation (D.11). By trigonometry,

$$\cos[\ \pi(sR/a-x/a)]=\cos\pi sR/a\ \cos\pi x/a\ -\ \sin\pi sR/a\ \sin\pi x/a \qquad (D.13)$$

Now, examining the r.h.s. terms in equation (D.13) then for $s<<1$, which is true for the main-beam region and if $R/a\leq 1$, then

$$\sin(\pi sR/a) \rightarrow 0\ .$$

Therefore,

$$\cos[\pi(sR/a - x/a)] \simeq \cos \pi x/a \quad , \qquad (D.14)$$

$s \ll 1$

i.e., the required expression, equal to that needed in equation (D.12), has been achieved.

Hence, summarizing, it can be stated that the far-field main-beam is approximated from near-field measurements by the following procedure:

- (1) The signal should be integrated over the receiving aperture placed in parallel to the transmitting array and having the same aperture length.
- (2) The seperation between the receiving and transmitting apertures should be small, of the order of $R/a \lesssim 1$.

Thus the system described in Fig. 6.3 will also be adequate for monitoring a cosine illuminated aperture scanning-beam, if only the seperation between receiving and transmitting antenna is decreased according to (2) above.

APPENDIX E

Computer programs listing

The following computer programs will be listed.

		Page
JACK18	Far field of N element array with random phase error	251
JACK19	Far field of N=8 element array, with mutual coupling (uses values computed in JACK20), and with random phase error.	258
COREL03	Subroutine to compute the correlation function of the angular spectrum for JACK18 (or JACK19)	265
JACK20	Mutual coupling between broadside parallel dipoles.	268
JACK30	Near field measurements, far field NN element array.	271
EJIX	Subroutine to be used with JACK30. Simulation of near field measurements.	279
SHIFT01	Subroutine to be used with JACK30 to introduce controlled shift of measured data.	280
DBMES1	A program to change measured values from x-y plot in centimeters into db and phase angle, using linear calibration.	281

		Page
SHIFT1	A Subroutine to be used with DBMES1 for shifting data.	283
JACK37	Monitoring in the near field with a focused antenna, cosine illumination.	284
JACK38	Monitoring in the near field with a focused antenna, cosine square over pedestal.	287
JACK39	Monitoring in the near field with a focused antenna, sine illumination.	290
JACK42	Near field of an aperture antenna with uniform illumination.	293
JACK45	Angular spectrum of a Pyramidal horn with $\pi/2$ phase error, Fresnel integral.	295

```
C-      FAR FIELD OF  N  ELEMENT ARRAY
C      UNIFORM DISTRIBUTION , RANDOM PHASE ERROR
C      THIS PROGRAM IS LINEAR WITH SIN(ANGLE)
       PROGRAM JACK18(INPUT=500B,OUTPUT,TAPE5=INPUT,TAPE6=OUTPUT)
       COMMON X(4,400),Y(4,400),Z(4,400),AX(500),BY(500),CY(500),
      1       BZ(500),CZ(500),DZ(500),YC(500),XC(500),
      2       ARXY(500),AIXY(500),VAS(50)  ,
      3       AXY(350),SXY(350),V(350),SVS(350),SVA(350)
       DIMENSION W1(250), W2(20),AR(250),BJ(250), IW(250) , AFT(350)
       DIMENSION MS(350)
       DIMENSION XDB(100),XPH(100),XAM(100),YDB(100),YPH(100),YAM(100)
       DIMENSION AATZ(100),AAZ(100),AXZ(100) ,XYZ(350),ZC(100)
       DIMENSION Y1(350)
       COMPLEX AMPT ,AMPT1, AMPTZ ,AMPY
       COMPLEX AMPTX,AMPTY,AMPZ
       COMPLEX AMPTO
       NOLIST
C  CHOOSE  INVERSE(INVFT=1)  OR FORWARD(INVFT=0)  FOR F.F.T.
       INVFT=0
C  INITIALIZE  100 SIZE ARRAYS DIMENSION
       IXNIL=0
       DO 51 NIL=1,100
       IXNIL=IXNIL+1
       XDB(NIL)=0.0
       XPH(NIL)=0.0
       XAM(NIL)=0.0
       YDB(NIL)=0.0
       YPH(NIL)=0.0
       YAM(NIL)=0.0
       AATZ(NIL)=0.0
       AAZ(NIL)=0.0
       AXZ(IXNIL)= FLOAT(IXNIL)
       MS(NIL)=0
       ZC(NIL)=0.0
       AR(NIL)=0.0
       BJ(NIL)=0.0
   51  CONTINUE
       WRITE(6,19)
   19  FORMAT(1X//3X," LMIN LMAX MMIN MMAX   KX   I0   I1",
      * "      RP       PRO"//)
       READ(5,13) LMIN
       READ( 5,13)LMAX
       READ(5,13) MMIN
       READ(5,13)MMAX
       READ(5,13) KX
       READ(5,13) I0
       READ(5,13) I1
       READ(5,13) INEAR
       READ(5,13) IAMPL
       READ(5,13) NN
   13  FORMAT(I4)
       READ(5,15)RP
       READ(5,15) PRO
   15  FORMAT(F10.2)
       PI=4.*ATAN(1.)
```

```
      P=180./PI
      READ(5, 791)  A1
      READ(5,793) IAM, IPH
  791 FORMAT( F10.3 )
  793 FORMAT(2(I4))
      LX=0
      AMX=0.0
      IXSTOP=1
      IYSTOP=1
 6666  CONTINUE
      WRITE(6,17)LMIN,LMAX,MMIN,MMAX,KX,IO,I1,RP,  PRO,INEAR,IAMPL,NN
   17 FORMAT(3X,  7(1X,I4),2(F10.2),7H INEAR=,I1,7H IAMPL=,I1,4H NN=,I3)
      WRITE(6,90)

C  RANDOM NOISE GENERATOR IS RESET WHEN RP .LT.-.1 , OTHERWISE NONRESET
      IRESET=0
      IF(RP.LT.-.1) IRESET=1
      RPP=ABS(RP)
      AL=2.*PI/RPP

      S=0.61
C  INITIALIZE 350 SIZE ARRAYS DIMENSION

      DO 65 INIL=1,350
      X(1,INIL)=0.0
      X(2,INIL)=0.0
      X(3,INIL)=0.0
      X(4,INIL)=0.0
      Y(1,INIL)=0.0
      Y(2,INIL)=0.0
      Y(3,INIL)=0.0
      Y(4,INIL)=0.0
      Y1(INIL)= 0.0
      AX(INIL)=0.0
      ARXY(INIL)=0.0
      AIXY(INIL)=0.0
      SVA(INIL)=0.0
      SVS(INIL)=0.0
      SXY(INIL)=0.0
      AXY(INIL)=0.0
      XC(INIL)=0.0
      YC(INIL)=0.0
      AFT(INIL)=0.0
   65 CONTINUE
      N=KX
      NV=KX
      KS=KX
      NIW=250
      NW1=250
      NW2=20
      IFAIL=0
      DEL=0.00001
      THO=0.0
      K=0

      KC=240
      THO=0.0
```

```
      EN=0.0
      EN1=0.0
      CN=NN
C     NN IS THE NUMBER OF ELEMENTS IN THE ARRAY
      RL=FLOAT(I0)/CN
      RU=FLOAT(I1)/CN
      CALL RANSET(PI)

      WRITE(6,90)
      WRITE(6,90)
      WRITE(6,31)
   31 FORMAT(3X,"J  ANG       PHE     AME       QE         RE        PH1
     1AM1        QE1        RE1       PH0       AM0        Q0        R0"//)
      DO 9 J= LMIN,LMAX
C       CHANGE INITIAL VALUE  OF  RANSET FOR DIFF. EXPERIMENTS
      IF(IRESET.EQ.1) CALL RANSET(PI)
      C=J
      CC=C
C     THE FOLLOWING 4 STATEMENTS ARE INTENDED TO  CHANGE X SCALE TO SIN
      MOD=J/KC
      IF(ABS(C).GT.FLOAT(KC)) CC=2.*FLOAT(MOD)*KC - C
      IF(ABS(FLOAT(MOD)).GT.1.)CC=0.0
      SIC=CC/FLOAT(KC)
      THP=ASIN(SIC)
      AMPT=0.0
      AMPTZ=0.0
      AMPT1=0.0
      AMPY=0.0
11223 CONTINUE
      II3=0
C  CHOOSE  NUMBER OF ELEMENTS IN SUBARRAY NSUB=
      NSUB=6
      IF(I1.EQ.0) NSUB=1
      IF((I1+NSUB-1).GT.NN) NSUB=NN-I1+1
      G=FLOAT(I1)+FLOAT(NSUB-1)*0.5
C  CHOOSE DEFECTIVE ELEMENT AMPLITUDE RATIO  A1=  AND PHASE P1=
      A1=1.
      P1=0.0

      APY=1.0
      I4=0
      AMPT0=0.0
      AMPT1=0.0
      AMPY=0.0
      AMPZ=0.0
      AMPTZ=0.0
C  CALCULATE  NORMALIZED FAR-FIELD OF THE NN ELEMENT ARRAY
      DO 10 I=1,NN
      I3=0
      RIJ=0.0
      RA=RANF(0.0)
      PR=(RA-0.5)*AL*PRO
      D=I
      F=2.*PI*S*(D-(CN+1.)*.5)*SIN(THO)
      APS=-(2.*PI*S*(D-(CN+1.)*.5)*SIN(THP))+ PR
      FT=F+APS
      A=1.
```

```
C-  CHANGES FOR NEAR FIELD MONITORING
      XI1= S*(D-(CN+1.)*.5)
      IF(INEAR.EQ.1) RIJ=-2.*PI*SQRT((XI1-XJ2)**2.+PD**2.)
      FT=F+APS+RIJ
C- FOR CS SQUARE OVER A PEDESTAL , CHANGE A AS FOLLOWES
      IF(IAMPL.EQ.1) AI1=1./7.+6./7.*(COS(XI1/((CN+1.)*.5)*PI*.5))**2.
      IF(IAMPL.EQ.1) A=AI1
      A2=A
      IF( I.EQ.IFIX(G+.5)) A2=A
      AMPT=A*CEXP(CMPLX(0.,FT))+AMPT
      IF(I.GE.I1.AND.I.LE.(I1+NSUB-1)) I3=1


      IF(I3.EQ.1) FF=F+P1+RIJ
      IF( I3.EQ.1) AMPT0=A*CEXP(CMPLX(0.,FT))+AMPT0
      IF(I3.EQ.1) AMPY=A1*A*CEXP(CMPLX(0.,FF))+AMPY
      IF(I3.EQ.1) MS(I)=I
   10 CONTINUE
      K=K+1
      RIJ=0.0
      F=2.*PI*S*(G-(CN+1.)*.5)*SIN(THO)
      APS=-(2.*PI*S*(G-(CN+1.)*.5)*SIN(THP))
      FT1=F+APS
      FT2=F+P1
C- TO CHANGE REF. MIS/STUCK FROM FAR  FIELD INTO NEAR FIELD
      XI1=S*(G-(CN+1.)*.5)
      IF(INEAR.EQ.1) RIJ=-2.*PI*SQRT((XI1-XJ2)**2.+PD**2.)
      FT1=F+APS+RIJ
      FT2=F+P1+RIJ
      AMPZ=A2*CEXP(CMPLX(0.,FT1))
      AMPTZ=A1*CEXP(CMPLX(0.,FT2))-AMPZ
      AMPT1=AMPT-AMPT0+AMPY
      AMPT1=APY*AMPT1
      X(1,K)=(CABS(AMPT)/CN)
      X(3,K)=AIMAG(AMPT)+1.E-10
      X(4,K)=REAL(AMPT)
      X(2,K)=ATAN2(X(3,K),X(4,K)) *180./PI
      Y(3,K)=AIMAG(AMPT1)+1.E-10
      Y(4,K)=REAL (AMPT1)
      Y(2,K)=ATAN2(Y(3,K),Y(4,K))*180./PI
      Y(1,K)=(CABS(AMPT1)/CN)
      Z(3,K)=Y(3,K)-X(3,K)+1.E-10
      Z(4,K)=Y(4,K)-X(4,K)+1.E-10
      Z(2,K)=ATAN2(Z(3,K),Z(4,K))*180./PI
      Z(1,K)=SQRT(Z(4,K)*Z(4,K)+Z(3,K)*Z(3,K))
      ARXY(K)=X(4,K)
      AIXY(K)=X(3,K)
      IF(INVFT.EQ.1) AIXY(K)=-AIXY(K)
      SVA(K)=Y(3,K)
      SVS(K)=Y(4,K)
      IF(INVFT. EQ.1) SVA(K)=-SVA(K)
      AR(K)=Z(4,K)
      BJ(K)=Z(3,K)
      IF(INVFT.EQ.1) BJ(K)=-BJ(K)
      AIM1=AIMAG(AMPZ)+1.E-10
      REL1=REAL(AMPZ)
      Y1(K)=ATAN2(AIM1,REL1)*180./PI
```

```
      AIM2=AIMAG(AMPTZ)+1.E-10
      REL2=REAL(AMPTZ)
      DZ(K)=ATAN2(AIM2,REL2)*180./ PI
      AX(K)=SIC
      XC(K)=20.*ALOG10(X(1,K))
      IF(IX1.GT.1) Y(1,K)= .00001
      YC(K)=20.*(ALOG10(Y(1,K)))
      ZC(K)=20.*(ALOG10(Z(1,K)))
C  REARRANGE CORRECT ORDER OF F.F.T. COMPONENTS
      V(K)=FLOAT(K-1)
      KKX=KX/2 +1
      IF(K.GT.KKX) V(K)=FLOAT(K-1) - FLOAT(KX)
      WRITE(6,33)J,THP*P ,         Z(2,K),Z(1,K),Z(3,K),Z(4,K),Y(2,K),
     1Y(1,K),Y(3,K),Y(4,K),X(2,K)     ,X(1,K),X(3,K),X(4,K)
   33 FORMAT(1X,I4,   F6.1,3(2X,F6.1,1X,F8.4,1X,F9.4,1X,F9.4))
      BY(K)= X(1,K)
      CY(K)= Y(1,K)
      BZ(K)= Z(1,K)
      CZ(K)= Z(2,K)
      IF(BY(K).GT.0.3) BY(K)=0.3
      IF(CY(K).GT.0.3) CY(K)=0.3
      EN1=(Y(1,K)+EN1)
      EN=(Y(1,K)*Y(1,K)+EN)
    9 CONTINUE
      WRITE(6,90)
      WRITE(6,90)
      CLL=FLOAT(LMAX-LMIN)
      IF(CLL.LE.1.0)CLL=1.
      EN1=EN1/CLL
      EN=EN/CLL
      WRITE (6,1230) II3
C  DESCRIBE ARRAY OF ELEMENTS WHERE "0"= NO DEFECT  , "(.NE.0)"=DEFECT
 1230 FORMAT(3X,"MISSING ELEMENTS=",I3,"  MISS. ELEMENTS NUMBERS ARE"//)
      WRITE(6,1240) (MS(K),K=1,40)
      WRITE(6,1240)(MS(K),K=41,80)
      WRITE(6,1240)(MS(K),K=81,100)
 1240 FORMAT(3X,40I3//)
      WRITE(6,1200)
 1200 FORMAT(1H///3X,"I0    I1    MIS.ELS     ABS       ENERGY"///)
      WRITE(6,1220) I0,I1, II3   ,EN1,EN
 1220 FORMAT(2X,3(I3,3X),2(F10.5,2X))
      GOTO13131
      CALL CORELO3(LMIN,LMAX,MMIN,MMAX,KP)
13131 CONTINUE
      SQN=NV
      SQN=SQRT(SQN)
      CALL C06ADF( ARXY,AIXY,N,NV,KS,IW,NIW,W1,NW1,W2,NW2,IFAIL  )
      IF(IFAIL.NE.0)GOTO 210

      DO 3100 L=1,N
      AXY(L)=SQRT(ARXY(L)*ARXY(L)+AIXY(L)*AIXY( L))/SQN
      IF(ABS(ARXY(L)).LE.DEL)ARXY(L)=DEL
      IF(INVFT.EQ.1) AIXY(L)=-AIXY(L)
      SXY(L)= ATAN2(AIXY(L) , ARXY(L))*180./PI
 3100 CONTINUE
      CALL C06ADF(SVS,SVA, N,NV,KS, IW,NIW,W1,NW1,W2,NW2,IFAIL )
      DO 3120 L=1,N
```

```
      SVS(L)=SVS(L)/SQN
      IF( ABS(SVS(L)).LE.DEL) SVS(L)=DEL
      SVA(L)=SVA(L)/SQN
      IF(INVFT.EQ. 1) SVA(L)=-SVA(L)
      AFT(L)=SQRT(SVS(L)*SVS(L)+SVA(L)*SVA(L))
 3120 CONTINUE
      CALL C06ADF(AR, BJ , N, NV,KS, IW, NIW,W1,NW1,W2,NW2,IFAIL )
      DO 3110   L=1,N
      IF(ABS(AR(L)).LE.DEL) AR(L)=DEL
      ARL=AR(L)/SQN
      BJL=BJ(L)/SQN
      AR(L)=SQRT(ARL*ARL+BJL*BJL)
      IF(INVFT.EQ.1) BJL=-BJL
      BJ(L)=ATAN2(BJL,ARL)*180./PI
 3110 CONTINUE
      WRITE(6,992) (IW(I),I=1,5)
  992 FORMAT(1H///3X, 18HOPTIMUM VALUES ARE/2X,3HKF=, I7/2X,
     *5HKMAX=,I5/2X,4HNIW=, I6/2X, 4HNW1=, I6/2X, 4HNW2=, I6///)
      GOTO 800
  210 WRITE(6,991) IFAIL
  991 FORMAT (1H ,24HFAILURE IN C06ADF,IFAIL=, I4)
      WRITE(6,992) (IW(I),I=1,5)
  800 CONTINUE
      WRITE(6,90)
      WRITE(6,90)
   90 FORMAT(1X//)
      WRITE(6,880)
  880 FORMAT(9X,"SIN   REL FX     IMG  FX      ABS  FX        PHASE FX" ,"
     *       FTRY       FTJY      AFTY       AFXZ      PH.Z"//)
      DO 21 MM=1,KX
      LD=MM
      MN=MM-1
      WRITE (6,850) MN, AX(LD), ARXY(MM),AIXY(MM), AXY(MM),SXY(MM)
     * , SVS(MM),SVA(MM),  AFT(MM), AR(MM), BJ(MM)
  850 FORMAT(1X,I4,1X, F6.3 , 3(3X,F8.4),5X,F6.1, 4(3X,F8.4),5X,F6.1    )
   21 CONTINUE

C  LINE PRINTER GRAPHICS OUTPUT
      KK=KX
      K=KX
      KKZ=2*KK
      KKK=3*KK
      KZ=0
      AFT(1)=0.0
      AR(1)=0.0
      DO 777 LXY=1,KKK
      KZ=KZ+1
      K2Z=KZ
      IF(KZ.GT.KK)K2Z=KZ-KK
      IF(KZ.GT.2*KK)K2Z=KZ-2*KK
      AX(KZ)=AX(K2Z)
      V(KZ)=V(K2Z)
      IF(KZ.LE.KK)XYZ(KZ)=XC(K2Z)
      IF(KZ.LE.2*KK.AND.KZ.GT.KK)XYZ(KZ)=YC(K2Z)
      IF(KZ.LE.3*KK.AND.KZ.GT.2*KK)XYZ(KZ)=ZC(K2Z)
      IF(KZ.LE.2*KK.AND.KZ.GT.KK) CZ(KZ)=Y1(K2Z)
      IF(KZ.LE.3*KK.AND.KZ.GT.2*KK) CZ(KZ)=DZ(K2Z)
```

```
      IF(KZ.LE.2*KK.AND.KZ.GT.KK) AXY(KZ)= AFT(K2Z)
      IF(KZ.LE.3*KK.AND.KZ.GT.2*KK)AXY(KZ)=AR(K2Z)
      IF(KZ.LE.2*KK.AND.KZ.GT.KK) SXY(KZ)=ATAN2( SVA(K2Z),SVS(K2Z))*P
      IF(KZ.LE.3*KK.AND.KZ.GT.2*KK)SXY(KZ)=BJ(K2Z)
      IF(XYZ(KZ).LE.-50.) XYZ(KZ)=-50.
  777 CONTINUE
      LKK=LX*2
      MZ=0

      CALL GRAFIT(AX, XYZ, KKK, KK, KK, -70)
C- X=SINE ANG. "*"-DB FULL ARRAY,,"X"-DB DEFECT. ARRAY, "O"-DB MISS. EL.
      WRITE(6,173)
  173 FORMAT(2X,"X=SIN ANG. Y=FAR FLD. DB , *- FULL ARRAY, X-DEF. O-MS")
      CALL GRAFIC(AX,CZ,KK)
      WRITE(6,45)
   45 FORMAT(2X,"X=SIN ANG.Y=*-PHASE SB.A.,X-PH. MS EL(CTR),O-PH.ST.C")
      WRITE(6,3000) LMIN,LMAX,MMIN,MMAX, KX,IO,I1,IRESET,PRO,RPP
      CALL GRAFIT( V, AXY,KKK,KK,KK,-70)
      WRITE(6,4120)
 4120 FORMAT( 10X,"X=APERTUR,Y=*-MAG FFT X,X-FFT Y , O-FFT Z ")
      WRITE(6,3003) LMIN,LMAX,MMIN,MMAX, KX,IO,I1,IRESET,PRO,RPP,
     * INEAR,IAMPL
      CALL GRAFIT( V, SXY,KKK,KK,KK,-70)
      WRITE(6,450)
  450 FORMAT(10X,"X=APERTURE,Y=*-FFT X PHASE, X- FFT PHASE Y, O-FT P Z")
 3000 FORMAT(3X,6H LMIN=,I4,6H LMAX=,I4,6H MMIN=,I4,6H MMAX=,I4,
     1 12H NO SAMPLES=,I4,11H MISS ELEM= ,I3,1X,I3,8H IRESET= ,I1 ,
     27H PHASE=,F2.0 ,4H*PI/,F5.1                                    )
 3003 FORMAT(3X,6H LMIN=,I4,6H LMAX=,I4,6H MMIN=,I4,6H MMAX=,I4,
     1 12H NO SAMPLES=,I4,11H MISS ELEM= ,I3,1X,I3,8H IRESET= ,I1 ,
     27H PHASE=,F2.0 ,4H*PI/,F5.1, 7H INEAR=,I1,7H IAMPL=,I1        )
 1000 STOP
      END
END OF FILE
```

```
C-      FAR FIELD OF  N  ELEMENT ARRAY
C  INCLUDING MUTUAL COUPLING EFFECTS
C  DATA OF MUTUAL COUPLING FOR 8-ELEMENT ARRAY IS GIVEN IN
C  NORMALIZED AMPLITUDE=AZA12( )  AND PHASE=APH12( )
C       UNIFORM DISTRIBUTION , RANDOM PHASE ERROR
C       THIS PROGRAM IS LINEAR WITH SIN(ANGLE)
      PROGRAM JACK19(INPUT=131B,OUTPUT=131B,TAPE5=INPUT,TAPE6=OUTPUT)
      COMMON X(4,350),Y(4,350),Z(4,350),AX(500),BY(500),CY(500),
     1       BZ(500),CZ(500),DZ(500),YC(500),XC(500),
     2       ARXY(450),AIXY(450),VAS(50)  ,
     3       AXY(350),SXY(350),V(350),SVS(350),SVA(350)
      DIMENSION W1(250), W2(20),AR(250),BJ(250), IW(250) , AFT(350)
      DIMENSION MS(350)
      DIMENSION XDB(100),XPH(100),XAM(100),YDB(100),YPH(100),YAM(100)
      DIMENSION AATZ(100),AAZ(100),AXZ(100) ,XYZ(350),ZC(100)
      DIMENSION Y1(350),AZA12(10),APH12(10)
      COMPLEX AMPT ,AMPT1, AMPTZ ,AMPY
      COMPLEX AMPTX,AMPTY,AMPZ
      COMPLEX AMPT0
      DATA(AZA12(M),M=1,8)/.0,.0547,.0808,.1488,1.0,.1488,.0808,.0547/
      DATA(APH12(L),L=1,8)/0.0,112.,-10.,-126.,0.0,-126.,-10.,112./
C  CHOOSE INVERSE(INVFT=1) OR FORWARD(INVFT=0) FOR F.F.T.
      INVFT=0
C  INITIALIZE  100 SIZE ARRAYS DIMENSION
      IXNIL=0
      DO 51 NIL=1,100
      IXNIL=IXNIL+1
      XDB(NIL)=0.0
      XPH(NIL)=0.0
      XAM(NIL)=0.0
      YDB(NIL)=0.0
      YPH(NIL)=0.0
      YAM(NIL)=0.0
      AATZ(NIL)=0.0
      AAZ(NIL)=0.0
      AXZ(IXNIL)= FLOAT(IXNIL)
      MS(NIL)=0
      ZC(NIL)=0.0
      AR(NIL)=0.0
      BJ(NIL)=0.0
   51 CONTINUE
      WRITE(6,16)
   16 FORMAT(5X,"VALUES LMIN,LMAX,MMIN,MMAX,KX,I0,I1,INEAR,IAMPL,NN")
      READ(5, )LMIN,LMAX,MMIN,MMAX,KX,I0,I1,INEAR,IAMPL,NN
      WRITE(6,18)
   18 FORMAT(5X,"VALUES  A1,RP,PRO , IAM,IPH, NSUB , KC  ")
      READ(5, )A1,RP,PRO,IAM,IPH,NSUB,KC
      WRITE(6,19)NSUB
   19 FORMAT(1X//3X," LMIN LMAX MMIN MMAX   KX   I0   I1",
     * "      RP       PRO  NSUB=",I4//)
      PI=4.*ATAN(1.)
      P=180./PI
      IX1=0
      LX=0
      AMX=0.0
      IXSTOP=1
      IYSTOP=1
 6666  CONTINUE
```

```
      WRITE(6,17)LMIN,LMAX,MMIN,MMAX,KX,I0,I1,RP,  PRO,INEAR,IAMPL,NN
   17 FORMAT(3X,  7(1X,I4),2(F10.2),7H INEAR=,I1,7H IAMPL=,I1,4H NN=,I3)
      WRITE(6,90)

C  RANDOM NOISE GENERATOR IS RESET WHEN RP .LT.-.1 , OTHERWISE NONRESET
      IRESET=0
      IF(RP.LT.-.1) IRESET=1
      RPP=ABS(RP)
      AL=2.*PI/RPP


C  CHOOSE S=.61 FOR MLS (100 ELEMENT )  S=.687 FOR 8 ELEMENTS ARRAY
      S=0.687
C  INITIALIZE  350 SIZE ARRAYS DIMENSION
      DO 65 INIL=1,350
      X(1,INIL)=0.0
      X(2,INIL)=0.0
      X(3,INIL)=0.0
      X(4,INIL)=0.0
      Y(1,INIL)=0.0
      Y(2,INIL)=0.0
      Y(3,INIL)=0.0
      Y(4,INIL)=0.0
      Y1(INIL)= 0.0
      AX(INIL)=0.0
      ARXY(INIL)=0.0
      AIXY(INIL)=0.0
      SVA(INIL)=0.0
      SVS(INIL)=0.0
      SXY(INIL)=0.0
      AXY(INIL)=0.0
      XC(INIL)=0.0
      YC(INIL)=0.0
      AFT(INIL)=0.0
   65 CONTINUE
      N=KX
      NV=KX
      KS=KX
      NIW=250
      NW1=250
      NW2=20
      IFAIL=0
      DEL=0.00001
      THO=0.0
      K=0
      THO=ASIN(0.18)
      EN=0.0
      EN1=0.0
      CN=NN
C     NN IS THE NUMBER OF ELEMENTS IN THE ARRAY
      RL=FLOAT(I0)/CN
      RU=FLOAT(I1)/CN
      CALL RANSET(PI)

      WRITE(6,90)
      WRITE(6,90)
      WRITE(6,31)
```

```
   31 FORMAT(3X,"J  ANG       PHE     AME       QE         RE        PH1
     1AM1        QE1        RE1       PH0       AM0        Q0        R0"//)
      DO 9 J= LMIN,LMAX
C       CHANGE INITIAL VALUE  OF  RANSET FOR DIFF. EXPERIMENTS
      IF(IRESET.EQ.1) CALL RANSET(PI)
      C=J
      CC=C
C     THE FOLLOWING 4 STATEMENTS ARE INTENDED TO  CHANGE X SCALE TO SIN
      MOD=J/KC
      IF(ABS(C).GT.FLOAT(KC)) CC=2.*FLOAT(MOD)*KC - C
      IF(ABS(FLOAT(MOD)).GT.1.)CC=0.0
      SIC=CC/FLOAT(KC)
      THP=ASIN(SIC)
      AMPT=0.0
      AMPTZ=0.0
      AMPT1=0.0
      AMPY=0.0
11223 CONTINUE
      II3=0
      IF(I1.EQ.0) NSUB=1
      NSBB=(NSUB-1)/2
      NSB=4-NSBB
      A2=1.
      KM=1
      G=FLOAT(I1)
      A1=0.

      APY=1.0
      P1=0.0
      I4=0
      AMPT0=0.0
      AMPT1=0.0
      AMPY=0.0
      AMPZ=0.0
      AMPTZ=0.0
      DO 10 I=1,NN
      I3=0
      RIJ=0.0
      RA=RANF(0.0)
      PR=(RA-0.5)*AL*PRO
      D=I
      F=2.*PI*S*(D-(CN+1.)*.5)*SIN(THO)
      APS=-(2.*PI*S*(D-(CN+1.)*.5)*SIN(THP))+ PR
      FT=F+APS
      A=1.
C-  CHANGES FOR NEAR FIELD MONITORING
      XI1= S*(D-(CN+1.)*.5)
      IF(INEAR.EQ.1) RIJ=-2.*PI*SQRT((XI1-XJ2)**2.+PD**2.)
      FT=F+APS+RIJ
C- FOR CS SQUARF OVER A PEDESTAL , CHANGE A AS FOLLOWES
      IF(IAMPL.EQ.1) AI1=1./7.+6./7.*(COS(XI1/((CN+1.)*.5)*PI*.5))**2.
      IF(IAMPL.EQ.1) A=AI1
      IF( I.EQ.IFIX(G+.5)) A2=A
      AMPT=A*CEXP(CMPLX(0.,FT))+AMPT
      IF(I.GE.(I1-NSBB).AND.I.LE.(I1+NSBB))I3=1
      IF(I3.EQ.1)KM=I-I1+5
      IF(I.GT.(I1+NSBB))KM=1
```

```
      PH12=APH12(KM)/P
      AM12=AZA12(KM)


      IF(I3.EQ.1) FF=FT+PH12
      IF( I3.EQ.1) AMPTO=A*CEXP(CMPLX(0.,FT))+AMPTO
      IF(I3.EQ.1) AMPY=AM12*CEXP(CMPLX(0.,FF))+AMPY
      IF(I3.EQ.1) MS(I)=I
   10 CONTINUE
      K=K+1
      RIJ=0.0
      F=2.*PI*S*(G-(CN+1.)*.5)*SIN(THO)
      APS=-(2.*PI*S*(G-(CN+1.)*.5)*SIN(THP))
      FT1=F+APS
      FT2=F+P1
C- TO CHANGE REF. MIS/STUCK FROM FAR  FIELD INTO NEAR FIELD
      XI1=S*(G-(CN+1.)*.5)
      IF(INEAR.EQ.1) RIJ=-2.*PI*SQRT((XI1-XJ2)**2.+PD**2.)
      FT1=F+APS+RIJ
      FT2=F+P1+RIJ
      AMPZ=A2*CEXP(CMPLX(0.,FT1))
      AMPTZ=A1*CEXP(CMPLX(0.,FT2))-AMPZ
      AMPT1=AMPT-AMPTO+AMPY
      AMPT1=APY*AMPT1
      AMPT1=AMPT-A2*AMPY
      X(1,K)=(CABS(AMPT)/CN)
      X(3,K)=AIMAG(AMPT)+1.E-10
      X(4,K)=REAL(AMPT)
      X(2,K)=ATAN2(X(3,K),X(4,K)) *180./PI
      Y(3,K)=AIMAG(AMPT1)+1.E-10
      Y(4,K)=REAL (AMPT1)
      Y(2,K)=ATAN2(Y(3,K),Y(4,K))*180./PI
      Y(1,K)=(CABS(AMPT1)/CN)
      Z(3,K)=Y(3,K)-X(3,K)+1.E-10
      Z(4,K)=Y(4,K)-X(4,K)+1.E-10
      Z(2,K)=ATAN2(Z(3,K),Z(4,K))*180./PI
      Z(1,K)=SQRT(Z(4,K)*Z(4,K)+Z(3,K)*Z(3,K))
      ARXY(K)=X(4,K)
      AIXY(K)=X(3,K)
      IF(INVFT.EQ.1) AIXY(K)=-AIXY(K)
      SVA(K)=Y(3,K)
      SVS(K)=Y(4,K)
      IF(INVFT. EQ.1) SVA(K)=-SVA(K)
      AR(K)=Z(4,K)
      BJ(K)=Z(3,K)
      IF(INVFT.EQ.1) BJ(K)=-BJ(K)
      AIM1=AIMAG(AMPZ)+1.E-10
      REL1=REAL(AMPZ)
      Y1(K)=ATAN2(AIM1,REL1)*180./PI
      AIM2=AIMAG(AMPTZ)+1.E-10
      REL2=REAL(AMPTZ)
      DZ(K)=ATAN2(AIM2,REL2)*180./ PI
      AX(K)=SIC
      XC(K)=20.*ALOG10(X(1,K))
      IF(IX1.GT.1) Y(1,K)= .00001
      YC(K)=20.*(ALOG10(Y(1,K)))
      ZC(K)=20.*(ALOG10(Z(1,K)))
```

```
C  REARRANGE CORRECT ORDER OF F.F.T. COMPONENTS
      V(K)=FLOAT(K-1)
      KKX=KX/2 +1
      IF(K.GT.KKX) V(K)=FLOAT(K-1) - FLOAT(KX)
      WRITE(6,33)J,THP*P ,         Z(2,K),Z(1,K),Z(3,K),Z(4,K),Y(2,K),
     1Y(1,K),Y(3,K),Y(4,K),X(2,K)     ,X(1,K),X(3,K),X(4,K)
   33 FORMAT(1X,I4,   F6.1,3(2X,F6.1,1X,F8.4,1X,F9.4,1X,F9.4))
      BY(K)= X(1,K)
      CY(K)= Y(1,K)
      BZ(K)= Z(1,K)
      CZ(K)= Z(2,K)
      IF(BY(K).GT.0.3) BY(K)=0.3
      IF(CY(K).GT.0.3) CY(K)=0.3
      EN1=(Y(1,K)+EN1)
      EN=(Y(1,K)*Y(1,K)+EN)
    9 CONTINUE
      WRITE(6,90)
      WRITE(6,90)
      CLL=FLOAT(LMAX-LMIN)
      IF(CLL.LE.1.0)CLL=1.
      EN1=EN1/CLL
      EN=EN/CLL
C  DESCRIBE ARRAY OF ELEMENTS WHERE "0"=NO DEFECT , "(.NE.0)"=DEFECT
C
      WRITE (6,1230)  II3
 1230 FORMAT(3X,"MISSING ELEMENTS=",I3,"  MISS. ELEMENTS NUMBERS ARE"//)
      WRITE(6,1240) (MS(K),K=1,40)
      WRITE(6,1240)(MS(K),K=41,80)
      WRITE(6,1240)(MS(K),K=81,100)
 1240 FORMAT(3X,40I3//)
      WRITE(6,1200)
 1200 FORMAT(1H///3X,"I0     I1     MIS.ELS      ABS        ENERGY"///)
      WRITE(6,1220) I0,I1, II3    ,EN1,EN
 1220 FORMAT(2X,3(I3,3X),2(F10.5,2X))
C  CANCEL NEXT LINE (GOTO  ....) IF USE OF COREL IS REQUIRED
      GOTO13131
      CALL COREL03(LMIN,LMAX,MMIN,MMAX,KP)
13131 CONTINUE
      SQN=NV
      SQN=SQRT(SQN)
      CALL C06ADF( ARXY,AIXY,N,NV,KS,IW,NIW,W1,NW1,W2,NW2,IFAIL  )
      IF(IFAIL.NE.0)GOTO 210

      DO 3100 L=1,N
      AXY(L)=SQRT(ARXY(L)*ARXY(L)+AIXY(L)*AIXY( L))/SQN
      IF(ABS(ARXY(L)).LE.DEL)ARXY(L)=DEL
      IF(INVFT.EQ.1) AIXY(L)=-AIXY(L)
      SXY(L)= ATAN2(AIXY(L) , ARXY(L))*180./PI
 3100 CONTINUE
      CALL C06ADF(SVS,SVA, N,NV,KS, IW,NIW,W1,NW1,W2,NW2,IFAIL )
      DO 3120 L=1,N
      SVS(L)=SVS(L)/SQN
      IF( ABS(SVS(L)).LE.DEL) SVS(L)=DEL
      SVA(L)=SVA(L)/SQN
      IF(INVFT.EQ. 1) SVA(L)=-SVA(L)
      AFT(L)=SQRT(SVS(L)*SVS(L)+SVA(L)*SVA(L))
 3120 CONTINUE
```

```
      CALL C06ADF(AR, BJ , N, NV,KS, IW, NIW,W1,NW1,W2,NW2,IFAIL )
      DO 3110   L=1,N
      IF(ABS(AR(L)).LE.DEL) AR(L)=DEL
      ARL=AR(L)/SQN
      BJL=BJ(L)/SQN
      AR(L)=SQRT(ARL*ARL+BJL*BJL)
      IF(INVFT.EQ.1) BJL=-BJL
      BJ(L)=ATAN2(BJL,ARL)*180./PI
 3110 CONTINUE
      WRITE(6,992) (IW(I),I=1,5)
  992 FORMAT(1H///3X, 18HOPTIMUM VALUES ARE/2X,3HKF=, I7/2X,
     *5HKMAX=,I5/2X,4HNIW=, I6/2X, 4HNW1=, I6/2X, 4HNW2=, I6///)
      GOTO 800
  210 WRITE(6,991) IFAIL
  991 FORMAT (1H ,24HFAILURE IN C06ADF,IFAIL=, I4)
      WRITE(6,992) (IW(I),I=1,5)
  800 CONTINUE
      WRITE(6,90)
      WRITE(6,90)
   90 FORMAT(1X//)
      WRITE(6,880)
  880 FORMAT(9X,"SIN   REL FX     IMG  FX      ABS  FX        PHASE FX" ,"
     *       FTRY       FTJY      AFTY       AFXZ      PH.Z"//)
      DO 21 MM=1,KX
      LD=MM
      MN=MM-1
      WRITE (6,850) MN, AX(LD), ARXY(MM),AIXY(MM), AXY(MM),SXY(MM)
     * , SVS(MM),SVA(MM),  AFT(MM), AR(MM), BJ(MM)
  850 FORMAT(1X,I4,1X, F6.3 , 3(3X,F8.4),5X,F6.1, 4(3X,F8.4),5X,F6.1    )
   21 CONTINUE
C
C   LINE PRINTER GRAF OUTPUT SECTION
C
      KK=KX
      K=KX
      KKZ=2*KK
      KKK=3*KK
      KZ=0
      DO 777 LXY=1,KKK
      KZ=KZ+1
      K2Z=KZ
      IF(KZ.GT.KK)K2Z=KZ-KK
      IF(KZ.GT.2*KK)K2Z=KZ-2*KK
      AX(KZ)=AX(K2Z)
      V(KZ)=V(K2Z)
      IF(KZ.LE.KK)XYZ(KZ)=XC(K2Z)
      IF(KZ.LE.2*KK.AND.KZ.GT.KK)XYZ(KZ)=YC(K2Z)
      IF(KZ.LE.3*KK.AND.KZ.GT.2*KK)XYZ(KZ)=ZC(K2Z)
      IF(KZ.LE.2*KK.AND.KZ.GT.KK) CZ(KZ)=Y1(K2Z)
      IF(KZ.LE.3*KK.AND.KZ.GT.2*KK) CZ(KZ)=DZ(K2Z)
      IF(KZ.LE.2*KK.AND.KZ.GT.KK) AXY(KZ)= AFT(K2Z)
      IF(KZ.LE.3*KK.AND.KZ.GT.2*KK)AXY(KZ)=AR(K2Z)
      IF(KZ.LE.2*KK.AND.KZ.GT.KK) SXY(KZ)=ATAN2( SVA(K2Z),SVS(K2Z))*P
      IF(KZ.LE.3*KK.AND.KZ.GT.2*KK)SXY(KZ)=BJ(K2Z)
      IF(XYZ(KZ).LE.-50.) XYZ(KZ)=-50.
  777 CONTINUE
      LKK=LX*2
```

```
      MZ=0

   50 FORMAT(1H1)
      CALL GRAFIT(AX, XYZ, KKK, KK, KK, -70)
C- X=SINE ANG. "*"-DB FULL ARRAY,,"X"-DB DEFECT. ARRAY, "0"-DB MISS. EL.
      WRITE(6,173)
  173 FORMAT(2X,"X=SIN ANG. Y=FAR FLD. DB ,  - FULL ARRAY, X-DEF. 0-MS")
      CALL GRAFIC(AX,CZ,KK)
      WRITE(6,45)
   45 FORMAT(2X,"X=SIN ANG.Y= -PHASE SB.A.,X-PH. MS EL(CTR),0-PH.ST.C")
      WRITE(6,3000) LMIN,LMAX,MMIN,MMAX, KX,I0,I1,IRESET,PRO,RPP
      CALL GRAFIT( V, AXY,KKK,KK,KK,-70)
      WRITE(6,4120)
 4120 FORMAT( 10X,"X=APERTUR,Y= -MAG FFT X,X-FFT Y , 0-FFT Z ")
      WRITE(6,3003) LMIN,LMAX,MMIN,MMAX, KX,I0,I1,IRESET,PRO,RPP,
     * INEAR,IAMPL
      CALL GRAFIT( V, SXY,KKK,KK,KK,-70)
      WRITE(6,450)
  450 FORMAT(10X,"X=APERTURE,Y= -FFT X PHASE, X- FFT PHASE Y, 0-FT P Z")
 3000 FORMAT(3X,6H LMIN=,I4,6H LMAX=,I4,6H MMIN=,I4,6H MMAX=,I4,
     1 12H NO SAMPLES=,I4,11H MISS ELEM= ,I3,1X,I3,8H IRESET= ,I1 ,
     27H PHASE=,F2.0 ,4H*PI/,F5.1                                    )
 3003 FORMAT(3X,6H LMIN=,I4,6H LMAX=,I4,6H MMIN=,I4,6H MMAX=,I4,
     1 12H NO SAMPLES=,I4,11H MISS ELEM= ,I3,1X,I3,8H IRESET= ,I1 ,
     27H PHASE=,F2.0 ,4H*PI/,F5.1, 7H INEAR=,I1,7H IAMPL=,I1         )
 1000 STOP
      END
END OF FILE
```

```
         SUBROUTINE COREL03(LMIN,LMAX,MMIN,MMAX,KP          )
       COMMON Y(4,400),X(4,400),Z(4,400),AX(500),BY(500),CY(500),
      1       BZ(500),CZ(500),DZ(500),YC(500),XC(500),
      2       ARXY(500),AIXY(500),VAS(50)  ,
      3       AXY(350),SXY(350),V(350),SVS(350),SVA(350)
C      KP - NUMBER OF TERM IN THE OUTPUT ARRAY OF COREL
C      M IS THE DIFFERENCE INDEX OF THE CORELATION COEFICIENT -   C(M)
C
       KP=0
C
       DO 6 M=MMIN,MMAX
       KL=0
       S44=0.0
       S33=0.0
       S43=0.0
       S34=0.0
       S11=0.0
       S11S=0.0
       S4A=0.0
       S3A=0.0
       S1A=0.0
       S11A=0.0
       S4B=0.0
       S3B=0.0
       S1B=0.0
       S11B=0.0
       V4A=0.0
       V3A=0.0
       V1A=0.0
       V11A=0.0
       V4B=0.0
       V3B=0.0
       V1B=0.0
       V11B=0.0
       LL=0
       KP=KP+1
       L=M+1
       NM=LMAX-LMIN-M
C
C  LL IS THE INDEX OF DISCRETE ANG . SPECT. IN THE (LMIN+LL) DIRECTION
C   OR LL IS THE INDEX OF THE SUMATION     X1
C      LM IS THE INDEX OF THE SUMATION  X2 -   LM=LL+M
C      THE SUMATION IS PERFORMED ONLY OVER (N-M) TERMS
C      N IS THE NUMBER OF TERMS  -  N=LMAX-LMIN+1  .  HENCE
C      THE IF STATMENT TERMINATES THE DO 5 AFTER  INDEX (LMAX-M)
C      X(1, )=ABS   X(3, ) = IMAGINARY     X(4, ) = REAL
C
       DO 5 K=LMIN,LMAX
       LL=LL+1
       KL=KL+1
       LM=LL+M
       IF(LL.GT.NM) GOTO 3
C    A SUMATION  OVER  X1  INDEX LL
       S4A=X(4,LL)+S4A
       S3A=X(3,LL)+S3A
       S1A=X(1,LL)+S1A
       S11A=X(1,LL)**2.+S11A
C    B SUMATION OVER X2  INDEX LM=LL+M
       S4B=X(4,LM)+S4B
       S3B=X(3,LM)+S3B
```

```
       S1B=X(1,LM)+S1B
       S11B=X(1,LM)**2.+S11B
C      SUMATION OVER  CROSS MULTIPLICATIONS
       S44=X(4,LL)*X(4,LM)+S44
       S33=X(3,LL)*X(3,LM)+S33
       S43=X(4,LL)*X(3,LM)+S43
       S34=X(3,LL)*X(4,LM)+S34
       S11=X(1,LL)*X(1,LM)+S11
       S11S=X(1,LL)**2.*X(1,LM)**2. +S11S
C      SUMATION OF SQUARE TERMS FOR THE VARIANCE CALCULATION
C    A SUMATION OVER THE X1 TERMS
       V4A=X(4,LL)*X(4,LL)+V4A
       V3A=X(3,LL)*X(3,LL)+V3A
       V1A=X(1,LL)*X(1,LL)+V1A
       V11A=X(1,LL)**4. +V11A
C    B SUMATION OVER THE X2 TERMS
       V4B=X(4,LM)*X(4,LM)+V4B
       V3B=X(3,LM)*X(3,LM)+V3B
       V1B=X(1,LM)*X(1,LM)+V1B
       V11B=X(1,LM)**4. +V11B
     5 CONTINUE
       KS=KL
     3 IF(LL.GT.NM) KS=KL-1
       IF(KL.LE.1) KS=1
       CL=FLOAT(KS)
       IF(KS.LT.1)GOTO 4
       VRZA=V4A-S4A*S4A/CL
       VIZA=V3A-S3A*S3A/CL
       VRZB=V4B-S4B*S4B/CL
       VIZB=V3B-S3B*S3B/CL
       VZA=VRZA+VIZA
       VZB=VRZB+VIZB
       SAZ=SQRT(VZA)
       SBZ=SQRT(VZB)
       VAB=SAZ*SBZ
       VSA=V1A-S1A*S1A/CL
       VSB=V1B-S1B*S1B/CL
       IF(VSA.LT.0.0)VSA=ABS(VSA)
       IF(VSB.LT.0.0) VSB=ABS(VSB)
       VA=SQRT(VSA*VSB)
       VSSA=V11A-S11A*S11A/CL
       VSSB=V11B-S11B*S11B/CL
       IF(VSSA.LT.0.0) VSSA=ABS(VSSA)
       IF(VSSB.LT.0.0) VSSB=ABS(VSSB)
       VSS=SQRT(VSSA*VSSB)
       ARXY(L)=((S44+S33)-(S4A*S4B+S3A*S3B)/CL)/VAB
       AIXY(L)=((S43-S34)-(S4A*S3B-S3A*S4B)/CL)/VAB
       AXY(L)=(S11-S1A*S1B/CL)/VA
       SXY(L)=(S11S-S11A*S11B/CL)/VSS
       SVS(L)=ARXY(L)
       SVA(L)=AIXY(L)
     4 CONTINUE
       IF(KP.GT.1)GOTO 8
       VAS(1)=CL
       VAS(2)=S44
       VAS(3)=S33
       VAS(4)=S43
       VAS(5)=S34
       VAS(6)=S4A
       VAS(7)=S3A
```

```
      VAS(8)=S4B
      VAS(9)=S3B
      VAS(10)=VRZA
      VAS(11)=VIZA
      VAS(12)=VRZB
      VAS(13)=VIZB
      VAS(14)=VZA
      VAS(15)=VZB
      VAS(16)=VAB
      VAS(17)=VSA
      VAS(18)=VSB
      VAS(19)=VA
      VAS(20)=VSSA
      VAS(21)=VSSB
      VAS(22)=VSS
      VAS(23)=FLOAT(L)
    8 CONTINUE
    6 CONTINUE
      RETURN
      END
END OF FILE
```

```
C-   - MUTUAL COUPLING BETWEEN BROADSIDE PARALLEL DIPOLES
      PROGRAM JACK20(INPUT,OUTPUT,TAPE5=INPUT,TAPE6=OUTPUT)
      DIMENSION X(500),Y(500),X1(150),X2(150),X3(150),X4(150)
     *,X5(150),X6(150),X7(150),X8(150),X9(150),X10(150),X11(150),XX(120)
      COMPLEX Z,Z1,Z11,Z21,XPS1
      PI=4.*ATAN(1.)
      DEL=0.0000001
      GAMA=0.57721566490153
      EXGAMA=1.78107241799019
      P=180./PI
      D1=0.5
      C=30.
      GHZ=5.0
      WRITE(6,70)
   70 FORMAT(5X,"VALUES  EL.LENGTH=D1,GHZ,LMIN,LMAX,KC  ")
      READ(5,*)D1,GHZ,LMIN,LMAX,KC
      LAMBDA=C/GHZ
      AK=2.*PI/LAMBDA
      D=2.*PI*D1
      CI= S13ACF(2.*D,1)
      SI=S13ADF(2.*D,1)
      REL1=GAMA+ALOG(2.*D)-CI
      AIM1=SI- PI/2.
      REL1=30.*REL1
      IF(ABS(REL1).LE.DEL) REL1=DEL
      AIM1=30.*AIM1
      Z11=  CMPLX(REL1,AIM1)
      AT=ATAN2(REL1,AIM1)*180./PI
      WRITE(6,52)
   52 FORMAT(3X////     )
      WRITE(6,90) REL1,AIM1,AT
   90 FORMAT(3X,"RLZ=",F10.5,5X,"IM.Z=",F10.5, 5X,"PH.Z=",F6.1  )
      WRITE(6,52)
      WRITE(6,80)
   80 FORMAT(2X,"   K     S       DB.C     PH.12     IM12"
     *,"   RE 12     IM Z1    RE.Z1    PH(Z1-Z11)   Z120  PH.120  C1DB"
     2 ,"   V(Z1)/V(Z11)")
      WRITE(6,50)
   50 FORMAT(1X//)
      K=0
      DO10 I=LMIN,LMAX
      K=K+1
      S=FLOAT( I)/FLOAT(KC)
      A=2.*PI*S
      G=SQRT( A*A+D*D)
      D1=A
      D2=G+D
      D3=G-D
      SI1=S13ADF(D1,1)-PI/2.
      SI2=S13ADF(D2,1)-PI/2.
      SI3=S13ADF(D3,1)-PI/2.
      CI1=S13ACF(D1,1)
      CI2=S13ACF(D2,1)
      CI3=S13ACF(D3,1)
      REL=2.*CI1-CI2-CI3
      IF(ABS(REL).LE.DEL*.01) REL=DEL*.01
      AIM=-(2.*SI1-SI2-SI3)
      IF(ABS(REL).LE.DEL*.01) REL=DEL*.01
```

```
      AIM=-(2.*SI1-SI2-SI3)
      Z21=30.*CMPLX(REL,AIM)
      CP= CABS(Z21) / (2.*REL1)
      PHZ=ATAN2(REAL(Z21),AIMAG(Z21))*180./PI
      Z1=Z11+Z21
      X1(K)=S
      X2(K)=20.*ALOG10(CP)
      PS1=(A-PI/2.)
      XPS1=CEXP(CMPLX(0.,PS1))
      REXPS1=REAL(XPS1)
      IF(ABS(REXPS1).LE.DEL)REXPS1=DEL
      AIMXPS1=AIMAG(XPS1)
      PSM=ATAN2(REXPS1,-AIMXPS1)
      X10(K)=PSM*P
      X3(K)= PHZ- X10(K)
      AX3=X3(K)
      IF(AX3.GE.180.)X3(K)=AX3-180.
      IF(AX3.GE.270.)X3(K)=360.-AX3
      IF(AX3.LE.-180.)X3(K)=AX3+180.
      IF(AX3.LE.-270.)X3(K)=AX3+360.
      X3(K)=-X3(K)
      X4(K)=AIMAG(Z21)
      X5(K)= REAL(Z21)
      X6(K)=AIMAG(Z1)
      X7(K)=  REAL(Z1)
      APH=( ATAN2(REAL(Z1),AIMAG(Z1))-ATAN2(REAL(Z11),AIMAG(Z11)))*P
      X8(K)=APH
      REL2=X7(K)
      CP1= CABS(Z21)/(2.*REL2)
      X11(K)= 20.*ALOG10(CP1)
C     Z120=120./A*CEXP(0.0,-(A-PI/2.))
      X9(K)= 120./A
      XX(K)= CABS(Z1)/CABS(Z11)
      WRITE(6,100) K,X1(K),X2(K),X3(K),X4(K),X5(K),X6(K),X7(K)
     *, X8(K),X9(K),X10(K)  ,X11(K) ,XX(K)
   10 CONTINUE
  100 FORMAT(3X,I4,2X,F8.4,2X,F6.2,2X,F6.1,2X,4(F8.4,2X),F6.1
     *,2X,F8.4,2X,F6.1,2X,F8.2,2X,F8.4  )
      CALL GRAFIC(X1,X2,K)
      WRITE(6,110)
  110 FORMAT(10X,"X=SPACING S/LAMBDA, Y= MUTUAL COUPLING DB. "      )
      CALL GRAFIC(X1,X3,K)
      WRITE(6,120)
  120 FORMAT(10X,"X=SPACING S/LAMBDA, Y= PH.Z21 - PH. Z120   ")
      CALL GRAFIC(X1,X4,K)
      WRITE(6,130)
  130 FORMAT(10X,"X=SPACING S/LAMBDA, Y= IMAG Z21")
      CALL GRAFIC(X1,X5,K)
      WRITE(6,140)
  140 FORMAT( 10X," X=SPACING S/LAMBDA, Y=REAL Z21"  )
      CALL GRAFIC(X1,X8,K)
      WRITE(6,150)
  150 FORMAT(10X,"X=SPACING S/LAMBDA, Y= PH.Z1-PH.Z11")
      CALL GRAFIC(X1, X11,K)
      WRITE(6,160)
  160 FORMAT(10X,"X=SPACING, Y=CORRECTED COUPLING DB.(REAL(Z1))  ")
      CALL GRAFIC(X1,XX,K)
```

```
      WRITE(6,170)
  170 FORMAT( 10X,"X=SPACING, Y=VOLTAGE RATIO COUPLED/UNCOUPLED EL.    ")
      STOP
      END
END OF FILE
```

```
C-       NEAR FIELD MEASURMENTS , FAR FIELD  NN  ELEMENT ARRAY
C      XDB(),YDB() MEASURED FIELD IN DB. XPH YPH MEASURED PHASE IN DEG
C       THIS PROGRAM IS LINEAR WITH SIN(ANGLE)
       PROGRAM JACK30(INPUT=131B,OUTPUT=131B,FINX,TAPE5=INPUT,
      * TAPE6=OUTPUT,TAPE7=FINX)
       COMMON X(4,400),Y(4,400),Z(4,400),AX(500),BY(500),
      1       BZ(500),CZ(500),DZ(500),YC(500),XC(500),
      2       ARXY(500),AIXY(500),VAS(100)    ,
      3       AXY(350),SXY(350),V(350),SVS(350),SVA(350)
       DIMENSION W1(250), W2(20),AR(250),BJ(250), IW(250) , AFT(350)
       DIMENSION MS(350)
       DIMENSION XDB(100),XPH(100),XAM(100),YDB(100),YPH(100),YAM(100)
       DIMENSION AATZ(100),AAZ(100),AXZ(100) ,XYZ(350),ZC(100)
       DIMENSION Y1(350)
       COMPLEX AMPT ,AMPT1, AMPTZ ,AMPY
       COMPLEX AMPTX,AMPTY,AMPZ
       COMPLEX AMPTO
       NOLIST
       INVFT=0
C  INITIALIZE 100 SIZE ARRAYS DIMENSION
       IXNIL=0
       DO 51 NIL=1,100
       IXNIL=IXNIL+1
       XDB(NIL)=0.0
       XPH(NIL)=0.0
       XAM(NIL)=0.0
       YDB(NIL)=0.0
       YPH(NIL)=0.0
       YAM(NIL)=0.0
       AATZ(NIL)=0.0
       AAZ(NIL)=0.0
       AXZ(IXNIL)= FLOAT(IXNIL)
       MS(NIL)=0
       ZC(NIL)=0.0
       AR(NIL)=0.0
       BJ(NIL)=0.0
       VAS(NIL)=0.0
    51 CONTINUE
       WRITE(6,19)
    19 FORMAT(1X//3X," LMIN LMAX MMIN MMAX   KX   IO   I1",
      * "      RP       PRO"//)
       READ(5,13) LMIN
       READ( 5,13)LMAX
       READ(5,13) MMIN
       READ(5,13)MMAX
       READ(5,13) KX
       READ(5,13) IO
       READ(5,13) I1
       READ(5,13) INEAR
       READ(5,13) IAMPL
       READ(5,13) NN
    13 FORMAT(I4)
       READ(5,15)RP
       READ(5,15) PRO
    15 FORMAT(F10.2)
       PI=4.*ATAN(1.)
       P=180./PI
       DEL=0.00001
```

```
      READ(5, 791)  A1
      READ(5,793) IAM, IPH
  791 FORMAT( F10.3 )
  793 FORMAT(2(I4))
      LX=0
      AMX=0.0
      IXSTOP=1
      IYSTOP=1
      IZOK=0
      IEJIX=0
      IF(IAM.GE.10.AND.IPH.GE.10 )IEJIX=1
      IF(IEJIX.EQ.1) LX=41
      IF(IEJIX.EQ.1) GOTO 666
      DO 53 LLX=1,100
      LX=LX+1
C  READ NEAR FIELD MEASUREMENTS DATA FROM TAPE7
      READ(7,55) XDB(LX),XPH(LX),IXSTOP  ,IZOK
      IF(IXSTOP.LT.0)GOTO   121
      DBX=XDB(LX)/20.0
      XAM(LX)=FLOAT(NN)*10.0**DBX
      XPH(LX)=XPH(LX)/P
      AMX=AMX+XAM(LX)
   53 CONTINUE
  121 CONTINUE
      LX=LX-1
   55 FORMAT(F10.2,F10.2,I4,I6             )
      I11=0
      IF(I1.EQ.0.AND.I0.EQ.0)I11=1
      IF( (-IXSTOP).GT.1)   GOTO 666
      LY=0
      DO 57 LLY=1,100
      LY=LY+1
      READ(7,55) YDB(LY),YPH(LY),IYSTOP
      IF((-IYSTOP).GT.1)I1=(-IYSTOP)
      IF(I11.EQ.1)I1=0
      IF(LY.EQ.I1) MS(LY)=LY
      IF(IYSTOP.LT.0) GOTO 23
      DBY=YDB(LY)/20.0
      YPH(LY)=YPH(LY)/P
      YAM(LY)= FLOAT(NN)*10.0**DBY
   57 CONTINUE
   23 CONTINUE
      LY=LY-1
  666 CONTINUE
      IX1=0
      IF( (-IXSTOP).GT.1) I1=(-IXSTOP)
      IF( (-IXSTOP).GT.1)IX1= (-IXSTOP)
      NN2=NN
      NN=LX
      WRITE(6,17)LMIN,LMAX,MMIN,MMAX,KX,I0,I1,RP,  PRO,INEAR,IAMPL,NN
   17 FORMAT(3X,  7(1X,I4),2(F10.2),7H INEAR=,I1,7H IAMPL=,I1,4H NN=,I3)
      WRITE(6,90)
      ST8=.18
      ST16=.08
      S2= .404
      N8=8
      S=0.404
```

```
      N1= N8
      N2=LX
      STHO=ST8
      S8=.687
      S1=S8
      ZOK=20.
      IF(IZOK.LT.0)ZOK=ABS(FLOAT(IZOK))*0.1
      WRITE(6, 178)
  178 FORMAT( 3X,"  N1    N2     S1       S2       ZOK      STHO      "//)
      WRITE(6,176)  N1,N2, S1,S2,ZOK, STHO
  176 FORMAT( 3X,2(I4), 4(2X, F8.4)        //)
      WRITE(6,129)
  129 FORMAT(3X," II     X DB      XAMP     XPHASE     Y DB      Y AMP      ",
     *"  Y PHASE    REAL Z     IMAG Z    AMP Z    PHASE Z",11X,"VAS PH.Z"//)
      AMPTX=0.
      AMPTY=0.
      AMPZ=0.
      IL=0
      PD=ZOK/5.26
      CN=LX
      LI=0
      IF(IEJIX.EQ.0) GOTO 6161
            CALL EJIX(XAM,XPH,N1,N2,S1,S2,PD ,STHO,  0,  0  , AMX,1,10 )

            CALL EJIX(YAM,YPH,N1,N2,S1,S2,PD ,STHO,  0, I1  , AMX,1,10 )
 6161 CONTINUE
      H=1.
      IF(IEJIX.EQ.1) H=-1.
      DO  125 II=1,LX
      IL=IL+1
      PX=XPH(IL)
      AMPTX=XAM(IL)*CEXP(CMPLX(0.,PX))
      PY=YPH(IL)
      AMPTY=YAM(IL)*CEXP(CMPLX(0.,PY))
      AMPZ= AMPTY - AMPTX
      RIZ=REAL(AMPZ)
      AIZ=AIMAG(AMPZ)
      IF(ABS(RIZ).LE.DEL) RIZ=DEL
      ATZ= ATAN2(AIZ,RIZ)*P
      AZ=CABS(AMPZ)
      AATZ( IL)= ATZ
      AAZ(IL)=AZ

      D=FLOAT(IL)
      TANTO=S*(D-(CN+1.)*.5)/PD
      THP=ATAN(TANTO)
      F=H*2.*PI*PD*COS(THP)
      SUBT=0.
      IMT=1
      IF(IL.GT.1)SUBT=AATZ(IL-1)-AATZ(IL)
      IF(SUBT.GT.0.)IMT=-1
      IF(ABS(SUBT).GT.180.) LI=LI+IMT
      FT= F+ATZ/P
      VASI= FT    -FLOAT(LI)*2.*PI
      IF(IL.EQ.1)VASO=VASI
      VAS(IL)=VASI-VASO
      WRITE(6,127) IL,XDB(IL),XAM(IL),XPH(IL)*P, YDB(IL),YAM(IL),
```

```
     1 YPH(IL)*P,RIZ,AIZ,AZ,ATZ  ,VAS(IL)/(2.*PI)
  127 FORMAT( 3X, I4, 11(2X,F8.3))
  125 CONTINUE
12521 CONTINUE
C  START NEAR FIELD TO FAR FIELD TRANSFORMATION
C  INITIALIZE 350 SIZE ARRAYS DIMENSION
      DO 65 INIL=1,350
      X(1,INIL)=0.0
      X(2,INIL)=0.0
      X(3,INIL)=0.0
      X(4,INIL)=0.0
      Y(1,INIL)=0.0
      Y(2,INIL)=0.0
      Y(3,INIL)=0.0
      Y(4,INIL)=0.0
      Y1(INIL)= 0.0
      AX(INIL)=0.0
      ARXY(INIL)=0.0
      AIXY(INIL)=0.0
      SVA(INIL)=0.0
      SVS(INIL)=0.0
      SXY(INIL)=0.0
      AXY(INIL)=0.0
      XC(INIL)=0.0
      YC(INIL)=0.0
      AFT(INIL)=0.0
   65 CONTINUE
      N=KX
      NV=KX
      KS=KX
      NIW=250
      NW1=250
      NW2=20
      IFAIL=0
      THO=0.0
      K=0
      KC=50

      PD=ZOK/5.26
      THO=0.0
      EN=0.0
      EN1=0.0
      CN=NN
C     NN IS THE NUMBER OF ELEMENTS IN THE ARRAY
      RL=FLOAT(I0)/CN
      RU=FLOAT(I1)/CN
      WRITE(6,90)
      WRITE(6,31)
   31 FORMAT(3X,"J  ANG      PHE    AME      QE        RE       PH1
     1AM1       QE1       RE1      PH0      AM0       Q0       R0"//)

      DO 9 J= LMIN,LMAX
      C=J
      CC=C
C     THE FOLLOWING 4 STATEMENTS ARE INTENDED TO  CHANGE X SCALE TO SIN
      MOD=J/KC
      IF(ABS(C).GT.FLOAT(KC)) CC=2.*FLOAT(MOD)*KC - C
```

```
      IF(ABS(FLOAT(MOD)).GT.1.)CC=0.0
      SIC=CC/FLOAT(KC)
      THP=ASIN(SIC)
      AMPT=0.0
      AMPTZ=0.0
      AMPT1=0.0
      AMPY=0.0
11223 CONTINUE
      II3=0
      P1=0.0
      I4=0
      AMPT0=0.0
      AMPT1=0.0
      AMPY=0.0
      AMPZ=0.0
      AMPTZ=0.0

C  START D.F.T.  LOOP
      DO 11 I=1,LX
      D=FLOAT(I)
      F=H*2.*PI*PD*COS(THP)
      APS=-(2.*PI*S*(D-(CN+1.)*.5)*SIN(THP))- XPH(I)
      APY=-(2.*PI*S*(D-(CN+1.)*.5)*SIN(THP))- YPH(I)
      FT=F+APS
      TF=F+APY
      A=XAM(I)/AMX
      B=YAM(I)/AMX
      AMPT=A*CEXP(CMPLX(0.,FT))+AMPT
      AMPY=B*CEXP(CMPLX(0.,TF))+AMPY
      IF(I11.EQ.1)AMPY=AMPT
   11 CONTINUE
      AMPT1=AMPY
      K=K+1
      X(1,K)=(CABS(AMPT)/CN)
      X(3,K)=AIMAG(AMPT)+1.E-10
      X(4,K)=REAL(AMPT)
      X(2,K)=ATAN2(X(3,K),X(4,K)) *180./PI
      Y(3,K)=AIMAG(AMPT1)+1.E-10
      Y(4,K)=REAL (AMPT1)
      Y(2,K)=ATAN2(Y(3,K),Y(4,K))*180./PI
      Y(1,K)=(CABS(AMPT1)/CN)
      Z(3,K)=Y(3,K)-X(3,K)+1.E-10
      Z(4,K)=Y(4,K)-X(4,K)+1.E-10
      Z(2,K)=ATAN2(Z(3,K),Z(4,K))*180./PI
      Z(1,K)=SQRT(Z(4,K)*Z(4,K)+Z(3,K)*Z(3,K))
      ARXY(K)=X(4,K)
      AIXY(K)=X(3,K)
      IF(INVFT.EQ.1) AIXY(K)=-AIXY(K)
      SVA(K)=Y(3,K)
      SVS(K)=Y(4,K)
      IF(INVFT. EQ.1) SVA(K)=-SVA(K)
      AR(K)=Z(4,K)
      BJ(K)=Z(3,K)
      IF(INVFT.EQ.1) BJ(K)=-BJ(K)
      AIM1=AIMAG(AMPZ)+1.E-10
      REL1=REAL(AMPZ)
      Y1(K)=ATAN2(AIM1,REL1)*180./PI
```

```
      AIM2=AIMAG(AMPTZ)+1.E-10
      REL2=REAL(AMPTZ)
      DZ(K)=ATAN2(AIM2,REL2)*180./ PI
      AX(K)=SIC
      XC(K)=20.*ALOG10(X(1,K))
      IF(IX1.GT.1) Y(1,K)= .00001
      YC(K)=20.*(ALOG10(Y(1,K)))
      ZC(K)=20.*(ALOG10(Z(1,K)))
      V(K)=FLOAT(K-1)
      KKX=KX/2 +1
      IF(K.GT.KKX) V(K)=FLOAT(K-1) - FLOAT(KX)
      WRITE(6,33)J,THP*P ,         Z(2,K),Z(1,K),Z(3,K),Z(4,K),Y(2,K),
     1Y(1,K),Y(3,K),Y(4,K),X(2,K)     ,X(1,K),X(3,K),X(4,K)
   33 FORMAT(1X,I4,   F6.1,3(2X,F6.1,1X,F8.4,1X,F9.4,1X,F9.4))
      BY(K)= X(1,K)
      BZ(K)= Z(1,K)
      CZ(K)= Z(2,K)
      IF(BY(K).GT.0.3) BY(K)=0.3
      EN1=(Y(1,K)+EN1)
      EN=(Y(1,K)*Y(1,K)+EN)
    9 CONTINUE
      WRITE(6,90)
      WRITE(6,90)
      CLL=FLOAT(LMAX-LMIN)
      IF(CLL.LE.1.0)CLL=1.
      EN1=EN1/CLL
      EN=EN/CLL
      WRITE (6,1230) II3
 1230 FORMAT(3X,"MISSING ELEMENTS=",I3,"  MISS. ELEMENTS NUMBERS ARE"//)
      WRITE(6,1240) (MS(K),K=1,40)
      WRITE(6,1240)(MS(K),K=41,80)
      WRITE(6,1240)(MS(K),K=81,100)
 1240 FORMAT(3X,40I3//)
      WRITE(6,1200)
 1200 FORMAT(1H///3X,"I0    I1    MIS.ELS     ABS        ENERGY"///)
      WRITE(6,1220) I0,I1, II3    ,EN1,EN
 1220 FORMAT(2X,3(I3,3X),2(F10.5,2X))
      SQN=NV
      SQN=SQRT(SQN)
      CALL C06ADF( ARXY,AIXY,N,NV,KS,IW,NIW,W1,NW1,W2,NW2,IFAIL  )
      IF(IFAIL.NE.0)GOTO 210
      DO 3100 L=1,N
      AXY(L)=SQRT(ARXY(L)*ARXY(L)+AIXY(L)*AIXY( L))/SQN
      IF(ABS(ARXY(L)).LE.DEL)ARXY(L)=DEL
      IF(INVFT.EQ.1) AIXY(L)=-AIXY(L)
      SXY(L)= ATAN2(AIXY(L) , ARXY(L))*180./PI
 3100 CONTINUE
      CALL C06ADF(SVS,SVA, N,NV,KS, IW,NIW,W1,NW1,W2,NW2,IFAIL )
      DO 3120 L=1,N
      SVS(L)=SVS(L)/SQN
      IF( ABS(SVS(L)).LE.DEL) SVS(L)=DEL
      SVA(L)=SVA(L)/SQN
      IF(INVFT.EQ. 1) SVA(L)=-SVA(L)
      AFT(L)=SQRT(SVS(L)*SVS(L)+SVA(L)*SVA(L))
 3120 CONTINUE
      CALL C06ADF(AR, BJ , N, NV,KS, IW, NIW,W1,NW1,W2,NW2,IFAIL )
      DO 3110   L=1,N
```

```
      IF(ABS(AR(L)).LE.DEL) AR(L)=DEL
      ARL=AR(L)/SQN
      BJL=BJ(L)/SQN
      AR(L)=SQRT(ARL*ARL+BJL*BJL)
      IF(INVFT.EQ.1) BJL=-BJL
      BJ(L)=ATAN2(BJL,ARL)*180./PI
 3110 CONTINUE
      WRITE(6,992) (IW(I),I=1,5)
  992 FORMAT(1H///3X, 18HOPTIMUM VALUES ARE/2X,3HKF=, I7/2X,
     *5HKMAX=,I5/2X,4HNIW=, I6/2X, 4HNW1=, I6/2X, 4HNW2=, I6///)
      GOTO 800
  210 WRITE(6,991) IFAIL
  991 FORMAT (1H ,24HFAILURE IN C06ADF,IFAIL=, I4)
      WRITE(6,992) (IW(I),I=1,5)
  800 CONTINUE
      WRITE(6,90)
      WRITE(6,90)
      WRITE(6,880)
  880 FORMAT(9X,"SIN   REL FX    IMG  FX     ABS  FX       PHASE FX" ,"
     *       FTRY       FTJY      AFTY       AFXZ     PH.Z"//)
      DO 21 MM=1,KX
      LD=MM
      MN=MM-1
      WRITE (6,850) MN, AX(LD), ARXY(MM),AIXY(MM), AXY(MM),SXY(MM)
     * , SVS(MM),SVA(MM),  AFT(MM), AR(MM), BJ(MM)
  850 FORMAT(1X,I4,1X, F6.3 , 3(3X,F8.4),5X,F6.1, 4(3X,F8.4),5X,F6.1    )
   21 CONTINUE

   90 FORMAT(1X//)

C  LINE PRINTER GRAPHICS OUTPUT
      KK=KX
      K=KX
      KKZ=2*KK
      KKK=3*KK
      KZ=0
      DO 777 LXY=1,KKK
      KZ=KZ+1
      K2Z=KZ
      IF(KZ.GT.KK)K2Z=KZ-KK
      IF(KZ.GT.2*KK)K2Z=KZ-2*KK
      AX(KZ)=AX(K2Z)
      V(KZ)=V(K2Z)
      IF(KZ.LE.KK)XYZ(KZ)=XC(K2Z)
      IF(KZ.LE.2*KK.AND.KZ.GT.KK)XYZ(KZ)=YC(K2Z)
      IF(KZ.LE.3*KK.AND.KZ.GT.2*KK)XYZ(KZ)=ZC(K2Z)
      IF(KZ.LE.2*KK.AND.KZ.GT.KK) CZ(KZ)=Y1(K2Z)
      IF(KZ.LE.3*KK.AND.KZ.GT.2*KK) CZ(KZ)=DZ(K2Z)
      IF(KZ.LE.2*KK.AND.KZ.GT.KK) AXY(KZ)= AFT(K2Z)
      IF(KZ.LE.3*KK.AND.KZ.GT.2*KK)AXY(KZ)=AR(K2Z)
      IF(KZ.LE.3*KK.AND.KZ.GT.2*KK)AXY(KZ)=ABS(AR(K2Z)-AR(N/2))
      IF(KZ.LE.2*KK.AND.KZ.GT.KK) SXY(KZ)=ATAN2( SVA(K2Z),SVS(K2Z))*P
      IF(KZ.LE.3*KK.AND.KZ.GT.2*KK)SXY(KZ)=BJ(K2Z)
      IF(XYZ(KZ).LE.-70.) XYZ(KZ)=-70.
  777 CONTINUE
      LKK=LX*2
      MZ=0
```

```
      DO 779 LZZ=1,LKK
      MZ=MZ+1
      M2Z=MZ
      IF(MZ.GT.LX)M2Z=MZ-LX
      IF(MZ.GT.2*LX)M2Z=MZ-2*LX
      AXZ(MZ)=AXZ(M2Z)
      IF(MZ.LE.LX)AATZ(MZ)=AATZ(M2Z)
      IF(MZ.LE.2*LX.AND.MZ.GT.LX)AATZ(MZ)=AAZ(M2Z)*15.
  779 CONTINUE
   50 FORMAT(1H1)
      CALL GRAFIT(AXZ,AATZ,LKK,LX,LX,-70)
C - X=APERTURE LINEAR SCALE. "*"- PHASE(Z),"X"- =15.*AMP(Z),NEAR FIELD.
      WRITE(6,171)
  171 FORMAT(10X,"X=APERTURE AXIS. Y= *- PHASE Z , X- 15.*AMP(Z),NR.FL")

      CALL GRAFIT(AX, XYZ, KKK, KK, KK, -70)
C- X=SINE ANG. "*"-DB FULL ARRAY,,"X"-DB DEFECT. ARRAY, "0"-DB MISS. EL.
      WRITE(6,173)
  173 FORMAT(2X,"X=SIN ANG. Y=FAR FLD. DB , *- FULL ARRAY, X-DEF. 0-MS")
      CALL GRAFIC(AX,CZ,KK)
      WRITE(6,45)
   45 FORMAT(2X,"X=SIN ANG.Y=*-PHASE SB.A.,X-PH. MS EL(CTR),0-PH.ST.C")
      WRITE(6,3000) LMIN,LMAX,MMIN,MMAX, KX,I0,I1,IRESET,PRO,RPP
      CALL GRAFIT( V, AXY,KKK,KK,KK,-70)
      WRITE(6,4120)
 4120 FORMAT( 10X,"X=APERTUR,Y=*-MAG FFT X,X-FFT Y , 0-FFT Z ")
      WRITE(6,3003) LMIN,LMAX,MMIN,MMAX, KX,I0,I1,IRESET,PRO,RPP,
     * INEAR,IAMPL
      CALL GRAFIT( V, SXY,KKK,KK,KK,-70)
      WRITE(6,450)
  450 FORMAT(10X,"X=APERTURE,Y=*-FFT X PHASE, X- FFT PHASE Y, 0-FT P Z")
 3000 FORMAT(3X,6H LMIN=,I4,6H LMAX=,I4,6H MMIN=,I4,6H MMAX=,I4,
     1 12H NO SAMPLES=,I4,11H MISS ELEM= ,I3,1X,I3,8H IRESET= ,I1 ,
     27H PHASE=,F2.0 ,4H*PI/,F5.1                                    )
 3003 FORMAT(3X,6H LMIN=,I4,6H LMAX=,I4,6H MMIN=,I4,6H MMAX=,I4,
     1 12H NO SAMPLES=,I4,11H MISS ELEM= ,I3,1X,I3,8H IRESET= ,I1 ,
     27H PHASE=,F2.0 ,4H*PI/,F5.1, 7H INEAR=,I1,7H IAMPL=,I1        )
 1000 STOP
      END
```

```
      SUBROUTINE EJIX(XAM,XPH,N1,N2,S1,S2,PD ,STHO,I0,I1  ,AMX ,IT,M   )
C
C  SIMULATION OF NEAR FIELD
C
C      M=0 FOR SYMETRICAL COUPLING
C   M=1 FOR ASYMETRICAL COUPLING
C    M=10 FOR NO INTERNAL COUPLING
      DIMENSION XAM(100), XPH(100)
      COMPLEX EJI , EJ , EJ1
      PI=4.*ATAN(1.)
      P=180./PI
      DEL=.0000001
      AMX=0.0
C  THE FOLLOWING 4 STATEMENTS ARE INTENDED  INTERNAL COUPLING IN W/G
      GL=5.26/9.233
      G1=FLOAT(I1)
      XX1=(G1-FLOAT(N1+1)*.5)*S1
      AA1=1./6.+6./7.*(COS(XX1/(FLOAT(N1+1)*.5)*PI*.5))**2.
      XX2=-2.*PI*XX1  *STHO
      DO 3 J=1,N2
      EJ=0.0
      JE=J
      XJ2=  (FLOAT(JE) - FLOAT(N2+1)*.5 )*S2
      DO 5 I=1,N1
      XI1=(FLOAT(I)-FLOAT(N1+1)*.5)*S1
      AI1= 1./7. + 6./7.*(COS(XI1/(FLOAT(N1+1)*.5)*PI*.5))**2.
      RIJ=SQRT((XI1-XJ2)**2.+PD **2.)
      IF(I.EQ.I0.OR.I.EQ.I1) AI1=0.0
      AIJ= -2.*PI*(   XI1*STHO   +RIJ)
C  THE FOLLOWING 7 STATEMENTS ARE INTENDED  INTERNAL COUPLING IN W/G
      B=SQRT(2.)/2.
      IF(M.EQ.1.AND.I.LT.I1)B=-SQRT(2.)/2.
      IF(M.EQ.2)B=0.
      IF(M.EQ.2.AND.I.GT.I1)B=1.
      XI3=(G1-FLOAT(I))*S1*2.*PI*GL
      XI2=-ABS(XI3)  +XX2
      EJ1=B*AA1*CEXP(CMPLX(0.,XI2))
      IF(M.EQ.10)EJ1=0.0
      EJI=AI1*(1.+EJ1)/RIJ*CEXP(CMPLX(0.,AIJ))
      TETA=ATAN2((XJ2-XI1),PD)
      IF(IT.EQ.1) EJI=EJI*COS(TETA)
      IF(IT.EQ.2) EJI=EJI*(COS(TETA))**2.
      EJ=EJI+EJ
    5 CONTINUE
      XAM(J)= CABS(EJ) *10.
      XRM= REAL(EJ)
      XIM= AIMAG(EJ)
      IF( ABS(XRM).LE.DEL)XRM=DEL
      XPH(J)= ATAN2(XIM,XRM)
      AMX=AMX+XAM( J)
    3 CONTINUE
      RETURN
      END
END OF FILE
```

```
      SUBROUTINE SHIFT01( XDB, XAM,XPH,YDB,YAM,YPH , A1, IAM,IPH,NN,NN2)
     DIMENSION XDB(100),XAM(100),XPH(100),YDB(100),YAM(100),YPH(100),
    *DB(100),PH(100)
     IF(IAM.EQ.0.AND.IPH.EQ.0)GOTO 10
     PI=4.*ATAN(1.)
     DEL= .01
     IX=0
     IF(A1.LE.-DEL)IX=-1
     DO 2 K=1,NN
     DB(K)=YDB(K)
     IF(IX.EQ.-1)DB(K)=XDB(K)
     PH(K)=YPH(K)
     IF(IX.EQ.-1)PH(K)= XPH(K)
   2 CONTINUE
     H1=ABS(A1)
     IH1=INT(H1)
     H1=H1 - ABS(FLOAT(IH1))
     G1= 1.0 -H1
     JX=INT(ABS(A1))
     L=0
     DO 3 I=1,NN
     L=L+1
     IF(I.GT.(NN-JX-1)) GOTO 9
     IF(IAM.EQ.0) GOTO 11
     YD=G1*DB(I+JX) +H1*DB(I+JX+1)
  11 IF(IPH.EQ.0) GOTO 13
     YPP=PH(I+JX+1) - PH(I+JX)
     IPM=0
     IF(ABS(YPP).GT.PI)IPM=1
     B=1.
     IF(YPP.LT.0.0) B=-1.
     PM=PH(I+JX)+B*2.* PI
     YP=G1*PH(I+JX)+H1*PH(I+JX+1)
     IF(IPM.EQ.1) YP=G1*PM +H1*PH(I+JX+1)
     IF(ABS(YP).GT.PI.AND.YP.GT.0.0) YP=YP-2.*PI
     IF(ABS(YP).GT.PI.AND.YP.LT.0.0) YP=2.*PI+YP
  13 CONTINUE
     IF(IAM.EQ.0) YD=DB(I)
     IF(IPH.EQ.0) YP=PH(I)
     DBY= YD/20.
     AMY=FLOAT(NN2)*10.0**DBY
     IF(IX.EQ.0) YDB(I) =YD
     IF(IX.EQ.0) YAM(I)=AMY
     IF(IX.EQ.0) YPH(I)=YP
     IF(IX.EQ.-1)XDB(I)=YD
     IF(IX.EQ. -1) XAM(I)=AMY
     IF(IX.EQ.-1)XPH(I)= YP
   3 CONTINUE
   9 CONTINUE
     NN2=L-1
  10 CONTINUE
     RETURN
     END
END OF FILE
```

```
C-     THIS PROGRAM CHANGES MEASURED VALUES IN CM OF X-Y PLOT TO
C     DB AND PHASE(DEG) ACCORDING TO CALIBRATION CHART ASSUMED
C      TO BE LINEAR IN DB AND PHASE
       PROGRAM DBPMES1(INPUT=131B,OUTPUT=131B,FIGX,FIGY,
      * TAPE5=INPUT,TAPE6=OUTPUT,TAPE7=FIGX,TAPE8=FIGY)
       DIMENSION XDCM(100),XPCM(100),YDCM(100),YPCM(100)
       DIMENSION XDB(100),XPH(100),YDB(100),YPH(100)
       INORDER=1
       READ(5, )DELX,DELYDB,DELYPH
C     DELX IS THE ABSISA SHIFT OF THE GRAPH IN CM TO THE REF.
C     DELYDB IS THE ORDINATE SHIFT OF DB IN CM TO THE REF.
C     DELYPH IS THE ORDINATE SHIFT OF PH IN CM TO THE REF.
       DEL=0.000001

       PI=ATAN(1.)*4.
       DB0=10.25
       PH0=8.15
       CONSTDB=-10.25*40./9.3
       CONSTPH=8.15*360./15.7
       APH=-360./15.7
       ADB=40./9.3
       I=0
       DO 10 M=1,100
       READ(7, )XDCM(M),XPCM(M)
       I=I+1
       IF(XPCM(M).GT.0.0)GOTO 120
       READ(7, )IXSTOP,IZOK
       GOTO 122
  120  CONTINUE
   10  CONTINUE
  122  CONTINUE
       IL=I-1
       LX=I
       CALL SHIFT1(XDCM,XPCM,  0.0,  0.0,  0.0,  LX        )
       DO 1000 I=1,IL
       XDB(I)=XDCM(I)*ADB+CONSTDB
       XPH(I)=XPCM(I)*APH+CONSTPH
       GOTO 15
       WRITE(6,12)XDB(I),XPH(I),ZOK,I
   12  FORMAT(5X, "XDB=",F7.2,"  XPH=",F7.2,"  ZOK=",F7.2,4X,I4)
   15  CONTINUE
 1000  CONTINUE
       XDB(IL+1)=XPH(IL+1)=DEL
       ZOK=FLOAT(IABS(IZOK))
       K=0
       DO 20 M=1,100
       READ(8, )YDCM(M),YPCM(M)
       K=K+1
       IF(YPCM(M).GT.0.0)GOTO 130
       READ(8, )IYSTOP
       GOTO 133
  130  CONTINUE
   20  CONTINUE
  133  CONTINUE
       CALL SHIFT1(YDCM,YPCM,DELX,DELYDB,DELYPH,LX       )
       DO 2000 K=1,IL
       YDB(K) =YDCM(K)*ADB +CONSTDB
       YPH(K)=YPCM(K)*APH +CONSTPH
```

```
2000 CONTINUE
     YDB(IL+1)=YPH(IL+1)=DEL
     IIXSTOP=0
     IIZOK=0
     IIYSTOP=0
     IF(INORDER.EQ.1)GOTO 45
     DO 22 I=1,IL
     K=IL+1-I
     XDCM(K)=XDB(I)
     XPCM(K)=XPH(I)
     YDCM(K)=YDB(I)
     YPCM(K)=YPH(I)
  22 CONTINUE
     DO 55 I=1,IL+1
     IF(I.EQ.IL+1)IIXSTOP=IXSTOP
     IF(I.EQ.IL+1)IIZOK=IZOK
     XDCM(IL+1)=XPCM(IL+1)=YDCM(IL+1)=YPCM(IL+1)=DEL
     WRITE(6,80)XDCM(I),XPCM(I),IIXSTOP,IIZOK
  55 CONTINUE
     DO 65 I=1,IL+1
     IF(I.EQ.IL+1)IIYSTOP=IYSTOP
     WRITE(6,80)YDCM(I),YPCM(I),IIYSTOP
  65 CONTINUE
     GOTO 75
  45 CONTINUE
     DO 40 I=1,IL+1
     IF(I.EQ.IL+1)IIXSTOP=IXSTOP
     IF(I.EQ.IL+1)IIZOK=  IZOK
     WRITE(6,80)XDB(I),XPH(I),IIXSTOP,IIZOK
  40 CONTINUE
  80 FORMAT(1X,F9.2,F10.2,I4,I6)
     DO 60 I=1,IL+1
     IF(I.EQ.IL+1)IIYSTOP=IYSTOP
     WRITE(6,80)YDB(I),YPH(I),IIYSTOP
  60 CONTINUE
  75 CONTINUE
     STOP
     END
```

```
      SUBROUTINE SHIFT1(XDCM,XPCM,DELX,DELYDB,DELYPH,LX      )
      DIMENSION XDCM(100),XPCM(100)
      DEL=0.000001
      PI=4.*ATAN(1.)
      IF(ABS(DELX).LE.DEL)GO TO 100
      K=0
      DO 10 I=1,LX-1
      K=K+1
      DCM=XDCM(I)
      DDCM=XDCM(I+1)
      A=DDCM-DCM
      PCM=XPCM(I)
      DPCM=XPCM(I+1)
      P=DPCM-PCM
      IF(ABS(P).GE.7.)P=0.0
      XDCM(I)=DCM+A*DELX
      XPCM(I)=PCM+P*DELX
   10 CONTINUE
  100 CONTINUE
      IF(ABS(DELYDB).LE.DEL)GOTO 200
      DO 20 I=1,LX
      DCM=XDCM(I)
      XDCM(I)=DCM+DELYDB
   20 CONTINUE
  200 CONTINUE
      IF(ABS(DELYPH).LE.DEL)GOTO 300
      DO 30 I=1,LX
      PCM=XPCM(I)
      XPCM(I)=PCM+DELYPH
   30 CONTINUE
  300 CONTINUE
      RETURN
      END
END OF FILE
```

```
C-      MONITORING IN THE NEAR FIELD WITH A FOCUSED ANTENNA, COS ILLUMIN
        PROGRAM JACK37(INPUT=131B,OUTPUT=131B,TAPE5=INPUT
       *,TAPE61,TAPE66,TAPE6=OUTPUT)
        COMMON X(500),Y(500),Z1(500),Z2(500),Z3(500),Z4(500),Z5(500)
        DIMENSION IBCD(3),NUM(4),XN(10)
        COMPLEX F00,AJ,V1,VV,V20,VA,VP,VM
        DATA(IBCD(M),M=1,3)/10H A  B R  W,10H LMIN LMAX,10H  KC NG DX/
        PI=4.*ATAN(1.)
        DEL=0.0001
        AJ=0.5*CMPLX(1., 1.)
        WRITE(6,50)
        IIS=IPH=0
   50 FORMAT(10X,"VALUES,A,B,R,W,LMIN,LMAX,KC,IMAX")
        READ(5,*)A,B,R,W,LMIN,LMAX,KC,IMAX
        WRITE(6,70)IIS,IPH
   70 FORMAT(5X,"   IIS(CORRECTION)=",I2,"   IPH=",I2)
        READ(5,*)IIS,IPH
        WRITE(6,60)A,B,R,W,LMIN,LMAX,KC,IMAX
        WRITE(6,70)IIS,IPH
   60 FORMAT(5X,4(F10.5,2X),4(I5,2X))
        IF((LMAX-LMIN).GT.150)LMAX=LMIN+150
        KK=LMAX-LMIN+1
        R=R*A
        A=A*W
        B=B*A
        R=R*W
        P=SQRT(2./(R*W))
        K=0
        BK=FLOAT(IMAX-1)
        IF(ABS(BK).LE.DEL)BK=1.
        DX=B/BK
        CC=1./(FLOAT(IMAX))
        WRITE(6,150)
  150  FORMAT(10X,"K  S  V2  DF  V6  V7  AT  "//)
        DO 5 L=LMIN,LMAX
        K=K+1
        S=FLOAT(L)/FLOAT(KC)
        V1=0.0
        VA=0.0
        DO 7 I=1,IMAX
        XX=(FLOAT(I)-FLOAT(IMAX+1)*0.5)*DX
        U1=(+(S*R-XX)+A/2.)*P
        U2=(-(S*R-XX)+A/2.)*P
        U3=P*A/2.-1./P*(2.*(S-XX/R)/W+1./A)
        U4=P*A/2.+1./P*(2.*(S-XX/R)/W+1./A)
        U5=P*A/2.-1./P*(2.*(S-XX/R)/W-1./A)
        U6=P*A/2.+1./P*(2.*(S-XX/R)/W-1./A)
        FM=PI*( R*S/A-XX/A-2.*S*XX/W)
        FP=PI*(-R*S/A+XX/A-2.*S*XX/W)
        X1=S20ADF(U1,1)
        Y1=S20ACF(U1,1)
        X2=S20ADF(U2,1)
        Y2=S20ACF(U2,1)
        X3=S20ADF(U3,1)
        Y3=S20ACF(U3,1)
        X4=S20ADF(U4,1)
        Y4=S20ACF(U4,1)
        X5=S20ADF(U5,1)
        Y5=S20ACF(U5,1)
        X6=S20ADF(U6,1)
```

```
      Y6=S20ACF(U6,1)
      VV=CMPLX(X1,-Y1)+CMPLX(X2,-Y2)
      VP=(CMPLX(X3,-Y3)+CMPLX(X4,-Y4))*CEXP(CMPLX(0.,FP))
      VM=(CMPLX(X5,-Y5)+CMPLX(X6,-Y6))*CEXP(CMPLX(0.,FM))
      F=-2.*PI/W*XX*S
      FF=PI*XX/A
      CSNR=COS(FF)
      SSNR=SIN(FF)
      XDR=-PI*XX*XX/(W*R)
      SRA=PI*S*R/A
      CSSR=COS(SRA)
      IF(ABS(CSSR).LE.DEL)CSSR=DEL
      SSSR=SIN(SRA)
      CISR=1./CSSR
      TGSR=SSSR*CISR
      SIGN=1.0
      IF(IIS.LT.0)SIGN=-1.0
      CF=1.0
      IF(IABS(IIS).EQ.1)CF=CISR
        IF(IABS(IIS).EQ.2)CF=CISR*(1.0+SIGN*TGSR*SSNR)
      IF(IABS(IIS).EQ.3)CF=CISR*(SIGN*TGSR*SSNR)
      VA=VA+(VP+VM)*CF
      V1=V1+CSNR*VV*CEXP(CMPLX(0.,F))
    7 CONTINUE
      V1=VA
      V8=CABS(VA)
      V2=CABS(V1)*CC
      REL1=REAL(V1)
      AIM1=AIMAG(V1)
      IF(ABS(REL1).LE.DEL)REL1=DEL
      AT=ATAN2(REL1,AIM1)*180./PI
      V3=AT
      VF1=V2
      IF(VF1.LE.DEL)VF1=DEL
      DF=20.*ALOG10(VF1)
      TETA=PI*A*S/W
      TET1=TETA+PI/2.
      TET2=TETA-PI/2.
      IF(ABS(TET1).LE.DEL)TET1=DEL
      IF(ABS(TET2).LE.DEL)TET2=DEL
      ASN1=SIN(TET1)
      ASN2=SIN(TET2)
      ACSN=ASN1/TET1+ASN2/TET2
      ASN=SIN(TETA)
      IF(ABS(TETA).LE.DEL)TETA=DEL
      IF(ABS(TETA).LE.DEL)ASN=DEL
      ASNX=ASN/TETA
      V6=ABS(ASNX)
      V6=ABS(ACSN)
      V66=V6
      IF(V66.LE.DEL)V66=DEL
      V7=20.*ALOG10(V66)
      WRITE(6,200)K,S,V2,DF,V6,V7,AT
  200 FORMAT(1X,I4,6(F10.5))
      FD1=DF+10.
      DF=FD1
      IF(DF.LE.-40.)DF=-40.
      IF(DF.GE.30.)DF=30.
      IF(V7.LE.-40.)V7=-40.
```

```
      X(K)=S
      X(K+KK)=S
      Z2(K)=V2
      Z3(K)=V3
      Z5(K)=DF
      Y(K)=V6
      Z1(K)=V7
      IF(IPH.EQ.1)Z1(K)=AT/10.
      Z5(K+KK)=Z1(K)
      NUM(1)=NUM(2)=NUM(3)=KK
    5  CONTINUE
      KK=LMAX-LMIN+1
      XN(1)=A
      XN(2)=0.0
      XN(3)=R
      XN(4)=W
      XN(5)=FLOAT(LMIN)
      XN(6)=FLOAT(LMAX)
      XN(7)=FLOAT(KC)
      XN(8)=0.0
      XN(9)=DX
      NDEC=0
      CC=0.75
      YY=2.0
      DO 3  I=1,9
      XX1=CC*FLOAT(I)
    3 CONTINUE
      CALL GRAFIT(X,Z5,2*KK,KK,KK,-70)
      WRITE(6,100)
  100 FORMAT(10X,"X=SIN ANGL, Y=DB.*NR FLD+10.DB,X=FAR FLD")
      WRITE(6,50)
      WRITE(6,60)A,B,R,W,LMIN,LMAX,KC,IMAX
      WRITE(6,70)IIS,IPH
      STOP
      END
END OF FILE
```

```
C-      MONITORING IN THE NEAR FIELD WITH A FOCUSED ANTENNA, COS.SQ.+PED
        PROGRAM JACK38(INPUT=131B,OUTPUT=131B,TAPE5=INPUT
       *,TAPE61,TAPE66,TAPE6=OUTPUT)
        COMMON X(500),Y(500),Z1(500),Z2(500),Z3(500),Z4(500),Z5(500)
        DIMENSION IBCD(3),NUM(4),XN(10)
        COMPLEX F00,AJ,V1,VV,V20,VA,VP,VM
        DATA(IBCD(M),M=1,3)/10H A  B R  W,10H LMIN LMAX,10H  KC NG DX/
        PI=4.*ATAN(1.)
        DEL=0.0001
        AJ=0.5*CMPLX(1., 1.)
        WRITE(6,50)
        IIS=IPH=0
        CF1=0.5714
        CF2=0.4285
   50 FORMAT(10X,"VALUES,A,B,R,W,LMIN,LMAX,KC,IMAX")
        READ(5,*)A,B,R,W,LMIN,LMAX,KC,IMAX
        WRITE(6,70)CF1,CF2,IPH
   70 FORMAT(5X,"  CF1(0.5714)=",F6.3,"  CF2(0.4285)=",F6.3,"  IPH=",I2)
        READ(5,*)CF1,CF2,IPH
        WRITE(6,60)A,B,R,W,LMIN,LMAX,KC,IMAX
        WRITE(6,70)CF1,CF2,IPH
   60 FORMAT(5X,4(F10.5,2X),4(I5,2X))
        IF((LMAX-LMIN).GT.150)LMAX=LMIN+150
        KK=LMAX-LMIN+1
        R=R*A
        A=A*W
        B=B*A
        R=R*W
        P=SQRT(2./(R*W))
        K=0
        BK=FLOAT(IMAX-1)
        IF(ABS(BK).LE.DEL)BK=1.
        DX=B/BK
        CC=1./(FLOAT(IMAX))
        WRITE(6,150)
  150  FORMAT(10X,"K  S  V2  DF  V6  V7  AT  "//)
        DO 5 L=LMIN,LMAX
        K=K+1
        S=FLOAT(L)/FLOAT(KC)
        V1=0.0
        VA=0.0
        DO 7 I=1,IMAX
        XX=(FLOAT(I)-FLOAT(IMAX+1)*0.5)*DX
        U1=(+(S*R-XX)+A/2.)*P
        U2=(-(S*R-XX)+A/2.)*P
        U3=P*A/2.-1./P*(2.*(S-XX/R)/W+2./A)
        U4=P*A/2.+1./P*(2.*(S-XX/R)/W+2./A)
        U5=P*A/2.-1./P*(2.*(S-XX/R)/W-2./A)
        U6=P*A/2.+1./P*(2.*(S-XX/R)/W-2./A)
        AA=1./(A*A)
        FM=PI*( 2.*R*S/A-2.*XX/A-2.*S*XX/W+W*R*AA)
        FP=PI*(-2.*R*S/A+2.*XX/A-2.*S*XX/W+W*R*AA)
        X1=S20ADF(U1,1)
        Y1=S20ACF(U1,1)
        X2=S20ADF(U2,1)
        Y2=S20ACF(U2,1)
        X3=S20ADF(U3,1)
        Y3=S20ACF(U3,1)
        X4=S20ADF(U4,1)
        Y4=S20ACF(U4,1)
```

```
      X5=S20ADF(U5,1)
      Y5=S20ACF(U5,1)
      X6=S20ADF(U6,1)
      Y6=S20ACF(U6,1)
      VV=CMPLX(X1,-Y1)+CMPLX(X2,-Y2)
      VP=(CMPLX(X3,-Y3)+CMPLX(X4,-Y4))*CEXP(CMPLX(0.,FP))
      VM=(CMPLX(X5,-Y5)+CMPLX(X6,-Y6))*CEXP(CMPLX(0.,FM))
      F=-2.*PI/W*XX*S
      FF=PI*XX/A
      CSNR=COS(FF)
      SSNR=SIN(FF)
      XDR=-PI*XX*XX/(W*R)
      SRA=PI*S*R/A
      CSSR=COS(SRA)
      IF(ABS(CSSR).LE.DEL)CSSR=DEL
      SSSR=SIN(SRA)
      CISR=1./CSSR
      TGSR=SSSR*CISR
      SIGN=1.0
      IF(IIS.LT.0)SIGN=-1.0
      CF=1.0
      IF(IABS(IIS).EQ.1)CF=CISR
        IF(IABS(IIS).EQ.2)CF=CISR*(1.0+SIGN*TGSR*SSNR)
      IF(IABS(IIS).EQ.3)CF=CISR*(SIGN*TGSR*SSNR)
      VA=VA+CF2*(VP+VM)+CF1*VV*CEXP(CMPLX(0.,F))
      V1=V1+CSNR*VV*CEXP(CMPLX(0.,F))
    7 CONTINUE
      V1=VA
      V8=CABS(VA)
      V2=CABS(V1)*CC
      REL1=REAL(V1)
      AIM1=AIMAG(V1)
      IF(ABS(REL1).LE.DEL)REL1=DEL
      AT=ATAN2(REL1,AIM1)*180./PI
      V3=AT
      VF1=V2
      IF(VF1.LE.DEL)VF1=DEL
      DF=20.*ALOG10(VF1)
      TETA=PI*A*S/W
      TET1=TETA+PI
      TET2=TETA-PI
      IF(ABS(TET1).LE.DEL)TET1=DEL
      IF(ABS(TET2).LE.DEL)TET2=DEL
      ASN1=SIN(TET1)
      ASN2=SIN(TET2)
      ACSN=ASN1/TET1+ASN2/TET2
      ACSN=CF2*ACSN
      ASN=SIN(TETA)
      IF(ABS(TETA).LE.DEL)TETA=DEL
      IF(ABS(TETA).LE.DEL)ASN=DEL
      ASNX=ASN/TETA
      ASNX=CF1*ASNX
      V6=ABS(ASNX)
      V6=ABS(ACSN+ASNX)
      V66=V6
      IF(V66.LE.DEL)V66=DEL
      V7=20.*ALOG10(V66)
      WRITE(6,200)K,S,V2,DF,V6,V7,AT
  200 FORMAT(1X,I4,6(F10.5))
```

```
      FD1=DF+10.
      DF=FD1
      IF(DF.LE.-40.)DF=-40.
      IF(DF.GE.30.)DF=30.
      IF(V7.LE.-40.)V7=-40.
      X(K)=S
      X(K+KK)=S
      Z2(K)=V2
      Z3(K)=V3
      Z5(K)=DF
      Y(K)=V6
      Z1(K)=V7
      IF(IPH.EQ.1)Z1(K)=AT/10.
      Z5(K+KK)=Z1(K)
      NUM(1)=NUM(2)=NUM(3)=KK
    5  CONTINUE
      KK=LMAX-LMIN+1
      XN(1)=A
      XN(2)=0.0
      XN(3)=R
      XN(4)=W
      XN(5)=FLOAT(LMIN)
      XN(6)=FLOAT(LMAX)
      XN(7)=FLOAT(KC)
      XN(8)=0.0
      XN(9)=DX
      NDEC=0
      CC=0.75
      YY=2.0
      DO 3  I=1,9
      XX1=CC*FLOAT(I)
    3 CONTINUE
      CALL GRAFIT(X,Z5,2*KK,KK,KK,-70)
      WRITE(6,100)
  100 FORMAT(10X,"X=SIN ANGL, Y=DB.*NR FLD+10.DB,X=FAR FLD")
      WRITE(6,50)
      WRITE(6,60)A,B,R,W,LMIN,LMAX,KC,IMAX
      WRITE(6,70)CF1,CF2,IPH
      STOP
      END
END OF FILE
```

```
C       MONITORING IN THE NEAR FIELD WITH A FOCUSED ANTENNA, SIN ILLUMIN
        PROGRAM JACK39(INPUT=131B,OUTPUT=131B,TAPE5=INPUT
       *,TAPE61,TAPE66,TAPE6=OUTPUT)
        COMMON X(500),Y(500),Z1(500),Z2(500),Z3(500),Z4(500),Z5(500)
        DIMENSION IBCD(3),NUM(4),XN(10)
        COMPLEX FOO,AJ,V1,VV,V2O,VA,VP,VM
        DATA(IBCD(M),M=1,3)/10H A  B R  W,10H LMIN LMAX,10H  KC NG DX/
        PI=4.*ATAN(1.)
        DEL=0.0001
        AJ=0.5*CMPLX(1., 1.)
        WRITE(6,50)
        IIS=IPH=0
   50 FORMAT(10X,"VALUES,A,B,R,W,LMIN,LMAX,KC,IMAX")
        READ(5,*)A,B,R,W,LMIN,LMAX,KC,IMAX
        WRITE(6,70)IIS,IPH
   70 FORMAT(5X,"   IIS(CORRECTION)=",I2,"   IPH=",I2)
        READ(5,*)IIS,IPH
        WRITE(6,60)A,B,R,W,LMIN,LMAX,KC,IMAX
        WRITE(6,70)IIS,IPH
   60 FORMAT(5X,4(F10.5,2X),4(I5,2X))
        IF((LMAX-LMIN).GT.150)LMAX=LMIN+150
        KK=LMAX-LMIN+1
        R=R*A
        A=A*W
        B=B*A
        R=R*W
        P=SQRT(2./(R*W))
        K=0
        BK=FLOAT(IMAX-1)
        IF(ABS(BK).LE.DEL)BK=1.
        DX=B/BK
        CC=1./(FLOAT(IMAX))
        WRITE(6,150)
  150  FORMAT(10X,"K  S  V2  DF  V6  V7  AT  "//)
        DO 5 L=LMIN,LMAX
        K=K+1
        S=FLOAT(L)/FLOAT(KC)
        V1=0.0
        VA=0.0
        DO 7 I=1,IMAX
        XX=(FLOAT(I)-FLOAT(IMAX+1)*0.5)*DX
        U1=(+(S*R-XX)+A/2.)*P
        U2=(-(S*R-XX)+A/2.)*P
        U3=P*A/2.-1./P*(2.*(S-XX/R)/W+1./A)
        U4=P*A/2.+1./P*(2.*(S-XX/R)/W+1./A)
        U5=P*A/2.-1./P*(2.*(S-XX/R)/W-1./A)
        U6=P*A/2.+1./P*(2.*(S-XX/R)/W-1./A)
        FM=PI*( R*S/A-XX/A-2.*S*XX/W)
        FP=PI*(-R*S/A+XX/A-2.*S*XX/W)
        X1=S20ADF(U1,1)
        Y1=S20ACF(U1,1)
        X2=S20ADF(U2,1)
        Y2=S20ACF(U2,1)
        X3=S20ADF(U3,1)
        Y3=S20ACF(U3,1)
        X4=S20ADF(U4,1)
        Y4=S20ACF(U4,1)
        X5=S20ADF(U5,1)
```

```
      Y5=S20ACF(U5,1)
      X6=S20ADF(U6,1)
      Y6=S20ACF(U6,1)
      VV=CMPLX(X1,-Y1)+CMPLX(X2,-Y2)
      VP=(CMPLX(X3,-Y3)+CMPLX(X4,-Y4))*CEXP(CMPLX(0.,FP))
      VM=(CMPLX(X5,-Y5)+CMPLX(X6,-Y6))*CEXP(CMPLX(0.,FM))
      F=-2.*PI/W*XX*S
      FF=PI*XX/A
      CSNR=COS(FF)
      SSNR=SIN(FF)
      XDR=-PI*XX*XX/(W*R)
      SRA=PI*S*R/A
      CSSR=COS(SRA)
      IF(ABS(CSSR).LE.DEL)CSSR=DEL
      SSSR=SIN(SRA)
      CISR=1./CSSR
      TGSR=SSSR*CISR
      SIGN=1.0
      IF(IIS.LT.0)SIGN=-1.0
      CF=1.0
      IF(IABS(IIS).EQ.1)CF=CISR
        IF(IABS(IIS).EQ.2)CF=CISR*(1.0+SIGN*TGSR*SSNR)
      IF(IABS(IIS).EQ.3)CF=CISR*(SIGN*TGSR*SSNR)
      VA=VA+(VP-VM)*CF
      V1=V1+CSNR*VV*CEXP(CMPLX(0.,F))
    7 CONTINUE
      V1=VA
      V8=CABS(VA)
      V2=CABS(V1)*CC
      REL1=REAL(V1)
      AIM1=AIMAG(V1)
      IF(ABS(REL1).LE.DEL)REL1=DEL
      AT=ATAN2(REL1,AIM1)*180./PI
      V3=AT
      VF1=V2
      IF(VF1.LE.DEL)VF1=DEL
      DF=20.*ALOG10(VF1)
      TETA=PI*A*S/W
      TET1=TETA+PI/2.
      TET2=TETA-PI/2.
      IF(ABS(TET1).LE.DEL)TET1=DEL
      IF(ABS(TET2).LE.DEL)TET2=DEL
      ASN1=SIN(TET1)
      ASN2=SIN(TET2)
      ACSN=ASN1/TET1-ASN2/TET2
      ASN=SIN(TETA)
      IF(ABS(TETA).LE.DEL)TETA=DEL
      IF(ABS(TETA).LE.DEL)ASN=DEL
      ASNX=ASN/TETA
      V6=ABS(ASNX)
      V6=ABS(ACSN)
      V66=V6
      IF(V66.LE.DEL)V66=DEL
      V7=20.*ALOG10(V66)
      WRITE(6,200)K,S,V2,DF,V6,V7,AT
  200 FORMAT(1X,I4,6(F10.5))
      FD1=DF+10.
```

```
      DF=FD1
      IF(DF.LE.-40.)DF=-40.
      IF(DF.GE.30.)DF=30.
      IF(V7.LE.-40.)V7=-40.
      X(K)=S
      X(K+KK)=S
      Z2(K)=V2
      Z3(K)=V3
      Z5(K)=DF
      Y(K)=V6
      Z1(K)=V7
      IF(IPH.EQ.1)Z1(K)=AT/10.
      Z5(K+KK)=Z1(K)
      NUM(1)=NUM(2)=NUM(3)=KK
    5  CONTINUE
      KK=LMAX-LMIN+1
      XN(1)=A
      XN(2)=0.0
      XN(3)=R
      XN(4)=W
      XN(5)=FLOAT(LMIN)
      XN(6)=FLOAT(LMAX)
      XN(7)=FLOAT(KC)
      XN(8)=0.0
      XN(9)=DX
      NDEC=0
      CC=0.75
      YY=2.0
      DO 3  I=1,9
      XX1=CC*FLOAT(I)
    3 CONTINUE
      CALL GRAFIT(X,Z5,2*KK,KK,KK,-70)
      WRITE(6,100)
  100 FORMAT(10X,"X=SIN ANGL, Y=DB.*NR FLD+10.DB,X=FAR FLD")
      WRITE(6,50)
      WRITE(6,60)A,B,R,W,LMIN,LMAX,KC,IMAX
      WRITE(6,70)IIS,IPH
      STOP
      END
END OF FILE
```

```
C         NEAR FIELD OF APERTURE ANTENNA UNIFORM ILLUMINATION
      PROGRAM JACK42(INPUT=131B,OUTPUT, TAPE5=INPUT,TAPE6=OUTPUT)
      DIMENSION X(500),Y(500),Z1(500),Z2(500),Z3(500),Z4(500)
      COMPLEX F00,AJ,V1,VV ,V20
      PI=4.*ATAN(1.)
      DEL=0.0000001
      AJ=0.5*CMPLX(1., 1.)
      KC=20
      KC=40
      KC=10
      KC=100
      ALZ=1.
      W=1.
      A=10.*W
      A=50.*W
      ALZ=A*A
      ALZ=A*A/30.
      ALZ=A*A/3.
      ALZ=A*A*10.
      ALZ=A*W
      ALZ=2.*A*W
      ALZ=A*A/2.
      ALZ=A*A*2.
      P=SQRT(2./ALZ)
      K=0
      WRITE(6,3)
    3 FORMAT(2X," NO        X       U1          U2          C(U1) ",
     *"  S(U1)          C(U2)       S(U2)      ABS( W(U))   20LOG(W)  "//)
      DO 5 L=0,100
      K=K+1
      S=FLOAT(L)/FLOAT(KC)*A
      U1=(-S+A/2.)*P
      U1=S
      U2=(-S-A/2.)*P
      X1=S20ADF(U1,1)
      Y1=S20ACF(U1,1)
      V1=CMPLX(X1,-Y1)
      X2=S20ADF(U2,1)
      Y2=S20ACF(U2,1)
      V20=CMPLX(X2,-Y2)
      VV=AJ*(V1-V20)
      V2=CABS(VV)
      V2=CABS(V1)
      V22=V2
      IF(V22.LE.DEL)V22=DEL
      V3=20.*ALOG10(V22)
      REL=X1
      IF(ABS(REL).LE.DEL)REL=DEL
      V3=ATAN2(REL,-Y1)*180./PI
      X(K)=S
      Y(K)=V2
      Z1(K)=V3
      WRITE(6,8) K,S,U1,U2,X1,-Y1,X2,-Y2,V2,V3
    8 FORMAT(2X,I4,9(2X,F10.5))
      IF(V3.LE.-80.) V3=-80.
    5 CONTINUE
      WRITE(6,30)
   30 FORMAT( 2X///)
```

```
      CALL GRAFIC(X,Y,100)
      WRITE(6,10)
   10 FORMAT(10X,"X=X , Y=AMPLITUDE W(U) . N.B. U=X*SQRT(2./ALZ)   ")
      CALL GRAFIC(X,Z1,100)
      WRITE(6,12)
   12 FORMAT(10X,"X=X , Y=AMPLITUDE W(U)IN DB.  N.B. U=X*SQRT(2./ALZ)")
      STOP
      END
END OF FILE
```

```
C       ANGULAR SPECTRUM OF PYRAMIDAL HORN WITH PI/2 PHASE ERROR .FRESNEL INT
        PROGRAM JACK45(INPUT=131B,OUTPUT, TAPE5=INPUT,TAPE6=OUTPUT)
        DIMENSION X(500),Y(500),Z1(500),Z2(500),Z3(500),Z4(500) ,Z5(500)
        COMPLEX FOO,AJ,V1,VV ,V20  ,V0,V9,VU,VD
        PI=4.*ATAN(1.)
        DEL=0.0000001
        AJ=0.5*CMPLX(1., 1.)
        KC=50
        W=1.
        A=10.*W
        B=A
        EL=0.5*A*A/W
        HL=EL
        ALZ=EL*W
        ZLA=EL/W
        P=SQRT(2./ALZ)
        P1=P*A/2.
        Q=SQRT(2.*ZLA)
        R=1./SQRT(2.*ALZ)
        T=SQRT(ALZ/2.)
        WRITE(6,3)
      3 FORMAT(2X,"  NO  SIN ANG      ABS(INT 1)   AMP UNT 1 DB  ",
       * " ABS(INT 2)   ABS(INT 2) DB  ABS(SINC)   SINC DB" //)
        K=0
        DO 5 L=0,100
        K=K+1
        S=FLOAT(L)/FLOAT(KC)
        U1=(P1-Q*S)
        U2=(P1+Q*S)
        U3=B*R+(2.*S/W-1./B)*T
        U4=B*R-(2.*S/W-1./B)*T
        U5=B*R+(2.*S/W+1./B)*T
        U6=B*R-(2.*S/W+1./B)*T
        FM=PI/4.*ALZ*(2.*S/W-1./B)**2
        FP=PI/4.*ALZ*(2.*S/W+1./B)**2
        X1=S20ADF(U1,1)
        Y1=S20ACF(U1,1)
        X2=S20ADF(U2,1)
        Y2=S20ACF(U2,1)
        X3=S20ADF(U3,1)
        Y3=S20ACF(U3,1)
        X4=S20ADF(U4,1)
        Y4=S20ACF(U4,1)
        X5=S20ADF(U5,1)
        Y5=S20ACF(U5,1)
        X6=S20ADF(U6,1)
        Y6=S20ACF(U6,1)
        V1=CMPLX(X1,-Y1)+CMPLX(X2,-Y2)
        VV=(CMPLX(X3,-Y3)+CMPLX(X4,-Y4))*CEXP(CMPLX(0.,FM))+
       *(CMPLX(X5,-Y5)+CMPLX(X6,-Y6))*CEXP(CMPLX(0.,FP))
        V2=CABS(V1)
        V22=V2
        IF(V22.LE.DEL)V22=DEL
        V3=20.*ALOG10(V22)
        V4=CABS(VV)
        V44=V4
        IF(V44.LE.DEL)V44=DEL
        V5=20.*ALOG10(V44)
```

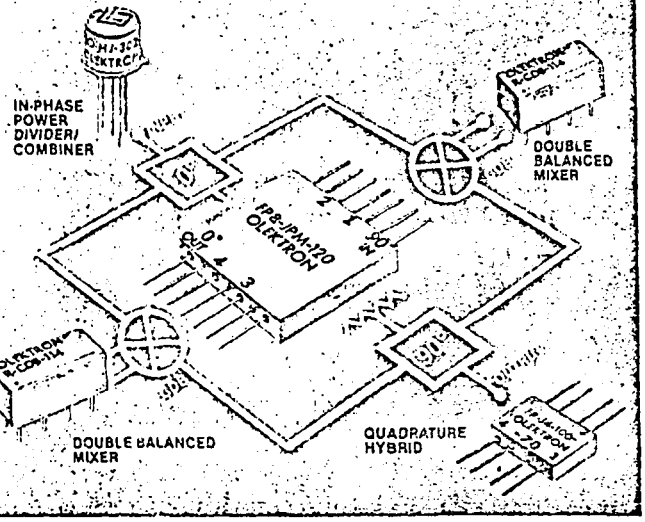
```
      TETA=PI*A*S/W
      ASN=SIN(TETA)
      IF(ABS(TETA).LE.DEL)TETA=DEL
      IF(ABS(TETA) .LE. DEL) ASN=DEL
      ASNX=ASN/TETA
      V6=ABS(ASNX)
      V66=V6
      IF(V66.LE.DEL)V66=DEL
      V7=20.*ALOG10( V66)
      WRITE(6,8) K,S,V2,V3,V4,V5,V6,V7
    8 FORMAT(2X,I4,7(2X,F10.5))
      IF(V3.LE.-60.) V3=-60.
      IF(V5.LE.-60.) V5=-60.
      IF(V7.LE.-60.) V7=-60.
      X(K)=S
      Z2(K)=V2
      Z3(K)=V3
      Z4(K)=V4
      Z5(K)=V5
      Y(K)=V6
      Z1(K)=V7
    5 CONTINUE
      WRITE(6,30)
   30 FORMAT( 2X///)
      CALL GRAFIC(X,Z2,100)
      WRITE(6,10)
   10 FORMAT(10X," X=SIN ANGLE, Y=AMP       UNIFORM+PI/2  ")
      CALL GRAFIC(X,Z3,100)
      WRITE(6,12)
   12 FORMAT(10X," X=SIN ANGLE, Y=AMP  DB   UNIFORM+PI/2  ")
      CALL GRAFIC(X,Z4,100)
      WRITE(6,14)
   14 FORMAT(10X," X=SIN ANGLE, Y=AMP        COSINE+PI/2  ")
      CALL GRAFIC(X,Z5,100)
      WRITE(6,16)
   16 FORMAT(10X," X=SIN ANGLE, Y=AMP    DB  COSINE+PI/2  ")
      CALL GRAFIC(X,Y ,100)
      WRITE(6,18)
   18 FORMAT(10X," X=SIN ANGLE, Y=AMP         SIN(X)/X")
      CALL GRAFIC(X,Z1,100)
      WRITE(6,20)
   20 FORMAT(10X," X=SIN ANGLE, Y=AMP   DB    SIN(X)/X")
      STOP
      END
END OF FILE
```

APPENDIX F

Commercially advertized electronic products

Company	Page
Olektron	298
R.H.G.	302
M.C.L.	314

Improved Performance through Package Integration



OLEKTRON's Series FP8 Modulators, which include the JPM Quadriphase Modulator illustrated, cover the range from 1 to 500 MHz in octave bands. The increased circuit density and package integration have resulted in overall improved performance. Integrated FP8 style packages are available for the following devices.

- ☐ JPM Series Quadriphase Modulator — use TTL or ECL gates directly for modulation drive.
- ☐ PC Series Phase Comparator or Quadriphase Demodulator or Resolver — using same basic circuit.
- ☐ CDBQ Series Quadrature IF Mixer — IF outputs are in phase quadrature.
- ☐ SSB Series Single Sideband Modulator — quadrature modulation signals applied at IF ports can be analog or digital I and Q signals.
- ☐ IRM Series Image Reject Mixer — IF signals are applied into an external quadrature combiner and image responses are suppressed.

Model FP8-JPM Series Modulator measures 0.81 x 0.81 x 0.14 inches. Delivery 6 to 8 weeks from receipt of order.

Whatever your application or degree of complexity, if not in stock, we can supply it in a matter of several weeks.
For additional information write or call today . . .
Tel: (617) 943-7440

OLEKTRON
CORPORATION
61 Sutton Road/Webster, Mass 01570
YOUR CHALLENGE IS OUR PROGRESS

Circle Reader Service No. 5

MSN
MICROWAVE SYSTEMS NEWS
(USPS 461-030)

Microwave Systems News
August 1980, Volume 10 Number 8. Published monthly by EW Communications, Inc., 1170 East Meadow Drive, Palo Alto, CA 94303, U.S.A. Copyright 1980.

Change of Address
Send new and old addresses (including mailing label) with ZIP code numbers to P.O. Box 50249, Palo Alto, CA 94303.

Controlled circulation postage paid at Olive Branch, Mississippi.

Subscriptions
MICROWAVE SYSTEMS NEWS is sent free each month to individuals actively engaged in microwave programs and projects. If your copy does not contain an application form, check Number 300 on the Reader Service card or write to the Circulation Director. Paid subscription rates for non-qualified recipients are: USA & Canada, $25 one year and $45 two years; international (surface), $35 one year and $65 two years; international (air), $45 one year and $85 two years. Single copies and back issues (if available), $5.00 each.

Publisher assumes no responsibility for unsolicited material. Contributors are responsible for the proper release of proprietary and/or classified information

Advertising Sales Offices

Anthony Yaconelli
Associate Publisher

New York State, New England, Northeast, Mid-Atlantic, Southeast and Midwest
Anthony Yaconelli
13 Reynolds Road
Glen Cove, NY 11542
(516) 671-8758

Northern California, Southwest Washington, Oregon, Southern California and Colorado
Joseph R. Hinojosa
1170 East Meadow Drive
Palo Alto, CA 94303
(415) 494-2800

Western Europe
Robert Broerman
L'Avant-Seine
4-8 Rue Robert de Flers
75015 Paris, France
Phone 331-579-0627
331-609-9595 TLX 270560

Far East
Shigeo Kazama
6-2-3, Hirayama, Hino-shi
Tokyo, Japan, T 191
Phone: 0 425-91-2477

VBPA ABP

Sales Administrator
Kimberley S. Hanson

Advertising Coordinator/Recruitment Advertising
Anne Marie St John

Assistant
Sue Murphy
(415) 494-2500
TWX 910-379-6584

Answer Back: EW MSN HQ PLA

Circle Reader Service No. 6 ⟶

Phase Comparators

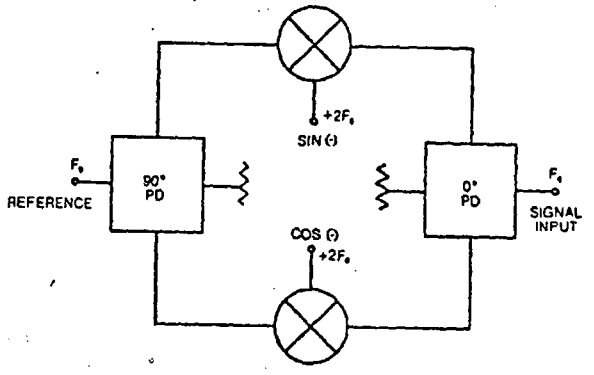
SERIES PC

The PC Series of phase comparators provide two dc outputs proportional to the sine and cosine of the phase difference between a reference and an input RF signal. Standard units are available in Flatpack (prefix FPS) or Pin Header (prefix P) or in connector version (prefix with connector type).

MODEL NO. PREFIX	CONNECTOR TYPE
O-	SMA (3MM)
B-	BNC
T-	TNC
S-	SEALECTRO

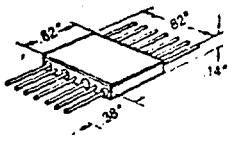
NOTE: The two F_o signals must be properly terminated in order to realize the full capability of the device. Olektron manufactures miniature diplexers for this special purpose.

FUNCTIONAL SCHEMATIC, PHASE COMPARATOR

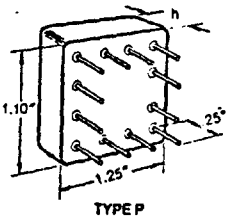


SERIES PC PHASE COMPARATORS

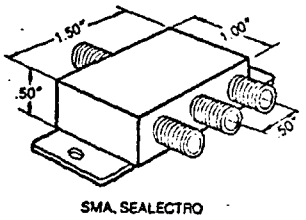
MODEL NO.	FREQUENCY RANGE (MHz)	REF LEVEL (+dBm)	INPUT LEVEL (dBm)	OUTPUT mV P-P (nominal)	PHASE RANGE	PHASE ERROR (max)
PC-15	10-20	10	0	300	0-360°	5°
PC-30	20-40	10	0	300	0-360°	5°
PC-60	40-80	10	0	300	0-360°	5°
PC-120	80-160	10	0	300	0-360°	5°
PC-150	100-200	10	0	300	0-360°	5°
PC-240	160-320	10	0	300	0-360°	5°
PC-300	225-400	10	0	300	0-360°	5°
PC-400	300-500	10	0	300	0-360°	5°
PC-500	400-600	10	0	300	0-360°	5°
PC-800	700-900	10	0	300	0-360°	5°
PC-1000	800-1200	10	0	300	0-360°	5°



TYPE FPS



TYPE P

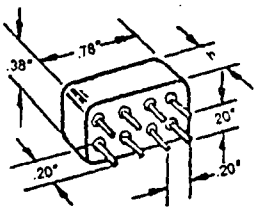


SMA, SEALECTRO

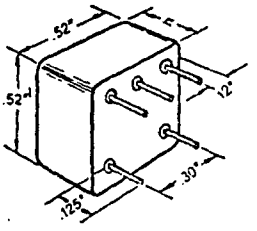
Attenuators and Phase Shifters

OLEKTRON's line of impedance matched attenuators and phase shifters are designed for radar and signal processing applications. Units include both analog and digital control types. Attenuators utilize PIN diodes as the control element and analog phase shifters utilize varactor diodes. For applications where RF impedance match is not required at high attenuation levels the Balanced PIN Diode modulators described on page 10 may be used as current control attenuators. These economical units cover bandwidths in excess of a decade.

The Series ATT-100 impedance matched PIN diode attenuators utilize quadrature matching networks and PIN diode with long minority carrier lifetimes. This series is designed for IF system applications where small size is required. Standard packages include the illustrated P1 Header and Relay Header. Pairs with matched phase and amplitude characteristics can be supplied on request.



TYPE R

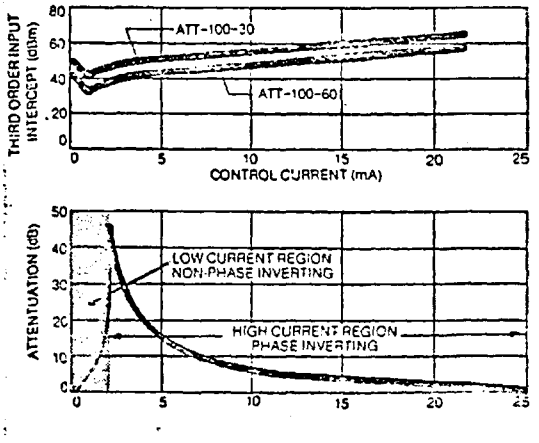


TYPE P1

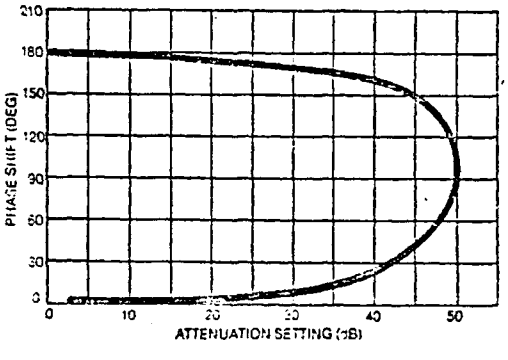
SERIES ATT-100 MATCHED PIN DIODE ATTENUATORS

MODEL NO.	FREQUENCY RANGE (MHz)	INSERTION LOSS (min) (dB)	ATTENUATION RANGE (dB)	IMPEDANCE Zo (ohms)	IMPEDANCE VSWR (max)
P1-ATT-100-60	60 ± 6	1.5	32	50	1.5:1
P1-ATT-110-60	60 ± 6	1.5	32	75	1.5:1
P1-ATT-100-30	30 ± 3	1.5	32	50	1.5:1
P1-ATT-110-30	30 ± 3	1.5	32	75	1.5:1
P1-ATT-100-120	120 ± 10	1.5	32	50	1.5:1
P1-ATT-100-200	200 ± 20	1.5	30	50	1.5:1

CHARACTERISTIC CURVES OF MATCHED PIN DIODE ATTENUATORS



TYPICAL TRANSMISSION PHASE SHIFT



PIN Diode Bridge Attenuators

OLEKTRON's PIN diode bridge attenuators are designed for signal amplitude control applications where extreme flatness of attenuation versus frequency, and low inherent phase shift versus control setting are required. The PIN diode bridge attenuators require a symmetrical source of bias such as standard ±5 volts used in systems with high performance and control voltage source. Bridges are inherently biphasal and a reversal of control voltage polarity results in a reversal of transmitted RF or IF signals.

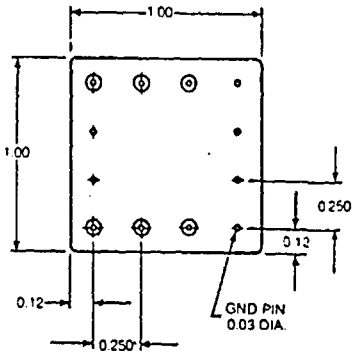
The ATTB Series of attenuators tabulated on page 35 are illustrations of standard units available in standard relay leader, R package, or our FP8 flatpack. We can supply custom units tailored to your requirements including special control and bias voltage and dynamic range requirements.

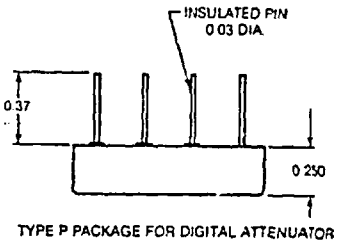
Digital Attenuators

OLEKTRON's digital attenuators are designed primarily for RF/IF signal processing applications requiring rapid discrete level changing under TTL control. Units feature TTL compatible control and balanced PIN diode switches to switch attenuator sections. The leakage of control transients into the attenuator RF output or input is kept below 50 MV peak by the balanced circuits.

The basic DATT Series is offered in the illustrated pin package. Several attenuator steps can be cascaded to form multiple step attenuators. Only a single 5-volt supply is required.

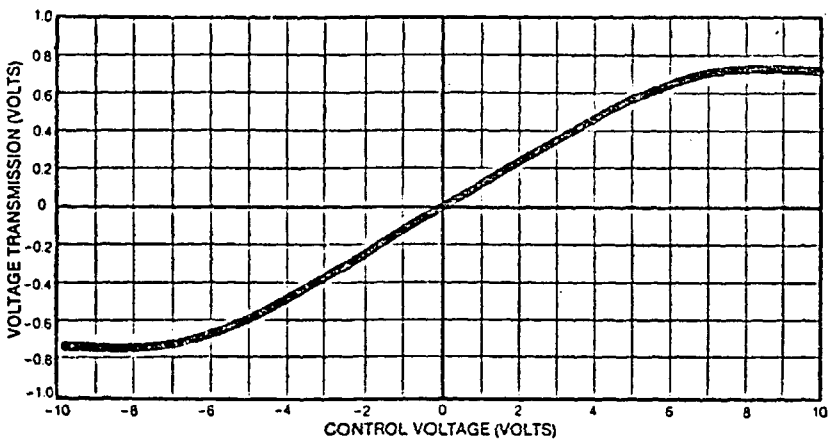
OLEKTRON can supply on request other package configurations with multiple step binary or decimal coded attenuators for your special applications.





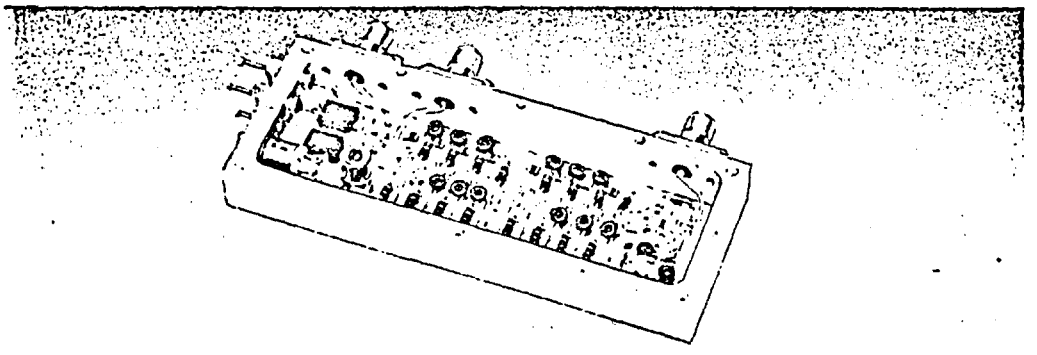
TYPE P PACKAGE FOR DIGITAL ATTENUATOR

TYPICAL TRANSMISSION CHARACTERISTIC FOR R-ATT B-70



RHG

IC LOG AMPS TO 1 GHz



- **For high resolution systems:** <10 nanosecond rise times.
- **For frequency agile systems:** Identical log curves over wide frequency swaths.

The combination of microwave transistors and IC technology results in an extension of frequency up to 1 Gigahertz where the performance shown in figure A was achieved. In the UHF band, frequency swaths of 200-300 MHz are covered in a single amplifier. This results in extremely fast rise times for very wide-band signals and, in addition, a shifting center frequency will produce virtually identical log curves anywhere in the band (see figure B).

Model	Center Freq. (MHz)	Operating BW (MHz)	Dynamic Range (dB)[1]	Linearity[2] (dB)	Price[3]
ICLT150	150	100-200	70	±1	$ 975
ICLT300	300	200-400	60	±1	1100
ICLT375	375	250-500	60	±1.5	1150
ICLT450	450	300-600	60	±1.5	1250
ICLT475	475	400-550	60	±1.5	1100
ICLT625	625	550-700	60	±1.5	1200
ICLT775	775	700-850	60	±2	1300
ICLT925	925	850-1000	60	±2	1400
ICLT1000	1000	950-1050	60	±2	1400

STANDARD SPECIFICATIONS:

a) DC Coupled video.
b) Output voltage: 1.25 Volts into 93Ω
c) Input impedance: 50Ω
d) Power: ± 12 VDC at 80 ma typ. (± 15 VDC, add Suffix "C", no charge).
e) Size: 3-25/32" × 1-1/2" × 15/32"
f) Weight: <4 oz.

NOTES:

1. Input range is from −65 to −5 dBm. (0 to −70 dBm on 70 dB range units).
2. Nominal at center frequency for standard units. Add ±1 dB for −30 °C to +71 °C.
3. Standard Units: Prices shown are for standard units optimized for operation at center frequency with pulse rise times of <10 nanoseconds.
4. Frequency Agile Units: $250 additional. Add Suffix "A". These units are optimized for use over entire operating band with CW or pulsed signals—see reverse side for additional specifications.
5. Limited IF output: $75 additional, add Suffix "B".

OPTIONS (Contact Factory)

1. Up to 80 dB dynamic range units available.
2. Units with hermetically sealed transistors available.
3. Special configurations.
4. Special center frequency/bandwidth combinations.

LOGARITHMIC IF AMPLIFIERS

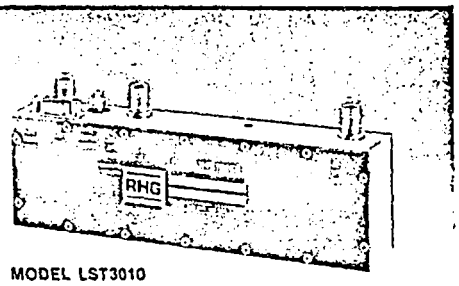
■ True Log Compression ■ Dynamic Ranges to 80 dB

LST SERIES

Model	Center Freq. (MHz)	Bandwidth (MHz)	Rise time (μsec)	Input Range (dB)	Price
LST1003	10	3	0.30	80	$700
LST2005	20	5	0.20	80	700
LST3002	30	2	0.50	80	620
LST3010	30	10	0.10	80	620
LST6010	60	10	0.10	80	620
LST6020	60	20	0.05	80	650
LST7010	70	10	0.10	80	650
LST7030	70	30	0.04	80	700
LST12040	120	40	0.03	80	825
LST16020	160	20	0.05	80	825
LST16040	160	40	0.03	80	825

NOTES:
1. Input dynamic range referenced to 0 dBm high end (nominal).
2. Video output 0.25 to 2.5V (typ) into 93Ω. Units direct coupled.
3. Linearity ± 1 dB over input range
4. Limited IF output: 0 dBm
5. Power: ± 12V @ 70 ma (± 15V, add Suffix "C", N/C)

OPTIONS:
1. RFI protection—includes power line filtering and RFI gasketed covers. Add suffix "RFI" $40 additional.
2. SMA connectors: add suffix "SMA" additional cost $25.
3. 90 dB dynamic ranges, contact factory.



MODEL LST3010

STANDARD MODELS

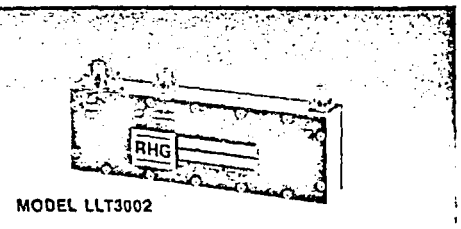
■ 93 ohm Video Load Capability ■ DC Coupled Video

This series offers the user high fidelity "logging" of wide dynamic signal ranges thru the use of successive detection and video summing.

LLT SERIES

Model	Center Freq. (MHz)	Bandwidth (MHz)	Rise time (μsec)	Input Range (dB)	Price
LLT1003	10	3	0.30	80	$795
LLT2005	20	5	0.20	80	795
LLT3002	30	2	0.50	80	680
LLT3010	30	10	0.10	80	680
LLT6010	60	10	0.10	80	680
LLT6020	60	20	0.05	80	750
LLT7010	70	10	0.10	80	750

NOTES:
1. Input dynamic range referenced to 0 dBm high end (nominal).
2. Video output: 0.25 to 2.5V (typ) into 93Ω direct coupled.
3. Linearity: ± 1 dB over 80 dB.
4. Limited IF output: 0 dBm
5. Power: ± 12V @ 70 ma (± 15V, add suffix "C", N/C)

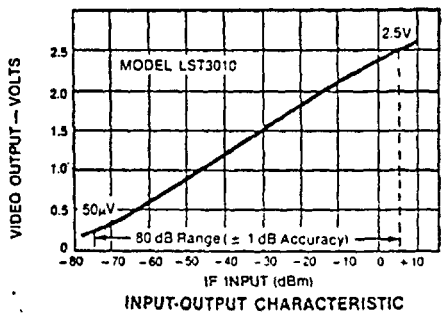


MODEL LLT3002

MINIATURE MODELS

■ Reduced Volume ■ RFI Protected

The "LLT" series duplicates the "LST" performance in 1/2 the package volume.



INPUT-OUTPUT CHARACTERISTIC

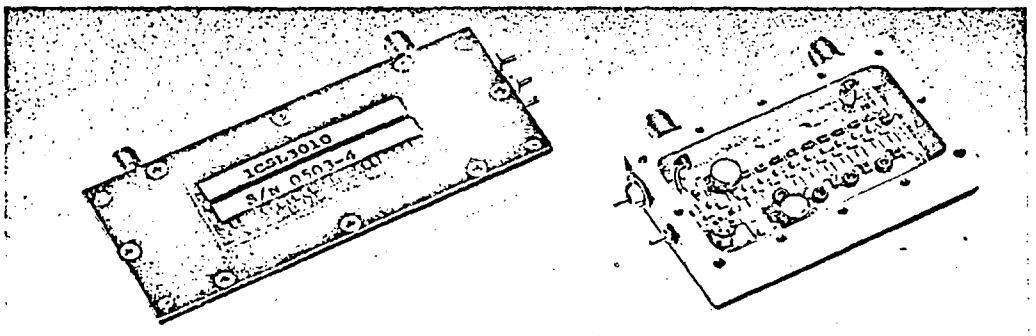
This chart shows a typical transfer curve of a log amplifier. Note that input signals from –80 to 0 dBm may be accommodated and will provide an output which is compressed so that it varies from 0.25 to 2.5 or 20 dB. Note also that ± 1 dB accuracy is obtained over an 80 dB portion of that range and that the average slope of the transfer characteristic is equal to 28 mv per dB.

Units are available with wider dynamic ranges and/or better linearity. For details, contact factory.

RHG

HYBRID IC IF LIMITERS

■ Constant Transmission Phase Shift ■ Wide Dynamic Range ■ Models to 400 MHz
■ Matched Sets Available ■ Pulse and CW Operation ■ Small Size



MODEL ICSL3010 MODEL ICUL400

STANDARD MODELS

The ICSL limiters offer outstanding performance over a wide dynamic range. The use of input filters, multiple limiting stages and a buffered output help to reduce internally generated phase error as well as load change variations. The amplifiers utilize selected components and are stabilized from – 40° to + 70°C.

MINIATURE MODELS

The ICUL series of constant phase IF limiters feature higher operating frequencies and smaller size and weight than have been previously available. The aluminum housed units measure only 2-1/2" × 1-1/2" × 15/32" and weigh only two ounces.

STANDARD MODELS

ICSL SERIES

Model	Center Freq. (MHz)	Min. Bandwidth (MHz)	Nominal Output (dBm)	Price
ICSL3010	30	10	+ 10	$675
ICSL6010	60	10	+ 10	675
ICSL6020	60	20	+ 10	675
ICSL7010	70	10	+ 10	675
ICSL16020	160	20	+ 10	750

MINIATURE MODELS

ICUL SERIES

Model	Center Freq. (MHz)	Min. Bandwidth (MHz)	Nominal Output (dBm)	Price
ICUL3010	30	10	+ 10	$750
ICUL6010	60	10	+ 10	750
ICUL7010	70	10	+ 10	750
ICUL16020	160	20	+ 10	825
ICUL200	200	50	+ 10	895
ICUL400	400	100	+ 10	995

SPECIFICATIONS:

1. Input dynamic range: – 70 to – 5 dBm
2. Phase shift over input range: < 5° (< 10° for 160, 200 and 400 MHz models)
3. Output level variation over input range: < 0.5 dB
4. Noise figure: < 10 dB
5. Input Z: 50 ohms, VSWR 1.5:1 max
6. Output Z: 50 ohms, VSWR 1.5:1 max
7. Operating Temperature Range: – 40°C to + 70°C
8. Power: – 12 VDC at 150 ma (typ)
   (– 15 VDC, add Suffix "C", N/C)

NOTE: Units designed to work with pulsed or CW signals. Typically 100 nanosecond pulses for 10 MHz bandwidths and 50 nanosecond pulses for 20 MHz bandwidths.

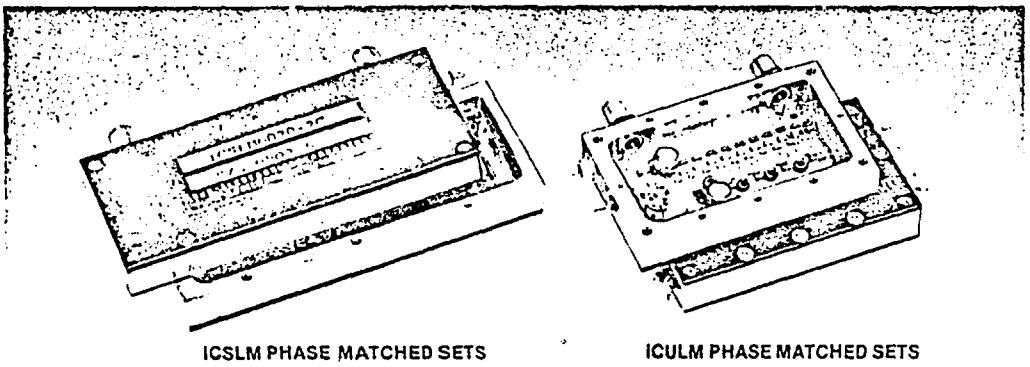
All RHG limiting amplifiers and subsystems are dynamically aligned and tested utilizing the amplitude sweeping RHG Log Test Set (TSL series). This technique presents an instantaneous dynamic display of phase vs. input amplitude on a standard oscilloscope. The overall affects of adjusting any part of the device or subsystem are immediately seen. It is particularly advantageous when matching multiple channels.

This technique is made possible by the wide range amplitude sweeping characteristics of the RHG TSL test set. The linear sweep range of 80 dB allows straightforward scope calibration for the horizontal (in dB/cm). The use of a conventional output phase detector provides a direct readout of phase shift in degrees on the vertical axis.

RHG

IC LIMITERS—MATCHED SETS

■ 2 and 3 Channels ■ Frequencies to 400 MHz ■ Matching to ±2.5°



ICSLM PHASE MATCHED SETS

ICULM PHASE MATCHED SETS

Matched sets of limiters are available for monopulse and other applications requiring constant phase transmission characteristics and accurate matching over input dynamic range and temperature. Offered in 2 or 3 channel sets, they utilize the Super ICSL and ICUL limiters (see reverse side) and meet all of the specifications of that series.

ICSLM SERIES Model	Center Freq. (MHz)	Min. Bandwidth (MHz)	Price for 2 channels	Price for 3 channels
ICSLM3010	30	10	$1550	$2325
ICSLM6010	60	10	1550	2325
ICSLM6020	60	20	1550	2325
ICSLM7010	70	10	1550	2325
ICSLM16020	160	20	2000	3000

Basic Specifications:
The basic specifications are the same as those of the standard ICSL series.

ADDITIONAL SPECIFICATIONS

2 Channels—phase matched over −70 to −5 dBm input range:
- ±2.5° at room temperature (30 thru 160 MHz)
- ±5.0° from −40°C to +70°C
- ±5.0° at room temperature (200 thru 400 MHz)
- ±10° from −40°C to +70°C

To Order: 2 channel set, add suffix—"2C"

ICULM SERIES Model	Center Freq. (MHz)	Min. Bandwidth (MHz)	Price for 2 channels	Price for 3 channels
ICULM3010	30	10	$1700	$2550
ICULM6010	60	10	1700	2550
ICULM7010	70	10	1700	2550
ICULM16020	160	20	1850	2775
ICULM200	200	50	1930	2985
ICULM400	400	100	2190	3285

Basic Specifications:
The basic specifications are the same as those of the standard ICUL series.

3 Channels—phase matched over −70 to −5 dBm input range:
- ±3.0° at room temperature
- ±6.0° from −40°C to +70°C (30 thru 160 MHz)
- ±6.0° at room temperature
- ±12° from −40°C to +70°C (200 thru 400 MHz)

To Order: 3 channel set, add suffix—"3C"

RHG

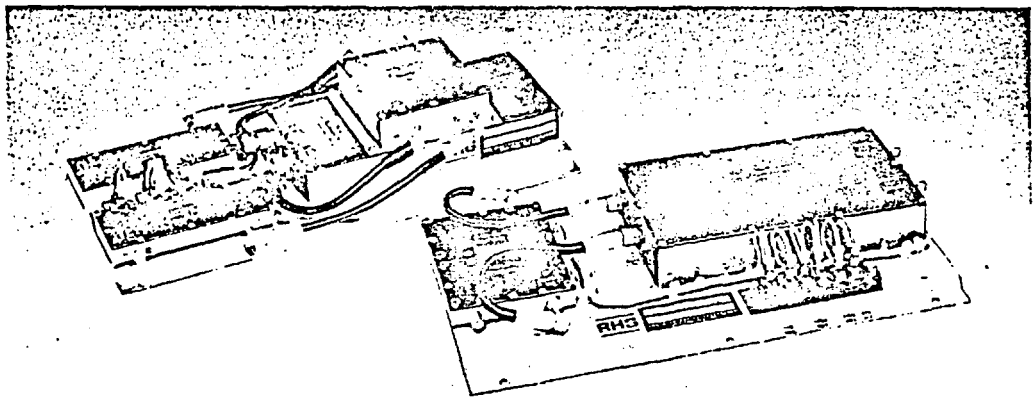
RHG ELECTRONICS LABORATORY, INC

161 East Industry Court ◻ Deer Park, New York 11729 ◻ (516) 242-1100 ◻ TWX 510-227-6083

RHG

IF PHASE DETECTOR SUBSYSTEMS

■ Self-contained ■ Small size ■ IC construction ■ MIL grade
■ Tracking radars ■ Interferometers ■ Direction Finders ■ Test Equipment



RHG now offers a line of complete IF phase detector subsystems. These phase detectors produce direct-coupled video output(s) that are functions of the instantaneous phase difference between the IF inputs, over a wide range of input levels. The phase detectors are optimized for pulsed signals, but are equally useable for CW or analog inputs.

The phase detector subsystems are intended for use in monopulse and interferometer receivers as well as for use in instrumentation. They are complete subsystems, incorporating all necessary limiters, IF components, and video amplifiers, requiring only IF input and video output connections and DC power for operation. Each subsystem is fully calibrated and characterized. This eliminates the usual interfacing and alignment difficulties encountered when assembling a system from individual components.

This data sheet describes three of the most common types of phase detectors. Other configurations are available on special order.

RHG is pleased to provide this section to assist professional engineering personnel with some of the new "language" being used in the field.

Angular Accuracy

Angular accuracy is defined as the difference, in degrees, between the actual input phase difference and the phase difference determined from the output voltage using the nominal phase detector transfer function. In these phase detectors, accuracy is guaranteed for phase angles within ± 45° of crossover.

For example:
For cosine output:
$-135° < \phi < -45°, 45° < \phi < 135°$
For sine output:
$-180° < \phi < -135°; -45° < \phi < 45°,$
$135° < \phi < 180°$

Ratio Accuracy

On a return to boresight system, the levels and phase polarity of the Δ (difference) inputs relative to the Σ (sum) input, are measured. The accuracy is defined as how closely the system can detect crossover, i.e., zero Δ level. This accuracy is stated as the highest ratio of Δ/Σ that will produce a zero output voltage.

Settling Time

Settling time is the time required for the phase detector output to stabilize within rated accuracy limits, for a pulsed IF input.

Dynamic Range

The phase detector is guaranteed to be within rated accuracy as long as both input levels are within the specified dynamic range, and as long as the difference in input levels is no greater than 30 dB.

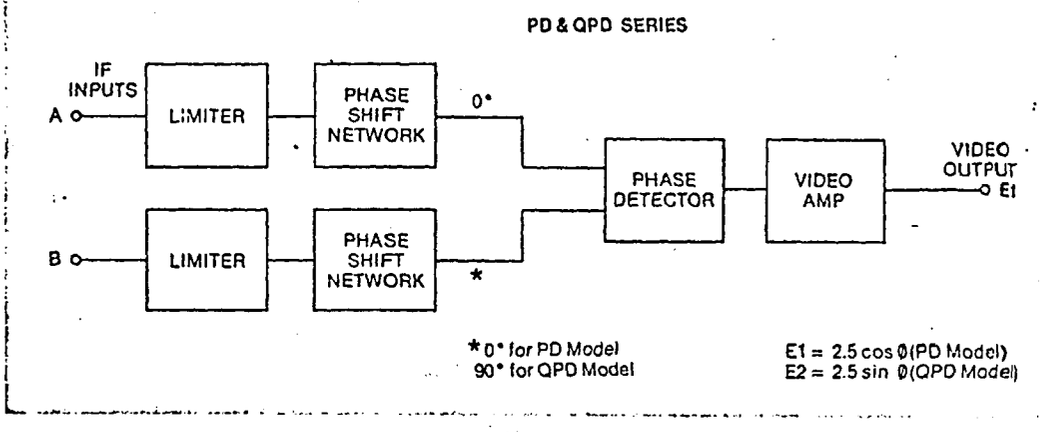
Information Bandwidth

The information bandwidth is the subsystem 3 dB IF bandwidth (*referred to the input*). The video bandwidth is amply wide to be transparent to the information bandwidth.

Accuracy Bandwidth

The accuracy bandwidth is the range of center frequencies over which rated accuracy is maintained. This is of necessity less than the information bandwidth.

TWO CHANNEL, SINGLE OUTPUT PHASE DETECTOR SUBSYSTEM!



The two channel, single output phase detector subsystems are intended for use in phase demodulator systems where the expected input phase difference is less than ±90°. Both in-phase (cos Ø output) and quadrature (sin Ø output) models are available.

Separate limiters and IF processing modules are mounted to a common base plate with all power connections made to a single barrier strip.

Model	Center Freq. (MHz)	Information Bandwidth (MHz)	Accuracy Bandwidth (MHz)	Settling Time (μsec)	Angular Accuracy (degrees)	Price
In-Phase						
PD3010	30	10	2	0.1	±5	$2,250
PD6010	60	10	2	0.1	±5	2,250
PD6020	60	20	4	0.08	±5	2,350
PD7020	70	20	4	0.08	±5	2,350
PD16020	160	20	4	0.08	±7	2,650
Quadrature						
QPD3010	30	10	2	0.1	±5	2,275
QPD6010	60	10	2	0.1	±5	2,275
QPD6020	60	20	4	0.08	±5	2,375
QPD7020	70	20	4	0.08	±5	2,375
QPD16020	160	20	4	0.08	±7	2,675

ADDITIONAL SPECIFICATIONS

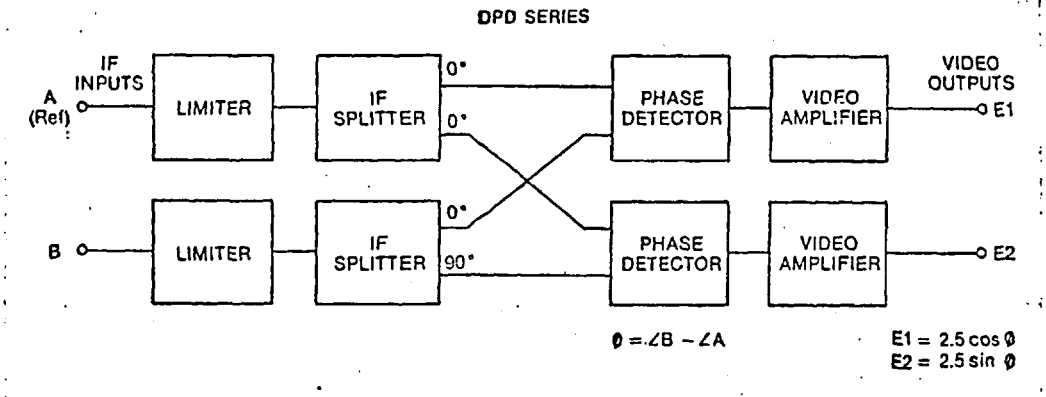
1. Input Impedance: 50 Ω (VSWR 1.5:1 nom)
2. Input Dynamic Range: 0 to −60 dBm (−5 to −60 dBm for 160 MHz units)
3. Input Level Difference: 0 to 30 dB
4. Output Impedance: 75Ω
5. Connectors: SMA
6. Power: ± 12V (± 15V available N/C, add Suffix "C")

NOTES

1. See Glossary (page 33) for detailed definitions of terms.
2. Special parameters, other frequencies, etc. are available—Contact factory.
3. PD and QPD models are available for use with one limiter channel and an external reference—Contact factory.

RHG ELECTRONICS LABORATORY, INC
161 East Industry Court ▫ Deer Park, New York 11729 ▫ (516) 242-1100 ▫ TWX 510-227-6083

TWO CHANNEL, DUAL OUTPUT PHASE DETECTOR SUBSYSTEMS



The two channel, dual output phase detector subsystem offers, by means of the two quadrature outputs, an unambiguous measurement of the input phase difference. This technique is used in angular measuring devices such as interferometers, direction finders and instrumentation.

The two limiters and the IF processor are mounted to an aluminum base plate with all power connections brought out to a single barrier strip.

Model	Center Freq. (MHz)	Information Bandwidth (MHz)	Accuracy Bandwidth (MHz)	Settling Time (μsec)	Angular Accuracy (degrees)	Price
DPD3010	30	10	2	0.1	±5°	$2,500
DPD6010	60	10	2	0.1	±5°	2,500
DPD6020	60	20	4	0.08	±5°	2,600
DPD7020	70	20	4	0.08	±5°	2,600
DPD16020	160	20	4	0.08	±7°	2,950

ADDITIONAL SPECIFICATIONS

1. Input Dynamic Range: 0 to −60 dBm (−5 to −60 dBm for 160 MHz)
2. Input Level Difference: 0 to 30 dB
3. Input Impedance: 50 Ω (VSWR 1.5:1 nom)
4. Output Impedance: 75 Ω
5. Connectors: SMA
6. Power: ± 12V (± 15V available N/C, add Suffix "C".)

NOTES

1. See Glossary (page 33) for detailed definitions of terms.
2. Special parameters, other frequencies, etc. are available—Contact factory.

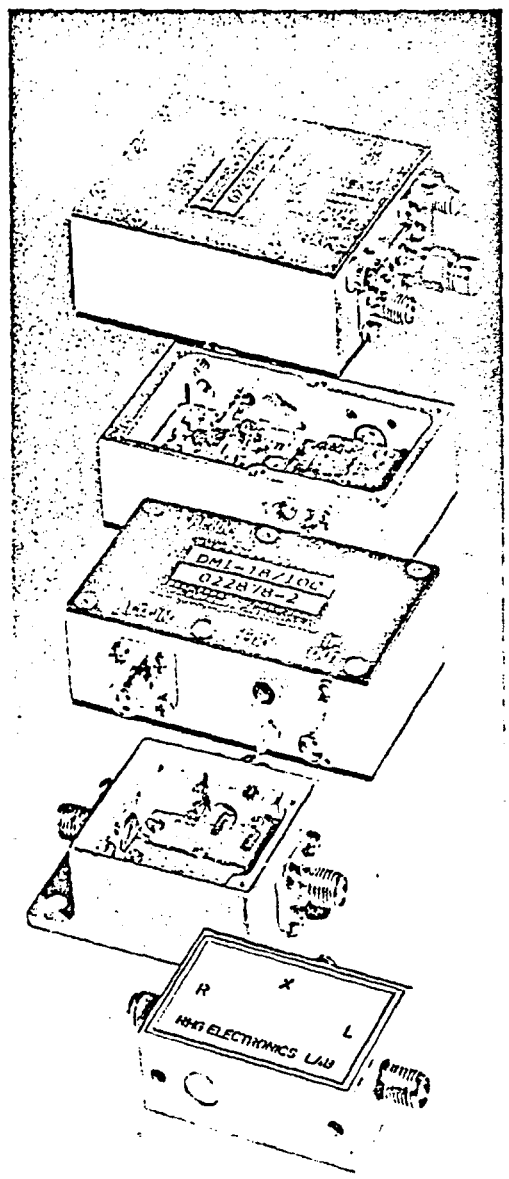
RHG ELECTRONICS LABORATORY, INC.
131 East Industry Court ▫ Deer Park, New York 11729 ▫ (516) 242-1100 ▫ TWX 510-227-6063

For Reliability, Innovation, and Service

TECHNICAL DATA

RHG

DOUBLE BALANCED MIC MIXERS AND MIXER PREAMPS



To fill the growing need for multioctave devices in surveillance, ECM, and other specialized receiver applications, RHG has developed a complete line of double balanced mixers, and double balanced imageless mixers—obtainable with or without built in IF preamplifiers.

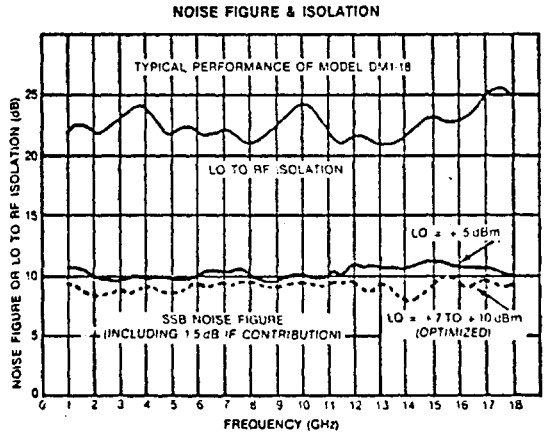
These MIC (Microwave Integrated Circuitry) mixers provide coverage of up to 1 to 26 GHz in a single assembly. This performance has been achieved through the use of a unique microwave configuration. Excellent performance is maintained over five octaves with extremely low intermodulation distortion and high isolation.

Available since late 1969 the "DM" series of double balanced mixers, in standard octave or multioctave versions, has gained wide acceptance in both prototype and production applications.

Recent developments at RHG have produced a 1 to 26 GHz unit, and the industry's smallest 1 to 18 GHz mixer (1/2" × 1/2" × 1/2"). RHG's leadership in the mixer field is evidenced by the growing number of imitators. However, only at RHG can the customer receive the latest technology coupled with custom designs and ongoing service.

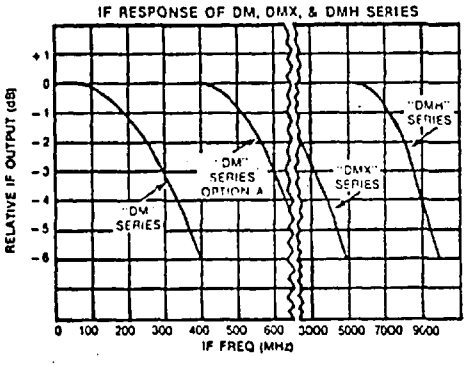
In addition, all RHG mixers can be provided with a fully integrated IF preamp, with IF coverage spanning 1 MHz to 4 GHz.

NOISE FIGURE & ISOLATION

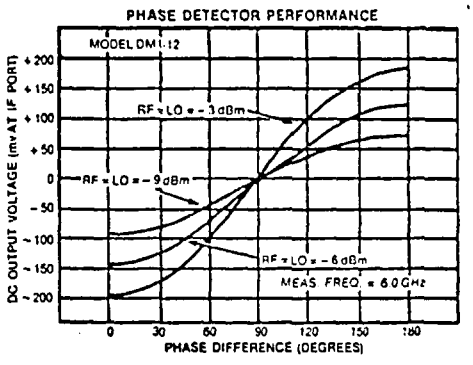


DM SERIES TECHNICAL DATA

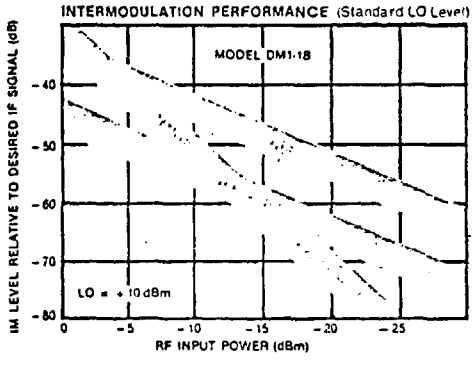
IF RESPONSE OF DM, DMX, & DMH SERIES



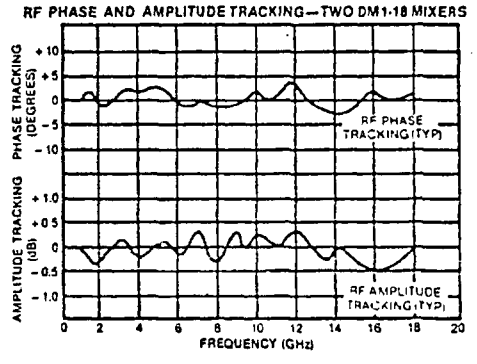
PHASE DETECTOR PERFORMANCE



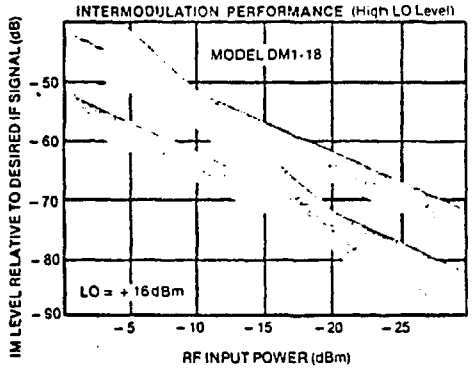
INTERMODULATION PERFORMANCE (Standard LO Level)



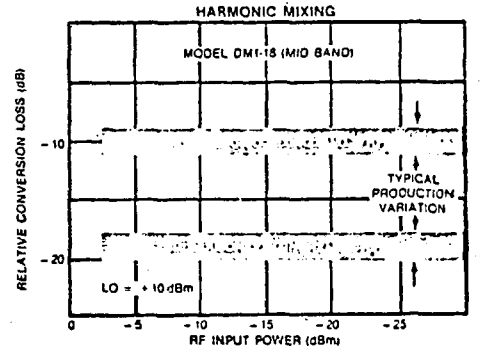
RF PHASE AND AMPLITUDE TRACKING—TWO DM1-18 MIXERS



INTERMODULATION PERFORMANCE (High LO Level)



HARMONIC MIXING



RHG ELECTRONICS LABORATORY, INC.
161 East Industry Court ▪ Deer Park, New York 11729 ▪ (516) 242-1100 ▪ TWX 510-227-6083

RHG

DOUBLE BALANCED MIC MIXERS

■ 1.0 to 18 GHz in one mixer ■ Low IM

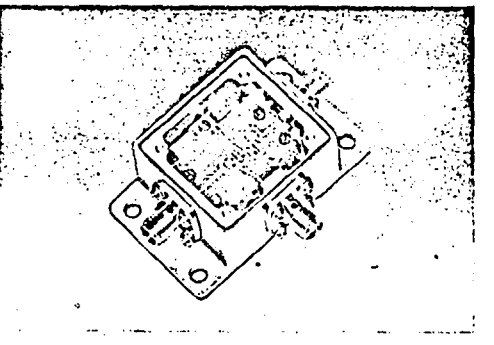
OCTAVE MODELS

Model No.	Freq. (GHz)	Typ N.F. (1) (dB)	Max N.F. (1) (dB)	Price
DM1-2	1.0 to 2.0	6.5	7.5	$250
DM2-4	2.0 to 4.0	7.0	8.0	250
DM4-8	4.0 to 8.0	7.0	8.0	280
DM8-12	8.0 to 12.0	8.0	9.0	315
DM12-18	12.0 to 18.0	9.0	10.0	395
MULTIOCTAVE MODELS				
DM1-4	1.0 to 4.0	7.0	8.0	280
DM1-8	1.0 to 8.0	7.0	8.0	295
DM1-12	1.0 to 12.0	8.0	9.0	350
DM1-18	1.0 to 18.0	9.0	10.0	450
DMS1-26	1.0 to 26.0	8.0	9.5	695

The DMS 1-26 is fully described on an individual DMS 1-26 data sheet.

NOTES:
1. Based on 1.5 dB IF noise figure.
2. RF & LO VSWR: 2.5:1 (typ).
3. LO injection: +5 to +10 dBm (typ).
4. Connectors: SMA all ports (for feed thru terminal at IF output—add Suffix "PT"—no charge).
5. LO to RF ISO: > 20 dB.

STANDARD OPTIONS
1. IF response to 500 MHz: add suffix "A", $10 additional.
2. Low corner noise diodes: reduce 1/f noise in "zero IF" applications. Add suffix "B", $50 additional.



STANDARD MODELS

■ DC to 300 MHz IF ■ 1 to 26 GHz RF/LO

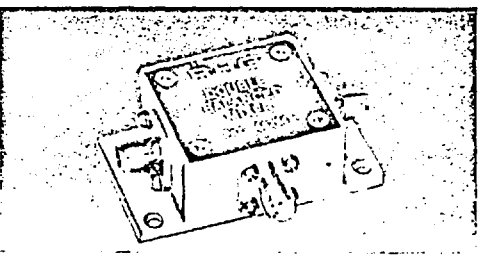
The "DM" series utilizes a rugged cast housing and special SMA connectors to provide reliable performance.

OCTAVE MODELS

Model No.	Freq. (GHz)	Typ. N.F. (dB) (1) 0 dBm LO	Typ. N.F. (dB) (1) −10 dBm LO	Price
DMB 1-2	1 to 2	8.0	12.0	$335
DMB 2-4	2 to 4	8.5	12.0	335
DMB 4-8	4 to 8	9.5	13.0	360
DMB 8-12	8 to 12	10.0	14.0	440
DMB 12-18	12 to 18	11.5	15.5	525
MULTIOCTAVE MODELS				
DMB 1-12	1 to 12	9.0	13.0	495
DMB 2-18	2 to 18	11.0	15.0	625

The DMB 2-18 is fully described on an individual DMB 2-18 data sheet.

NOTES:
1. NF includes: 1.5 dB IF contribution.
2. IF coverage: 10 to 300 MHz.
3. LO/RF isolation: 18 dB typ.
4. RF/LO VSWR: 2.0:1 typ.
5. Bias: +12V at 2 ma typ.
6. For IF to 500 MHz: add suffix "A", $50 additional (not available on DMB1-2 or DMB1-12.



STARVED LO MODELS

■ Operation at −10 dBm LO ■ 1 to 18 GHz

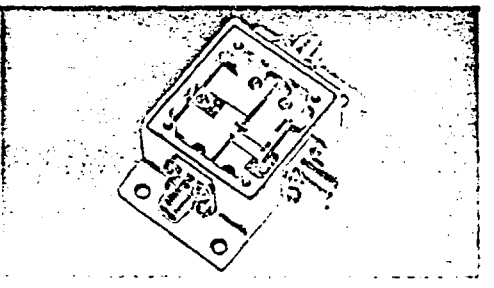
For application where LO power is minimal, the "DMB" series provides all the benefits of doubly balanced mixers.

DC to 2 GHz IF MODELS

Model No.	Freq. (GHz)	Typ. N.F. (1) (dB)	Max. N.F. (1) (dB)	Price
DMX 2-4	2 to 4	8.0	9.0	$395
DMX 4-8	4 to 8	8.0	9.0	425
DMX 8-12	8 to 12	9.0	10.0	450
DMX 12-18	2 to 18	10.0	11.0	475
1 to 8 GHz IF MODEL				
DMH2-18C	2.0 to 18.0	9.0	11.0	$560

The DMH2-18C is fully described on an individual DMH2-18C data sheet.

NOTES:
1. N.F. includes 1.5 dB IF contribution.
2. LO injection: +10 dBm.
3. LO to RF ISO: > 20 dB (> 16 dB on DMH).



MICROWAVE IF MODELS

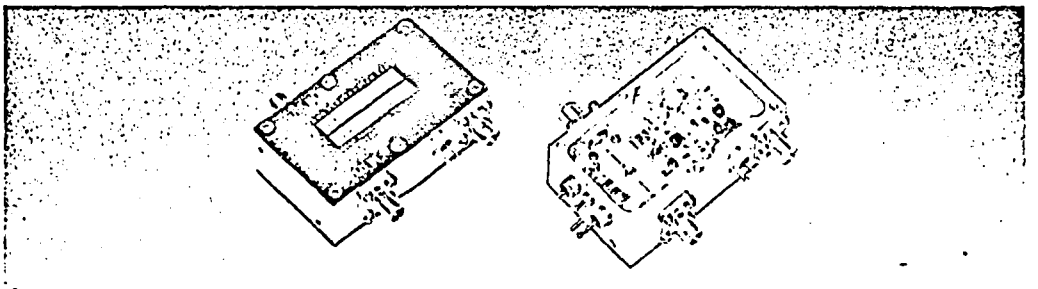
■ IF Coverage to 8 GHz ■ RF/LO to 18 GHz

IFs to 8 GHz for up or down conversion. The "DMX" and "DMH" series provide state-of-the-art performance.

RHG

DOUBLE BALANCED MIC MIXER PREAMPS

■ 1 to 26 GHz ◘ IC Preamps ◘ Small Size



STANDARD & SPECIAL PREAMP MODELS

Every RHG mixer can be supplied with a wide range of IF preamplifiers. These IC preamps are mechanically and electrically integrated with the mixer to provide optimum noise figure. The use of a mixer/preamp assures this optimum noise performance, since the mixer/preamp interface is a key factor and is often improperly established when separate mixers and preamps are used.

The models listed on the following pages reflect many of the most requested combinations. If your needs are not met by a standard, we will be happy to provide a special unit on request.

OCTAVE MODELS

RF Band	Model Number	IF Freq/BW MHz	TYP N.F. (dB)	MAX N.F. (dB)	Price
L-Band 1.0-2.0 GHz	DM1-2/10A	60/10	7.0	8.0	$575
	DM1-2/10B	60/20	7.0	8.0	575
	DM1-2/10C	30/10	7.0	8.0	575
S-Band 2.0-4.0 GHz	DM2-4/10A	60/10	7.5	8.5	575
	DM2-4/10B	60/20	7.5	8.5	575
	DM2-4/10C	30/10	7.5	8.5	575
C-Band 4.0-8.0 GHz	DM4-8/10A	60/10	7.5	8.5	575
	DM4-8/10B	60/20	7.5	8.5	575
	DM4-8/10C	30/10	7.5	8.5	575
X-Band 8.0-12.0 GHz	DM8-12/10A	60/10	8.5	9.5	625
	DM8-12/10B	60/20	8.5	9.5	625
	DM8-12/10C	30/10	8.5	9.5	625
Ku-Band 12.0-18.0 GHz	DM12-18/10A	60/10	9.5	10.5	745
	DM12-18/10B	60/20	9.5	10.5	745
	DM12-18/10C	30/10	9.5	10.5	745
K-Band 18.0-26.0 GHz	DM18-26/10A	60/10	8.5	10.0	995
	DM18-26/10B	60/20	8.5	10.0	995
	DM18-26/10C	30/10	8.5	10.0	995

SPECIAL PREAMPS: To order, replace suffix with preamp type desired

Preamp Type	Cent. Freq. (MHz)	Band-width (MHz min)	RF-IF Gain (dB min)	*Addit. N.F.	*Addit. Cost
10KK	10	2	25	0.5	$40
10LL	20	6	25	0.0	40
10D	70	10	25	0.0	25
10JJ	70	30	25	0.0	25
10BB	120	20	25	1.0	40
10DD	130	50	25	1.0	50
10HH	10 to 200		20	1.0	50

*Added to mixer preamp with 10A preamp type

For 160 MHz models, see "EF" series on reverse side

MULTIOCTAVE MODELS

RF Band	Model Number	IF Freq/BW MHz	N.F. (dB)	Price
0.1 to 1.0 GHz	DM0.1-1/10A	60/10	See	$ 675
	DM0.1-1/10B	60/20	note 1	675
	DM0.1-1/10C	30/10	below	675
1.0 to 8.0 GHz	DM1-8/10A	60/10	See	625
	DM1-8/10B	60/20	Note 1	625
	DM1-8/10C	30/10	below	625
1.0 to 12.0 GHz	DM1-12/10A	60/10	See	695
	DM1-12/10B	60/20	Note 1	695
	DM1-12/10C	30/10	below	695
1.0 to 18.0 GHz	DM1-18/10A	60/10	See	870
	DM1-18/10B	60/20	Note 1	870
	DM1-18/10C	30/10	below	870
1.0 to 26.0 GHz	DM1-26/10A	60/10	See	1050
	DM1-26/10B	60/20	Note 1	1050
	DM1-26/10C	30/10	below	1050

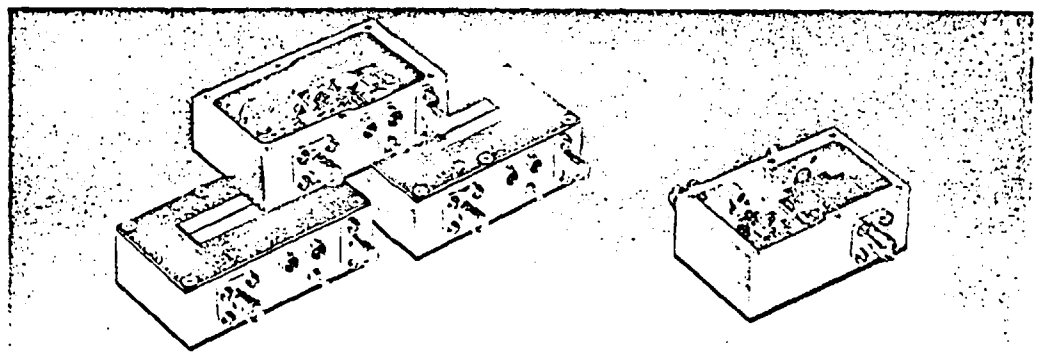
NOTES:

1. Noise figure of multioctave models is typically
   <10 dB 0.1 to 1.0 GHz
   < 8 dB 1.0 to 8 GHz
   <10 dB 8.0 to 26 GHz
2. VSWR: Typically 2.5:1
3. LO injection: +7 to +10 dBm
4. IF output capability: > 0 dBm (all models)
5. LO-RF isolation: 20 dB
6. Impedance level: 50Ω, all ports
7. Connectors: SMA
8. Gain (RF-IF): 25 dB (min) unless noted otherwise
9. Weight: Approx. 3 oz.
10. Power: +12 VDC at 20 ma (typ)
    For +15 VDC add suffix "C" (no charge).
11. Most units available with biasable mixers for low LO power. Contact factory for details.

RHG

DOUBLE BALANCED MIC MIXER PREAMPS

■ Special Purpose Mixer Preamps ■ MIC/IC Construction



GAIN AND PHASE MATCHED MODELS WITH ELECTRONIC GAIN CONTROL

OCTAVE MODELS

RF Band	Model Number	IF Freq/BW	N.F. (dB)	Price Per Channel (1)
L-Band 1.0 to 2.0 GHz	MDM1-2/12A	60/10	7.7	$ 675
	MDM1-2/12B	60/20	7.7	675
	MDM1-2/12C	30/10	7.7	675
S-Band 2.0 to 4.0 GHz	MDM2-4/12A	60/10	8.2	675
	MDM2-4/12B	60/20	8.2	675
	MDM2-4/12C	30/10	8.2	675
C-Band 4.0 to 8.0 GHz	MDM4-8/12A	60/10	8.2	675
	MDM4-8/12B	60/20	8.2	675
	MDM4-8/12C	30/10	8.2	675
X-Band 8 to 12 GHz	MDM8-12/12A	60/10	9.2	725
	MDM8-12/12B	60/20	9.2	725
	MDM8-12/12C	30/10	9.2	725
Ku-Band 12 to 18 GHz	MDM12-18/12A	60/10	9.7	845
	MDM12-18/12B	60/20	9.7	845
	MDM12-18/12C	30/10	9.7	845
K-Band 18 to 26 GHz	MDM18-26/10A	60/10	10.5	1095
	MDM18-26/10B	60/20	10.5	1095
	MDM18-26/10C	30/10	10.5	1095

MULTIOCTAVE MODELS

RF Band	Model Number	IF Freq/BW	N.F. (dB)	Price Per Channel (1)
1.0 to 12.0 GHz	MDM1-12/12A	60/10	See	795
	MDM1-12/12B	60/20	Note 2	795
	MDM1-12/12C	30/10		795
1.0 to 18.0 GHz	MDM1-18/12A	60/10	See	970
	MDM1-18/12B	60/20	Note 2	970
	MDM1-18/12C	30/10		970
1.0 to 26 GHz	MDM1-26/12A	60/10	See	1220
	MDM1-26/12B	60/20	Note 2	1220
	MDM1-26/12C	30/10		1220

NOTES:

1. For single channel with gain control, $50. less per unit.
2. NF: < 9 dB to 8 GHz; < 10 dB to 12 GHz; < 11 dB to 26 GHz
3. Overall RF-IF Gain: 20 dB min.
4. RF-LO Isolation: 20 dB min.
5. Power: + 12 VDC at 90 ma (typ).
   + 15 VDC available N/C, add suffix "C"
6. Matching: + 5° and ± 1 dB over specified gain control and temperature ranges.
7. Gain Control Range: 20 dB for 0 to − 3V (nom.)
8. Meets MIL-E 5400, Class II requirements (− 30° to + 71 °C)

ECM AND SURVEILLANCE MODELS WITH 160 MHz IF AND HIGH OUTPUT CAPABILITY

OCTAVE MODELS

RF Band	Model Number	TYP N.F. (dB)	MAX N.F. (dB)	Price
L-Band 1.0 to 2.0 GHz	DM1-2/14EF	7.0	8.0	$ 725
S-Band 2.0 to 4.0 GHz	DM2-4/14EF	7.5	8.5	725
C-Band 4.0 to 8.0 GHz	DM4-8/14EF	7.5	8.5	725
X-Band 8.0 to 12.0 GHz	DM8-12/14EF	8.5	9.5	800
Ku-Band 12.0 to 18.0 GHz	DM12-18/14EF	9.5	10.5	925
K-Band 18 to 26 GHz	DM18-26/14EF	10.0	11.0	117

MULTIOCTAVE MODELS

RF Band	Model Number	TYP N.F. (dB)	MAX N.F. (dB)	Price
0.25 to 1 GHz	DM0.25-1/14EF	10.0	11.0	$ 825
1.0 to 12 GHz	DM1-12/14EF	9.5	10.5	850
1.0 to 18 GHz	DM1-18/14EF	10.5	11.5	1025
1.0 to 26 GHz	DM1-26/14EF	11.0	12.0	1275

ADDITIONAL SPECIFICATIONS:

1. LO Power: + 10 dBm
2. LO-RF Isolation: 20 dB
3. RF-IF Gain: 25 dB (min)
4. Output Power: + 13 dBm at 1 dB compression.
5. IF Freq/Bandwidth: 160/50 MHz.
6. Units tested to: Temperature: − 54 °C to + 71 °C
   Vibration: Curve 1A of MIL-E-5400L (± 10g's to 2000 Hz)

Standard Level (+7 dBm LO)
DOUBLE-BALANCED MIXERS

TAK SERIES



MODEL	FREQUENCY	MIL-SPEC† DASH NO.	COST
TAK-5	10 KHz - 250 MHz	—	$17.95 (1-4)
TAK-5R	50 KHz - 200 MHz	01N	$14.45 (5-24)
TAK-6	0.5 MHz - 600 MHz	—	$17.95 (1-4)
TAK-6R	5 MHz - 500 MHz	02N	$14.45 (5-24)
•TAK-7	2 MHz - 1000 MHz	—	$19.95 (1-4)

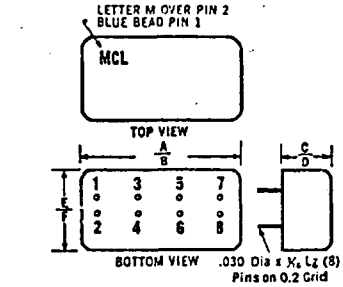
† MIL-M-28837/1A–
• IF port is not DC coupled

DESCRIPTION — Only 0.2 inches high, the low profile TAK series of double balanced mixers cover a very broad frequency ranges from 10 KHz to 1000 MHz. Exhibiting a flat conversion loss, these low profile units have a conversion loss typically 5.5 dB and isolation typically greater than 40 dB.

Packaged within an RFI shielded metal enclosure and hermetically sealed header, this low profile unit is only .064 cubic inches. The TAK series has its 8 pins located on a 0.2 inch grid.

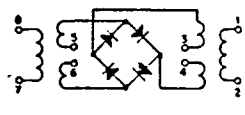
Internal components include well matched hot-carrier diodes and extra wideband transmission line transformers supported with silicone rubber for vibration and shock requirements.

DIMENSIONS AND CONNECTIONS



	A	B	C	D	E	F
IN	.8	.77	.21	.2	.4	.37
MM	20.3	19.5	5.3	5.0	10.1	9.3

PIN LAYOUT



	-5 -6	-7	-5R	-6R
LO	8	8	8	1
RF	1	3,4	1	8
IF	3,4	1	3,4	5,6
Ground	2,5,6,7	2,5,6,7	2,5,6,7	2,3,4,7
Case Ground	2	2,5,6,7	—	3,4,7

NOTE: PINS 3 AND 4 MUST BE CONNECTED TOGETHER

WEIGHT 3.7 grams .13 ounces

FEATURES

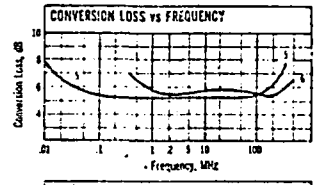
Broadband: 10 KHz to 1000 MHz
Low Conversion Loss: typically less than 5.5 dB
High Isolation: typically greater than 40 dB
Low Profile: 0.067 in.³, 0.4" x 0.8" PC area, 0.2" high
High Reliability: meets MIL-M-28837/1A, 100% tested, 1 year guarantee
Low Cost: as low as $14.95 in small quantity

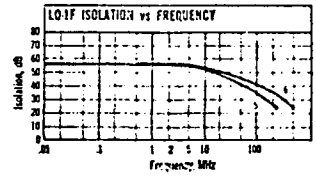
APPLICATIONS

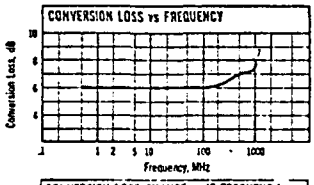
- Frequency mixing
- Pulse and amplitude modulation
- Phase detection
- Current controlled attenuation
- Bi-phase modulation

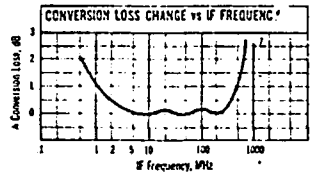
ABSOLUTE MAXIMUM RATINGS

- Input Power: 50 mW
- Peak IF Input Current: 40 mA
- Operating and Storage Temp.: −55°C to +100°C
- Pin Temperature: (10 sec.) +260°C
- Environmental Specifications: See Index Page









TAK Series
10 KHz to 1000 MHz

Mini-Circuits

SPECIFICATIONS: 50 Ohms

MIXING

CONVERSION LOSS AND ISOLATION

Model No.	Frequency Range, MHz LO	RF	IF	Conversion Loss, dB: One Octave From Band Edge Typ.	Max.	Total Range Typ.	Max.	Isolation, dB: Lower Band Edge To One Decade Higher LO-RF Typ.	Min.	LO-IF Typ.	Min.	Mid Range LO-RF Typ.	Min.	LO-IF Typ.	Min.	Upper Band Edge To One Octave Lower LO-RF Typ.	Min.	LO-IF Typ.	Min.	Pin Layout
TAK-5	.01-250	.01-250	DC-250	5.5	7.0	6.5	8.5	60	50	55	45	50	35	45	30	40	30	35	25	Fig. 1
TAK-5R	.05-200	.05-200	DC-200	5.5	6.5	6.5	8.0	55	50	50	45	45	35	40	30	45	35	40	30	Fig. 3
TAK-6	.5-500	.5-500	DC-600	5.5	7.5	6.5	8.5	60	50	55	45	50	30	45	30	40	25	30	20	Fig. 1
TAK-6R	5-500	5-500	DC-500	6.0	7.0	6.5	8.0	55	50	49	40	45	30	40	25	35	30	30	25	Fig. 4
TAK-7	2-1000	2-1000	.5-500	5.5	7.5	6.5	8.5	45	30	45	30	35	20	35	20	30	20	30	20	Fig. 2

SIGNAL 1 dB COMPRESSION LEVEL

Model No.	TAK-5	TAK-5R	TAK-6	TAK-6R	TAK-7
SIGNAL LEVEL, (dBm)	+1	+1	+1	+1	+1

ELECTRONIC ATTENUATION

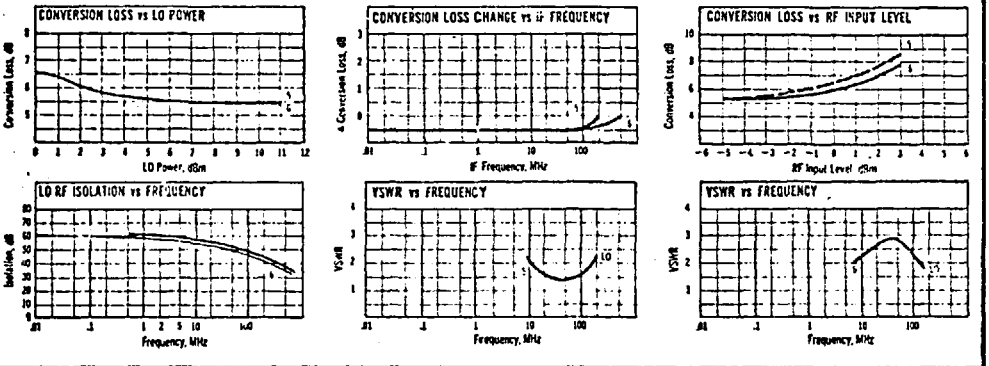
Model No.	TAK-5	TAK-5R	TAK-6	TAK-6R	TAK-7
MINIMUM ATTENUATION, (20 mA)	1.5 dB	1.7 dB	3.5 dB	3.5 dB	—

PHASE DETECTION

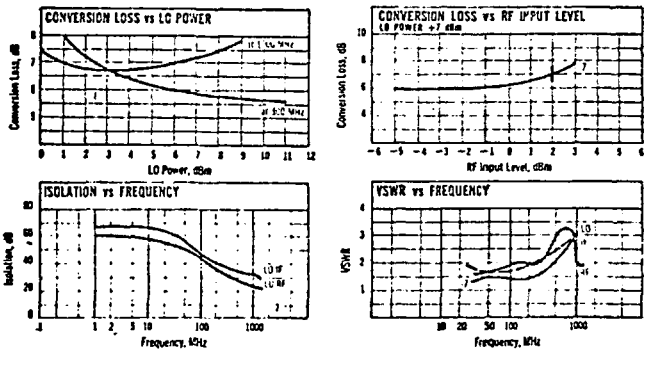
Model No.	TAK-5	TAK-5R	TAK-6	TAK-6R	TAK-7
DC OFFSET, (mV) TYP.	1	1	1	1	—
DC POLARITY	NEG	NEG	NEG	NEG	—
MAXIMUM OUTPUT, (VOLTS) TYP.	.25	.25	.25	.25	—

Models TAK-5R, TAK-6R . . .
Exact electrical and mechanical replacements for M6D and M6E respectively.

MODELS TAK-5, TAK-6



MODEL TAK-7



PROMPT SERVICE / ONE WEEK DELIVERY

Mini-Circuits

2-Way 0°
POWER SPLITTER/COMBINERS

PSC-2 SERIES



FEATURES

- Broadband, 2 KHz to 1000 MHz
- Excellent Balance, typically, phase balance within 1°, amplitude balance within 0.05 dB
- Low Insertion Loss, typically less than 0.6 dB
- High Isolation, typically better than 25 dB
- Hermetically Sealed & RFI Shielded
- Miniature, 0.128 in.³, 0.4" x 0.8" PC area 0.4" high
- High Reliability, 100% tested, one year guarantee
- Low Cost, as little as $9.95 in small quantity

APPLICATIONS

- Split an input signal into two equal in-phase outputs
- Combine signals from two different sources
- Add signals vectorially
- Provide RF logic capability

ABSOLUTE MAXIMUM RATINGS

- Operating and Storage Temp. -55°C to +100°C
- Pin Temperature: (10 sec.) +260°C
- Environmental Specifications: See Index Page

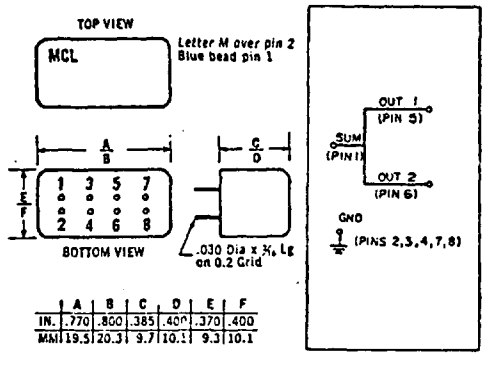
MODEL	FREQUENCY	Z (Ohms)	COST
PSC-2-1	100 KHz - 400 MHz	50	$ 9.95 (6-49)
PSC-2-1W	1 MHz - 650 MHz	50	$14.95 (6-49)
PSC-2-2	2 KHz - 60 MHz	50	$19.95 (6-49)
PSC-2-4	10 MHz - 1000 MHz	50	$19.95 (6-49)
NATIONAL STANDARD NUMBERS	PSC-2-1	NSN 5820-00-548-0739	

For 75Ω models see page 113.

DESCRIPTION — The Series PSC-2 2-way power splitter/combiner is a high performance broad band hybrid junction. Internally, terminations and transformers are provided to ensure a well matched 50 ohm impedance at all ports. Signals fed into the input S port are equally divided, in phase, to the two output (1 and 2) ports. Similarly, signals fed into ports 1 and 2 are vectorially summed at the output S port. Typically, over most of the frequency range, the phase balance is within 1 degree and the amplitude balance is within 0.5 dB.

High reliability is associated with every MCL unit. Every unit is 100% tested and carries a one year guarantee.

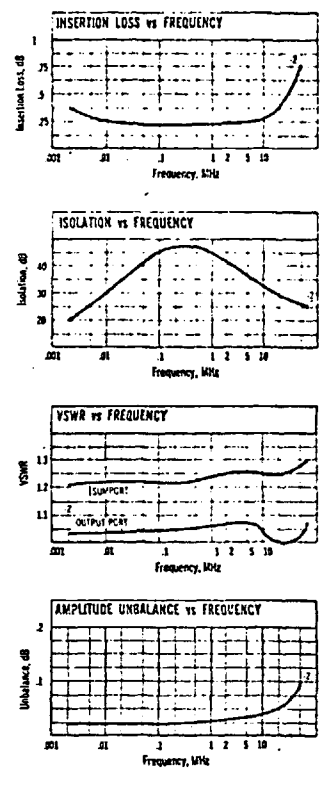
DIMENSIONS AND CONNECTIONS



	A	B	C	D	E	F
IN.	.770	.800	.385	.400	.370	.400
MM	19.5	20.3	9.7	10.1	9.3	10.1

WEIGHT 5.2 grams 0.18 ounces

MODEL PSC-2-2



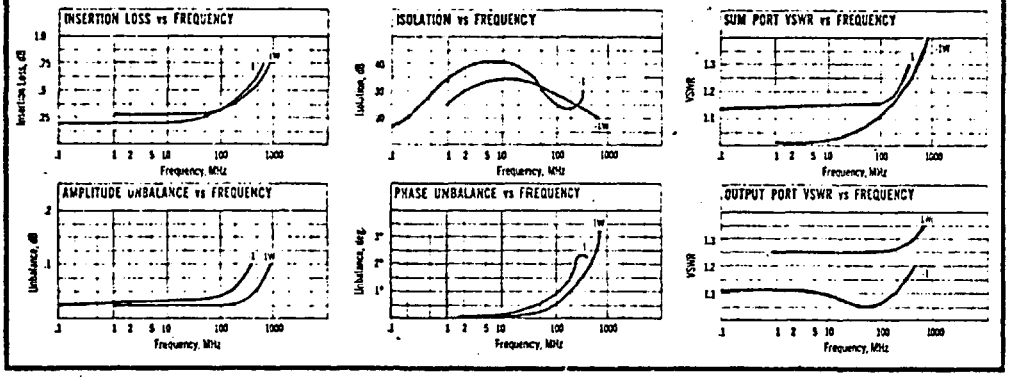
Mini-Circuits 2625 E. 14th St., Brooklyn, NY 11235 (212) 769-0200/Dom. Telex 125460/Int'l. Telex 620156

PSC-2 Series
2 KHz to 1000 MHz.

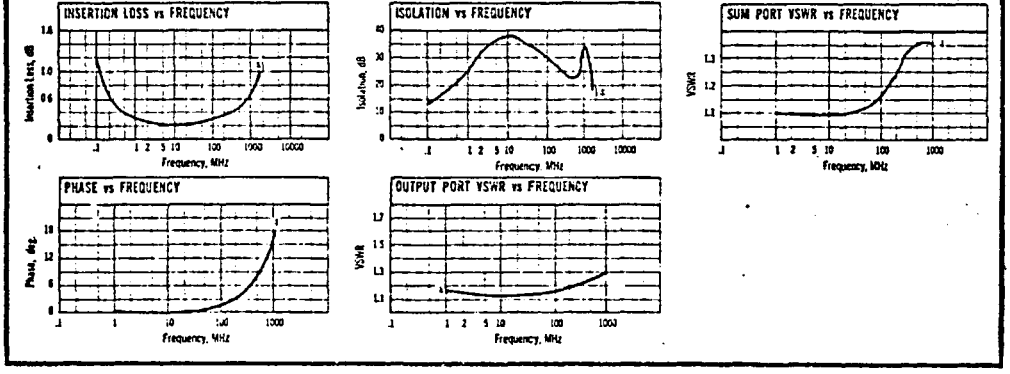
Mini-Circuits

MODEL	PSC-2-1	PSC-2-1W	PSC-2-2	PSC-2-4
FREQUENCY RANGE (MHz)	0.1 - 400	1 - 650	2 KHz - 60 MHz	10 - 1000
NOMINAL PHASE	0°	0°	0°	0°
IMPEDANCE, ALL PORTS	50 ohms	50 ohms	50 ohms	50 ohms
ISOLATION BETWEEN OUTPUT 1 and 2, dB	Typ. / Min. 2-40 MHz 40 30 0.4-400 MHz 25 20 0.1-0.4 MHz 20 15	Typ. / Min. 10-200 MHz 35 25 1-650 MHz 25 20	Typ. / Min. 15 KHz-6 MHz 40 30 4 KHz-60 MHz 27 20	Typ. / Min. 10-100 MHz 30 25 100-1000 MHz 25 20
INSERTION LOSS, dB (Above 3 dB Split)	Typ. / Max. 0.1-100 MHz 0.2 0.6 100-200 MHz 0.4 0.75 200-400 MHz 0.6 1.0	Typ. / Max. 1-200 MHz 0.3 0.6 200-500 MHz 0.5 0.9 500-650 MHz 0.7 1.0	Typ. / Max. 10 KHz-3 MHz 0.2 0.4 2 KHz-20 MHz 0.3 0.6 20 MHz-60 MHz 0.6 1.0	Typ. / Max. 10-100 MHz 0.6 1.0 100-1000 MHz 0.7 1.2
PHASE UNBALANCE, DEGREES	Typ. / Max. 0.1-100 MHz 0.5 2 100-200 MHz 1 3 200-400 MHz 2 4	Typ. / Max. 1-100 MHz 0.5 2.0 100-400 MHz 1.0 3.0 400-650 MHz 2.0 4.0	Typ. / Max. 10 KHz-3 MHz 0.5 2 2 KHz-20 MHz 1 3 20 MHz-60 MHz 2 4	Typ. / Max. 10-100 MHz 0.5 2 100-400 MHz 1.0 8 400-1000 MHz 8.0 20
AMPLITUDE UNBALANCE, dB	Typ. / Max. 0.1-100 MHz 0.05 0.15 100-200 MHz 0.05 0.2 200-400 MHz 0.1 0.3	Typ. / Max. 1-100 MHz 0.05 0.15 100-400 MHz 0.05 0.20 400-650 MHz 0.10 0.30	Typ. / Max. 2 KHz-20 MHz 0.05 0.15 20 MHz-60 MHz 0.1 0.3	Typ. / Max. 10-100 MHz 0.1 0.2 100-1000 MHz 0.2 0.4
VSWR	1.2 typ.	1.2 typ.	1.2 typ.	1.2 Typ.
MATCHED POWER RATING	1 watt max.	1 watt max.	1 watt max.	1 watt max.
INTERNAL LOAD DISS.	0.12 watt	0.12 watt	0.12 watt	0.12 watt

MODELS PSC-2-1, PSC-2-1W



MODEL PSC-2-4



PROMPT SERVICE / ONE WEEK DELIVERY

Mini-Circuits

2-Way 90°
POWER SPLITTER/COMBINERS

PSCQ-2 SERIES



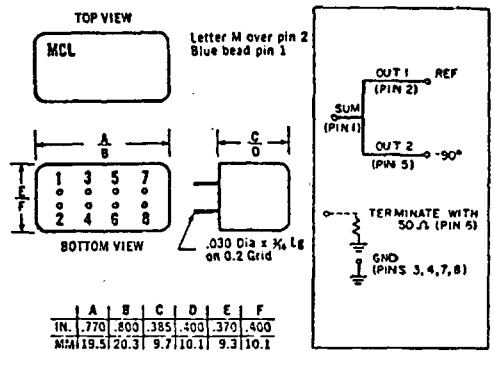
MODEL	FREQUENCY	Z (Ohms)	COST
PSCQ-2-13	12 MHz - 14 MHz	50	$12.95 (5-49)
PSCQ-2-14	12 MHz - 16 MHz	50	$12.95 (5-49)
PSCQ-2-40	23 MHz - 40 MHz	50	$16.95 (5-49)
PSCQ-2-50	25 MHz - 50 MHz	50	$19.95 (5-49)
PSCQ-2-90	55 MHz - 90 MHz	50	$19.95 (5-49)
PSCQ-2-160	120 MHz - 180 MHz	50	$19.95 (5-49)

DESCRIPTION — The Series PSCQ-2 2-way power splitter/combiner is a high performance broad band hybrid junction. Signals fed into the input S port are equally divided, 90° out of phase to the two output ports. Similarly, signals fed into ports 1 and 2 are vectorially summed at the output S port. Typically, over most of the frequency range, the phase balance is within 1 degree and the amplitude balance is within 0.6 dB.

The PSCQ-2 is ruggedly constructed to provide reliable service under severe environmental conditions. This hermetically sealed unit performs well under high relative humidity conditions and over temperature extremes from −55°C to +100°C.

High reliability is associated with every MCL unit. Every unit is 100% tested and carries a one year guarantee.

DIMENSIONS AND CONNECTIONS



	A	B	C	D	E	F
IN.	.770	.800	.385	.400	.370	.400
MM	19.5	20.3	9.7	10.1	9.3	10.1

WEIGHT 5.2 grams 0.18 ounces

FEATURES

- Broadband, 12 MHz to 180 MHz
- Excellent Balance, typically, phase deviation from quadrature less than 1°, amplitude unbalance 0.6 dB
- Low Insertion Loss, typically average loss is less than 0.3 dB
- High Isolation, typically better than 25 dB
- Hermetically Sealed & RFI Shielded
- Miniature, 0.128 in.³, 0.4" x 0.8" PC area 0.4" high
- High Reliability, 100% tested, one year guarantee
- Low Cost, as little as $12.95 in small quantity

APPLICATIONS

- Split an input signal into two equal phase quadrature outputs
- Add signals vectorially
- SSB modulators
- Image reject mixers

ABSOLUTE MAXIMUM RATINGS

- Operating and Storage Temp. −55°C to +100°C
- Pin Temperature: (10 sec.) +260°C
- Environmental Specifications: See Index Page

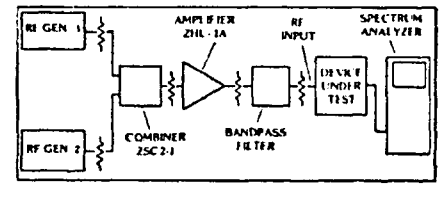
TWO-TONE INTERMODULATION MEASUREMENT

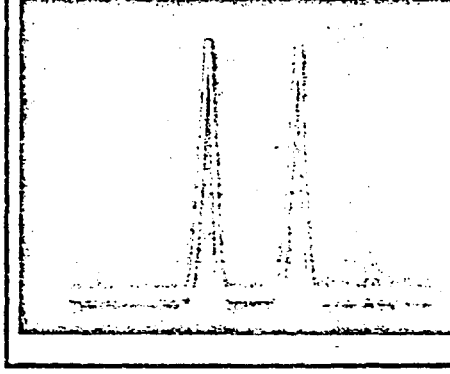
RF INPUT CONDITIONS

TONE 1 - 50 MHz at +7dBm INPUT
TONE 2 -51MHz at +7dBm INPUT

SPECTRUM DISPLAY

RESOLUTION - 500kHz PER DIVISION
VERTICAL - 10 dB PER DIVISION

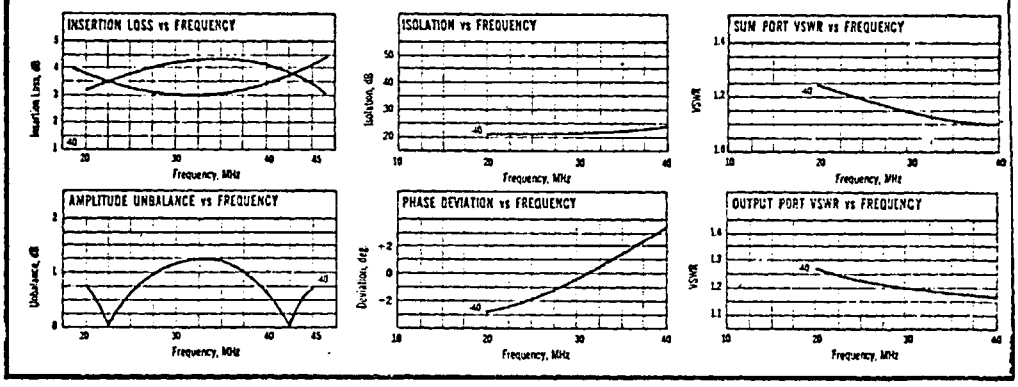




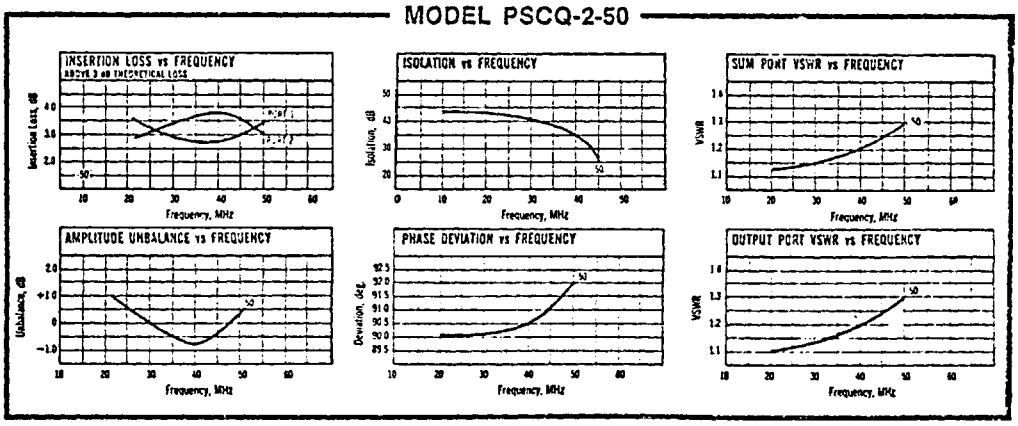
2-Way 90°
POWER SPLITTER/COMBINERS

MODEL	PSCQ-2-40		PSCQ-2-50		PSCQ-2-90		PSCQ-2-180	
FREQUENCY RANGE (MHz)	23 - 40		25 - 50		55 - 90		120 - 180	
NOMINAL PHASE	90°		90°		90°		90°	
IMPEDANCE, ALL PORTS	50 ohms		50 ohms		50 ohms		50 ohms	
ISOLATION BETWEEN OUTPUT 1 and 2, dB	Typ. 21	Min. 18	Typ. 30	Min. 20	Typ. 30	Min. 20	Typ. 23	Min. 15
INSERTION LOSS, dB (Average of Coupled Outputs Less 3 dB)	Typ. 0.3	Max. 0.7	Typ. 0.3	Max. 0.7	Typ. 0.3	Max. 0.7	Typ. 0.3	Max. 0.7
PHASE DEVIATION FROM QUADRATURE, DEGREES	Typ. 1	Max. 4	Typ. 1	Max. 3	Typ. 1	Max. 3	Typ. 2	Max. 4
AMPLITUDE UNBALANCE, dB	Typ. 1.0	Max. 1.5	Typ. 0.4	Max. 1.5	Typ. 0.4	Max. 1.2	Typ. 0.4	Max. 1.2
VSWR	1.2 typ.		1.2 typ.		1.2 typ.		1.35 typ.	
INPUT POWER RATING	2 watts max.		2 watts max.		2 watts max.		2 watts max.	

MODEL PSCQ-2-40



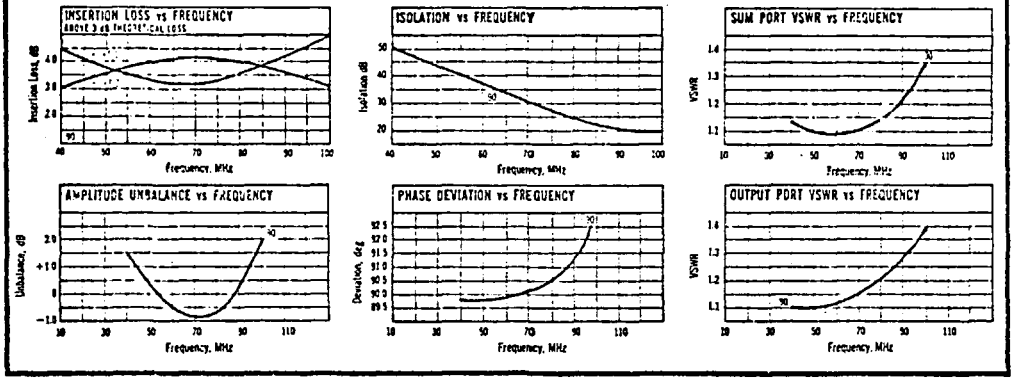
MODEL PSCQ-2-50



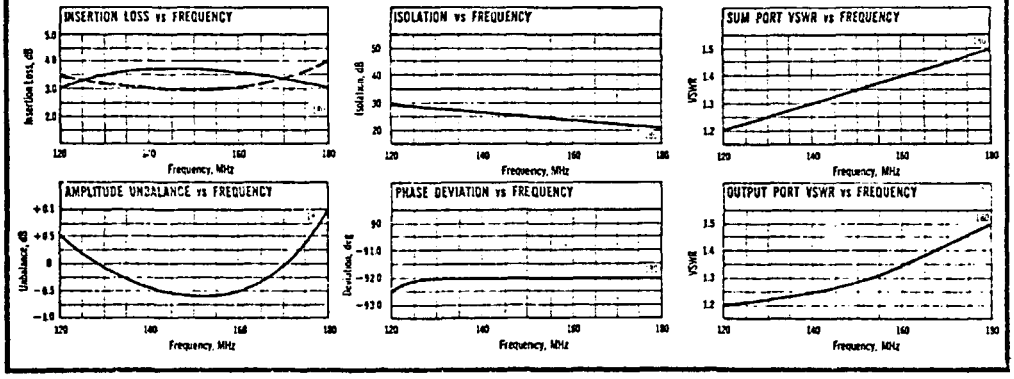
PSCQ-2 Series
12 MHz to 100 MHz

Mini-Circuits

MODEL PSCQ-2-90



MODEL PSCQ-2-180



PROMPT SERVICE / ONE WEEK DELIVERY

Mini-Circuits

Broadband LIMITERS

PLS SERIES



MODEL	FREQUENCY	Z (Ohms)	COST
PLS-1	100 KHz - 150 MHz	50	$18.95 (5-49)
PLS-2	100 MHz - 900 MHz	50	$18.95 (5-49)
PLS-6	3 KHz - 1 MHz	50	$29.95 (5-49)

DESCRIPTION—Having a volume of only .128 cu. inches, the PLS series covers a very broad frequency range from 3 KHz to 900 MHz. They have a dynamic range from +3 to +20 dBm and provide exceptionally hard limiting of a .05 dB output change per dB input change.

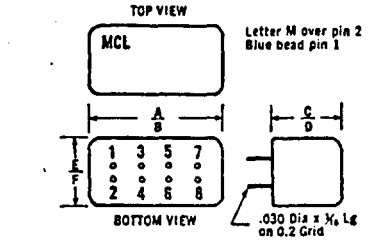
The PLS series has been designed to provide very small phase variations as the input level is changed. A bias current of about 3 mA from a 50 Ω source is required to excite the PLS limiter.

When the PLS series limiter is used with Mini-Circuits ZHL series amplifiers, a constant +15 dBm output can be obtained from .4 to 900 MHz.

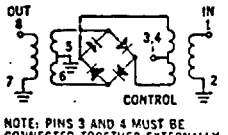
Packaged within an RFI shielded metal enclosure and hermetically sealed header, these high performance units have their pins oriented on a 0.2 inch grid.

Only well matched hot-carrier diodes and ruggedly constructed transmission line transformers are used. Internally, every component is bonded to the header and case with silicone rubber to provide super reliable protection against shock, vibration and acceleration.

DIMENSIONS AND CONNECTIONS



	A	B	C	D	E	F
IN.	.770	.800	.385	.400	.370	.400
MM	19.5	20.3	9.7	10.1	9.3	10.1



PINS FOR CASE GROUND	
Model No.	Pins
-1	2
-2	2,5,6,7
-6	—

NOTE: PINS 3 AND 4 MUST BE CONNECTED TOGETHER EXTERNALLY.

WEIGHT 5.2 grams .18 ounces

FEATURES

- **Broadband:** 3 KHz to 900 MHz
- **Large Dynamic Range:** +3 dBm to +20 dBm
- **Excellent Phase Characteristics**
- **Miniature:** 0.128 in³, 0.4" x 0.8" PC area, 0.4" high
- **High Reliability:** 100% tested
- **Low Cost:** as low as $18.95 (5-49)

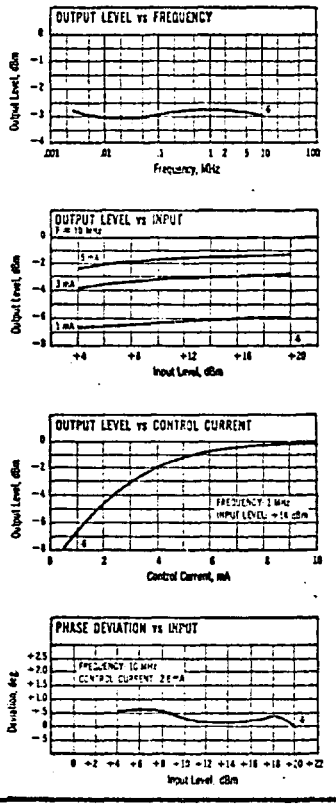
APPLICATIONS

- Stabilizing generator outputs
- Providing constant amplitude signals in phase sensitive systems
- Reducing amplitude variations in FM detection systems

ABSOLUTE MAXIMUM RATINGS

• Input Power:	100 mW
• Peak IF Input Current:	40 mA
• Operating and Storage Temp.:	−55°C to +100°C
• Pin Temperature:	(10 sec.) +260°C
• Environmental Specifications:	See Index Page

MODEL PLS-6



Mini-Circuits 2625 E. 14th St., Brooklyn, NY 11235 (212) 769-0200/Dom. Telex 125460/Int'l. Telex 620156

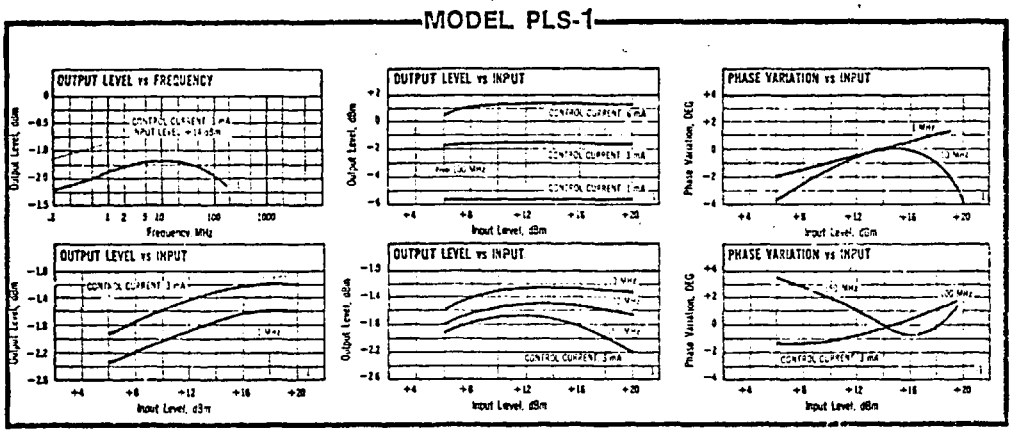
PLS Series
3 KHz to 900 MHz

Mini-Circuits

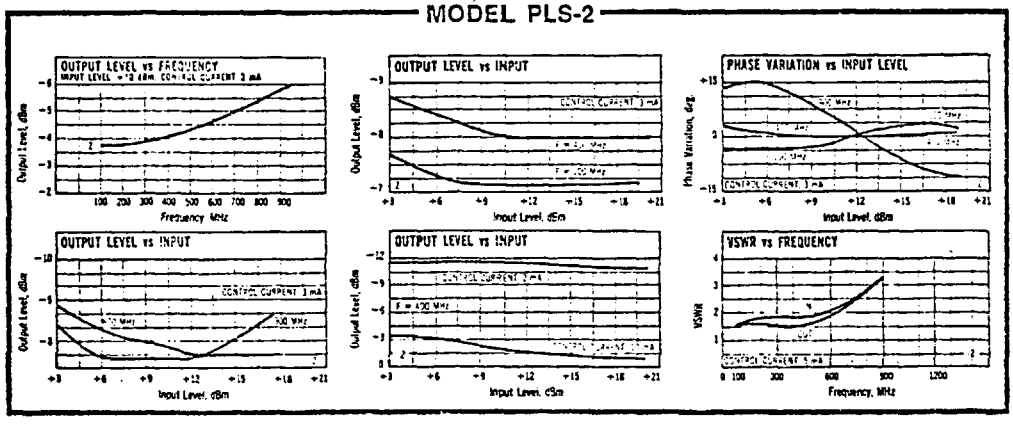
SPECIFICATIONS: 50 Ohms

Model No.	Frequency Range MHz	Input Level Range dBm	Output Level (Control Current 3 mA)	Control Current Source Impedance	RF Input Level, dBm — Limiting (Δ Out/Δin dB/dB)			RF Input Level, dBm — Relative Phase Variation			Typ. Control Current mA	Qty.	Price
					+6-+10	+10-+16	+16-+20	+6-+10	+10-+16	+16-+20			
PLS-1	0.1-150	+6-+20	−1.5 dBm Typ.	50 ohms	0.1	0.1	0.2	0.5	0.5	1.0	3	5-49	$18.95
PLS-2	100-900	+3-+15	−5 dBm Typ.	50 ohms	+3-+8 Typ. Max. 0.1 0.2	+8-+12 Typ. Max. 0.1 0.2	+12-+15 Typ. Max. 0.2 0.4	Entire Range 1° Typ. 2° Max.			10	5-49	$18.95
PLS-6	0.003-1	+6-+20	−3 dBm Typ.	50 ohms	+6-+10 Typ. Max. .10 .2	+10-+16 Typ. Max. .05 .1	+16-+20 Typ. Max. .05 .15	Full Range .2° Typ. 1.0° Max.			5	5-49	$29.95

MODEL PLS-1



MODEL PLS-2



PROMPT SERVICE / ONE WEEK DELIVERY

Mini-Circuits

REFERENCES

1. Blake, C.S., Schwartzman, L. and Esposito, F.J. (1972): "Evaluation of large phased-array antennas". Phased array antennas (Editors: Oliner A.A. and Knittel, G.H.) Aertech house.

2. Ransom, P.L. and Mittra, R. (1972): "A method of locating defective elements in large phased arrays". Phased array antennas (Editors: Oliner, A.A. and Knittel, G.H.) Aertech house.

3. Scharfman, W.E and August, G. "(1972): "Pattern measurements of phased-arrayed antennas by focusing into the near zone". Phased array antennas (Editors: Oliner, A.A. and Knittel, G.) Aertech house.

4. Bendix Company (1973): " MLS EL-1 antenna pattern monitor". Bendix company technical note MLS-BCD-TN082.

5. Bearsed, S.V. and Herbaugh, R.E. (1973): "Scanning beam landing system - endorsed as a global standard". Microwaves no 5, p.12.

6. International Committee for Aviation Organisation (ICAO) (1979): "Microwave Landing System (angle guidance documents)" AWOP,WGM/2 report Appendix A revised 10 October 1979.

7. Kummer, W.H. (1966): "Feeding and phase scanning" in "Microwave scanning antennas" (Ed. Hansen, R.C.) vol.3 Academic Press.

8. Taylor, P.J. (1979): "MLS beam forming" Plessey internal report.

9. Carter, P.S. (1932):
"Circuit relations in radiating systems and applications to antenna problems". Proc. IRE, Vol. 20 pp.1004-1041.

10. Kraus, J.D. (1950) :
"Antennas" McGraw-Hill.

11. Oliner, A.A. and Malech R.G.(1966):
"Radiating elements and mutual coupling" in "Microwave scanning antennas", Vol.2 (Ed. Hansen, R.C.) Academic Press.

12. Booker, H.G. and Clemmow, P.C. (1950):
"The concept of an angular spectrum of plane waves, and its relation to that of polar diagram and aperture distribution". Proc. IEE Vol. 97, Pt.III, pp.11-17.

13. Clarke, R.H. and Brown, J. (1980):
"Diffraction Theory and antennas" Ellis Horwood (Wiley).

14. Ratcliffe, J.A. (1956): "Some aspects of diffraction theory and their application to the ionosphere". Reports on progress in physics, Vol. 19, pp. 188-267.

15. Paris, D.T. Leach, W.M. and Joy, E.B. (1978):
"Basic theory of probe-compensated near-field measurements". Trans, IEEE, Vol.AP-26(3) pp.373-379.

16. Papoulis, A. (1962):
"The Fourier integral and its applications " , McGraw-Hill.

17. Kerns, D.M. (1970):

"Corrections of near-field measurements made with an arbitrary but known measuring antenna". Electronic Letters Vol. 6 No.11 pp. 346-347.

18. Born, M. and Wolf, E. (1975):

"Principles of optics" fifth edition,Pergamon.

19. Schelkunoff, S.A. (1952) :

"Advanced antenna theory". Wiley.

20. Jordan, E.C. and Balmain, K.G. (1960) :

" Electro-magnetic waves and radiating systems" Prentice-Hall.

21. Beckman, P. and Spizzichino, A. (1963) :

"The scattering of electro magnetic waves from rough surfaces". Macmillan.

22. Rotman, W. and Turner, R.F. (1963) :

"Wide-angle microwave lens for line source application". IEEE Trans. on Antenna and Propagation Vol. AP-11 (Nov), pp. 623-632.

23. Chignell, R.J.(1975):

"Slot loss coupling studies in stacked linear array application". Ph.D. Thesis, University of London.

24. Schelkunoff, S.A. (1948):

"Applied mathematics for engineers and scientists" Van Nostrand.

25. Abramowitz, M. and Stegun, I.A. (1964):

" Handbook of mathematical functions, graphs, and mathematical tables" National Bureau of Standards U.S. Government Printing Office.

26. Jahnke, E. and Emde, F. (1945) :

" Tables of functions with formulae and curves" Fourth edition, Dover.

27. Oliner, A.A. and Malech, R.G. (1966):

" Mutual coupling in infinite scanning arrays" in "Microwave scanning antennas" (Ed. Hansen, R.C.) Vol.2 , Academic Press.

28. Clemmow, P.C. (1966) : (*)

"The plane wave spectrum representation of elctro magnetic fields". Pergamon Press.

29. Blass, J. (1960):

" Multidirectional antenna a new approach to stacked beams" IRE National Convention Record. U.S.A.

30. Clarke, R.H. (1979) : (*)

"Random propagating fields". Post Graduate Course Notes, Imperial College, London.

31. Gradsteyn, I.S. and Ryzhik, I.M. (1965): (*)

" Tables of integrals, series, and products" Fourth Edition, Academic Press.

32. Champney, D.C. (1973): (*)

"Fourier transforms and their physical applications" Academic Press.

33. Schelkunoff, S.A. and Friis, A.T. (1952): (*)

"Antennas theory and practice", Wiley.

34. Lange F.H. (1967): (*)

"Correlation techniques" (English edition), Iliffe.

35. Williams, N. (1975): (*)

"Mutual coupling in waveguide slot arrays". Ph.D. Thesis, University of London.

(*) NOTE:

References marked with an asterisk (*) are not mentioned in the text but have been found to be very important for the study.